UNIVERSITY OF BELGRADE

FACULTY OF PHYSICS

Igor T. Franović

Collective Dynamics and Self-organization of Stochastic Neuronal Systems Influenced by Synaptic Time Delay

Doctoral Dissertation

Belgrade, 2013

UNIVERZITET U BEOGRADU

FIZIČKI FAKULTET

Igor T. Franović

Kolektivna dinamika i samoorganizacija stohastičkih neuronskih sistema pod uticajem sinaptičkog kašnjenja

doktorska disertacija

Beograd, 2013

Doctoral Committee

Thesis Adviser: **Dr Nikola Burić**, Research Professor at the Institute of Physics Zemun, Belgrade

1. Reviewer: **Dr Zoran Radović**, member of SANU, Professor at the Faculty of Physics, Belgrade

2. Reviewer: **Dr Milan Knežević**, Professor at the Faculty of Physics, Belgrade

3. Reviewer: **Dr Sunčica Elezović-Hadžić**, Professor at the Faculty of Physics, Belgrade

Day of the defense:

Belgrade,

Signature from head of the thesis committee:

Acknowledgements

I would like to thank my thesis advisor, Professor Nikola Burić, for the insightful discussions during the research. It has been a pleasure to work with and learn from him.

I also appreciate the support and collaboration of my dear friends and colleagues, Professor Kristina Todorović-Vasović and Professor Nebojša Vasović.

Abstract

Title of dissertation: Collective Dynamics and Self-organization of Stochastic Neuronal Systems Influenced by Synaptic Time Delay

by Igor Franović

The focus in the present thesis lies with the synchronization mediated self-organization phenomena in populations of globally coupled stochastic excitable or bursting units subjected to interaction delays. Excitable local dynamics follows the Fitzhugh-Nagumo model, canonical for type II excitability, whereas the bursting units are represented by the Hindmarsh-Rose model. The study comprises two complementary lines of research. One is aimed at extending the analogy regarding the complex forms of collective behavior exhibited by the assemblies of coupled nonlinear autonomous oscillators and those made up of excitable units. Within the second line of research, our main contribution consists in developing the mean-field based models for the collective dynamics of the assemblies of excitable or bursting units, whose microscopic dynamics is governed by large sets of coupled stochastic delay-differential equations. This is instigated by the notion that any population displaying a collective mode may be treated as macroscopic oscillator. While the framework itself rests on implementing the cumulant approach complemented by the Gaussian approximation, one of the principal gains presents the ability to recast the problem of (stochastic) bifurcations affecting the stability of the stationary state of the exact system

in terms of flows containing only several deterministic delay-differential equations, where noise intensity may act as a bifurcation parameter.

For the populations of excitable units, the two mean-field assumptions, the *quasi-independence* and the *Gaussian* one, are adapted to reflect the strong time-scale separation between the fast and slow motions, as well as the influence of noise. The conditions for the assumptions' validity are shown to involve matching between the qualitative features of the local and global dynamics, rather than being stated as common requirements for the small noise intensity and small coupling strengths. One also demonstrates that bistability in the dynamics of the mean-field model may indicate in a self-consistent fashion the parameter domains where the mean-field assumptions fail. Apart from single populations of excitable or bursting units, the mean-field approach has also been applied in case of two coupled populations, each comprised of excitable units, whereby the nonlinear interaction terms depend on the respective global variables. The latter setup involves noise acting within both the assemblies, and two types of coupling delays, the intra- and the inter-population ones. In all the considered instances, the mean-field model has been shown to qualitatively predict the parameter domains where the stationary state is stable, the scenarios for the onset and the time-delay induced suppression of the collective mode, as well as the parameter ranges admitting bistability between the equilibrium and the oscillatory state.

Regarding the complex forms of self-organization, we report on the novel phenomenon of spontaneous cluster formation in homogeneous assemblies of excitable units, which arises due to an interplay of the excitability feature and the co-effect of noise

and interaction delay. The phenomenon comprises the asymptotically stable two-cluster partitions, with units firmly bound to their subsets, and the dynamical three-cluster states, where the units may exchange subsets. The observed resonant-like behavior is explained in terms of competition between the collective effects occurring on the noise- and delay-dependent characteristic time scales. We also discuss the implications of the somewhat unexpected result, suggesting that the onset of the two-cluster states coincides with the global bifurcation of the corresponding mean-field model. Note that the content of the thesis is based on the results published in four research papers, including I. Franović, K. Todorović, N. Vasović, N. Burić, Physical Review Letters **108**, 094101 (2012); I. Franović, K. Todorović, N. Vasović, N. Burić, Physical Review E **87**, 012922 (2013); I. Franović, K. Todorović, N. Vasović, N. Burić, CHAOS **22**, 033147 (2012); I. Franović, K. Todorović, N. Vasović, N. Burić, CHAOS **21**, 033109 (2011).

key words: excitable dynamics, noise, interaction delays, synchronization, collective mode, cluster states, mean-field model, Gaussian approximation, bifurcation analysis, stochastic bifurcation

scientific field: Physics

specific scientific field: Condensed matter physics and statistical physics

UDK number:

Contents

List of Figures

List of Abbreviations

CR	Coherence resonance
DDE	Delay-differential equations
EQ	Equilibrium
FHN	Fitzhugh-Nagumo
FP	Fixed point
FS	Frequency synchronization
GA	Gaussian assumption
HR	Hindmarsh-Rose
ISI	Interspike interval
LC	Limit cycle
MF	Mean-field
MFA	Mean-field assumption
PS	Phase synchronization
QIA	Quasi-independence assumption
SDDE	Stochastic delay-differential equations
SISR	Self-induced stochastic resonance

Chapter 1

Introduction

1.1 Synchronization and the collective mode

Populations of coupled oscillators provide the elementary dynamical paradigm for modeling the collective motion in a variety of fields, ranging from physics, chemistry and biology to social sciences [1–6]. Such a framework has proven indispensable for understanding the onset and adjustment of coherent rhythms related to Josephson junction circuits [7], laser arrays [8] and electrochemical reactions [9], as well as the mechanisms regulating heartbeat [10] and circadian cycles [11], or underlying the normal and pathological patterns of brain activity [12–14] on one hand and even some forms of human social behavior [15, 16] on the other. The comprehensive analysis of the universal elements behind such phenomena requires one to combine and adapt the different concepts from the theory of nonlinear dynamics, statistical physics and pattern formation. All the mentioned systems, irrespective of the involved time scales and the degree of complexity, share the common tendency toward collective synchronization [17–19], facilitated by interaction between their constituents. Different forms of synchronization turn out to be the fundamental mechanism behind self-organization and structure formation in systems of coupled nonlinear oscillators [1, 3, 5].

Synchronization on a macroscopic scale refers to mutual adjustment of

rhythms between a large number or all units in the assembly, which gives rise to a collective mode, whose frequency matches that of the synchronized majority [2]. Note that a system may admit one or perhaps several collective modes, whereby the larger is the synchronized group, the higher is the amplitude of the collective mode. Analytical approaches to local and global periodic behavior in systems of autonomous (self-sustained) nonlinear oscillators heavily relies on the notion of phase [17, 20, 21]. Having properly defined the phase variable, the dynamics of any single unit may be recast in terms of the simplified, one-dimensional description, which allows one to characterize all the main aspects of oscillations, such as regularity or sensitivity to external forcing [22, 23].

On many occasions, sufficient insight into collective phenomena may be gained by assuming that the units are coupled in the all-to-all fashion (global coupling) [1, 3, 6], rendering each oscillator as being driven by the mean-field generated by all the members of the assembly. In case of weak interactions, population activity can be handled within the framework of phase approximation. For the canonical setup involving globally coupled Kuramoto phase oscillators [20, 24], one may derive the equations for the global variable (order parameter), explicitly demonstrating that the transition from asynchrony, characterized by the zero mean-field, to synchronous regime under increasing coupling strength has the properties of nonequilibrium phase transition. In particular, if the units are identical or their natural frequencies follow a unimodal distribution, the mean-field grows smoothly with supercritical coupling strength, indicating a second-order transition [1, 6, 24, 25]. Nonetheless, if the distribution of natural frequencies is uniform, the non-zero mean-field appears by a jump, analogous to a first-order transition [26].

Apart from the onset and suppression of the collective mode [1, 27], the most frequently addressed issues include the effects of the external forcing [3, 28] or feedback [29], as well as the interaction between the different

collective modes [30–32]. Added complexity of individual units' dynamics and/or coupling function may further result in a number of interesting phenomena, such as chaos in the mean-field [33, 34], multistability [2], clustering [1] [35–37] as well as splay-states [38, 39]. These well known forms of behavior in assemblies of coupled phase oscillators have recently been complemented by the novel highly non-trivial phenomena of self organization, namely the self-organized quasiperiodicity [2, 40–42] and the chimera states [43–48], both of which may be cast as partially synchronous states. The former refers to a scenario where the mean-field is unable to entrain the single units, but they still remain coherent, attaining a frequency incommensurate to that of the mean-field. This is facilitated by the non-linear global coupling, that changes its attractive/repulsive character depending on the mean-field: for a weak (strong) mean-field, the coupling supports in-phase (antiphase) synchronization. Self-organized quasiperiodicity arises in an intermediate case, having the interaction tuned exactly at the border between attraction and repulsion [40, 41]. On the other hand, chimera states involve a symmetry breaking scenario, where a spatially homogeneous population of identical coupled oscillators displays a self-organized pattern comprised of regions with synchronous and asynchronous motion. The most important ingredient for such patterns to emerge is the non-local form of connectivity between the units, whose characteristic range is sufficiently distinct from both the global and the local next-nearest neighbor coupling [47]. For the general class of systems comprised of coupled phase oscillators, the issues regarding the above collective states, including the onset, dynamical features, as well as the transitions between them, are susceptible to analytical treatment. The appropriate framework is provided by the Watanabe-Strogatz theory [49], complemented by the Ott-Antonsen Ansatz [25, 50]. The latter allows one to derive closed equations for the

[1] Cluster synchronization refers to a phenomenon where subsets of network nodes display isochronous synchronization internally, but synchronization between the subsets either does not occur, or is of non-isochronous type, with the latter most often involving a phase lag. [21, 35].

amplitude and the frequency of the mean-field, obtaining the corresponding stationary solutions.

1.2 Noise and interaction delay

In real-world applications, the evolution of macroscopic systems is naturally attended by noise and interaction delays, whose particular or combined effects may substantially alter the ”bare” dynamics, conforming to the noise- and delay-free case. On the modeling side, one should note several recent studies suggesting that coexistence of noise and interaction delays is ubiquitous in nature rather than rare [51, 52], with the most prominent examples referring to biophysiological systems [53] and the laser dynamics in optical cavities [54]. While introducing noise provides a standard paradigm to account for the small random perturbations due to fluctuations of the internal origin or variability in the embedding environment [55, 56], the interaction delays usually arise for the finite signal transmission velocities along the appropriate communication channels, though the time-lag may also be a corollary of finite processing times, causing latency in the system's responses [57–59].

Focussing on the impact of time delay in systems of globally coupled phase oscillators [60–62], the major effect presents the ability to control, viz. suppress or enhance the collective mode by feeding the delayed mean-field back to the assembly [1, 29, 63]. This effectively introduces another characteristic time scale to the system dynamics. What makes the delayed feedback mechanism generic is the fact that it does not depend on the features of the local dynamics, nor does it affect its corresponding frequency, but it only acts in direction of improving or spoiling the coherence between the single oscillators [1]. Among the less important effects of time delay, one may count in the roles in introducing different forms of multistability, as well as in facilitating the transition to chaos [64] or inducing synchrony

in systems of coupled chaotic elements [65, 66].

Regarding the isolated effects of noise, a clear distinction should be made between the scenarios where oscillations are noise-induced [56, 67] and only noise-perturbed [68]. In the latter instance, it is well known that rather than being detrimental, noise can actually prove constructive with respect to improving regularity of the system's behavior. This particularly refers to the interplay of noise and nonlinearity, whose combined effects have been seen to bring order into the unperturbed irregular dynamics [69]. Therefore, instead of looking into the ways of minimizing the influence of noise, the proper strategy consists in finding the parameter domains where the impact of noise is optimal. Within this context, one should mention the phenomena of noise-induced order in chaotic dynamics, then the enhanced synchronization by external noise [55] and most importantly, the stochastic resonance feature[1] [70–72]. The latter refers to the existence of a certain intermediate noise intensity at which the response of a system to a weak subthreshold periodic signal becomes optimal. In effect, this may be interpreted as if the weak signal changes the energetically most favorable state of the system, with the hopping to such state, elicited by noise, occurring precisely when its rate matches the one provided by the frequency of forcing [67].

On the modeling side, two types of stochastic models may loosely be distinguished when their dynamics is compared to their deterministic counterparts [67]:

i) the models where noise acts inhomogeneously in different regions of phase space, such that it dampens or amplifies certain processes and events; this does not result in the introduction of novel characteristic time-scales, but in modification and noise-dependence of the existing ones;

[1] The discovery of stochastic resonance in 1981 marks the turning point in the perception of the role of noise in nonlinear systems, changing the earlier perspective strictly relating noise and disorder.

ii) models associated with presence of unstable barriers, such as thresholds, separatrices and saddles in the system dynamics; with noise coming into play, such barriers may be exceeded with finite probability.

At variance with type *i*), the stochastic models of type *ii*) attain a novel characteristic time-scale, given that noise evokes processes absent in the deterministic case.

The above physical picture is significantly modified in the case of noise-induced oscillations, which brings us closer to the main topic of this thesis. For the most part, the focus here lies with the synchronization mediated self-organization phenomena in fully connected networks of excitable units subjected to noise and coupling delays. Much less space is dedicated to analogous phenomena in networks of bursting units. The common feature for both forms of local dynamics is that the proper phase description is unavailable, though certain phase-like variables, such as the effective phase [4, 73, 74] or protophase, may yet be defined.

1.3 Excitable dynamics

Excitable dynamics constitutes a specific type of motion found in systems whose equilibrium is poised close to a bifurcation toward sustained periodic activity [67, 75]. In a nutshell, excitability refers to a form of behavior where a perturbed system may generate *small-amplitude* linear or *large-amplitude*, highly-nonlinear types of responses, this depending sensitively on the magnitude of the stimulus. In particular, if perturbation is interpreted as a setting of initial conditions, it follows that two nearby conditions may evoke qualitatively distinct excitations: after a linear response, the system promptly settles back to equilibrium, whereas for the nonlinear one, referred to as *spike*, the system's representative point performs a stereotypical large excursion in phase space before relaxing to equilibrium. Note that the boundary separating the two pertaining sets of initial

conditions in phase space may be hard or soft [67, 75, 76], which is reflected in the threshold-like or smooth crossover between the small- and large-amplitude responses, respectively. Arguably the best example of an excitable system is provided by a neuron cell membrane [75, 76], where a stimulus may either set off post-synaptic potentials, analogous to small-amplitude graded responses, or may elicit action potentials (spikes), with the outcome contingent on the stimulus strength.

The basic paradigm behind excitable dynamics is built on the sharp time-scale separation involving the fast (excitatory, activator) variable, coupled to a slow (recovery, inhibitory) variable, whereby the latter is responsible for the relaxation stage following the excitation [77–80]. In terms of the fast-slow decomposition, a single oscillation is made up of slow motion, confined to the slow manifold, and fast motion, consisting in rapid jumps between different pieces of the slow manifold. All excitable systems possess a *unique stable equilibrium*, but may further visit two unstable states, namely the *excited* (firing) and the *refractory* (recovery) one. The latter two are unstable in a sense that a system escapes from them even in the perturbation-free case. In other words, in the absence of external perturbations, an excitable system resides in equilibrium (rest state). If a weak perturbation kicks in, the system fluctuates in the vicinity of fixed point for a short while, then regaining the steady state. On the other hand, being adequately perturbed, an excitable unit engages in a large-amplitude excursion, passing through the firing and rest states before equilibrium is reinstated. Once a spike has been elicited, a certain amount of time, known as *refractory time*, has to pass before another excitation is possible.

One should be careful not to confound excitability with bistability, given that the former is not facilitated by coexistence between a fixed point and a limit cycle. As iterated above, all excitable systems are monostable, having a stable equilibrium as the sole attractor, whereas the existence of orbits corresponding to large-amplitude responses is tied to the structure of the

respective systems' phase spaces, especially their geometry in the vicinity of equilibrium. The latter point also indicates that excitability per se is an intrinsic feature of the system, rendering its manifestation completely independent on the deterministic/stochastic character of the stimuli. Under deterministic scenario, the large-amplitude responses may be envisioned as a corollary of the system traversing states far from equilibrium [67]. Regarding the stochastic effects, one readily realizes how noise may act as an excitability amplifier [75]. This refers to the point that excitable systems are capable of generating sustained oscillations under permanent perturbation, whereby a sequence of excitations makes up a *spike (pulse) train* [67]. On the surface, the ensuing noise-induced oscillations may even appear quite regular, so that their profile becomes virtually indistinguishable from what is commonly seen in relaxation oscillators. However, oscillations evoked in excitable systems are conceptually more intricate than those found in self-sustained oscillators, be it the phase or the relaxation ones. Regarding the potential analytical approaches, the key difference lies in the ability to derive the proper phase description. The latter provides the means for implementing the phase resetting framework, which allows one to gain insight into the system's responses to external stimuli or its synchronizability with other systems [22, 81]. In this context, for autonomous oscillators there is a basic phase description, which can easily be modified to account for the effects of noise perturbatively [73]. On the other hand, the phase variable cannot be attributed at all to excitable systems, essentially because they reside in equilibrium [4].

1.3.1 Classification of excitable systems

As already mentioned, by the theory of nonlinear dynamics, excitable behavior arises because the deterministic system lies just below the bifurcation threshold between the stationary state and the oscillatory motion [67, 77, 78, 80]. In the subthreshold regime, any oscillation is merely a

transient triggered by the sufficiently strong perturbation that temporarily kicks the system into a supercritical state. According to the generic mechanism by which the bifurcation toward the limit cycle takes place, all excitable systems may be cast into two classes [67, 75]. The *type I* excitable systems are poised near the saddle-node-on-invariant circle bifurcation. Then, in the vicinity of the bifurcation point, the ensuing oscillations can attain an arbitrary low frequency due to creation of a homoclinic orbit. On the other hand, at the critical value of the bifurcation parameter, the *type II* excitable systems would undergo a supercritical Hopf bifurcation, meaning that the oscillation frequency near the critical threshold remains finite. For type II excitability, the boundary between perturbations yielding small- or large-amplitude oscillations is less clear, so that the transition between the two appears continuous. Type I excitability class is usually represented by the Morris-Lecar model [82], whereas the Fitzhugh-Nagumo model [83, 84] is considered canonical for type II class. Both models are two-dimensional and derive from the field of neuroscience. There are also simpler, one-dimensional models of excitability, including the integrate-and-fire model [85] and the noisy Adler equation [67]. Throughout the thesis, we are concerned with the systems composed of type II stochastic excitable units with delayed couplings, with each unit following the Fitzhugh-Nagumo model.

1.3.2 Excitability and noise: resonance phenomena in single unit dynamics

Excitable systems influenced by noise are encountered in a wide variety of areas, including chemical reactions, semiconductors [86], lasers [87, 88], combustion and climate dynamics [67], but the most prominent examples come from biophysiological context, where they are known to underlie the behavior of cardiac [10, 89, 90] and neuronal tissues [4, 75, 91]. Sources of noise in excitable systems are just as diverse as the origins of excitability

itself [67]. In case of chemical reactions, noise is related to finite-size effects, whereas in laser dynamics, the quantum fluctuations provide the main physical basis for noise. Nonetheless, in neuronal systems, there are multiple coexisting sources of noise, including the random synaptic input due to background neuronal activity on one hand, and the stochastic kinetics of the ion-gating channels as well as the quasi-random synaptic release of neurotransmitters on the other.

For understanding the impact of noise on excitable systems, a point to single out is that noise affects the excitation and refractory stages of oscillation in a quite different fashion. The latter is reflected in the means and variances of the underlying characteristic time-scales [51, 55, 67]. In particular, the activation time, required for the phase point to escape from the equilibrium, is noise-controlled, with the excitation events approximately obeying the Poisson statistics [67, 76–78]. On the other hand, the excursion time, which describes the decay of the unstable excited and refractory states, is mostly governed by the deterministic dynamics, which justifies the term ”stereotypical oscillation” in the definition of excitability. While the mean excursion time varies weakly with noise, the dependence of its variance becomes apparent at large noise intensities.

What has been stated so far implies that noise-induced oscillations can be made coherent by the appropriate (optimal) noise intensity. For a single excitable unit, there are in fact two distinct scenarios for such resonance phenomena, namely the *coherence resonance* (CR) [55, 77] and the *self-induced stochastic resonance* (SISR) [78, 79]. To a certain extent, one may compare them to stochastic resonance in autonomous oscillators, though they take place in the absence of external forcing. CR explicitly relies on different dependencies of means and variations of the activation and excursion times on noise. The resonance is achieved by a tradeoff between two different effects: for one, noise should be large enough to make the activation time considerably smaller than the excursion time, while on the

other hand, noise intensity should not be overly large, such that the fluctuations of the excursion time remain small [55, 67]. The mechanism behind SISR is considerably more intricate, and rests on keeping an excitable unit frustrated, such that its representative point is prevented from reaching the vicinity of equilibrium. Put succinctly, differences between CR and SISR concern three important aspects [77]:

i) the limit cycle within CR is the precursor of the deterministic one, whereas the limit cycle in SISR has no deterministic counterpart;

ii) in CR, the bifurcation parameter has to be fine-tuned to close vicinity of the critical threshold, whereas in SISR one does not require fine tuning;

iii) in SISR, coherence of the oscillations is sensitive both to noise and the separation ratio between the fast and slow characteristic time-scales; noise can also be used as a control parameter to make the coherence arbitrarily large.

Note that the arguments from this discussion will partly be revisited when drawing an analogy to local mechanism behind clustering in Chapter 5.

1.3.3 Noise-induced regimes of collective behavior

Due to rapid expansion in recent years, the study of collective dynamics in excitable media has come to be appreciated as a distinct field, where the phenomena are characterized by specific modes of behavior in their own right. Still, comparing the self-sustained and noise-excited oscillations, several analogies may be drawn. In particular, the latter may also get synchronized when coupled into an assembly of excitable units [92, 93], or may be controlled by the time-delayed feedback [63]. Important roles of noise in spatially extended excitable media consist in facilitating and enhancing periodic signal transmission and wave propagation, as well as

promoting synchronization and influencing the pattern formation [67, 94]. Nevertheless, the most substantial effect related to noise in excitable media is that it may enact a control parameter, such that its increase causes the system to switch between the three generic regimes [95]. The latter include

i) *the subthreshold motion* at low noise intensities, where the firing of individual units is sporadic and incoherent;

ii) *coherent regime* at intermediate noise, where the system displays the collective mode due to approximate synchronization between the comparably high-frequency, regular spiking activities of single units;

iii) *chaotic collective state* at large noise intensities, where the single units fire at high frequencies, but their action remains incoherent.

In this thesis, it is argued that taking into account the effects of interaction delays profoundly alters the above physical picture. In particular, it is demonstrated that the interplay of excitability, noise and delays in completely homogeneous networks leads to formation of cluster states, a complex form of self-organization which exhibits the features of resonance phenomena.

1.4 Background on bursting dynamics

As indicated earlier, a much smaller segment of the thesis is concerned with the study of the self-organization phenomena in networks of globally coupled bursting units subjected to noise and coupling delays. Bursting activity is typically found in biophysiological context [75], with the examples including the neuronal systems [96, 97], populations of pancreatic β-cells or the circuits responsible for rhythmogenesis, such as the central pattern generators [98].

Bursting is a form of complex oscillation, where the *active phases*, comprised of series of closely spaced spikes, are interspersed with periods of

quiescence, viz. the *silent phases*. Models of bursting generally involve coaction of a fast subsystem giving rise to repetitive spiking within the active phases, and the slow subsystem, that modulates spiking by controlling its onset and termination. In qualitative terms, the models may be classified topologically according to the type of bifurcations the system undergoes when passing from resting to spiking phases and vice versa. The most widely encountered is the fold-homoclinic class, which is known for generating the square-wave bursting profiles [75]. The Hindmarsh-Rose model [99], considered within the thesis, comes from the field of neuroscience and is canonical for the class of square-wave bursters. One may loosely regard it as analogous to Fitzhugh-Nagumo model, augmented with another slow variable. Note that our analysis covers both the noise-perturbed (endogenous bursters) and the noise-induced bursting activities.

As with the systems of coupled excitable units, onset of the collective mode is related to synchronization between the local oscillations. Nevertheless, the synchronization phenomena between the units engaged in bursting activity are significantly more complex, and may take place on a larger or a shorter time-scale. On a larger time-scale, one may encounter *burst synchronization*, a manifestation of *chaotic phase synchronization* [100–102], characterized by an overlap between the respective times of triggering and cessation of active phases between the units, though the spikes themselves may not be correlated. The phenomenon on a shorter time-scale is referred to as *spike synchronization* [75], where spikes generated within the active phases of two neurons are closely matched.

1.5 Mean-field models for systems of coupled stochastic delay-differential equations

Conceptually, given a population of coupled oscillators which exhibits a collective mode, a pervasive idea within the theory of nonlinear dynamics

is to treat it as a macroscopic oscillator [3]. Going a step further, the idea is to develop a formalism that would provide a macroscopic description of the system's behavior, instead of the one based on the local dynamics. Such an approach is motivated on theoretical and practical grounds, the former of which will be discussed shortly. The practical reasons for attempting to reduce the motion of a large system of units to that of global variables is pretty much apparent: the computational time required to simulate an N-size assembly of coupled oscillating units grows with N^2 [103], whereas additional demand is imposed when performing averages over different realizations of stochastic processes.

Dynamics of nonlinear macroscopic oscillators can be studied in a fashion similar to that of the single units. In particular, one may examine the response to external stimuli by determining the collective phase-resetting curves [21, 22, 104], analyze the enhancement or the suppression of oscillations via time-delayed feedback [1, 27, 105], observe the mode entrainment via external forcing [3, 25] or address the issue of mutual adjustment between the collective modes from different assemblies [32]. As mentioned earlier, for populations made up of autonomous oscillators, there are powerful phase reduction techniques, which allow one to analytically treat the behavior of global variables, obtaining exact solutions related to the above and more complex collective phenomena. However, this does not apply in case of assemblies comprised of excitable units, given that phase cannot be attributed to systems residing in equilibrium [4]. Nevertheless, there are other more convenient methods that may be adapted to capture the collective motion of populations of noise-driven oscillating units subjected to interaction delays. In mathematical terms, dynamics of such assemblies is represented by large systems of coupled nonlinear stochastic delay-differential equations (SDDE), for which a systematic statistical description is still lacking. The study so far has mostly been confined to determining the parameter domains admitting the stationary solu-

tion of the system of coupled Langevin equations, implementing the step-by-step or the moments methods [64, 106]. In case of instantaneous interactions, the collective motion of stochastic systems in the thermodynamic limit $N \to \infty$ could also be handled within the Fokker-Planck formalism [107, 108]. Then, the usual approach consists in applying the mean-field and diffusion approximations to obtain the stationary probability distribution [103]. The problems involving the time-dependent solutions for probability distribution have recently been considered by performing series expansions in terms of Hermitian polynomials, such that the system's evolution is expressed through the dynamics of expansion coefficients. The drawback with the Fokker-Planck formalism is that it does not provide analytically tractable solutions for the setups involving time-delays, because the SDDE-governed processes are essentially non-Markovian [64, 103]. In other words, having included the interaction delays, the stochastic process is no longer memoryless, since the future states of the system depend not only on the current state at moment t, but also require the knowledge of history at time $t - \tau$, where τ denotes the time-delay.[1] A notable exception to the lack of analytical solutions for SDDE systems within the Fokker-Planck approach presents the class of *linear* stochastic differential equations with additive noise.

Instead of considering hierarchies of probability densities[2], an alternative approach to describing collective motion led by a stochastic process consists in deriving equations for the complete sets of cumulants or moments of distribution. Either of the two latter methods applies in presence

[1] This point is readily illustrated on the example of a single stochastic variable $x(t)$, whose evolution is given by some nonlinear equation that incorporates a delayed feedback. Then, one is faced with the problem of determining the two-point joint probability distribution $p[x(t), x_\tau]$, having defined $x_\tau \equiv x(t - \tau)$, or equivalently, is required to calculate the so-called conditional drift term of the form $\langle x_\tau | x(t) \rangle = \int_0^\infty x_\tau p(x_\tau|x) dx_\tau$, where $p(x_\tau|x)$ stands for the appropriate conditional probability [109, 110]. Note that if τ is larger than the correlation time of x, a simplifying assumption of statistical independence $p[x(t), x_\tau] = p[x(t)]p[x_\tau]$ may be in order. Also, certain approximations are available in the limit of small time-delay.

[2] For the globally coupled systems, it is sufficient to consider one particle probability density given the assumption of molecular chaos. On the other hand, considering more involved types of connectivity patterns would require taking into account two- or higher degree-particle probability densities.

of time-delays, but the one with cumulants is preferred because it allows one to introduce a number of convenient approximations in a controlled fashion [67]. Such approximations are intended as a form of closure hypothesis for the set of equations guiding the evolution of cumulants. By default, this set is unclosed due to nonlinear terms in the original SDDE system, causing the dynamics of the lower-order cumulants to be intertwined with that of the higher-order ones. In this context, the most widely applied is the *Gaussian approximation* [5, 67, 111, 112], by which all the cumulants above the second order are assumed to vanish, such that the collective motion is described in terms of averages and fluctuations of global variables. Compared to the original system, the form of the ensuing mean-field model is substantially more compact, and further involves only deterministic DDEs, where noise is represented solely by its intensity [5, 67].

From the theoretical point of view, multiple gains can be drawn from developing a mean-field description of collective motion. Apart from offering insight into the system's behavior in the thermodynamic limit $N \to \infty$, it may advance understanding of the relationship between the local and global dynamics, in particular with respect to isolating the key ingredients of the local dynamics that affect the macroscopic phenomena. A benefit for itself presents the point that the collective motion is described in terms of variables with a transparent meaning, allowing one to see more clearly the role of system parameters in shaping the global dynamics. Nevertheless, the most valuable gain lies in the ability to trace the *stochastic bifurcations* [64, 111, 113] of the exact system. In deterministic systems, the notion of bifurcation refers to the qualitative change of the asymptotic dynamics above the critical value of the bifurcation parameter. For the phenomenological stochastic bifurcations, the proper definition is still lacking, though one may relate them to qualitative changes in some time-averaged measure, like the probability density function or the power spectrum. For instance, the steady state distribution could undergo transition, turning from uni-

modal to bimodal. At variance with deterministic bifurcations, the noise-driven ones may be smeared over a certain parameter range, rather than occurring at the critical parameter value. Having derived the mean-field approximation for the exact system, the stochastic bifurcations exhibited by the original SDDE may be qualitatively compared to deterministic bifurcations of the approximate system, where the noise intensity can act as a genuine bifurcation parameter.

Within the thesis, we present the derivation of the mean-field based approximations for the collective motion of populations of globally coupled excitable or bursting units, subjected to noise and interaction delays. Carrying out the bifurcation analysis on the respective approximate models, it will be demonstrated that the latter predict in a qualitative sense the conditions for the stability of equilibrium, the scenarios for the onset of the collective mode and its suppression by the effects of time-delay, as well as the parameter domains admitting bistability exhibited by the corresponding exact system. On the quantitative side, it is shown that the models are capable of capturing the frequency of the collective mode. Moreover, instances may be found where the time series of the mean-field variables closely match those of the global variables of the exact system.

1.6 Outline of the thesis

The purpose of the introductory chapter so far has been to provide the appropriate context for the issues discussed within the thesis. To do so, we have laid out the basic terminology and have made brief remarks on the relation between what has previously been known and the results to be reported in detail here. The intention now is to make a preview on the content of the thesis, briefly indicating the key points. In particular, two complementary lines of research have been followed. For one, the interest has been to examine whether and how much can the complex forms

of collective behavior exhibited by the populations of autonomous oscillators carry over to assemblies of excitable units, aiming to highlight the common elements and isolate the potential specific features that arise due to excitability. The second line of research pursued here focuses on deriving the mean-field based approximations to collective motion of the corresponding exact systems. Apart from examining the conditions for the validity of the mean-field assumptions, the main goal is to demonstrate that the scenarios related to the onset of the collective mode in the original system, governed by the large set of SDDEs, can qualitatively be predicted by the approximate model, represented by a small set of deterministic DDEs. The remaining chapters are organized as follows.

Chapter 2 is comprised of three sections: the first contains background information on the dynamics of a single Fitzhugh-Nagumo unit, the second illustrates the three generic regimes of noise-induced collective behavior for the assembly of Fitzhugh-Nagumo units, whereas the third one concerns the detailed derivation of the mean-field model for the population of excitable units influenced both by noise and interaction delays. The first section stresses the interplay of strong time-scale separation and the vicinity of the supercritical Hopf bifurcation, showing that the noise-induced oscillations are reminiscent of those displayed by the relaxation oscillators. The second section indicates the main features of the collective motion in the absence of interaction delays. Apart from the details of the derivation, in the third section one points out how the two mean-field assumptions, the quasi-independence and Gaussian one, fit within the cumulant approach.

In Chapter 3, we provide the more precise formulation of the two mean-field assumptions, adapted to the conditions of strong time-scale separation and the presence of noise. The analysis shows that their validity cannot simply be linked to the requirements for small noise and small coupling strength, but should rather be stated in terms of the qualitative features of local and global dynamics. It is further demonstrated that bistability of the

mean-field model's dynamics may indicate in a self-consistent fashion the parameter ranges where the mean-field assumption s fail. The content of this Chapter is based on the paper considered for publication in Physical Review E [114].

Chapters 4 and 5 address the spontaneous formation of synchrony clusters in homogeneous assemblies of stochastic delay-coupled excitable units, this being a novel form of self-organization which we recently reported on in [115, 116]. In Chapter 4 is described the basic phenomenology of the noise-delay co-effect leading to the asymptotically stable two-cluster partitions and the dynamical three-cluster states, having introduced the appropriate analytical tools to characterize them. In Chapter 5, the resonant character of clustering with respect to interaction delays is explained in terms of competition between the noise-driven and delay-driven collective modes. The local mechanism, showing how clustering is reflected in the adjustment of single units, is considered by drawing an analogy to particle motion in a double-well potential. We also comment on the unexpected result that the onset of clustering coincides with the global bifurcation of the corresponding mean-field model.

In Chapter 6 the focus lies with the collective dynamics displayed by two populations of excitable units, having assumed that the coupling term between populations is a nonlinear function of global variables. The presented results follow our recently published paper [117]. In particular, the system dynamics is influenced by noise acting locally on each unit within the assemblies, as well as the intra- and inter-population coupling delays. The main idea behind constructing the approximate model for this setup has been to replace each population with its mean-field counterpart. The behavior of such an approximate system is compared with that of the exact system to demonstrate the qualitative agreement in terms of the conditions for the stability of equilibrium, scenarios for the onset of the collective mode or its suppression by time-delay, as well as the parameter domains

supporting bistable regimes.

The similar agenda is followed in Chapter 7, but in case of an assembly of coupled bursting units. It is shown that the collective mode admitting bursting may arise directly from equilibrium, or via an intermediate spiking mode. A remarkable point is that there may be instances where the series for the global variables of the exact system are exactly matched by those of the respective mean-field variables. The results of this Chapter rest on our recent article [118].

Chapter 8 contains the concluding remarks, together with the discussion on possible directions of future research.

Chapter 2

Assembly of excitable units: exact system and the mean-field model

---

Chapter abstract Focussing on the Fitzhugh-Nagumo model, the first two sections provide an overview of the known facts regarding the dynamics of a single excitable unit and specify more closely the regimes of collective behavior making up the paradigm for excitable media prior to our research. On the former, we highlight the importance of interplay between nonlinearity and sharp separation of characteristic time scales for manifestation of the excitability feature. Relying on the phase plane analysis, one demonstrates how the period of noise-induced oscillations is calculated, followed by several notes on their regularity within the CR phenomenon. The types of collective dynamics controlled by noise in the absence of interaction delays are characterized in several ways, including the phase portraits for the macroscopic variables, the regularity and synchronization properties of the local dynamics, as well as the stationary probability distributions for the assembly averages. Last but not least, the third section is highly relevant for the main body of the thesis, because it concerns one of our main contributions, presenting

the derivation of the mean-field model for the population of excitable units subjected to noise and interaction delays.

2.1 Dynamics of an isolated Fitzhugh-Nagumo unit

Throughout the thesis, the Fitzhugh-Nagumo system (FHN) is used as a generic model for excitable local dynamics. Prior to discussing the three regimes of collective behavior typically encountered in noise-driven excitable media, let us consider the dynamics of an isolated FHN unit, first for the deterministic setup and then under the action of noise. This approach is aimed at highlighting the interplay between the strong time-scale separation and the vicinity of Hopf bifurcation threshold in shaping the key features of excitable dynamics.

Note that the equations of the FHN model can be interpreted as a generalization of the van der Pol oscillator, and are better known under the name Bonhoeffer-van der Pol oscillator [119] when considered in the regime of self-sustained oscillations. For its excitable dynamics, this system has first been analyzed in independent works of Fitzhugh (1961) [83] and Nagumo (1962) [84], who regarded it as a simplification of the Hodgkin-Huxley model [85], describing the excitable response of a nerve membrane to an external current stimuli. Though derived in the field of neuroscience, FHN model has since been applied in several other areas, including the formation of spiral and scroll waves in the kinetics of Belousov-Zhabotinsky reaction [120], as well as the transmission of pulses in cardiac tissue [10, 90]. FHN model has particularly gained attention for it allows one to study the key ingredients behind excitable dynamics within the framework of phase plane analysis.

For the moment, the discussion is confined to the deterministic case,

such that the equations for an isolated FHN unit read [75]

$$\begin{aligned} \epsilon dx &= F(x,y)dt = (x - x^3/3 - y)dt \\ dy &= G(x,y)dt = (x + b)dt. \end{aligned} \tag{2.1}$$

The parameter ϵ is deliberately set to a small value $\epsilon << 1$ to enforce a large separation between the characteristic time-scales for the evolution of $x(t)$ and $y(t)$. Throughout the thesis, the time-scale separation ratio between the two variables is $\epsilon = 0.01$. Interpreted in the context of neuroscience, the fast (activator) variable embodies the membrane potential of a neuron, whereas the slow variable, referred to as recovery or refractory, accounts for the gross kinetics of the potassium ion-gating channels. Nevertheless, such an analogy should be viewed in a qualitative, rather than quantitative sense [76].

b plays the role of excitability parameter, which can be established as follows. We first invoke the point that the system (7.1) possesses a unique equilibrium given by

$$x_0 = -b, \;\; y_0 = -b + b^3/3, \tag{2.2}$$

whose characteristic exponents read

$$\lambda_{\pm} = \frac{b^2 - 1 \pm \sqrt{(b^2-1)^2 - 4\epsilon}}{2\epsilon}. \tag{2.3}$$

Therefore, the fixed point is stable if and only if $|b| > 1$, whereas the system undergoes supercritical Hopf bifurcation at $|b| = 1$. For $|b| < 1$, there exists a limit cycle, which is globally stable. Selecting different values of b, the system (7.1) may effectively switch between the excitable and oscillatory regimes. Given that (7.1) is invariant under the transformation $(x, y, b) \longrightarrow (-x, -y, -b)$, it suffices to consider only the case $b > 0$ [79].

Now let us consider by means of phase plane analysis the excitable dynamics obtained for b lying slightly above 1. The basic framework rests

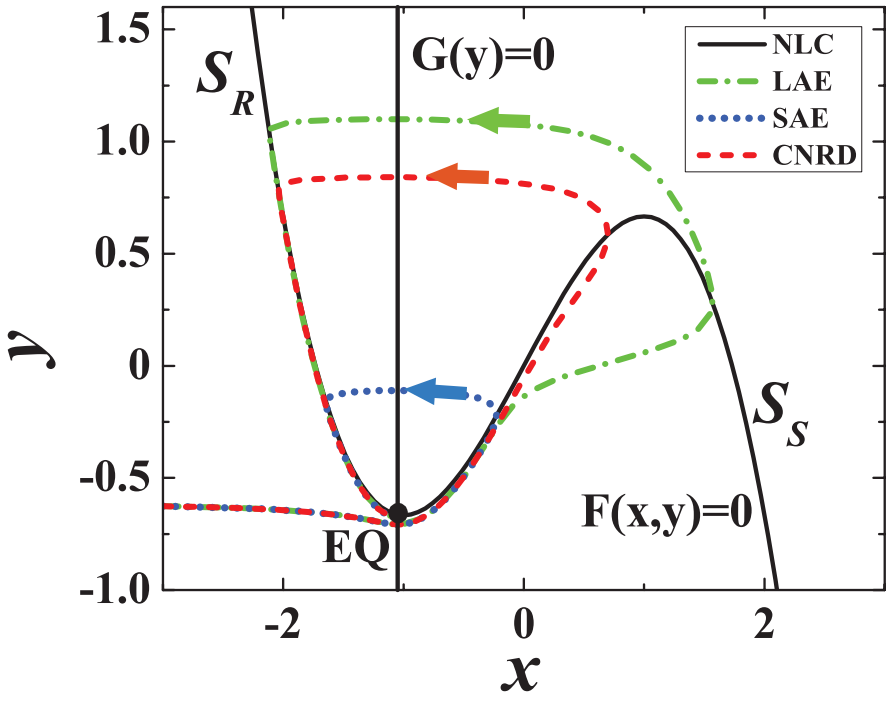

Figure 2.1: Phase plane analysis for an excitable Fitzhugh-Nagumo unit. The black solid lines indicate the two nullclines (NLC) $F(x, y) = 0$ and $G(y) = 0$, with the equilibrium EQ lying at their intersection point. The refractory and spiking branches of the cubic nullcline are denoted by S_R and S_S, respectively. Focus is on illustrating the two types of responses that may be elicited depending on the perturbation strength. Trajectory corresponding to the small-amplitude excitation (SAE) is presented by the blue dotted line, whereas the trajectory typical for the large-amplitude excitation (LAE) is shown by the green dash-dotted line. Since the effects of perturbation are interpreted as setting of the initial conditions, the obtained trajectories are in fact solutions of an initial value problem. Sensitivity of the form of response to initial conditions is most apparent around the canard-like trajectory ($CNRD$), denoted by the red dashed line, which makes up a soft boundary between the domains leading to SAE or LAE. The data are obtained by iterating system (7.1) for $\epsilon = 0.05$ and $b = 1.05$.

on the nullclines $F(x, y) = 0$ and $G(x) = 0$, displayed by the black solid lines in Fig. 7.1. These two curves outline the boundary between the respective regions where the derivatives $\dot{x}(t)$ and $\dot{y}(t)$ attain opposite signs. The location of the intersection point between the two nullclines depends on b and determines the equilibrium of system (7.1). The cubic nullcline $F(x, y) = 0$ can be divided into three branches, whereby the *(refractory)* branch S_R on the left side of Fig. 7.1 and the *(spiking)* branch S_S on the right are stable, whereas the middle one is unstable. The excitable regime

is characterized by the fixed point lying close to the knee of the left branch. Throughout the thesis, this is achieved by setting $b = 1.05$. On the other hand, for $b < 1$ the fixed point gets shifted to the middle branch, thus becoming unstable.

Excitable behavior is crucially influenced by the cubic nonlinearity of the fast nullcline and the strong separation between the fast and slow characteristic time-scales [80]. Note that an external perturbation injected into the system can be regarded as a setting of the initial conditions [76]. If the latter are such that the trajectory reaches S_R first, the phase point subsequently slides down toward the equilibrium, where it settles until the next perturbation. This provides a description of a small-amplitude, non-spiking event for the variable $x(t)$, viz. Fig. 7.1. On the other hand, if the initial conditions cause the trajectory to reach the S_S branch first, the system undergoes a large excursion in phase space [77]. Along this transient, one finds the representative point first traveling upward toward the fold point $(x, y) = (1, 2/3)$, then executing a jump to S_R and proceeding as described above. In other words, instead of rapidly decaying to the fixed point, as in case of the small perturbation, the sufficiently large perturbation elicits a large-amplitude (spiking) response of the system (7.1).

The use of terms ”small” and ”large enough” perturbation suggest the existence of the threshold-like behavior in the FHN model. Typically, presence of a threshold would be associated with the saddle states or sets, which separate between the attractor basins of the two stable states. In our case, having varied the initial conditions, one can single out a boundary delineating two regions of the phase plane, such that the boundary itself makes up the trajectory of the system (7.1) obtained under particular initial conditions. Such a trajectory, indicated in Fig. 7.1, is reminiscent of a canard [80], with the region around it being extremely sensitive to initial conditions. This is why the crossover from small to large-amplitude events appears continuous, rather than threshold-like. The described type

of boundary is inherited from the singular limit $\epsilon \rightarrow 0$, where S_R and S_S may be regarded as attractors. In this case, the separatrix between the two attractors actually includes the middle branch of the cubic nullcline. Nevertheless, for finite ϵ the separatrix vanishes, but an infinite number of lines, forming a layer, can be specified as carrying out the similar role. Still, within the distance $d >> \epsilon$ of the fold point $(x, y) = (1, 2/3)$, this layer decays into a single line, resembling a clear boundary. Therefore, for finite ϵ, it may be justified to refer to the canard-like trajectory illustrated in Fig. 7.1 as the "ghost-separatrix" [76].

As mentioned before, the deterministic system (7.1) undergoes supercritical Hopf bifurcation at $b = 1$, such that it displays sustained oscillations even in the absence of stimulation. Given the condition $\epsilon << 1$, the bifurcation itself acquires singular character, whereby its normal form, producing quasiharmonic oscillations, persists only in a narrow range of b values [79, 80]. Within this interval, the oscillation frequency is of the order $\nu(b) = \mathcal{O}(1)$, while the amplitudes in x and y are $\mathcal{O}(\epsilon) = \mathcal{O}(\sqrt{b-1})$ and $\mathcal{O}(\epsilon)$, respectively. On the other hand, above a certain value of b given by the condition $1 - b = \epsilon/8$, one finds a transition toward a relaxation cycle, whose amplitudes amount to $\mathcal{O}(1)$, both in x and y [121]. This scenario corresponds to a canard explosion [79, 80, 122].

While the non-zero frequency, viz. the finite period of oscillations at the bifurcation threshold constitutes a local property of the unstable focus, the large-amplitude oscillations are the corollary of the global dynamics of the system [80]. The period of large-amplitude oscillations is determined by the global structure of the phase space, and is primarily influenced by the slow motion along the S_R and S_S branches of the cubic nullcline. It is useful to attempt to assess its duration, bearing in mind that the noise-induced oscillations seen under the excitable regime we consider below, are just the precursor of the deterministic ones [77, 78]. When $b < 1$ and $\epsilon \rightarrow 0$ is fulfilled, the motion on the limit cycle may be broken into two

pieces of slow and two pieces of fast motion [77, 80]. Along the slow parts, occurring on the $\mathcal{O}(1)$ time-scale, the trajectory follows S_R and S_S, such that $\dot{x} = \frac{x+b}{1-x^2}$ and $y = x - \frac{1}{3}x^3$ holds. The slow parts are connected by the rapid jumps on the $\mathcal{O}(\epsilon)$ time-scale from S_R to S_S and vice versa, which are characterized by $\epsilon\dot{x} = x - \frac{1}{3}x^3 - y, y = \pm\frac{2}{3}$. The period of limit cycle T_{LC} may asymptotically be substituted by just the section on the S_R and S_S branches:

$$T_{LC} = \int_{-2}^{-1} \frac{1-x^2}{x+b}dx + \int_{2}^{1} \frac{1-x^2}{x+b}dx = 3 - (1-b^2)ln\frac{4-b^2}{1-b^2}. \tag{2.4}$$

In the vicinity of the bifurcation threshold, the above expression yields an estimate $\lim_{b\to 1^-} T_{LC}(b) \approx 3$.

Let us now turn to the case where a single FHN unit is embedded into a noisy environment. In the most general form, the equations for such a setup read

$$\begin{aligned} \epsilon dx &= (x - x^3/3 - y)dt + \sqrt{\epsilon}\sqrt{2D_1}dW_1 \\ dy &= (x+b)dt + \sqrt{2D_2}dW_2, \end{aligned} \tag{2.5}$$

having incorporated the stochastic effects in both the fast and slow subsystems to account for the potential existence of different noise sources. In particular, the $\sqrt{2D_i}dW_i$ terms represent the stochastic increments of the independent Wiener processes, such that the expectation values and the correlations satisfy $\langle dW_i \rangle = 0, \langle dW_i dW_j \rangle = \delta_{i,j}dt$ where $i, j \in \{1, 2\}$. In the field of neuroscience, presence of the D_1-term is typically interpreted as *synaptic noise*, arising due to irregular firing of peer neurons, whereas the D_2-term is associated with the intrinsic cell dynamics, such as fluctuations of currents in the ion-channels *(ion-channel noise)* [67, 76]. In the excitable lasers, noise may also be present in both the fast and the slow variable [76]. Treatment of the systems like (7.5) is inherently difficult, given that the forms of dynamics they display are complex even in case of

a single unit, let alone a whole assembly of units. In this context, note that the above system has been demonstrated to exhibit five different scaling regimes under variation of the noise amplitude $\delta = \sqrt{D_1 + D_2}$, including SISR, CR, bursting relaxation oscillations, rare clusters of several relaxation cycles and finally small-amplitude oscillations with sporadic isolated spikes [79], appearing in this order when δ is reduced.

The analysis in the present thesis is confined to the case $D_2 > 0, D_1 = 0$. One of the reasons for such a choice is that it enables a clear interpretation of the role of noise: within the phase plane, noise causes the vertical nullcline to change its position, effectively shifting the system between the excitable and the oscillatory regime. What also makes this setup a preferred one is the point that the noise-induced limit cycles are analogous to those obtained in the oscillatory regime $b < 1$. As indicated in the Introduction, there exists a range of D_2 values where the noise-induced oscillations appear coherent. This may be established by the standard measures for variability of spike trains, one of them being the *coefficient of variation* (jitter) R [55, 123]. The latter is defined as the standard deviation of the interspike interval T, normalized by its mean

$$R = \frac{\sqrt{\langle \Delta T^2 \rangle}}{\langle T \rangle}, \tag{2.6}$$

where $\langle \cdot \rangle$ stand for the time-averages, and $\langle \Delta T^2 \rangle = \langle T^2 \rangle - \langle T \rangle^2$ denotes the variance. Values of R belong to the interval $R \in [0, 1]$, with the smaller R indicating better coherence.[1] For an assembly of coupled excitable units, the coherent local oscillations may easily adjust their phases, hence contributing to the onset of the collective mode.

The phenomenon where noise-induced oscillations become regular under noise acting in the slow subsystem of (7.5) is known as the coher-

[1] Other possible measures for coherence of spike trains include the diffusion coefficient $D_{eff} = \frac{1}{2}R^2 r_0$ [67], where r_0 is the average firing rate, and the correlation time $\tau_{corr} = \frac{1}{\sigma^2}\int_0^\infty |\Psi(s)| ds$ [67, 80], such that $\Psi(s) = \langle [x(t-s) - < x >][x(t) - < x >] \rangle$ is the autocorrelation function and $\sigma^2 = |\Psi(0)|$ denotes its variance.

ence resonance [55, 77]. The mechanism behind CR has been briefly outlined in the Introduction, so that here we only specify some key elements. To this end, one first notes that an arbitrary interspike interval $T = t_a + t_e$ consists of the activation time t_a and the excursion time t_e, whose means and variances display quite different dependencies on noise [55, 67]. Regarding t_a, it may be adopted that the representative point escapes from the refractory to spiking branch at the Kramers rate $r = const \times \exp(-\frac{\Delta U(y)}{2D_2}) << 1$, where ΔU presents some y-dependent potential barrier [55, 77, 78, 124]. Then, the corresponding mean activation time can be estimated as $\langle t_a \rangle \sim r^{-1} \sim \exp(const \times D_2^{-1})$, which implies a rapid decay with increasing noise. On the other hand, $< t_e >$ is weakly dependent on noise, since it is primarily influenced by the system's deterministic relaxation properties. Nevertheless, fluctuations of the excursion time still grow with the noise intensity.

In view of the stated above, we are now able to provide a heuristic argument regarding the dependence of the squared coefficient of variation R^2 on noise. In particular, one may write [67]

$$R^2 = \frac{\langle \Delta(t_a + t_e)^2 \rangle}{\langle T \rangle} = \frac{\langle \Delta t_a \rangle^2}{\langle t_a \rangle^2} \frac{\langle t_a \rangle^2}{\langle T \rangle^2} + \frac{\langle \Delta t_e \rangle^2}{\langle t_e \rangle^2} \frac{\langle t_e \rangle^2}{\langle T \rangle^2}$$
$$= R_a^2 (\frac{\langle t_a \rangle}{\langle T \rangle})^2 + R_e^2 (\frac{\langle t_e \rangle}{\langle T \rangle})^2, \tag{2.7}$$

where R_a and R_e denote the respective coefficients of variation for t_a and t_e. The above expression has been obtained by assuming the statistical independence between the latter two, such that $\langle t_a t_e \rangle = \langle t_a \rangle \langle t_e \rangle$ holds. Should the spike trains be coherent, R^2 would have to be made as small as possible. Focussing on the first term, one may consider R_a^2 to be close to unity, given that the process it describes is Poisson-like. This leaves the ratio of the activation time vs. the interpike interval, which is small at large enough noise intensities. As for the second term, both the jitter R_e and the $\langle t_e \rangle / \langle T \rangle$ ratio grow with noise. Therefore, the minimum of R^2 is achieved if D_2 is

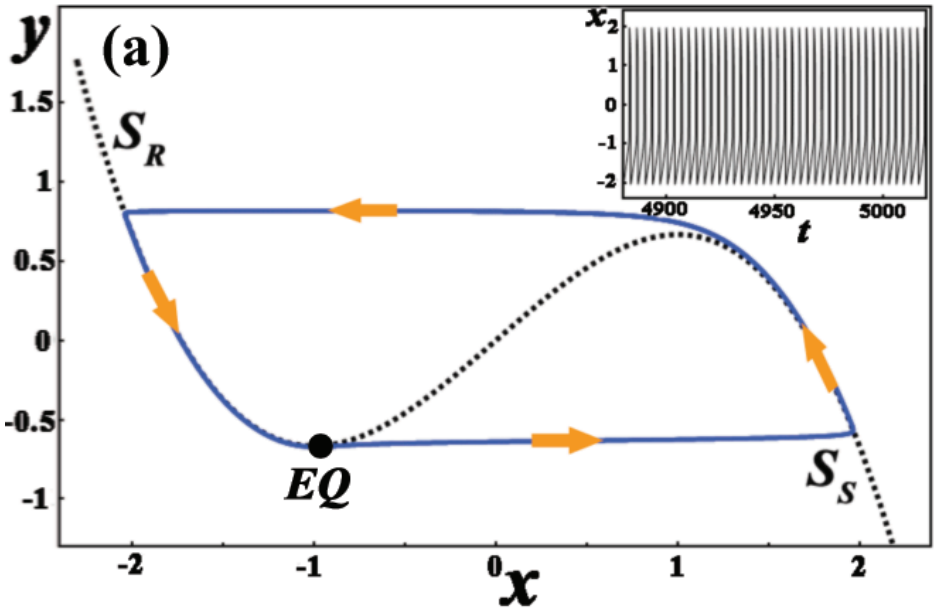

Figure 2.2: Typical phase portrait of a Fitzhugh-Nagumo unit in the regime of coherence resonance, where the stochastic limit cycle is just a precursor to the deterministic one. As such, it takes place on the attractive (outer) branches of the $\dot{x} = 0$ nullcline (dotted line), avoiding the unstable (middle) branch. EQ indicates the position of the equilibrium. A typical orbit (solid line) is made up of two portions of slow motion $\mathcal{O}(1)$, connected by two rapid transients $\mathcal{O}(\epsilon)$. The former include a descent down the refractory branch S_R until the left knee is reached, and the ascent along the spiking branch S_S. The inset shows a section from the time series $x(t)$ for $D = 0.003$.

large enough to substantially reduce the activation time, and small enough to keep the fluctuations of the excursion time low [55, 67].

In Fig. 2.2 is illustrated the typical phase portrait of a limit cycle displayed by the excitable Fitzhugh-Nagumo unit ($b = 1.05$) in the regime of coherence resonance. In dynamical terms, the cycle generated in this case is just the precursor of the deterministic one, found in the supercritical state above the Hopf bifurcation threshold ($b < 1$). An orbit consists of two pieces of slow motion connected by the rapid transients initiated around the fold points of the cubic nullcline $F(x, y) = 0$, the former being located at $(x, y) = (-1, -2/3)$ and $(x, y) = (1, 2/3)$. Such an oscillation profile is reminiscent to that of relaxation oscillators, whereby the motion of the phase point along the cycle proceeds as follows. The ascending stage of the spike coincides with the phase point jumping from the refractory

branch S_R to the spiking branch S_S, whereas the spike's descending stage corresponds to the upward motion along S_S. The beginning of the refractory period is marked by the phase point switching from S_S back to S_R, while during the interspike interval it travels down the refractory branch toward the left knee $(x, y) = (-1, -2/3)$. In the inset is shown a sequence from a time series of the fast variable $x(t)$, which corroborates the high degree of regularity for the noise-induced oscillations.

2.2 Assembly of Fitzhugh-Nagumo units: generic regimes of noise-induced collective dynamics

Apart from Chapter 7, the main body of the thesis concerns the collective behavior of an N-size population of *identical* stochastic Fitzhugh-Nagumo elements, viz. (7.5), interacting via delayed linear (diffusive) couplings. The intrinsic parameters b and ϵ, whose meaning has already been explained in Section 2.1, are set to $b = 1.05$ and $\epsilon = 0.01$, the former placing the individual units in the excitable regime and the latter allowing for a sharp separation between the fast and slow characteristic timescales. Also, the action of noise is incorporated within the slow subsystem for the reasons explained by the end of Section 2.1. In its most general form, the dynamics of a FHN unit embedded within a network then reads [75, 125, 126]

$$\begin{aligned} \epsilon dx_i &= (x_i - x_i^3/3 - y_i)dt + \frac{1}{n_i}\sum_{j=1}^{N} g_{ij}[x_j(t-\tau_{ij}) - x_i(t)]dt, \\ dy_i &= (x_i + b)dt + \sqrt{2D_i}dW_i, \end{aligned} \tag{2.8}$$

where the indices $i, j \in \{1, \dots N\}$ specify the members of the population, g_{ij} present the elements of the weighted connectivity matrix and n_i denotes the number of units which the given unit i is connected to. Within the thesis, n_i will be referred to as the (nodal) connectivity degree, the

term commonly applied in network theory. In the following, we adopt a simplifying assumption on the all-to-all type of connectivity between the units ($n_i = N, g_{ij} \neq 0$ for every i, j), adhering to the concept of building a minimal model capable of displaying certain forms of behavior. Consistent with the stated in Section 1.1, one notes that such an idealization has already proven useful, both on theoretical grounds [127, 128] and in applications related to neuroscience, especially regarding the emergence of healthy and pathological brain rhythms, or when studying the fashion in which the distributed brain areas communicate [1, 21, 27]. The linear interactions between the units are parametrized by the coupling strength g_{ij} and the time delay τ_{ij}, the latter accounting for the finite velocity by which the interactions propagate and/or latency in the units' responses. In our model, the coupling parameters are assumed to be uniform over the population, such that $g_{ij} = c, \tau_{ij} = \tau$ holds for each pair (i, j). Apart for simplicity, the latter is also aimed at eliminating the possible causes of secondary effects that could interfere with the considered core phenomena. For the same reason, the noise intensities are taken to be homogeneous across the assembly, meaning $D_i = D$ for each unit i. In the context of neuroscience, one can draw analogy between the linear couplings and the electrical synapses (gap-junctions) connecting the neurons, whereas the homogeneity of intrinsic and synaptic parameters conforms to the scenario where neurons belong to a small patch of the brain cortex. By including all the points stated above, the system (2.8) may be rewritten as

$$\begin{aligned} \epsilon dx_i &= (x_i - x_i^3/3 - y_i)dt + \frac{c}{N}\sum_{j=1}^{N}[x_j(t-\tau) - x_i(t)]dt, \\ dy_i &= (x_i + b)dt + \sqrt{2D}dW_i, \end{aligned} \tag{2.9}$$

which, for the most part of the thesis, presents the set of equations guiding the microscopic dynamics. Though generally considering the homogeneous populations, in Chapter 5 we also discuss the effects of heterogeneity

in the intrinsic unit parameters and the connectivity patterns.

Within this section, the primary intention is to lay out the facts that have been known on the collective dynamics of excitable media prior to our research. However, before proceeding in this direction, it is necessary to make a few brief remarks regarding the regimes displayed by a unit obeying (2.9), having left an extended discussion on this issue for the main body of the thesis. What is different from the setup analyzed in Section 1.1 is that now one has to account not only for the influence of noise, but also for the impact of the coupling terms, characterized by c and τ. Beginning with the noiseless case $D = 0$, c and τ may either be such to allow the unit to remain excitable, possessing equilibrium as the unique attractor, or they may give rise to oscillatory state via Hopf bifurcation, so that the excitability feature is lost. Adding a marginal amount of noise induces only small fluctuations around the attractors of the deterministic dynamics, obtained for $D = 0$. Nevertheless, as indicated earlier, a sufficiently strong noise can evoke a transition from stochastically stable fixed point to noise-induced oscillations, which may appear regular at the optimal noise intensity. Though we make this point more explicit later, the above arguments suggest that the oscillations under general c, D and τ are in fact influenced by two characteristic time scales [115], one which is noise-driven, and the other being adjusted with the delay. Naturally, such a paradigm can carry over to the collective motion due to synchronization of individual units.

Having clarified some of the details on the dynamics of units embedded within a network, we now use the population comprised of Fitzhugh-Nagumo elements to characterize more closely the three generic regimes of collective behavior in excitable media obtained under the scenario where noise enacts the control parameter. Recalling that these regimes have already been mentioned in Subsection 1.3.3 of the Introduction, the aim here is to define the appropriate macroscopic variables and examine the related phase portraits on one hand, but also to gain further insight into the un-

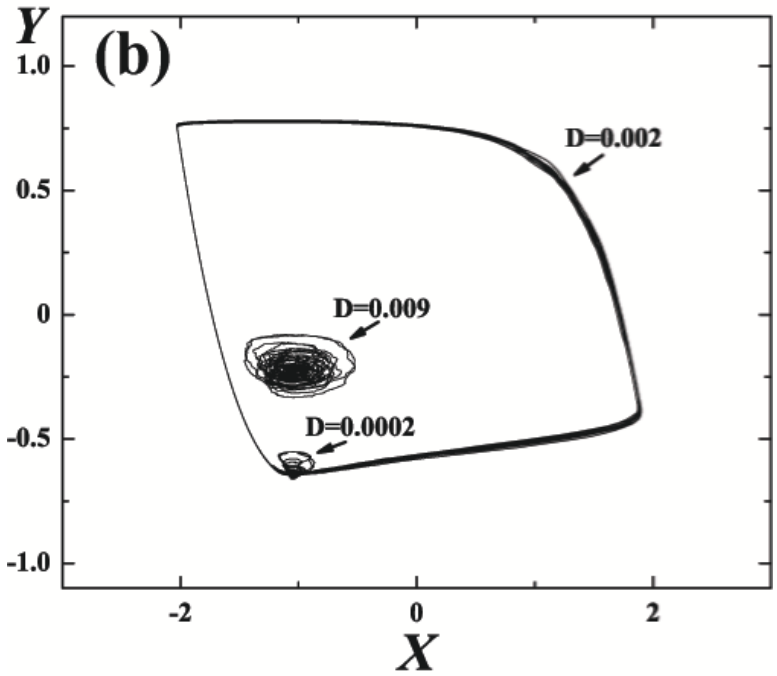

Figure 2.3: Three generic regimes exhibited by the excitable media under systematic increase of noise intensity D in case of instantaneous interactions are illustrated for the population of Fitzhugh-Nagumo elements. Phase portraits provided for the ensemble averages $X = N^{-1}\sum_{i=1}^{N} x_i$ and $Y = N^{-1}\sum_{i=1}^{N} y_i$ at $c = 0.1$ reflect incoherent motion ($D = 0.0002$), coherent collective oscillations ($D = 0.002$) and the decay into chaotic regime ($D = 0.009$).

derlying microscopic dynamics and the ensuing synchronization features. Note that the discussion in the remainder of this Section is confined to an assembly of excitable units interacting via instantaneous couplings, such that its evolution is described by the system (2.9) under the condition $\tau = 0$. This is so because the physical picture on global regimes identified prior to our research has been built without considering the effects of interaction delays.

The collective dynamics is typically described in terms of global (macro-

scopic) variables

$$X = \frac{1}{N}\sum_{i=1}^{N} x_i$$
$$Y = \frac{1}{N}\sum_{i=1}^{N} y_i, \tag{2.10}$$

which present the population (spatial) averages over the local variables. In Fig. 2.3 are displayed the phase portraits corresponding to the three regimes of collective behavior encountered when D is increased. For small D, there is a stochastically stable global equilibrium, which owes to the point that individual spiking is rare and incoherent, rendering the majority of units at rest at any given time. The latter is corroborated by the Fig. 2.4(a), showing together the sequences from the fast-variable time series for three arbitrary members of the assembly. At intermediate D, single units discharge more frequently, whereby the spiking events between the units become synchronized. Such synchronization of noise-induced oscillations gives rise to the collective coherent state, where the population effectively acts as a macroscopic oscillator, cf. the limit cycle in Fig. 2.3, whose frequency matches that of the individual units. Given the stochastic character of the dynamics, by the term frequency one actually refers to the reciprocal value of the time-averaged interspike interval (ISI) $\langle T_{x_i} \rangle$. The time series in the main frame of Fig. 2.4(b) indicate approximate synchronization between the single units, whereas the inset, showing the distribution of average ISIs $P(T_{x_i})$ over the population, demonstrates the level of mutual entrainment of units to a single frequency. In this context, we have also been interested in determining how the duration of the time-average ISI $\langle T_X \rangle$ for the global variable X depends on D within the coherent collective regime, cf. Fig. 2.4(c). Note that the variation of the period of noise-induced oscillations with D will prove important for the discussion in Chapter 5. The inset of Fig. 2.4(c) corroborates the regularity of col-

lective motion, indicating fairly small values of the coefficient of variation R_X for the global variable $X(t)$, cf. the definition (7.6) and the accompanying explanation. Nevertheless, further increasing D, the tendency of linear couplings to maintain approximate synchronization between units' activities is gradually suppressed by noise, which eventually takes the dynamics of assembly averages $(X(t), Y(t))$ into chaotic regime. While the local spiking frequencies continue to increase up to a certain point, the inter-unit synchronization systematically deteriorates until the frequency entrainment is lost, see the main frame and the inset of Fig. 2.4(d). For such a scenario, one infers that the bulk of the population is refractory at any instant, which renders the orbits of the global variables confined to an area of phase space much smaller than the one outlined by the limit cycle found in the coherent collective state.

As the final means to characterize the three regimes of global behavior controlled by the variation of D, we consider the stationary probability densities for the macroscopic variables $P(X, Y)$. In particular, the objective is to highlight the differences between the distribution profiles obtained for the D values matching those in Figures 2.4(a), 2.4(b) and 2.4(d), each being typical for one of the regimes. The stationary distributions are estimated numerically by recording the system's evolution for the sufficiently long time period. Having eliminated the transients, the method itself consists in counting the number of representative points that fall within each cell of a 110×110 grid, built by dividing the relevant ranges of the X and the Y variable values into 110 equal bins. As expected, for the stochastically stable equilibrium, $P(X, Y)$ shows a large peak about its location, cf. Fig. 7.5(a). For the coherent collective state at intermediate D, $P(X, Y)$ reflects the existence of the limit cycle by clearly indicating the two branches of slow motion, see Fig. 7.5(b), naturally with the states on the refractory branch, which correspond to the interspike intervals, being more salient. In case of the incoherent collective state, cf. Fig. 7.5(c), $P(X, Y)$ distribution

is concentrated in a small area of the $X - Y$ plane, which is a signature of the breakdown of frequency synchronization between the units. Note that the paradigm involving the three regimes of collective behavior has first been reported for fully connected networks [5, 67], but has later on been observed in layouts involving more complex interaction patterns [95, 123].

2.3 Derivation of the mean-field model

This section is intended to outline the key steps on how the MF model for the activity of an assembly of stochastic excitable units coupled via delayed linear couplings is derived. What is conveyed here presents our main contribution regarding the analysis of systems whose dynamics is expressed in terms of large sets of SDDEs, having applied the results throughout the thesis. In particular, within the MF approximation one aspires for a highly reduced set of nonlinear deterministic delay differential equations (DDE) to replace the original system (7.1) comprised of $2N$ nonlinear SDDEs. Though a simplified representation, the MF model should still be able to reproduce with sufficient accuracy the latter's behavior regarding the stability of the steady states, the scenarios for the onset of the collective mode and its suppression under the action of the cross-population coupling delay. The MF treatment draws on the all-to-all type of connectivity among neurons within each population, incorporating the thermodynamic limit $N \to \infty$ in a natural way [67]. In order to build a MF model, two different approaches are available to proceed with: one may either consider the time-dependence of a hierarchy of probability densities according to the Fokker-Planck formalism, or may focus on the evolution of cumulants, whereby the full density of states is factorized into a series of marginal densities. The latter alternative is preferred, as it allows for a number of convenient approximations to be introduced in a controlled fashion [67].

Note that one is bound to make some approximations for the nonlinear-

ity of the original system, given that the cumulants of the particular order are usually linked to those of the higher order, which apparently renders the underlying series unclosed. The way to resolve this issue consists in truncating the series by a form of a closure hypothesis. Such hypothesis typically integrates the cumulant approach with the Gaussian approximation [111, 129], recalling that the Gaussian distribution has vanishing cumulants above the second order. Such a method has previously been applied to study the influence of noise on bifurcations in maps [130], colored noise-induced transitions in bistable systems [131], phase transitions and SR in globally coupled bistable elements [132], and transitions in globally coupled noisy phase rotators [133].

Derivation of the MF model involves two elementary prepositions: first, that the instantaneous distributions of local variables $P(x_i)$ and $P(y_i)$ are Gaussian, and second, that the ensemble averages at any given moment coincide with the expectation values of the appropriate distributions in a sense $(1/N)\sum_{i=1}^{N} x_i \approx E[P(x_i)], (1/N)\sum_{i=1}^{N} y_i \approx E[P(y_i)]$ [111, 129]. For now, it suffices to say that the two above statements are referred to as the *Gaussian assumption (GA)* and the *quasi-independence assumption (QIA)* respectively, having left the refined formulation and the in-depth analysis of their implications to Chapter 3. If the two stated conditions are met, all the cumulants above the second order are supposed to vanish. Let us briefly comment on the constraints imposed on the system parameters by these assumptions. On the first point, the Gaussian distribution of local variables is maintained if the noise amplitude obeys $D << 1$. Nonetheless, the strong law of large numbers [134] implies that the second condition concerning the ensemble averages is fulfilled exactly in the thermodynamic limit $N \to \infty$ if the involved stochastic processes are independent ($c << 1$). However, the numerical results presented later on indicate that the MF approximation remains valid if the two latter conditions are relaxed, viz. when there is non-negligible interaction in the finite-size sys-

tems, provided that the requirement for not too large a noise amplitude is satisfied.

For convenience, let us first rewrite the system (7.1) by introducing an alternative notation $c \leftrightarrow g_{in}, \tau \leftrightarrow \tau_{in}$

$$\begin{aligned} \epsilon dx_i &= (x_i - x_i^3/3 - y_i)dt + \frac{g_{in}}{N}\sum_{j=1}^{N}[x_j(t-\tau_{in}) - x_i(t)]dt, \\ dy_i &= (x_i + b)dt + \sqrt{2D}dW_i, \end{aligned} \tag{2.11}$$

This notation anticipates for the case with two interacting populations discussed in Chapter 6, being primarily intended to enable an easier accommodation to such a setup. Given that the distributions of the stochastic local variables are assumed to take on the Gaussian form, one can fully characterize them by the set of the first and second order moments, which includes the mean values, the variances and the covariance. The mean values applied here

$$\begin{aligned} m_x(t) &= \langle x_i(t)\rangle = \lim_{N\to\infty}(1/N)\sum_{i=1}^{N} x_i(t) \\ m_y(t) &= \langle y_i(t)\rangle = \lim_{N\to\infty}(1/N)\sum_{i=1}^{N} y_i(t) \end{aligned} \tag{2.12}$$

should strictly speaking be distinguished from the global variables X and Y considered earlier for the large, but still finite-size populations. The angled brackets are generally used to denote averaging over the units making up the ensemble, whereas m_x and m_y are reserved solely for the averages of the local variables. Before introducing the second order moments, it is convenient to define the deviations from the mean $n_{x_i}(t) = \langle x_i(t)\rangle - x_i(t)$ and $n_{y_i}(t) = \langle y_i(t)\rangle - y_i(t)$, which obey the Gaussian distributions and are independent between the single elements. Then the appropriate variances

read

$$s_x(t) = \langle n_{x_i}^2(t)\rangle = \langle(\langle x_i(t)\rangle - x_i(t))^2\rangle$$
$$s_y(t) = \langle n_{y_i}^2(t)\rangle = \langle(\langle y_i(t)\rangle - y_i(t))^2\rangle, \tag{2.13}$$

whereas the covariance is given by

$$u(t) = \langle n_{x_i}(t) n_{y_i}(t)\rangle = \langle(\langle x_i(t)\rangle - x_i(t))(\langle y_i(t)\rangle - y_i(t))\rangle. \tag{2.14}$$

The evolution of the distributions' means m_x and m_y is obtained by performing the ensemble averages over the system (7.8), while the expressions for the dynamics of s_x, s_y and u follow from explicitly taking the time derivatives of the definitions (7.10) and (6.5). Note that the latter calculation also involves the derivatives of the compound functions of the stochastic variables such as $d\langle x_i^2\rangle/dt$ and $d\langle y_i^2\rangle/dt$, where one is required to apply the Ito's chain rule [1]. As for the higher order averages, like $\langle x_i^2\rangle$ and $\langle x_i^3\rangle$, it is necessary to tie them to the first and second order moments. In the simplest cases, this is accomplished by using the definitions (7.10) and (6.5), while in most instances one arrives at the required relations by setting the higher order cumulants [124] to zero, e.g. $\langle x_i^3\rangle_c = \langle x_i^3\rangle - 3\langle x_i^2\rangle\langle x_i\rangle + 2\langle x_i\rangle^3 = 0$, $\langle x_i^2 y_i\rangle_c = \langle x_i^2 y_i\rangle - \langle x_i^2\rangle\langle y_i\rangle - 2\langle x_i\rangle\langle x_i y_i\rangle + 2\langle x_i\rangle^2\langle y_i\rangle = 0$, and similar for $\langle x_i^3 y_i\rangle_c = 0$ and $\langle x_i^4\rangle_c = 0$. The ensuing auxiliary formulas for the higher

[1] According to the Ito's formula, the derivative dY of the twice-differentiable function $Y(t) = U(X,t)$, where $X(t)$ is a stochastic process given by $dX = F(t,X(t))dt + G(t,X(t))dW$, amounts to $dY = \frac{\partial U}{\partial t}dt + \frac{\partial U}{\partial X}dX + \frac{1}{2}\frac{\partial^2 U}{\partial X^2}G^2 dt$

order averages then read

$$\begin{aligned}
\langle x_i^2 \rangle &= s_x + m_x^2 \\
\langle x_i^3 \rangle &= m_x^3 + 3 m_x s_x \\
\langle x_i^4 \rangle &= m_x^4 + 6 m_x^2 s_x + 3 s_x^2 \\
\langle x_i y_i \rangle &= u + m_x m_y \\
\langle x_i^2 y_i \rangle &= m_y s_x + m_y m_x^2 + 2 m_x u \\
\langle x_i^3 y_i \rangle &= 3 s_x u + 3 m_x^2 u + m_y m_x^3 + 3 m_x m_y s_x .
\end{aligned} \tag{2.15}$$

After a series of steps which are too lengthy to convey in full detail, the closed system of equations for the first and second order moments finally becomes

$$\begin{aligned}
\epsilon \frac{dm_x(t)}{dt} &= m_x(t) - m_x(t)^3/3 - s_x(t) m_x(t) - m_y(t) + \\
&\qquad g_{in}(m_x(t-\tau_{in}) - m_x(t)) \\
\frac{dm_y(t)}{dt} &= m_x(t) + b \\
\frac{\epsilon}{2} \frac{ds_x(t)}{dt} &= s_x(t)(1 - m_x^2(t) - s_x(t) - g_{in}) - u(t) \\
\frac{1}{2} \frac{ds_y(t)}{dt} &= u(t) + D \\
\frac{du(t)}{dt} &= \frac{u(t)}{\epsilon}(1 - m_x^2(t) - s_x(t) - g_{in}) - \frac{1}{\epsilon} s_y(t) + s_x(t).
\end{aligned} \tag{2.16}$$

Note that (2.16) comprises a set of deterministic delay equations, where the impact of noise is absorbed into its amplitude D. Recalling the Introduction, one of the stated objectives has been to carry out the bifurcation analysis on the MF model analytically. However, the system (2.16) is still sufficiently complex to defy such a treatment. To ensure that the bifurcation analysis is analytically tractable, we consider an additional adiabatic-like approximation which draws on the relatively fast relaxation of the second order moments. In particular, given that the characteristic time scales, at least for s_x and u, are dominated by the small parameter ϵ, one may jus-

tify substituting their full dynamics by the stationary values reached when $\dot{s_x} = 0$, $\dot{s_y} = 0$ and $\dot{u} = 0$ are satisfied. The system (2.16) then becomes

$$\begin{aligned}\epsilon\frac{dm_x(t)}{dt} &= m_x(t) - \frac{m_x(t)^3}{3} - \frac{m_x(t)}{2}(1 - g_{in} - m_x(t)^2 + \\ &\sqrt{(g_{in} - 1 + m_x(t)^2)^2 + 4D}) - m_y(t) + g_{in}(m_x(t - \tau_{in}) - m_x(t)) \\ \frac{dm_y(t)}{dt} &= m_x(t) + b \end{aligned} \tag{2.17}$$

Though this may appear a crude approximation, it is not an uncommon one [67, 129]. In the language of neuroscience, the net result it yields is comparable to translating the initial MF model, given by the set of five equations, into an effective two-component neural-mass model [135], whereby the latter, at variance with the former, neglects the distribution of individual neuron states over the population. If and how much this is plausible strongly depends on the main objectives of the study, which here concern the stability of the stationary state, the onset of the collective mode and its suppression in an amplitude death-like phenomenon[1][136, 137]. As it stands, the described modification to the MF model should not substantially affect the latter set of issues, since the information supplied by the second order variables, like that on small fluctuations around the collective synchronous state, appears redundant in such a context. This is corroborated later on by the results indicating an agreement between the behavior of the exact system and the MF approximation.

Note that for $D = 0$, the obtained system (2.17) strongly resembles the one describing a single Fitzhugh-Nagumo element subjected to a delayed feedback. Consequently, it is not unexpected that the population dynamics can display excitable-like behavior akin to what is illustrated in Fig. 7.1, provided that g_{in}, D and τ_{in} admit equilibrium as the unique attractor. When this is satisfied, apart from the small amplitude oscillations remain-

[1] Amplitude death refers to the phenomenon where oscillatory solution collapses to a stable fixed point, with the possible bifurcation routes involving either an inverse Hopf or a saddle-node bifurcation.

ing nearby the equilibrium, external perturbations may also trigger large excursions of global potential, the latter reflecting the crucial feature of the exact system. Note that within the thesis are not provided the factual evidence on how the MF model of an isolated population is capable of accurately predicting the qualitative behavior of its exact counterpart, since this point has been addressed in a fair amount of detail prior to this research, cf. [138]. Here we adopt as a known fact that the sequence of local bifurcations under variation of D, τ_{in} and g_{in} can be used to highlight the parameter domains giving rise to oscillatory states or those leading to amplitude death [139]. Building on that, the MF model of a single ensemble will here be shown to reflect the global bifurcation imminent to the onset of clustering in the exact system [115]. Nonetheless, for the setup involving two populations that interact via delayed nonlinear couplings, the obtained approximate system is demonstrated to (i) outline the parameter domains where equilibrium is stable, (ii) specify the two distinct scenarios for the onset of the collective mode, (iii) pinpoint the regions admitting different forms of bistability and (iv) indicate the domains resulting in the suppression of the collective mode.

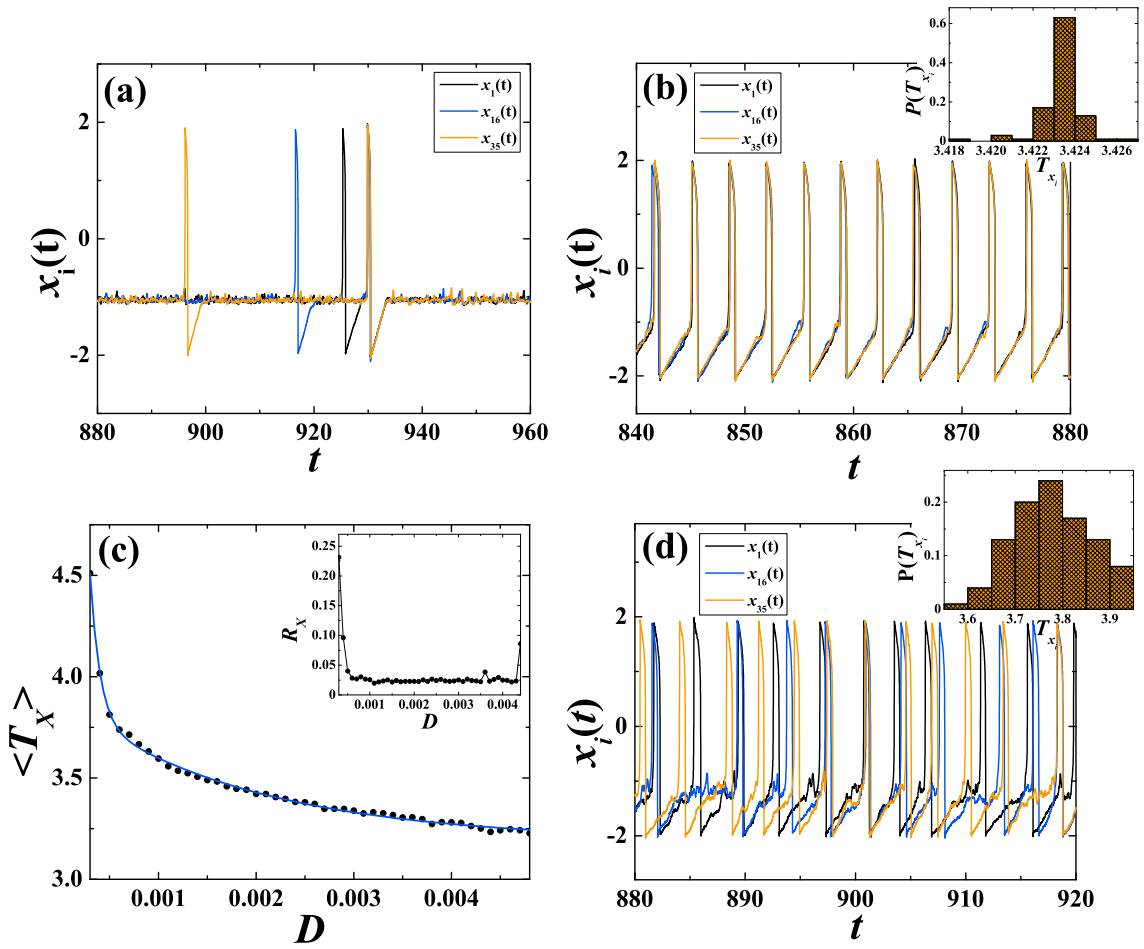

Figure 2.4: Local dynamics behind the three regimes of collective behavior. The main frames in (a), (b) and (d) show the corresponding sequences from the time series $x_i(t)$ of three arbitrary units, encoded in black, blue and orange, for the scenarios when the global dynamics exhibits the stochastically stable equilibrium ($D = 0.0002$), the coherent collective state ($D = 0.002$) and the incoherent state ($D = 0.009$), respectively. Insets of (b) and (d) refer to distributions $P(T_{x_i})$ of the time-averaged local ISIs T_{x_i}, indicating that the transition from coherent to an incoherent collective state is accompanied by the loss of frequency entrainment between the units. (c) is intended to provide further insight on the coherent collective state, with the dependence $\langle T_X \rangle(D)$ of the time-averaged ISI for the global variable X on noise presented in the main frame, and the associated dependence of the jitter $R_X(D)$ plotted in the inset.

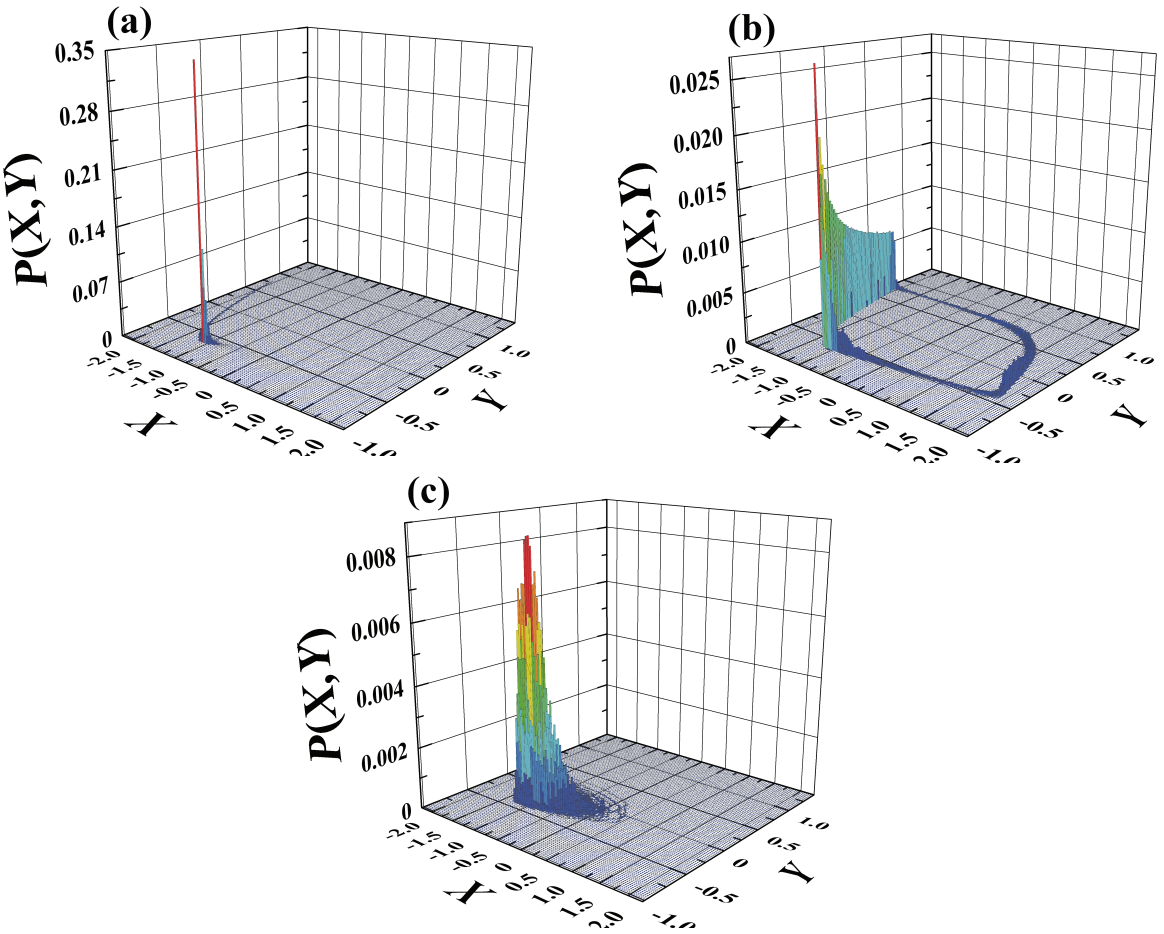

Figure 2.5: Profiles of the numerically estimated stationary probability distributions $P(X, Y)$ typical for the three regimes of collective behavior emerging under increasing D in the absence of interaction delays. (a) refers to the stochastically stable equilibrium ($D = 0.0002$), (b) corresponds to the collective coherent state ($D = 0.002$), whereas (c) is obtained for the incoherent (chaotic) regime ($D = 0.009$). The coupling strength is fixed to $c = 0.1$.

Chapter 3

Testing the assumptions of typical mean-field approximations of stochastic delay-differential systems

---

Chapter abstract Main assumptions of a typical mean-field approximation for a system of stochastic excitable units with delayed couplings are formulated and tested. Their validity is demonstrated to be primarily influenced by the qualitative properties of the system's dynamics, rather than stating the common requirements for the small noise and weak coupling strength. We analyze the generic regimes where the mean-field assumptions hold or fail, further characterizing their relation with certain forms of synchronization between the individual units.

The dynamics of complex systems with many interacting components is often modeled by the systems of nonlinear stochastic delay-differential

equations (SDDE), whose general form is given by

$$d\mathbf{x}_i(t) = f(\mathbf{x}_i(t)) + \sum_{i,j}^{N} g_{ij}(\mathbf{x}_i(t), \mathbf{x}_j(t-\tau_j)) + \sigma_i dW_i, \tag{3.1}$$

where $i, j = 1, ...N$, $\mathbf{x}_i$ are vectors of dynamical variables of the i-th unit, f is a nonlinear function, τ_i are the interaction delays and dW_i are stochastic increments of independent Wiener processes. Due to co-effects of nonlinearity, time-delay, stochastic character and a large number of components, such systems often defy analytical treatment. Very few nontrivial exact solutions of systems like (7.1) are known, whereas a limited number of analytical results so far may be used for the qualitative analysis of stochastic stability or stochastic bifurcations [124, 125, 140, 141]. Apart from a heavy demand on computational time, known to grow as N^2, numerical solving of systems like (7.1) may be prone to numerical errors that are difficult to control [142]. Therefore, much can be gained by introducing approximation techniques, especially if their domains of relative validity are well understood. Such approximations usually rely on some form of mean-field assumptions (MFAs) [5, 67, 111, 112]. For the systems described by (7.1), the two typical MFAs may loosely be formulated as: (i) the dynamics of $\mathbf{x}_i$ is given by the equally distributed quasi-independent processes and (ii) the processes $\mathbf{x}_i$ are Gaussian over small time intervals. Either of the MFAs is likely to be violated over large domains of the relevant parameter values. Nevertheless, the MF based approximations have still proven useful, providing qualitative predictions in terms of the stability of the equilibrium, as well as the onset and the suppression of the collective mode, or even the quantitative ones, regarding the frequency of macroscopic oscillations [117, 138]. Apart from the analysis of the domains where the MFAs apply, showing them to display the analogous qualitative features, we further demonstrate how the MF model's behavior may indicate MFAs' failure in a self-consistent fashion.

The domains of MFAs' validity depend on the details of the nonlinearity and the interaction terms in (7.1). This letter concerns the specific class of systems where $f(\mathbf{x}_i)$ yield excitable dynamics, whereas the globally connected units interact via linear couplings with uniform delays. Having already performed the bifurcation analysis of the corresponding MF system [138], here we examine whether the parameter domains where such predictions are accurate may extend beyond the domains of MFAs' validity.

3.1 Exact system, MFAs and MF system

Validity of MFAs is analyzed in case of a collection of N Fitzhugh-Nagumo excitable units, whose dynamics is set by:

$$\begin{aligned} \epsilon dx_i &= (x_i - x_i^3/3 - y_i)dt + \frac{c}{N}\sum_{j=1}^{N}(x_j(t-\tau) - x_i)dt \\ dy_i &= (x_i + b)dt + \sqrt{2D}dW_i, i = 1, \ldots N \end{aligned} \tag{3.2}$$

Each unit interacts with every other via diffusive delayed couplings, whereby the coupling strength c and the time-lag τ are taken uniform. Parameters $\epsilon = 0.01$ and $b = 1.05$ are such that the isolated units display excitable behavior, having stable fixed point (FP) as the only attractor. The terms $\sqrt{2D}dW_i$ represent stochastic increments of the independent Wiener processes, viz. dW_i satisfy $E(dW_i) = 0$, $E(dW_i dW_j) = \delta_{i,j}dt$, where $E()$ denotes the expectation over different realizations of the stochastic process.

Having proposed that the nontrivial conditions for the fulfilment of the MFAs derive from the qualitative properties of the underlying dynamics, we first summarize the typical regimes exhibited by $(x_i(t), y_i(t))$, beginning with the deterministic case $D = 0$. For small c and τ, the only attractor of each unit is FP and the dynamics is excitable. For larger c and/or larger τ, the FP undergoes a Hopf bifurcation and the asymptotic dynamics resides on a stable limit cycle (LC). The LC conforms to relaxation oscillations,

with two clearly distinguished slow branches, the refractory and the spiking one, and two fast transients in between, cf. Fig. 7.1(b) where small noise perturbations are added. Small D induces small fluctuations around the attractor of the deterministic dynamics. If the latter motion lies on LC, the impact of D is reflected mostly in the fluctuations of phase of the oscillatory dynamics between the different stochastic realizations. Apart from the increase of fluctuation amplitudes, enhancing D may give rise to the transition from the stochastically stable FP to the noise induced spiking. The latter can appear as nearly periodic or irregular depending on c, τ and D. It is known that in systems of excitable units subjected to D and τ, the length of inter-spike intervals (ISIs) is influenced by the competition between two characteristic time scales [115]. One is set by the self-oscillation "period" $T_0(D)$ obtained for $\tau = 0$, whereas the other is adjusted with τ. Loosely speaking, for $\tau < T_0(D)$ and intermediate c, the noise-led dynamics characterized by $T_0(D)$ prevails over the delay-driven one unless τ is commensurate or comparable to $T_0(D)$. This paradigm may carry over to the collective motion due to synchronization of individual units.

The first MFA derives from the strong law of large numbers, by which the sample average $S_N = N^{-1} \sum_{i=1}^{N} s_i$ of N independent and identically distributed random variables s_i converges almost surely to the expectation value $E(s_i)$ for $N \to \infty$. How S_N approaches $E(s_i)$ for large, but finite N and finite variances of s_i distributions σ^2, is specified by the central limit theorem, which implies that S_N follow the normal distribution $\mathcal{N}(E(s_i), \sigma^2/N)$. In our setup, the subsets $\{x_i(t)|i = 1, \ldots N\}$ and $\{y_i(t)|i = 1, \ldots N\}$ at any given t are obviously not made up of independent variables, but one may still consider the influence of interaction terms negligible if N is sufficiently large. The latter is referred to as the *quasi-independent assumption (QIA)*, whose precise formulation is:

Definition 1 . *random variables* $\{x_i(t)|i = 1, \ldots N\}$ *and* $\{y_i(t)|i = 1, \ldots N\}$

for each t and sufficiently large N satisfy the approximate equalities:

$$X(t) \equiv \frac{1}{N}\sum_{i}^{N} x_i(t) \approx E(x_i(t))$$
$$Y(t) \equiv \frac{1}{N}\sum_{i}^{N} y_i(t) \approx E(y_i(t)) \tag{3.3}$$

On the left of (7.3) are the *spatial averages*, used to define the global variables $X(t)$ and $Y(t)$. Need for the second approximation becomes apparent after carrying out the spatial average and applying the QIA on (7.2). The fashion in which the terms $E(x_i^3(t))$ are to be treated is resolved by the *Gaussian assumption* (GA), given as:

Definition 2 . *for most time instances t_0, the small random increments $dx_i(t), dy_i(t)$ for $t \in (t_0, t_0+\delta t)$ can be computed with sufficiently good accuracy by assuming that the random variables $x_i(t), y_i(t)$ for each $i = 1, \ldots N$ and for $t \in (t_0, t_0+\delta t)$ are normally distributed around $(E(x_i(t)), E(y_i(t))) \approx (X(t), Y(t))$.*

GA is intentionally stated in a weak sense, containing phrases "sufficiently good accuracy" and "for most time instances". The former implies that the approximate solutions should have the same qualitative features as the exact one, whereas the latter's meaning will become clear following the analysis on the typical scenarios where GA holds. Note that the GA does not require $\{x_i(t)|i = 1, \ldots N\}$ and $\{y_i(t)|i = 1, \ldots N\}$ to be Gaussian processes over asymptotically large time intervals, but rather to be Gaussian over small intervals $(t, t+\delta t)$ for most values of t. For such t one can express all the higher order moments that appear in the expressions for $dX(t)$ and $dY(t)$ in terms of only the means, viz. $X(t)$ and $Y(t)$, and the second-order moments, including variances $s_x(t) = E(n_{x_i}^2(t))$, $s_y(t) = E(n_{y_i}^2(t))$ and the covariance $u(t) = E(n_{x_i}(t)n_{y_i}(t))$, where $n_{x_i}(t) = X(t) - x_i(t), n_{y_i}(t) = Y(t) - y_i(t)$. Here, the QIA is reflected in the fashion in which the spatial and the stochastic averages are related. Use of GA in deriving the MF model rests

on the notion that the fraction of time where GA fails will not introduce significant differences between the MF and the exact solutions.

The MF counterpart of (7.2), incorporating QIA and GA, has been derived in Section 5.6. It constitutes the following system of five deterministic DDE:

$$\begin{aligned}
\epsilon \dot{m}_x &= m_x(t) - m_x(t)^3/3 - s_x(t)m_x(t) - m_y(t) \\
&\quad + c(m_x(t-\tau) - m_x(t)), \\
\dot{m}_y &= m_x(t) + b, \\
\frac{\epsilon}{2}\dot{s}_x &= s_x(t)(1 - m_x(t)^2 - s_x(t) - c) - u(t) \\
\frac{1}{2}\dot{s}_y &= u(t) + D, \\
\dot{u} &= (u(t)/\epsilon)(1 - m_x(t)^2 - s_x(t) - c) - s_y(t)/\epsilon + s_x(t)
\end{aligned} \tag{3.4}$$

assuming that MF solutions satisfy $m_x(t) \approx X(t), m_y(t) \approx Y(t)$. Note that some more sophisticated MF approaches [103] adopt the Gaussian decoupling approximation, yet do not require QIA, as their final form accounts for spatial averages of fluctuations of both local and global variables.

3.2 Domains where MFAs apply

The strategy is to first provide the qualitative explanation on the two typical scenarios where both the MFAs hold, associating the properties of the local and global dynamics with the appropriate parameter domains. We also demonstrate that the dynamics in different instances where GA, QIA or both break down, though apparently distinct, still shares a common feature which is more or less pronounced. The analysis then proceeds to the results of tests carried out to independently verify the validity of GA or the QIA, initially focussing on the paradigmatic cases. Note that for an excitable system influenced by D and τ, the MFAs are more likely to hold in relative than the absolute sense, which instigated us to introduce methods

to quantify the level in which the particular MFA is satisfied. This is convenient as one can explicitly show how their fulfilment deteriorates with the variation of the system parameters before the eventual failure. We also consider the relation between the MF model's behavior and the validity of the MFAs, discussing two issues: (i) whether the predictions of the MF model, inferred by the bifurcation analysis, may extend to the parameter domains where the MFAs no longer apply, and (ii) can the dynamics of the MF model serve to indicate the domains where the MFAs break down.

Intuitively, one expects the MFAs to hold if c and D are small. Though this is indeed so, the general conclusion cannot be put beforehand and in terms of the most likely parameter domains, but should rather refer to the qualitative properties of the system's dynamics. As a preview of the main result, it may be stated that the GA and QIA apply if both the local and the global dynamics are characterized by a single attractor, either a FP or a LC, provided that D is not too large. Conversely, if the local and the collective variables yield qualitatively different dynamics or exhibit multistability, the validity of either or both MFAs is lost. This occurs due to stochastic phase fluctuations, manifested more or less strongly, which may render the different realizations of both the local and the collective dynamics out of step.

Figures 7.1(a) and 7.1(b) illustrate two canonical examples where GA and the QIA hold. The value $c = 0.1$, fixed in both instances, is chosen from an intermediate range to stress that the MFAs' validity extends into such a domain. Figure 7.1(a) refers to scenario for small $D_1 = 0.0002$ and small $\tau_1 = 0.2$, where the local and collective dynamics display stochastically stable FP. Figure 7.1(b) concerns the case where the local and global dynamics exhibit the delay-driven LC with small superimposed fluctuations. The particular setup involves $D_2 = D_1$ but much larger $\tau_2 = 2.7$, having verified that the analogous conclusions apply for the noise-led oscillations. The main frames and insets of both figures are focussed on

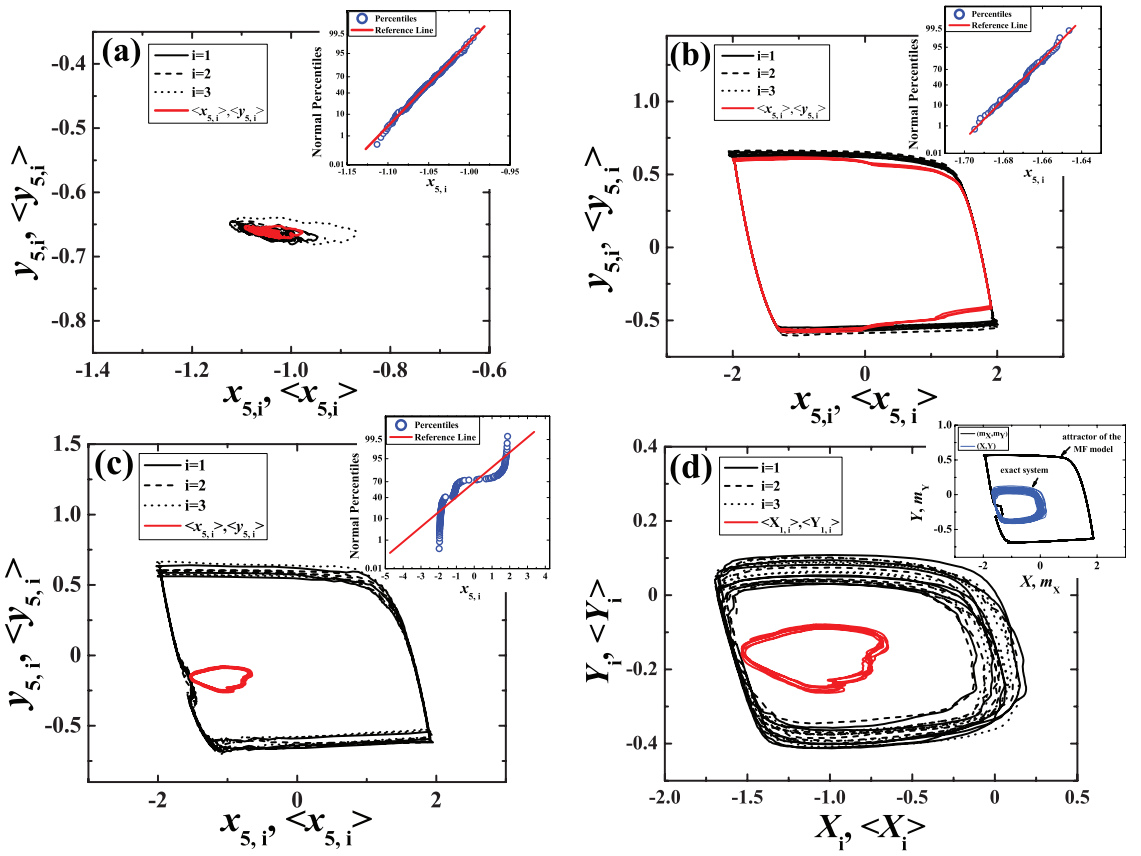

Figure 3.1: Main frames in (a), (b) and (c) display three different stochastic realizations $(x_{5,i}, y_{5,i})$ (black solid, dashed and dotted lines) for an arbitrary neuron, and $(E(x_{5,i}), E(y_{5,i}))$ for an ensemble of 10 realizations, shown by the solid red (grey) lines. The insets of (a), (b) and (c) refer to graphic normality tests. The data are obtained for $(c, D, \tau) = (0.1, 0.0002, 0.2)$ in (a), $(c, D, \tau) = (0.1, 0.0002, 2.7)$ in (b) and $(c, D, \tau) = (0.1, 0.003, 1.5)$ in (c). (d) illustrates the breakdown of GA for $X(t)$ under (c, D, τ) from (c). The inset shows the phase portraits for $(X(t), Y(t))$ (blue line) and $(m_x(t), m_y(t))$ (black line).

the validity of GA. The former show three different stochastic realizations $(x_{5,i}, y_{5,i})$ for an arbitrary neuron, encoded in black solid, dashed and dotted lines, as well as the expectation values $(E(x_{5,i}), E(y_{5,i}))$ for an ensemble of 10 realizations, drawn by the solid red (grey) lines. The index i accounts for the realizations. In case of Fig. 7.1(a), for any t, the expectation closely matches either of the realizations trivially. Regarding the scenario with LC, the analogous statement holds true if t is such that $(E(x_i(t)), E(y_i(t)) \approx (X(t), Y(t))$ lies on the slow branches of the given orbit. If $(E(x_i(t)), E(y_i(t))$ falls onto one of the transients, the expectation

departs substantially from the realizations, cf. Fig. 7.1(b). As mentioned in the definition, GA's validity is upheld if the number of former instances strongly prevails over the latter ones. This is verified for (c, D_2, τ_2) from Fig. 7.1(b), showing that the ratio of points lying on the transients vs those on the slow branches, approaches $n_t/n_s \approx 0.1$ for the sufficiently long time period along the trajectory of $(E(x_i(t)), E(y_i(t))$. Figure 7.1(c) illustrates the local dynamics for comparably large $D_3 = 0.003$, $c = 0.1$ and intermediate $\tau_3 = 1.5$, where the stochastic realizations fluctuate around the single LC. The fluctuations are large enough to induce strong phase desynchronization between the realizations. This is distinct from Fig. 7.1(b) in that the expectation substantially departs from each of the realizations at *any* t. For (c, D_3, τ_3), one can no longer interpret $(E(x_i(t)), E(y_i(t))$ in terms of clearly discernible slow and fast motions. Nonetheless, for some less pronounced examples of GA violation, say at $(c, D, \tau) = (0.1, 0.002, 1.2)$, one may estimate $n_t/n_s \approx 1.5$. Stochastic realizations of global variables' orbits $(X_i(t), Y_i(t))$ and their stochastic averages $(E(X_i(t)), E(Y_i(t)))$, shown in Fig. 7.1(d) for (c, D_3, τ_3) from Fig. 7.1(c), display qualitatively similar behavior as the local variables.

Apart from characterizing it by the n_t/n_s ratio, the GA validity has been tested directly for an arbitrary neuron at the given (c, D, τ). Having run many different realizations of the process $x_i(t), y_i(t)$ applying the same initial function, we have examined the properties of the distribution of different realizations $x_i(t_0 + \delta t), y_i(t_0 + \delta t)$ for small δt, taken to be of the order, in tens or hundreds of iteration steps. For LC dynamics, $(x_i(t_0), y_i(t_0))$ has lied on the refractory branch. The insets of (a), (b) and (c) display graphic normality tests, where the red lines indicate the theoretical percent of data points that would lie below the given value if obeying the Gaussian distribution, while the blue circles refer to the cumulative distribution of $(x_{5,i}, y_{5,i})$ for an ensemble of over 200 realizations. The data show that the distributions corresponding to (c, D, τ) in Fig. 7.1(a) and 7.1(b) are Gaus-

sian, whereas the one for Fig. 7.1(c) is not. The results of graphic tests are corroborated by the numerical Shapiro-Wilk method.

Note that the results above do not indicate how the GA's validity deteriorates with variation of the system parameters. The most interesting question is to assess the rate in which validity reduces with increasing D for fixed c and τ. The quantity appropriate to characterize this is determined as follows. For very small $D = 0.0002$, we select an arbitrary neuron and fix a point on the refractory branch of its LC orbit. Then, a large number of different stochastic realizations N_r for the given parameter set $(D, c, \tau) = (0.0002, 0.1, 2.7)$ is run. The goal is to find the maximal number of iteration steps T_{max}, for which the representative point in all the realizations still lies on the refractory branch. The curve plotted in Fig. 7.2 shows how the fraction of realizations N_{out}/N_r where the representative point has escaped the refractory branch in less than or exactly T_{max} steps increases with D. This may also be interpreted as an indication on how D gives rise to the number of instants where $(E(x_i(t)), E(y_i(t))$ belong to fast transients. According to validity of GA and the behavior predicted by the bifurcation analysis of the MF model [138], one may distinguish three characteristic noise domains. In (I), both the GA and the MF based bifurcation curves apply. For (II), the GA breaks down, but the MF model's dynamics still follows the one of the exact system. In domain (III), both the GA and the prediction based on the MF model's bifurcation analysis fail.

We proceed by the analysis on the fulfilment of QIA. One may either take (i) an indirect approach, derived from a corollary of the QIA formulation, or (ii) the direct approach, based on the notion that approximate synchronization between the units may render them virtually independent. Regarding (i), one invokes the central limit theorem, by which for large, but finite N holds that if local variables are normally distributed for most t, so too are the collective variables. Hence, GA validity for $X(t)$ and $Y(t)$ should imply that the local variables are independent. The normality test

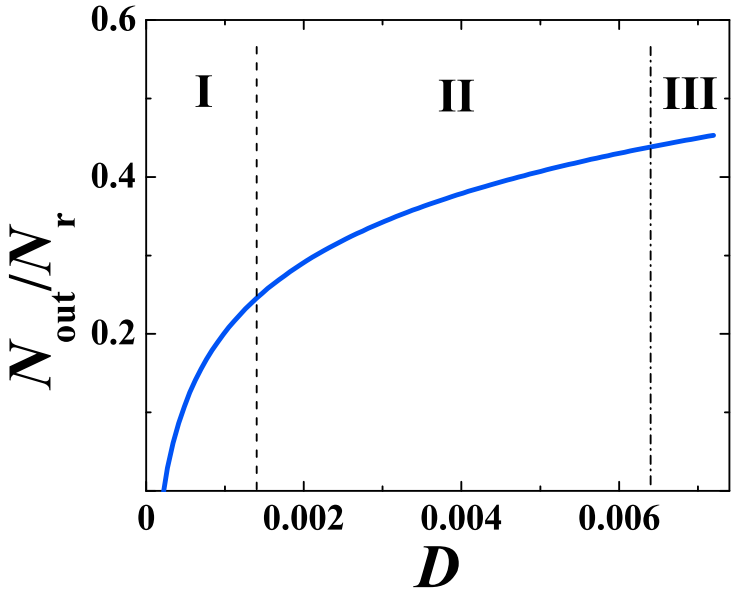

Figure 3.2: Fraction of stochastic realizations N_{out}/N_r in dependence of D for $(c, \tau) = (0.1, 2.7)$. The results converge to the given curve as N_r is increased.

on $X(t)$ and $Y(t)$ is carried out analogously to that for $x_i(t)$ and $y_i(t)$. The main frames (insets) of Fig. 7.3(a), (b) and (c) refer to graphic normality tests on the variable $X(t)$ ($Y(t)$) for the parameter sets exactly matching those in Fig. 7.1(a), (b) and (c). Figures 7.3(a) and (b) indicate the validity of GA for $X(t)$ and $Y(t)$ distributions, which suggests that QIA also applies. Nonetheless, an interesting point on Fig. 7.3(c) is that the distribution of $X_i(t_0+\delta t)$ over stochastic realizations conforms to, and the one for $Y_i(t_0+\delta t)$ sharply deviates from the Gaussian form. Such an outcome is often found for intermediate D and τ. One may cast this as a scenario where QIA is not violated strongly, since there are instances with normality violated for both $X(t)$ and $Y(t)$.

Let us consider the relation between behavior of the MF model and the validity of MFAs, especially QIA. It has already been indicated that GA for the collective motion may be violated in a weaker or the stronger sense, depending on (c, D, τ). Either way, stochastic phase desynchronization is reflected in the amplitude quenching of $X(t)$. What we argue is that

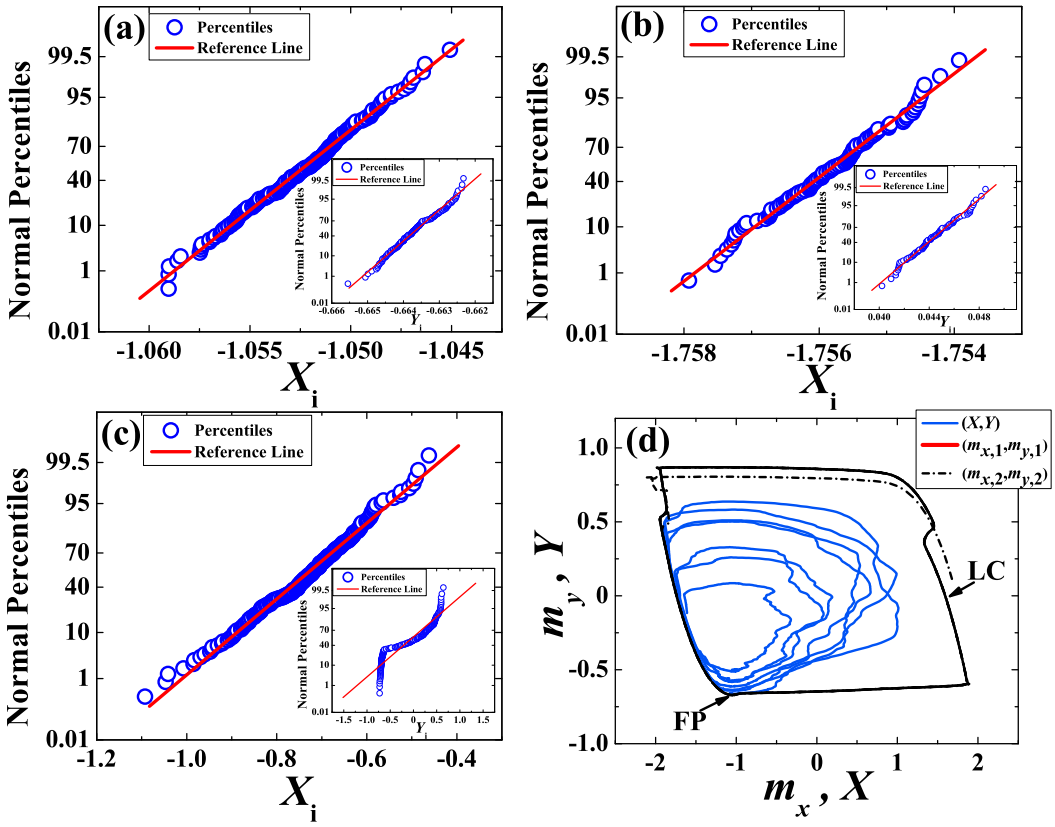

Figure 3.3: (a), (b) and (c) show normality tests for $X(t)$ (main frames) and $Y(t)$ (insets). Parameters are the same as in Fig. 7.1(a), (b) and (c), respectively. (d) illustrates coexistence of FP (red dot) and LC (black dashed line) for the MF variables $(m_x(t), m_y(t))$, as well as the typical orbit $(X(t), Y(t))$ of the exact system (blue solid line) at $(c, D, \tau) = (0.1, 0.002, 0.5)$.

the MF model is "sensitive" to instances of stronger violation, such that the bistability of its dynamics may indicate the failure of QIA in a self-consistent fashion. Namely, for moderate violation from Fig. 7.1(d) and Fig. 7.3(c), at variance with the exact system, MF model displays a large-amplitude LC, see the inset in Fig. 7.1(d). However, in cases of strong GA violation for the collective motion, found either at intermediate D for small and intermediate τ, or at large D and τ, the MF model exhibits coexistence between the FP and the large LC, see Fig. 7.3(d), or between the small and large LCs. Large LC is born via the global fold-cycle bifurcation and does not affect stability of the stationary state, whereas the small LC arises from the direct Hopf bifurcation. Mixed mode of the exact system in both instances may be interpreted as stochastic switching between two attrac-

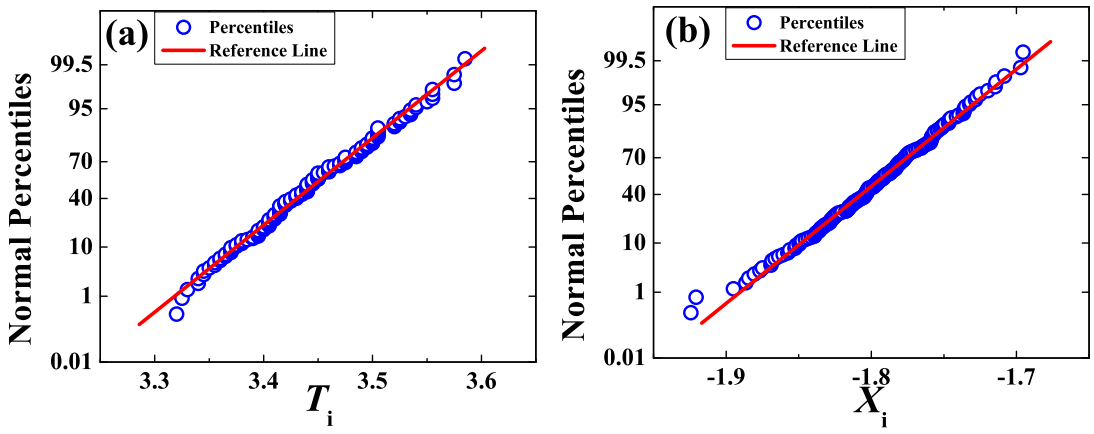

Figure 3.4: In (a) and (b) are displayed graphic normality tests indicating Gaussian distributions of ISIs and the return points for $X(t)$, respectively. The data refer to the noise-led dynamics at $(c, D, \tau) = (0.1, 0.0015, 0)$.

tors of the deterministic MF model, whereby such orbits are not normally distributed around the respective averages.

Before elaborating on the relation between the synchronization properties and the fulfilment of QIA, we consider two side topics intended to qualify more closely the terms ”frequency” and ”phase” used later on. The aim is to show that the effective frequency and phase description of system dynamics may be appropriate if MFAs hold. Regarding frequency, we present the results on the distribution of ISIs for $X(t)$. Note that there are two types of collective modes, one where the ISIs are dominated by $T_0(D)$, which occurs for small and intermediate D under very small τ, and the other corresponding to the delay-led dynamics, which is typically seen for small and intermediate D under large τ. Either way, we have verified that ISIs are normally distributed for an arbitrary stochastic realization under long simulation times. In Fig. 7.4(a), the normality test is provided for the more interesting case, showing persistence of Gaussian distribution for the noise-led dynamics under fairly large $D = 0.0015$ at $\tau = 0$. Thus, the description of collective motion in terms of the average period (frequency) appears justified if MFAs apply.

In the context of effective phase for the collective motion, we have examined whether the distributions of the return points $P(X_r)$ and $P(Y_r)$ fol-

lowing the average ISI may also be Gaussian, if MFAs are satisfied. $P(X_r)$ and $P(Y_r)$ are calculated in two steps: one first lets the simulation run for the sufficiently long time to determine the average ISI for $X(t)$, and then carries on by collecting data on the return points for another very long time period. The first point (X_0, Y_0) is chosen to lie on the refractory branch of the LC. In Fig. 7.4(b) is shown the graphic normality test for $P_r(X)$ along an arbitrary stochastic trajectory under the same parameter set as in Fig. 7.4(a). Given result implies that, in statistical sense, the return points remain fairly close to the "average" LC.

Now we proceed with the analysis on the relation between synchronization of units and the fulfillment of MFAs, in particular QIA. Being stochastic and excitable in nature, the units cannot exhibit complete synchronization. However, the discussion above suggests that one may speak of approximate frequency (FS) and phase synchronization (PS) in conditional terms, if MFAs are satisfied. Presence or absence of these forms of synchronization may give rise to three types of collective states: (i) coherent states where single units display both the approximate FS and PS, (ii) states that exhibit FS, but lack PS and (iii) collective states where approximate FS is not established. One may infer the relation between synchronization and QIA by examining the linear interaction terms of the form $c(x_i(t-\tau)-x_j(t))$. If there is approximate lag-synchronization, the latter become very small, which leaves the neurons virtually independent. Therefore, by identifying conditions under which the approximate lag-synchronization is achieved, one effectively looks for the parameter domains where QIA applies.

We have established that there exist only two scenarios for the approximate lag-synchronization, both of which amount to cases of approximate FS and PS. The interaction terms may substantially reduce either (i) for noise-led dynamics at $\tau \simeq 0$, or (ii) for delay-driven dynamics at very large $\tau \sim T_0(D)$. A way to characterize the approximate FS for the given parameter set is to calculate the ratio $r = \Delta T/\langle\overline{T_i}\rangle$, where $\Delta T = max|\overline{T_i} - \overline{T_j}|$

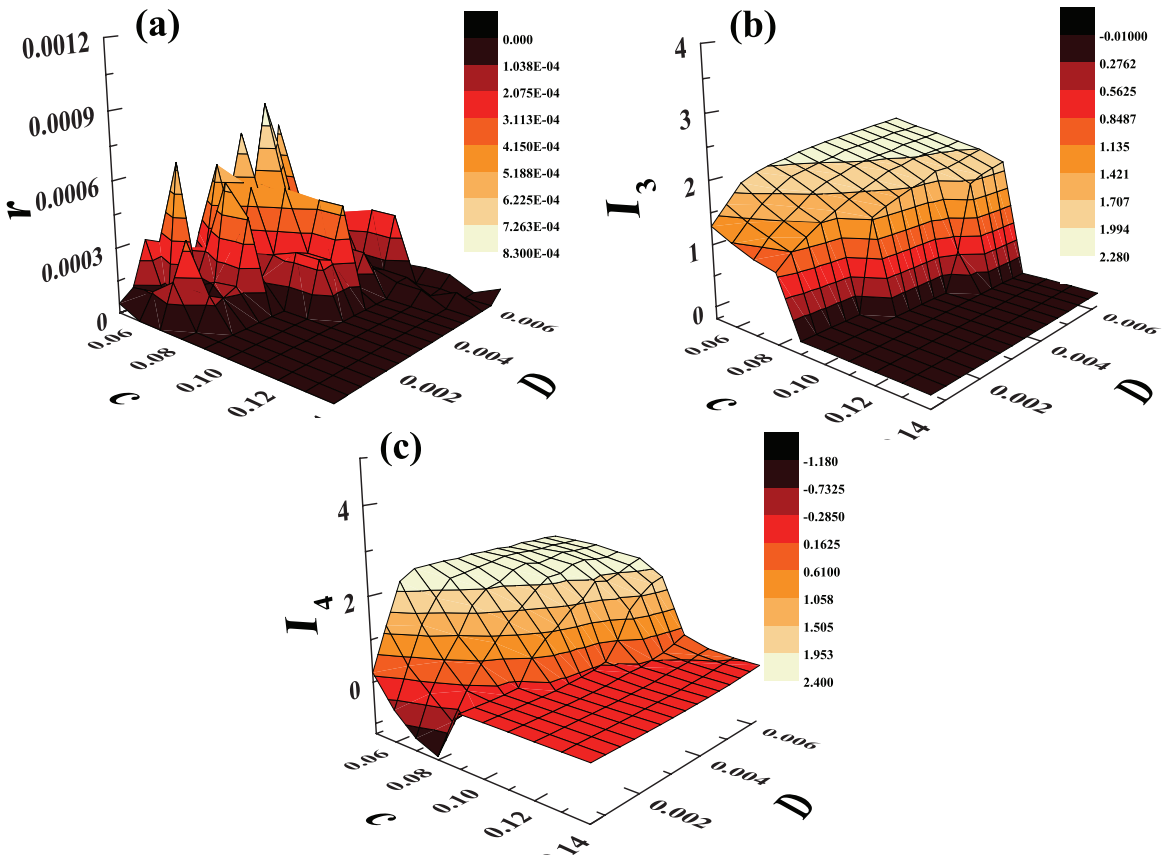

Figure 3.5: The parameter domains admitting the approximate frequency and phase synchronization between the units provide an indication of where the QIA holds. (a) shows $r(c, D)$ for the delay-driven dynamics at $\tau = 2.7$. (b) and (c) illustrate $\overline{I_3}(c, D)$ and $\overline{I_4}(c, D)$ for $\tau = 2.7$, respectively.

is the maximal difference between the time-averaged ISIs $\overline{T_i}$ of individual units, whereas $\langle \overline{T_i} \rangle$ denotes the population average $\langle \overline{T_i} \rangle = N^{-1} \sum_{i=1}^{N} \overline{T_i}$. The smaller r becomes, the better FS between the units is achieved. The results for $r(c, D)$ plotted in Fig. 7.5(a) refer to the (ii) case at $\tau = 2.7$. We have verified that setting $\tau = 0$, which corresponds to case (i), yields qualitatively similar results. As the main point, note a very large domain where r is small, which indicates the approximate FS. Expectedly, for small c and large D, r is seen to rise sharply, implying that FS is lost.

The drawback of the method above is that one cannot distinguish whether approximate FS is or is not accompanied by PS. To do so, we consider the time-averaged third and fourth order moments of the local potentials

$P(x_i(t))$ for the given parameter set, taking the average over a very long stochastic realization. By ergodic hypothesis, such an average equals the one taken over an ensemble of realizations. The third-order average moment is defined as $\overline{I_3} = (1/T)\sum_{t=1}^{T} I_3(t)$, where $I_3(t) = \sum_{x_i}(x_i - X(t))^3 P(x_i(t))$. The analogous relation holds for $\overline{I_4}$. $P(x_i(t))$ is obtained by dividing the range of possible x_i values into 110 bins $[x, x + \delta x]$, whereby one records the fraction of units whose potential falls within the given bin. If there is an approximate FS and PS, one expects x_i for most t to be Gaussian distributed around the mean $X(t)$. Then, both $\overline{I_3}$ and $\overline{I_4}$ should lie close to zero. If there is approximate FS, but PS is lacking, $\overline{I_3} \approx 0$ should hold, whereas $\overline{I_4}$ should substantially depart from zero. Finally, if there is no approximate FS, both $\overline{I_3}$ and $\overline{I_4}$ are supposed to lie away from zero. Results on $\overline{I_3}$ and $\overline{I_4}$ at $\tau = 2.7$ for a wide range of (c, D) values, cf. Fig. 7.5(b) and 7.5(c), suggest that domains with approximate FS closely match those with PS. Note the overlap between the areas with the smallest r, $\overline{I_3} \approx 0$ and $\overline{I_4} \approx 0$ in Fig. 7.5(a), 7.5(b) and 7.5(c), where QIA should hold.

3.3 Chapter summary and discussion

For the class of excitable systems influenced by D and τ, we have formulated the MFAs and discussed the typical scenarios where they hold or fail. The MFAs are adapted to reflect the excitable character of system dynamics and the strong time scale separation between fast and slow variables. Validity of MFAs is found to extend beyond the commonly expected parameter domains, demonstrating it to essentially depend on the qualitative properties of the local and global dynamics. If these two are characterized by a unique attractor of the same type, either a FP or LC, and D is not too large, both GA and QIA apply. We have introduced novel methods to quantify the level in which the MFAs' validity deteriorates with parameter variation. While the failure of GA is linked to stochastic phase fluctua-

tions between different process realizations, fulfilment of QIA is brought into context of synchronization of the local dynamics. For the MF model, the most important point shown is that bistability in its dynamics may indicate in the self-consistent fashion the domains where MFAs are violated.

Chapter 4

Clustering in excitable systems: basic phenomenology

Chapter abstract Spontaneous formation of clusters of synchronized spiking in a structureless ensemble of equal stochastically perturbed excitable neurons with delayed coupling is demonstrated for the first time. The effect is a consequence of a subtle interplay between interaction delays, noise and the excitable character of a single neuron. Dependence of the cluster properties on the time-lag, noise intensity and the synaptic strength is investigated.

Collective behavior in large ensembles of physiological and inorganic systems can be reduced to that of coupled oscillators engaged in various synchronization phenomena. In terms of macroscopic coherent rhythms, it may either be the case where all the units are recruited into a giant component or the case of cluster states characterized by exact or in-phase intra-subset and lag inter-subset synchronization. The spontaneous onset of cluster states is of particular interest to neuroscience [21] for the con-

jectured role in information encoding, as well as for participating in motor coordination or accompanying some neurological disorders. The approach to clustering has mostly relied on modeling neurons as autonomous oscillators, treating separately the question of whether the proposed mechanisms may be robust under noise [29, 57, 136, 137, 143] and transmission delays [144–147]. We explore a new mechanism which rests on the excitable character of neuronal dynamics and mutual adjustment between noise and time delay to yield the self-organization into functional modules within an otherwise unstructured network.

For the instantaneous couplings, the research on populations of excitable neurons has covered pattern formation due to local inhomogeneity [148], or has invoked a scenario where noise enacts a control parameter tuning the dynamics of ensemble averages between the three generic global regimes [95]. Distinct from the layout with complex connection topologies, here it is demonstrated how coupling delays do alter the latter landscape in a significant fashion, giving rise to an effect one may dub the cluster forming time-delay-induced coherence resonance. In part, the strategy to analyze global dynamics rests on deriving the mean-field (MF) approximation for the exact system. The likely gain from the MF treatment is at least twofold: except for allowing one to extrapolate what occurs in the thermodynamic limit $N \to \infty$, it may serve as an auxiliary means to discriminate between the effects of noise and time delay. Unexpectedly, the MF model undergoes a global bifurcation at certain parameter values where the exact system shows an onset of cluster states.

4.1 Network dynamics and the tools to analyze it

We focus on an N-size population of all-to-all diffusively coupled Fitzhugh-Nagumo neurons, whose local dynamics is set by

$$\begin{aligned} \epsilon dx_i &= (x_i - x_i^3/3 - y + I)dt + \frac{c}{N}\sum_{j=1}^{N}[x_j(t-\tau) - x_i(t)]dt, \\ dy_i &= (x + b)dt + \sqrt{2D}dW_i, \end{aligned} \tag{4.1}$$

where the activator variables x_i embody the membrane potentials, while the recovery variables y_i mimic the action of the K^+ membrane gating channels. c denotes the synaptic strength and τ stands for the coupling delay, both parameters for simplicity assumed homogeneous across the ensemble. The $\sqrt{2D}dW_i$ terms represent stochastic increments of the independent Wiener processes, i.e. the white noise. For the external stimulation holds $I = 0$, whereas the small parameter $\epsilon = 0.01$ warrants a clear separation between the fast and slow time scales. Selecting $b = 1.05$, the neurons are poised near the Hopf bifurcation threshold $b = 1$, which places them in an excitable regime where each possesses a single equilibrium. An adequate stimulation, be it by the noise or the interaction term, may evoke a large excursion of membrane potential, passing through the spiking and refractory states before it loops back to rest.

To characterize the degree of correlation between the firing events, we use primarily the interneuron spike train coherence [149, 150]

$$\kappa_{ij} = \sum_{k=1}^{m} X_i(k)X_j(k) / \sqrt{\sum_{k=1}^{m} X_i(k)X_j(k)}. \tag{4.2}$$

This requires one to split the simulation period T into bins k of length $\Delta = T/m$, awarding each neuron a variable $X_i(k) = 1(0)$, contingent on whether a spike was triggered or not within the given time bin, respectively. As with all the quantities below, we have been careful to exclude

from calculations the transient behavior. The spike threshold and the time bin are set to $X_0 = 1$ and $\Delta = 0.008$, verifying that no change of the results occurred if X_0 or Δ were reduced. The distribution of the κ_{ij} values may serve to distinguish between the homogeneous and clustered network states. Another aspect we are interested in is whether the clustered states are monostable or coexistent with the homogeneous ones at the given network size. To probe this, we have monitored if the values of the global coherence $\kappa = \frac{1}{N(N-1)} \sum_{i,j=1;i\neq j}^{N} \kappa_{ij}$ for different realizations at the fixed parameters clumped together, expecting bunching into distinct groups as evidence of multistable behavior.

Addressing the temporal structure of the network states, it is useful to look into the distribution of the local neuron jitters r_i [55, 123]. They represent the normalized variations of the interspike intervals T_k extracted from $x_i(t)$, $r_i = \sqrt{\langle T_k^2\rangle - \langle T_k\rangle^2}/\langle T_k\rangle$, with smaller values indicating better regularity. The modality and the width of the r_i distribution over the population may serve as rough indices on how the cluster dynamics is mutually adjusted. In the final part, we analyze the behavior of the ensemble averages $X = 1/N \sum_{i=1}^{N} x_i$ and $Y = 1/N \sum_{i=1}^{N} y_i$, where the former increases if a larger fraction of neurons fire in synchrony. The results for the exact system are compared to those of the approximate MF model [139]. The latter presents a two-dimensional set of delayed differential equations

$$\begin{aligned}
\epsilon\frac{dX(t)}{dt} &= X(t) - X(t)^3/3 - \frac{X(t)}{2}\left\{1 - c - X(t)^2 + \sqrt{[c - 1 + X(t)^2]^2 + 4D}\right\} \\
&\quad - Y(t) + c[X(t-\tau) - X(t)], \\
\frac{dY(t)}{dt} &= X(t) + b,
\end{aligned} \tag{4.3}$$

derived within a cumulant approach by employing the Gaussian approximation.

We note that the results for the exact system refer to a network of $N = 200$ neurons, applying independently a method from [151] to verify no

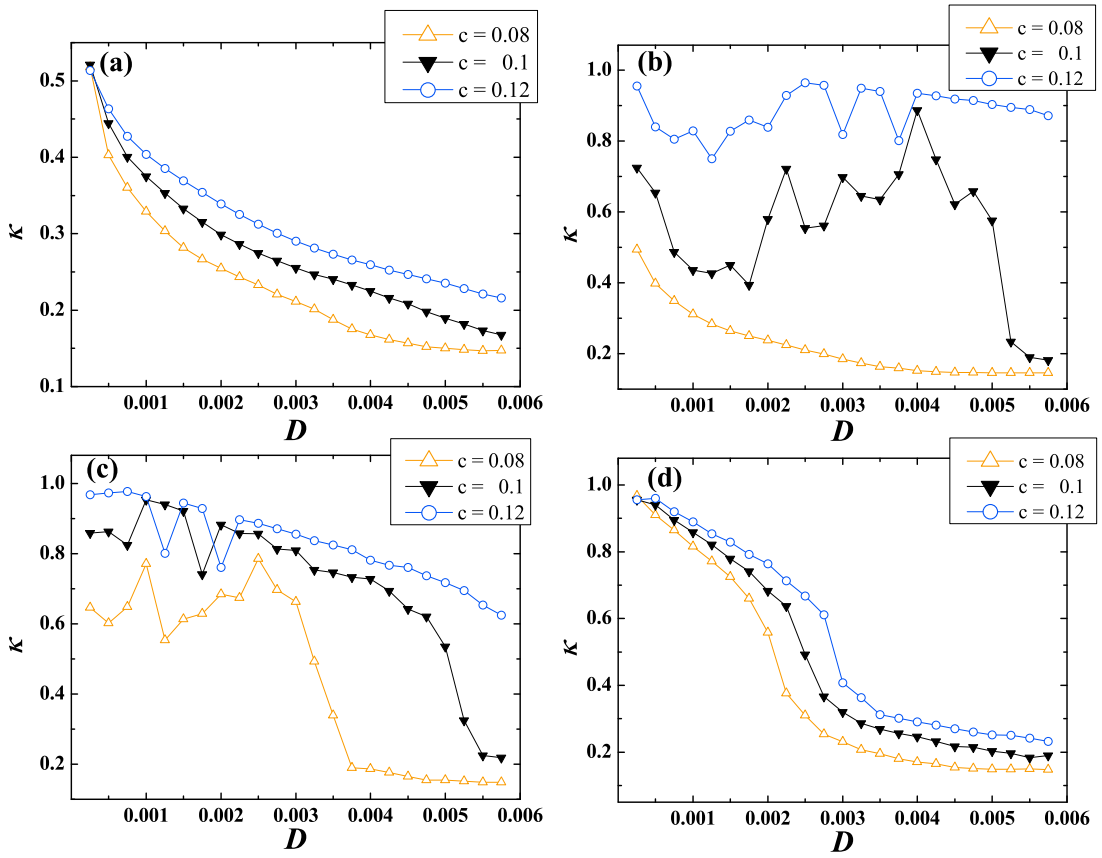

Figure 4.1: Profiles of the $\kappa(D)$ families of curves over the synaptic strengths $c = 0.08, 0.1$ and 0.12 display strong dependence on the delay, increasing from $\tau = 2$ in (a), $\tau = 6$ in (b), $\tau = 10$ in (c) to $\tau = 11$ in (d). The location of "wells" may point to the emergence of the clustered states.

qualitative changes in the clustering behavior for larger N.

4.2 Onset and characterization of cluster states

To get a sense of what may be the parameter ranges to admit the cluster states, we plot the c–families of the κ curves in dependence of D for different τ. Without the delay, the curves would conform to a stereotype profile, where one distinguishes between the three "regular" segments for very small, intermediate and large D, showing first a reduced κ due to incoherent oscillations, then steady high values for the coherent ones and the decaying segment at D where the stochastic dynamics prevails. However, from Fig. 7.1 we learn how this is upheld for some τ, say $\tau = 11$, but is violated

manifestly at the "cluster-resonant" values $\tau = 2, 6, 10$. The "wells" seen at approximately $D \in (0.001, 0.003)$ in Figs. 7.1(b) and 7.1(c) may occur for just two reasons, as κ decreases either for the incoherent or the clustered states. The latter alternative is supported by the coherence matrices in Fig. 7.3, which are discussed shortly. The importance of the D - τ adjustment for the clustering effect is also witnessed by the c-dependence within the families in Fig. 7.1: the stronger the interaction term, the more salient is the picture of "irregularity" sections immersed into a "regular" curve profile. Increasing the delay, the cluster states first occur, apparently monostable, around $\tau = 2$ for the small $D = 0.00025$, whereby the typical phase portrait (PP) projection shows twisted orbits with two clearly discernable segments, see Fig. 7.2(a). These reflect the two macroscopic fractions of the population firing alternately, such that the homogeneous network dynamically splits into clusters of mutually synchronized neurons, with the clusters locked in antiphase. The frequency entrainment is indicated by the shape of the r_i distribution, which peaks sharply around $< r >_m = 0.01$. We tested the invariance of clustering with N via the asymptotical behavior of the quantity $\chi^2_N = \frac{\sigma^2_X}{\frac{1}{N}\sum_{i=1}^{N}\sigma^2_{x_i}}$, where $\sigma^2_X =< X(t)^2 >_t - < X(t) >^2_t$ and $\sigma^2_{x_i} =< x_i(t)^2 >_t - < x_i(t) >^2_t$ holds. If the cluster states endure, there should be a residual component $\chi(\infty) \in (0, 1)$ in the large N limit [151]. For this and the remaining cases, the onset of such a regime is found around $N \approx 200$, implying that no qualitatively novel phenomena occur above this system size. An interesting observation is that the cluster configuration $\{N_1, N_2\}$, determined by the fractions' sizes, fluctuates around the ratio $2 : 1$ for different stochastic realizations and appears to aggregate with enhancing N. For certain τ, the two-cluster state also emerges outside the D-region delimiting the incoherent and coherent global regimes. This holds for $\tau = 5$ and $D \in (0.0004, 0.0008)$, where the cluster layout is also such that if one is active, the other remains refractory. The r_i distribution maintains a narrow form, but its maximum shifts to $< r >_m \approx 0.19$. Though

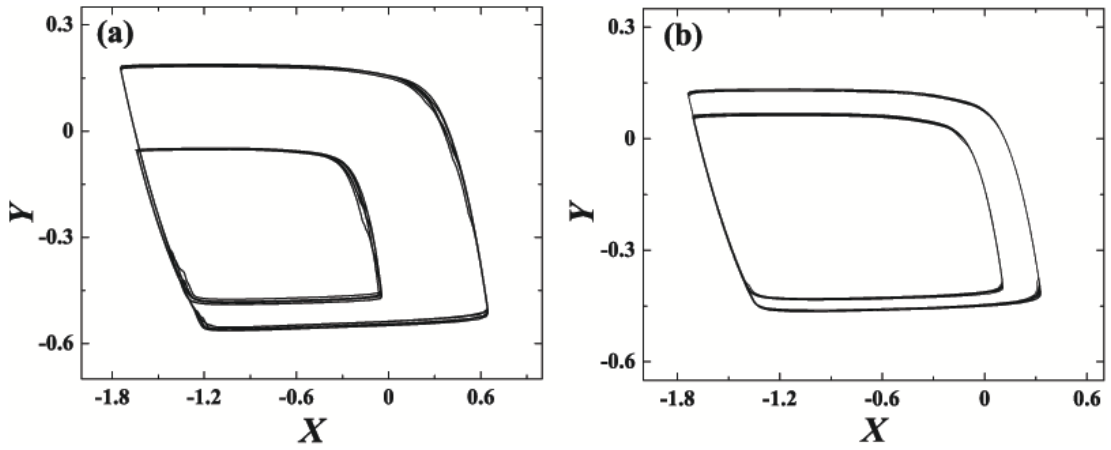

Figure 4.2: Global PPs for the two-cluster states show twisted LCs, whereby the two discernable segments reflect the alternate firing of the neuron subsets. The N_1/N_2 ratio depends on the interplay of D and τ, as seen from the examples $\tau = 2, D = 0.00025, c = 0.1$ in (a) and $\tau = 5, D = 0.0005, c = 0.1$ in (b).

one retrieves the general picture from above, a variance is that larger τ seems to favor the partition $N_1/N_2 \approx 1:1$, see PP in Fig. 7.2(b). The $1:1$ ratio is preferred both for increasing N and if the delay is set to $\tau = 6$.

The clustered states so far may be cast as stationary in the sense of stability against neurons switching between the clusters. We also report on the existence of three-cluster states that may be considered "dynamical", with the neurons able to jump to and from clusters. Such an outcome arises for the stronger noise $D \approx 0.0013$, once the delay is increased to $\tau = 10$. To underline the difference between the stationary and dynamical clustered states at $\tau = 5$ and $\tau = 10$, we plot side-by-side the corresponding pairwise coherence matrices $\{\kappa_{ij}\}$, see Figs. 7.3(a) and 7.3(b), where the network nodes have been rearranged by a hierarchical clustering algorithm according to a form of metric distance that has the most coherent nodes the closest. This makes it explicit how the intercluster coherence for the two-cluster state is virtually negligible with respect to the three-cluster case. Loosely speaking, within an unstable three-part population division, when a certain fraction is firing, the other is refractory and the neurons in the smallest cluster are at rest (excitable). This less clear separation is also apparent when comparing the nodal degree distributions in

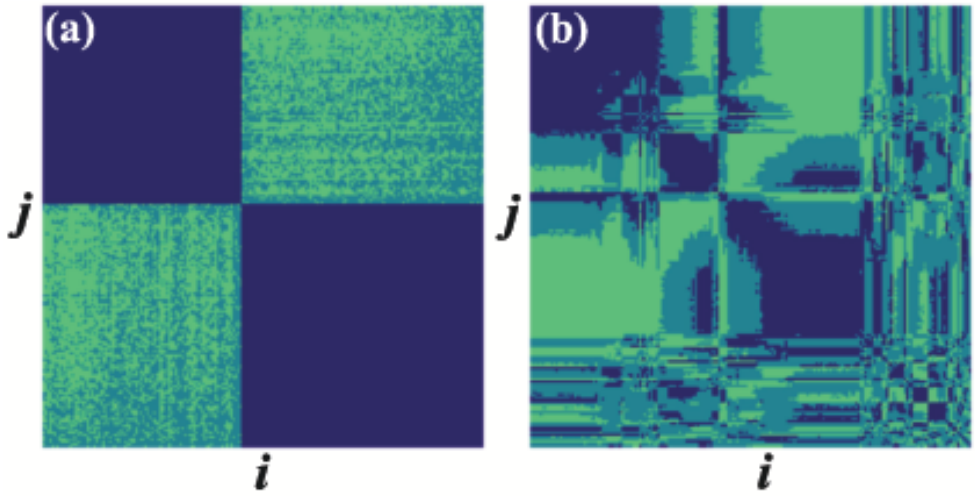

Figure 4.3: Rearranged coherence matrices for $\tau = 5, D = 0.0005, c = 0.1$ in (a) and $\tau = 10, D = 0.0013, c = 0.1$ in (b) imply the strong cluster separation in the two-cluster states and mixing between the clusters in the three-cluster case. Darker shading reflects higher coherence.

cases $\tau = 5$ and $\tau = 10$, obtained if one assumes $\left\{\kappa_{ij}\right\}$ to provide weights for the network whose links stand for the correlated dynamics between the neurons. For $\tau = 5$, the bimodal degree distribution is clearly seen without raising the connectivity threshold, whereas for $\tau = 10$ the initially smeared three-modal distribution refines after some thresholding is performed. The rationale of dynamical clustering may best be understood by analyzing the r_i distribution in the three-cluster state. Apart from being wider than in the two-cluster state, it peaks at a much smaller value $< r >_m \approx 0.09$, implying the more regular neuron firing. For this to hold, synchrony within the clusters has to be of intermittent nature, such that the neurons once engaged in synchronized spiking are much more likely to do so again.

Aa understanding of clustering mechanism is revealed by comparing the typical PPs of neurons participant in the homogeneous coherent state and the clustered states, see Figs. 7.4(a) and 7.4(b). A striking feature in the latter case is a kink at the refractory branch of the slow manifold. The appearance of a kink is the key manifestation of the $D - \tau$ co-effect, that consists in separating the ensemble into clusters and maintaining the proper phase difference between them. The purpose of the kink is to keep

the neurons frustrated long enough at the refractory branch before being allowed to slide down to its left knee. This may be imagined as a form of a lock-and-release behavior, where the delay primarily gives rise to the first, and noise to the second part. If a fraction of the ensemble were to move beyond the left knee and the other were to lag behind, the split should be amplified with each population cycle, eventually becoming resilient to perturbation precisely due to trapping at the refractory branch. For trapping to be successful, the kink has to be placed properly, approximately where the dynamics of the representative point is most susceptible to perturbation along the slow manifold. Then, for a brief period, due to an influence from x_i, the evolution of y_i is locally accelerated, becoming comparable to a speed of change in the direction orthogonal to the slow manifold, driven by the spiking fraction of the population. Note that the trapping interval has to be adjusted so that the entire population is entrained to a single frequency of firing. The latter matches the one in delay-free case, which warrants stability against perturbations. The arguments above and the numerical data seem to indicate how the delays where the coherence resonance is felt the strongest may be approximated by $\tau = T_0/2 + n * T_0$, with T_0 being the period of coherent oscillations at $\tau = 0$. Noise-wise, with increasing τ, D has to be adjusted to higher values to regulate the relaxation from the kink to the slow manifold while maintaining the entrainment to the proper frequency. In parallel, for stronger D, the representation cloud of the firing fraction tends to disperse more, requiring a sufficient τ for this effect to be averaged out.

The interplay between D and τ is further highlighted by exploring the behavior of the MF model (7.4). Local bifurcation analysis shows that the MF exhibits a succession of super- and subthreshold Hopf bifurcations [139], which account for the transition from the stochastically stable FP to the stable LC. Still, this scenario is confined to noise higher than here: analytical and numerical means corroborate the Hopf bifurcations to emerge

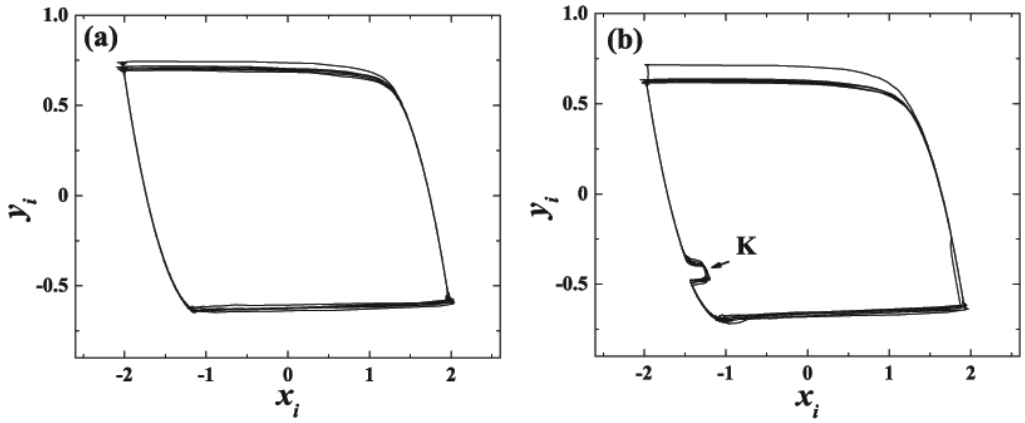

Figure 4.4: (a) and (b) show typical PPs of neurons participating the homogeneous global oscillations and clustered states, respectively. The latter are distinguished by a kink K, which is a signature of the $D-\tau$ co-effect. The parameter sets are $\tau = 6, D = 0.0005, c = 0.1$ in (a) and $\tau = 2, D = 0.00025, c = 0.1$ in (b).

about $D \approx 0.0025$ at relevant τ. Now we argue that the approximate model is in qualitative terms able to capture the clustering effect occurring for small D, c and τ. Focus is on the finding that MF system predicts an onset of cluster states by undergoing a global bifurcation for the parameter values around $\tau = 2, D = 0.00025$ and $c = 0.08$. At the given τ and D, for $c < 0.08$ the approximate model has only the equilibrium, whereas around $c \simeq 0.08$ a large and a small LC are born via a fold-cycle scenario. Note how then the PP of the MF acquires the form qualitatively similar to those of the exact system's in Figs. 7.2(a) and 7.2(b). The two sections of the emerging MF orbit mimic the action of the fractions within the full population. This structure of the LC becomes unstable under increasing c or τ, i.e. for the stronger impact of the interaction term. Another interesting aspect to the approximate system is that it shows the complex LC to coexist with the FP, viz. the basins of attraction in Fig. 7.5(b), which is a feature apparently absent in the exact model. However, the FP is located very close to the basins' boundary which indicates it to be stochastically unstable in the exact system for an arbitrary small noise.

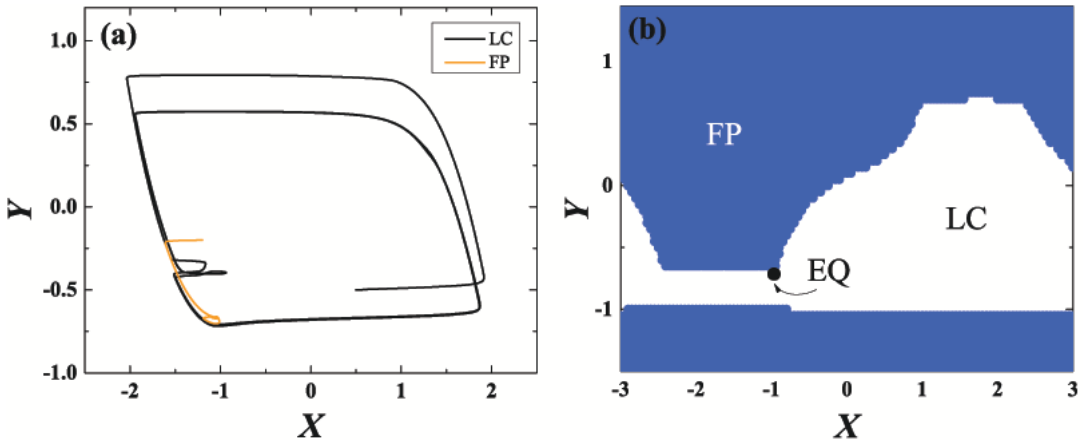

Figure 4.5: Bistability in the MF model: (a) shows the trajectories converging either to the FP or the LC, depending on the initial conditions, whereas in (b) are displayed the two basins of attraction for $\tau = 2, D = 0.00025, c = 0.1$.

4.3 Chapter summary and discussion

We have reported on a novel phenomenon where clustering within the homogeneous neural population is induced by an interplay of noise and time delay. This paradigm is distinct from most current explanations on how the clustered states may arise, for it does not treat D and τ as destabilizing and detrimental, but rather as biased toward the formation of dynamical structure in networks that are unstructured both in terms of topology and local parameters. The analyzed model is minimal yet sufficient to display an interesting type of behavior, possible only as an interplay of excitability, noise and interaction delay. Once the phenomenon is recognized as caused only by these qualitative properties one can study the effects of more realistic assumptions on the distribution of neuronal properties and connection patterns. An interesting point concerns the derived MF model, which can aid in understanding the precise roles played by D and τ. Notably, beneath the surface lies a more stratified phenomenon, where the subtle adjustment between the parameters affects the number of clusters, their configuration, stationary or dynamical character, as well as whether the cluster states occur monostable or coexist with the homogenous solution at the given population size. This framework could find application within the research on

neural systems and other excitable media.

Chapter 5

Cluster synchronization of spiking in homogenous assemblies of excitable units: analysis

---

Chapter abstract In the field of nonlinear dynamics, systematic exploration of the co-effects introduced by the simultaneous presence of noise and time delay has gained attention only recently. An interesting type of the ensuing synchronization phenomena may be splitting of a population into clusters, each made up of neurons oscillating in synchrony, whereby the activity between the clusters shows phase lags. Usually, the synchronization cluster formation is a consequence of some structural inhomogeneity, either in the local parameters or the network topology. Here we provide an in-depth analysis of the phenomenon where the interplay of noise, interaction time-delay and the excitable character of neuronal dynamics is found to be necessary and sufficient for the occurrence of the synchronization clusters, in spite of the network being completely structureless. In particular, the model we apply concerns a fully connected network of noisy excitable neurons interacting via delayed diffusive cou-

plings. Several tools have been applied to characterize the synchronization clusters and to study their dependence on the neuronal and the synaptic parameters. Qualitative explanation of the cluster formation is discussed. We have found the two-cluster partitions where neurons are firmly bound to their subsets, as well as the three-cluster ones, which are dynamical by nature. The former turn out to be stable under small disparity of the intrinsic neuronal parameters and the heterogeneity in the synaptic connectivity patterns.

Selective synchronization of relevant neural populations is a general principle for organizing communication in the brain, as it is associated with many cognitive processes [152–156], while also being crucial for movement preparation and execution [157–160]. It is commonly believed that synchronously oscillating neurons exchange information more effectively [13]. Neurons *in vivo* operate under the influence of many factors that can be modeled as noisy perturbation. Nontrivial and constructive role of noise in the dynamics of a single neuron, few neurons or large neuronal networks is well known [55, 67, 161–167]. The key to this lies in the fact that the excitable dynamics of a single neuron acts as an amplifier of the small noisy perturbation. The latter can shift a neuron near the stable fixed point of the excitable regime randomly into a state that yields a spike discharge. Such noise induced spiking resembles chaotic oscillations. However, for a certain range of noise intensity, which depends on the neuronal refractory period, spiking may appear as regular oscillation with a well defined frequency. Coupling to other neurons can then lead to synchronization between stochastic spiking or may induce deterministic oscillatory dynamics.

Transmission of neuronal impulses through an axon and synapses is not instantaneous. The transport time can be included phenomenologically into the modeling by using explicit time lag in the synaptic interaction terms. Relatively small interaction time delays are known to have profound effects on the neuronal dynamics [14, 29, 57, 136, 137, 143, 168, 169]. The time delay may induce oscillations through different mechanisms, like the Hopf or some global bifurcations, or it may suppress the existing oscillations. It is also widely recognized how time delay can profoundly influence the type of synchronization between the neurons.

The effects of the simultaneous influence of noise and the interaction delays on the dynamics of typical neuronal systems have been analyzed much less, viz. [138, 143] and the references therein. One such phenomenon, induced by combining the noise, interaction-delay and the excitable character of the local dynamics, constitutes the splitting of population into clusters, each made up of synchronously firing neurons. So far, the issues gaining significant attention have been the formation of clusters of synchronous dynamics either due to the inhomogeneous distributions of the neuronal parameters or the non-trivial network topologies, see [13, 21]. Appreciating such studies, one would imagine the clusters emerging in structureless networks less likely. Note that this does not connote to systems of globally coupled identical oscillators, where clustering already constitutes a well-known manifestation of multi-stability, usually being associated with more complex interaction functions [170–172]. However, it has recently been reported [115] that the synchronization clusters can be formed even in completely homogeneous networks of excitable units owing solely to a subtle interplay of noise, interaction delay and the neuronal excitability. In this chapter we provide an in-depth analysis of the spontaneous clustering phenomena. Several techniques are to be employed to characterize the aspects of local and the macroscopic dynamics related to the synchronization clusters, capturing the mechanisms that allow them to

arise and be maintained.

We consider a collection of N identical Fitzhugh-Nagumo excitable neurons perturbed by the white noise and interacting via the delayed linear couplings. Each neuron is connected to every other neuron, assuming uniform synaptic strength and the time-lag. Though the default setup involves a homogeneous ensemble, some of the cluster states are further shown to be robust with respect to small dispersions of the neuronal and network parameters. Results of the detailed numerical study on the properties of the cluster partition are discussed, making its dependence on the coupling strength, noise intensity and the time-lag explicit. Following on that, we provide an explanation of the observed phenomena using numerical and qualitative arguments, as well as the recently developed mean-field model of the stochastic delay-coupled network of excitable units [138, 139, 143].

The chapter is organized as follows. In Sec. 5.1 the focus lies with the details of the applied neuron and population models, further providing background on the global regimes generic for the extended excitable media. Section 5.2 is aimed at introducing the coherence measure appropriate to characterize the mutual adjustment between the neuron firing patterns, arriving at the means to analyze the structure of clustered states from the macroscopic perspective. The other major issue concerns the relationship between the cluster states and the already familiar global regimes, in particular in terms of anticipating the parameter regions that may facilitate clustering. Section 5.3 is dedicated entirely to the two-cluster states, examining whether and how are the regularity of local dynamics and the properties of cluster partition affected by variation of noise amplitude and the time delay. Another matter of interest is the asymptotic dynamics related to clustering, referring both to the long term stability and the behavior under increasing the system size. In Sec. 5.4 one shows the structure of the three-cluster states to be prone to reconfiguration, at variance with its two-cluster counterpart. The two following sections underlie the common

framework behind the clustering phenomena. On one hand, it is shown that the coaction of noise and delay induces a unique form of neuron phase portraits, whereas on the other, the developed mean-field (MF) model is demonstrated to undergo a global bifurcation reflecting the onset of clustered states. The final section contains the summary and the discussion on the results obtained.

5.1 Background on the neuron model and the population dynamics

Consistent with the assumption on neuron excitability, the local dynamics of an N-size population is built on the Fitzhugh-Nagumo model [75, 125, 126]

$$\begin{aligned} \epsilon dx_i &= (x_i - x_i^3/3 - y_i + I)dt + \frac{c}{n_i}\sum_{j=1}^{N} g_{ij}[x_j(t-\tau) - x_i(t)]dt, \\ dy_i &= (x_i + b)dt + \sqrt{2D}dW_i, \end{aligned} \tag{5.1}$$

where x_i and y_i are the respective activator and recovery variables, g_{ij} present the elements of the adjacency matrix and n_i refer to the number of neurons which the given neuron i is connected to. Setting $\epsilon = 0.01$ enforces a clear separation between the fast and slow variable subsystems, such that the former embodies the dynamics of membrane potentials, and the evolution of the latter may be linked to the action of the K^+ ion gating channels. The system is not subjected to external stimulation currents, so $I = 0$ holds. The neurons are nonetheless exposed to a noisy environment, a point reflected by the $\sqrt{2D}dW_i$ terms representing the stochastic increments of the independent Wiener processes, whose expectation values and correlations satisfy $\langle dW_i \rangle = 0$ and $\langle dW_i dW_j \rangle = \delta_{i,j}dt$. Communication between neurons occurs via diffusive couplings, parametrized by the synaptic strength c and the time delay τ, the latter accounting for the finite propa-

gation speed over the axons and/or the latency in postsynaptic responses. The synaptic parameters are taken to be uniform not least for simplicity, but rather to set aside all possible sources of secondary effects that may interfere with the core clustering phenomenon.

The key intrinsic parameter b is supposed to modulate the neuron excitability. To see how this may be so, one first recalls how the isolated neuron in the noiseless case undergoes a supercritical Hopf bifurcation for $|b| = 1$, such that it possesses a unique attractor, the fixed point (FP) above and the limit cycle (LC) below this value. Appreciating the invariance of the system (7.1) to transformation $(x_i, y_i, b) \to (-x_i, -y_i, -b)$, one can consider only the case $b > 0$ without any loss of generality. As a corollary of the strong time-scale separation, the Hopf threshold marks the onset of relaxation oscillations, where the phase point within each cycle spends $O(1)$ time along the spiking and refractory branches of the slow manifold, executing rapid $O(\epsilon)$ jumps in between them, recall Fig. 2.2. Translated to the stochastic version of the bifurcation, for vanishingly small D the trajectories still land on the appropriate attractor with probability 1 [79]. However, slightly above $b = 1$ the neurons are found in an excitable regime, meaning that an adequate stimulation, be it by the noise or the interaction term, may elicit large transients of membrane potential, whereby the orbit traverses the spiking and refractory states before the equilibrium is reinstated. A typical instance of such a behavior is obtained for $b = 1.05$, the value kept fixed throughout the chapter. Confined to the non-interacting case, one further encounters a range of intermediate noise amplitudes where the ensuing spike sequences show very little randomness. The particular setup with additive noise in the slow subsystem, like that in (7.1), may foster the coherence resonance (CR) [55], characterized by a tight analogy between the stochastic LC and its deterministic counterpart [77]. The latter does not hold for the alternative scenarios attending noise in the fast subsystem: letting it act alone or combined with that in the slow variable dynamics may

give rise to self-induced stochastic resonance (SISR) [77, 78] or several forms of mixed-mode oscillations [79], respectively.

Extending the above framework to excitable media, one typically invokes a scenario where noise enacts a control parameter, tuning between the different global regimes [64, 95, 103, 113]. In case of instantaneous couplings, the ensemble averages have been demonstrated to take up three generic forms of behavior, contingent solely on variation of the noise amplitudes, as illustrated earlier in Fig. 2.3. For small D, there is a stochastically stable global equilibrium, since the individual spiking is rare and incoherent, leaving most of the population at rest at any given time. The intermediate noise amplitudes give rise to a more frequent firing with most of the events synchronized, effectively turning the population into a macroscopic oscillator whose global frequency matches those of individual neurons due to mutual entrainment. Increasing D even further, one reaches a point when noise overwhelms the libration effects of coupling, with the ensemble averages decaying into chaotic regime. While the local spiking frequencies continue to increase, the synchronization systematically deteriorates by most of the spikes thrown out of step. These two points imply that at any instant the bulk of the population is refractory, which renders the trajectory of the global variables confined to an area of phase space much smaller than the one encircled by the LC.

The paradigm involving the three described types of behavior has first been reported for fully connected networks [5, 67], and has later been confirmed to endure for the layouts involving more complex interaction patterns [95, 123]. What we argue is that the inclusion of synaptic delay profoundly alters such a landscape, influencing in a meaningful way the succession of global variables' regimes. In particular, the coaction of noise and delay is found to facilitate a distinct form of synchronization that allows for the onset of the cluster states. As the effects of topology remain secondary to the core ingredients behind the phenomenon, namely

the noise, time delay and the neuron excitability feature, the results presented here refer to a globally connected network, viz. $g_{ij} = 1$ holds for each (i, j) pair of indices and $n_i = N$ applies to every node. This type of idealization has proven useful [127, 128], and populations with assumed all-to-all couplings, once subjected to external forcing or feedback control, have even been implemented in modeling the emergence of healthy and pathological brain rhythms, as well as the interaction between the distributed brain areas [1, 21, 27]. Nevertheless, in a discussion later on we consider an issue of removing a fraction of links between the neurons, showing that the phenomena laid out persist in randomly diluted networks on a condition that the sparseness level and the inhomogeneity in nodal degrees distribution are not excessive.

5.2 Observation of clustering

The main topic of this section concerns introducing the appropriate tools to monitor the emergence and describe the temporal structure of the cluster states. In particular, there are four issues we address: first, defining the quantities that may readily be implemented to distinguish between the homogeneous and the cluster states; second, gaining an insight on the set of parameters that admit clustering; third, examining whether the cluster states appear monostable or coexist with the homogeneous ones, and fourth, devising methods to discern and visualize how the neurons get distributed between clusters for each realization of the n-cluster state. In a nutshell, the aims stated are best achieved by means of pairwise and population coherence, which characterize the extent of correlation between the spiking events on the local and the global level.

To begin with, one is required to split the full iteration period T into bins k of length $\Delta = T/m$, such that each neuron i is awarded a binary variable $X_i(k) \in \{1, 0\}$, dependent on whether the neuron has fired or not within the

given bin, respectively. By doing so, the continuous time series of neuron membrane potentials are coarse-grained into binary sequences of ones and zeroes. Then the pairwise coherence κ_{ij} is defined as the cross-correlation between the neuron spike trains [149, 150]

$$\kappa_{ij} = \frac{\sum_{k=1}^{m} X_i(k)X_j(k)}{\sqrt{\sum_{k=1}^{m} X_i(k)X_j(k)}}. \tag{5.2}$$

Throughout the chapter, the time bin $\Delta = 0.008$ is set, whereas $X_0 = 1$ is the threshold assigned for the neuron potential to cross so to register a spike, verifying that the results withstand if either of these values is reduced further. We have made certain that the transients are excluded from calculations. Note that the distribution of κ_{ij} values may be used to distinguish between the homogeneous and the (different types) of cluster states, the information gained from its modality and the peaks' width.

Alternatively, $\{\kappa_{ij}\}$ can also be viewed as if it provides a template for defining *a posteriori* a connectivity matrix completely independent on the structural one, given by g_{ij}. One may envision this as an interpolation of the notion of functional networks [173–176], a well-known tool for analyzing the properties of the long-term dynamics within the large N systems, essentially intended to qualify some form of synchronization between the units. This is based on the idea of considering a pair of units (more strongly) coupled if their respective firing series are (better) synchronized. Hence, the way in which the functional network is built reflects the self-organization of neuron dynamics so that it places the units with precisely timed spikes within the same functional modules [21, 173, 175]. The latter role is here assumed by the clusters, so that the functional networks can be applied in exposing the structure of the cluster states. Since we introduce the coherence as a type of synchronization measure, the terms functional and coherence network are used alternatively.

The coherence networks [177] referred to here are by construction undi-

rected, but can involve either binary or weighted links. In the former case, a pair of neurons is considered connected if their pairwise coherence lies above a certain threshold Θ, be it nonzero or trivial [176]. Within this approach, the distinction between the homogeneous and the clustered states is apparent from the profile of the distribution of nodal connectedness degrees $P(k_i)$, as derived from the appropriate coherence network. Note that the nodal connectedness degree k_i is defined as the number of nodes which the given node i is connected to.

In Fig. 7.2(a) one sees the homogeneous state of global coherent oscillations typified by a unimodal distribution at $\Theta = 0$, such that all the neurons are interconnected, viz. the structural and the coherence networks are an exact match. On the other hand, for the cluster states one expects an n-modal degree distribution $P(k)$, whereby the threshold level necessary to arrive at clearly separated peaks depends on the ratio of intra- to inter-cluster correlations: the higher it becomes, the lesser Θ is required. For the two-cluster state in Fig. 7.2(b), coherence between neurons participating the different clusters is negligible, so one may take a marginal threshold value to obtain the coherence network whose nodal degree distribution reflects the cluster partition $\{N_1, N_2\}$.

Now let us explore the notion of the weighted coherence network, which rests on interpreting κ_{ij} as elements of a weight matrix that determines the scheme by which the nodes are interconnected. In order to visualize the structure of a cluster state, one is supposed to take two steps. The first is to introduce a distance metric which, loosely speaking, translates the least coherent neurons into the farthest ones, so that $\{\kappa_{ij}\}$ is effectively transformed into a matrix of distances $\{\gamma_{ij}\}$. The second step consists in applying an agglomerative hierarchical clustering algorithm on $\{\gamma_{ij}\}$, whereby the closest lying neuron groups are systematically merged into larger ones. Level-by-level, the groups to be joined are determined by a linkage criterion, expressing the intergroup distance as a function of pairwise distances

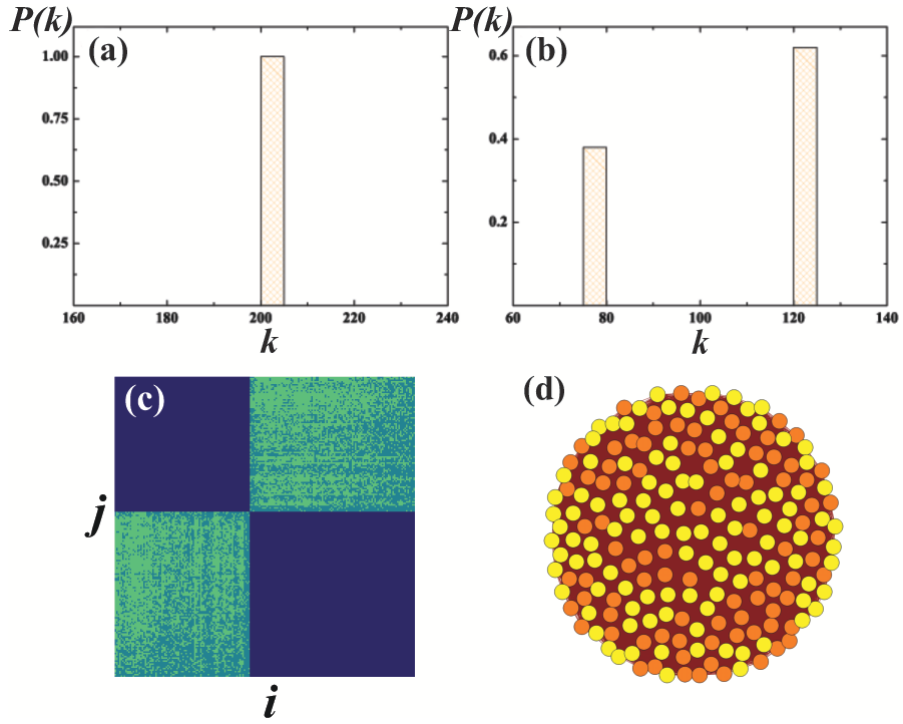

Figure 5.1: Characterization of the cluster states in terms of features of the corresponding binary and weighted coherence networks. In (a) and (b) it is demonstrated how the distinction between the homogeneous coherent states and the n-cluster states can be made explicit by the binary coherence network, which possesses a unimodal (an n-modal) distribution of the nodal connectedness degrees $P(k)$ in the former (latter) case. The data in (a) are obtained for the homogeneous coherent state at $c = 0.1, D = 0.001, \tau = 6$, whereas the parameter values for the two-cluster state in (b) are $c = 0.1, D = 0.00025, \tau = 2$. The weighted coherence network, represented by the weight matrix in (c), and the binary network in (d) may serve independently or combined to capture the structure of the given cluster state, as shown for the two-fraction partition at $c = 0.1, D = 0.0005, \tau = 5$.

between their respective members. In relation to the first step, it is convenient to adopt the distance metric $d(i, j) = 1 - \kappa_{ij}$. Completing the second stage, one readily obtains a dendrogram, where the layout of neurons in the lowest level may serve to rearrange $\{\kappa_{ij}\}$ so it assumes the block-diagonal form. The diagonal blocks mirror the clusters, and those off-diagonal represent the cross-correlations. What is displayed in Fig. 7.2(c) constitutes the outcome of the above strategy implemented in case of the two-cluster state obtained at $(D, \tau) = (0.0005, 5)$. A matter of some interest is to probe whether the binary and weighted coherence networks give rise to equivalent partitions for the same network state. Apparently, the binary networks,

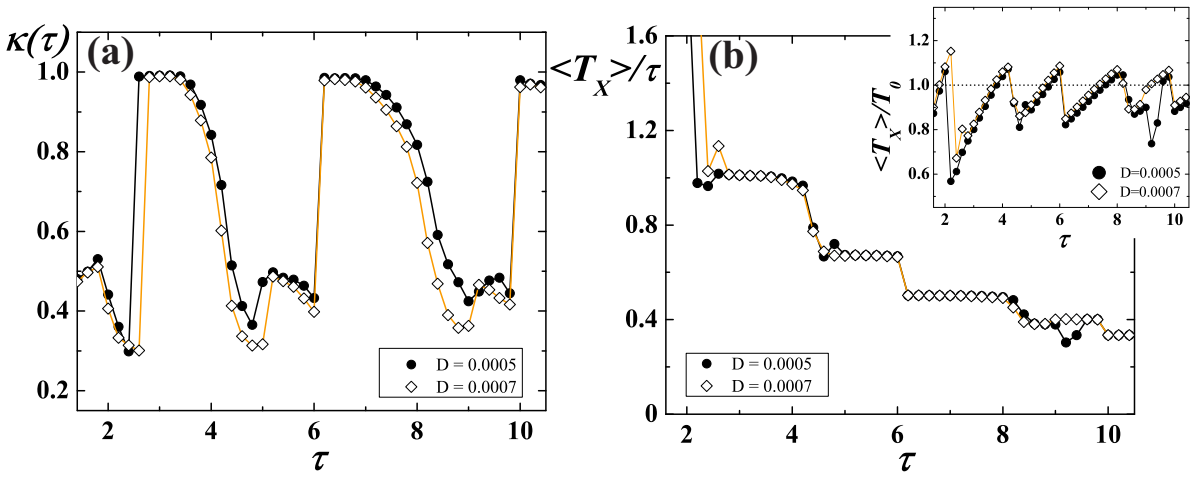

Figure 5.2: Focus on the impact of interaction delay on the system's behavior. (a) shows the $\kappa(\tau)$ plots for $D = 0.0005$ (solid circles) and $D = 0.0007$ (open diamonds) at fixed $c = 0.1$. Local minima exhibited by $\kappa(\tau)$ serve as an indication on the intervals of τ that foster the cluster states. (b) Representation scheme with respect to D is adopted from (a). The inset refers to the variation of the average oscillation period $\langle T_X \rangle / T_0$ with τ for the macroscopic variable X. In qualitative terms, the curves appear virtually the same for different noise, whereby the given profiles imply that the system's dynamics can be traced to the competition between the noise-driven and the delay-driven oscillation modes. The dashed line corresponds to the case $\langle T_X \rangle = T_0$. The main frame displays the dependence of the scaled average oscillation period $\langle T_X \rangle / T_0$ on τ for different D. For the homogeneous coherent states found within the approximate intervals $\tau \in [2.6, 4.2]$, $\tau \in [6.2, 8.2]$ and $\tau \gtrsim 9.8$, the above competition is resolved in favor of the delay-driven mode. For the two-cluster states around $\tau \in [4.8, 6]$ and $\tau \in [8.8, 9.8]$, the noise-driven mode prevails.

like the one in Fig. 7.2(d), provide less sophisticated information, but corroborate well with the weighted ones if the clusters are well separated, viz. when Θ should top only the very small cross-terms. Once there is more ambiguity to the separation, reaching the qualitative agreement rests with selecting the "proper" Θ for the binary network, as we see later on.

5.2.1 Where to look for the cluster states?

Having discussed the means of characterization, the next objective is to determine the parameter domains that facilitate the onset of the cluster states. For the most part, one is interested in the impact of D and τ, and to a lesser degree in the influence of c. Focussing initially on the isolated effects that each of the parameters brings in, we first consider how the sys-

tem's behavior is modified under variation of a single parameter, while the remaining ones are fixed. To this end, one invokes the global coherence [150] $\kappa = \frac{1}{N(N-1)} \sum_{i,j=1;i\neq j}^{N} \kappa_{ij}$, derived from the pairwise coherence by averaging over the neuron population. Given the definition, κ may assume values within the [0, 1] interval, with the upper and lower limits reflecting the completely coherent and incoherent firing between neurons, respectively. What is most useful about κ is that it decreases only for two reasons, either if the cluster states emerge or if some form of disordered states sets in. In the former case, should there be a two-cluster state with an approximate equipartition and a strong cluster separation, one expects to find $\kappa \approx 0.5$ or a slightly lesser value, depending on the deviations from the two assumptions we made. However, a larger reduction of κ can be considered a certain signature of the disordered states. Based on these two remarks, one should be able to read from any κ dependence where the cluster states are likely located. In particular, if there are no disordered states in the vicinity, the cluster states should coincide with the local minima of κ.

This is first probed for the $\kappa(\tau)$ dependence, viz. Fig. 7.3(a), having D fixed at two appropriate values, $D_1 = 0.0005$ and $D_2 = 0.0007$. Under this setup, the intention is to demonstrate that tuning the delay gives rise to the clustering effect, meaning that there exist some narrow intervals of τ which may be cast as the *cluster-resonant* ones [115]. We have indeed found by numerical simulation that the local minima around $\tau \approx 2, 6$ and 10 coincide with the onset of the two-cluster states, as to be expected from the curves' profile. The properties of such states will be analyzed in more detail in Section 5.3. However, one notes that clustering around $\tau \approx 2$ is distinct from the analogous phenomena for larger τ, given that in the former case, when increasing the delay, no homogenous coherent states arise prior to the cluster state, a point which in the latter case no longer applies. The other important observation is that $\kappa(\tau)$ acquires virtually a universal form for the fixed D values selected from the range relevant to clustering. The

minor differences around the local minima are the reflection of the noise-specified behavior of the global variables leading in to the formation or dissipation of the cluster states. Such background effects lie outside the scope of the present chapter. However, the argument on minor differences and the earlier statements on having to select the appropriate D values that admit clustering imply that one should also take into account the interplay between the effects of D and τ. In particular, apart from the characteristic time-scale determined by τ, note that the noise intensity as well brings in a characteristic time-scale, the one for "bare" oscillations in the delay-free case $\tau = 0$. The latter's period T_0 is solely determined by D, with $T_0(D)$ being a decaying function within the considered D-range, cf. Fig. 2.4(c) and the accompanying explanation. To get a sense on the values which T_0 may assume, we state two relevant instances, $T_0(D = 0.0005) \approx 3.78$ and $T_0(D = 0.0007) \approx 3.66$. It is not a surprising effect to find the system's behavior being determined by the competition between the two oscillation modes, one guided by noise and the other driven by the interaction delay. In this context, it is interesting that the cluster-resonant delays τ_r in Fig. 7.3(a) may roughly be approximated by the formula $\tau_r = T_0/2 + n * T_0$, which contains an implicit dependence on D through τ. Note that the given expression is similar to what is obtained in [62] for the coupled phase oscillators. Nevertheless, the formula may only be accepted in conditional terms, under two important constraints. First, it should not be read as if implying the existence of point-like resonances with delay, but rather as an indication on where the centers of the cluster-resonant intervals are situated. On the second constraint, note that Fig. 7.3(a) has the formula empirically confirmed only for $n = 0, 1, 2$. However, one should also take into account that considering overlong delays, viz. τ several times longer than the neuron refractory period, makes little sense in physiological terms.

Looking for further confirmation and additional details on how the system's behavior is driven by the competition of the delay and noise-driven

oscillation modes, we examine the variation with τ of the normalized average oscillation period for the global variable X, $< T_X > /T_0$, where averaging refers to an ensemble of different stochastic realizations. The plot is displayed in the inset of Fig. 7.3(b). Determining $< T_X >$ is the same as determining the average ISI [178], except for the two-cluster states, where the former is approximately twice as the latter. Apart for the non-trivial behavior in general, the curves for different D again qualitatively show a common form, with the minor noise-specific effects manifested mostly in the vicinity of $\tau \approx 2$. An important point is that around τ_r the $< T_X > /T_0$ values lie very close or slightly above the identity line $< T_X >= T_0$, indicated by dashes in the inset of Fig. 7.3(b). This should not be confound with the peaks around $\tau \approx 3.8$ and $\tau \approx 7.6$, where $\tau \approx n * T_0$ applies. These peaks are unrelated to clustering and reflect a form of global events in the phase space, which involve the limit cycle for the macroscopic variables approaching the vicinity of the saddle fixed point. Nonetheless, once the homogeneous coherent states first set in ($\tau \gtrsim 2.4$), $< T_X > /T_0(\tau)$ dependence exhibits nearly a periodic behavior approximately respecting the bare oscillation period T_0, viz. the sections $\tau \in [2.6, 6.2]$ and $\tau \in [6.2, 9.8]$.

To establish more firmly how are the homogeneous and the cluster states distinguished in terms of the prevailing oscillation modes, we also consider the variation with τ of the scaled average oscillation period for the global potential, $< T_X > /\tau$, see the main frame in Fig. 7.3(b). It strikes that the curves for different D again show nearly universal behavior. Essentially, one finds three plateaus approximately for $\tau \in [2.6, 4.2]$, $\tau \in [6.2, 8.2]$ and $\tau \gtrsim 9.8$, which are numerically confirmed to coincide with the homogeneous coherent states. Their average oscillation periods amount to $\tau, \tau/2$ and $\tau/3$, respectively, clearly implying the prevalence of the delay-dominated mode over the noise-driven one. Cross-referencing the results from the inset and the main frame, it also becomes clear that the sections for the approximate intervals $\tau \in [4.8, 6]$ and $\tau \in [8.8, 9.8]$ correspond to

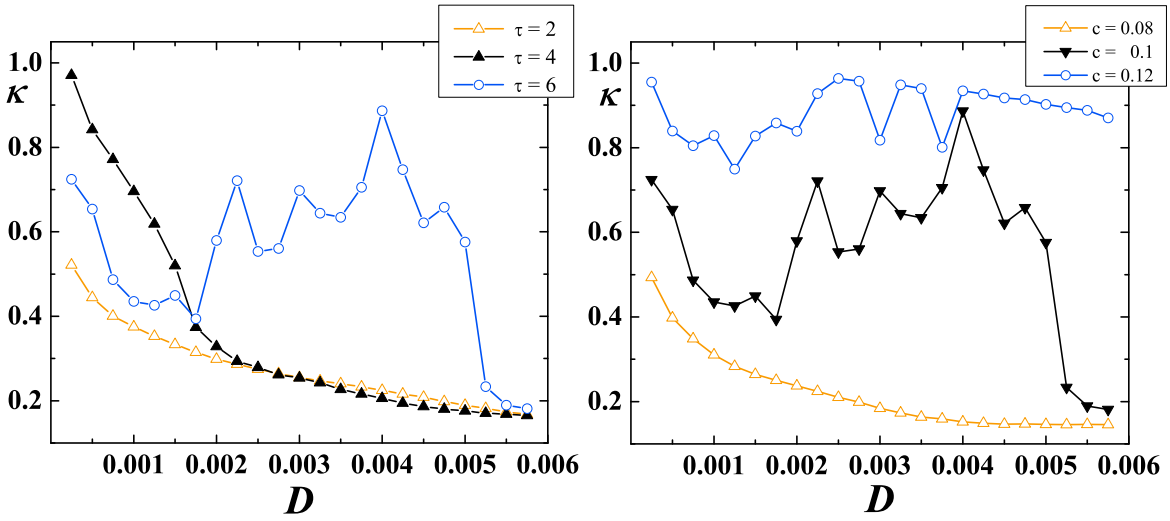

Figure 5.3: Insight on the impact of D and c on the system's dynamics. (a) shows the $\kappa(D)$ family of curves for the set of delay values including $\tau = 2$ (open triangles), $\tau = 4$ (solid triangles), as well as $\tau = 6$ (open circles), having $c = 0.1$ fixed. Two-cluster states are indicated for the noise amplitudes $D \lesssim 0.0008$ at $\tau = 2$, whereas the appropriate range of D is broader at $\tau = 6$. The curve's profile for $\tau = 4$ implies the lack of clustering within the considered interval of noise. (b) illustrates how the shape of the $\kappa(D)$ curves at fixed $\tau = 6$ is altered under variation of c, beginning with $c = 0.08$ (open triangles), over $c = 0.1$ (solid triangles) to $c = 0.12$ (open circles). Too strong a coupling appears to suppress the onset of the cluster states.

the two-cluster states, where the T_0-dominated oscillation mode wins over the τ-dominated one. In other words, it may be stated that in the noise-delay adjustment leading up to the cluster states, noise has the upper hand on determining the oscillation frequency, suppressing the forcing effect of the delay. As for the impact of bringing in the stronger noise, one only observes a minor broadening of the τ intervals where clustering can be found. This may be interpreted in the context of the finding that the delay-driven mode gives way to that driven by noise when the cluster states set in. Though it presents a simplification, note that the approximate formula on $\tau_r(T_0)$ is able to capture how the centers of the cluster-supporting delay intervals shift to smaller τ for larger D.

After an extensive overview focused mainly on the effects of τ on the formation of the cluster states, we direct our attention to demonstrating more explicitly how the system's behavior is influenced by the variation

of D. In this context, it is interesting to compare the $\kappa(D)$ curves for the different τ, examining how the cluster states interfere with the previously known picture involving three generic global regimes, contingent on the intensity of noise. To this end, in Fig. 7.4(a) are displayed the $\kappa(D)$ curves obtained by having fixed the delays at $\tau = 2, 4$ and 6. The value $\tau = 2$ has earlier been established to support clustering, $\tau = 6$ is in this respect marginal but still facilitates the cluster states, whereas $\tau = 4$ is identified as the value where no cluster states emerge. The latter curve serves to provide the point of reference, given that the deviations from its form may indicate clustering, among other phenomena. Note that the curve $\tau = 4$ conforms to a stereotype profile in the delay-free case $\tau = 0$. Following the explanation on the global regimes stated in the Introduction, one would expect to be able to discern three segments for the small, intermediate and large values of D, coinciding with the low initial κ values, significant κ increase through the middle section and a sharp decay for the latter part. This is basically confirmed for $\kappa(D)$ at $\tau = 4$, only the initial segment with low values is not apparent, as the required noise amplitudes are much smaller than the adopted, already small sampling step for noise. Note that the $\kappa(D)$ curves for $\tau = 2$ and $\tau = 6$ acquire quite different forms, though they both indicate clustering at certain D ranges. In the former case, $\kappa \approx 0.5$ implies the existence of two-cluster states for relatively small $D \lesssim 0.0008$. In the case $\tau = 6$, the D values that foster clustering seem to span the wider range. However, the overall picture may be somewhat smeared, since some average κ do not correspond to either the homogeneous coherent or the cluster states, reflecting bistability between the two, or even other types of multistability within some parameter ranges.

Finally, we touch upon the influence of varying the coupling strength c on the formation of the cluster states. To do so, we plot the $\kappa(D)$ families of curves for $c = 0.08, 0.1$ and 0.12 at fixed $\tau = 6$, see Fig. 7.4(b). It is apparent that the stronger the coupling, the more isolated become the

"irregularity" sections embedded into the flatter curve's profile, the latter being a corollary of the interaction term winning over the noise. Put differently, the stronger coupling confines the cluster states to smaller regions of the D-τ parameter space, making the resonance effect a more sharper one.

Once the existence of cluster states is established, κ may be put to use in determining whether they appear monostable or the dynamics exhibits multistable behavior for the given parameter set. If the κ values for different stochastic realizations were to bunch into distinct groups, it should be considered an evidence of the latter. On a cautionary note, this issue is likely to be sensitive on the system size.

Unless stated otherwise, the results presented throughout the chapter refer to a population of $N = 200$ neurons, with the numerical integration performed by an Euler method taking the iteration step $\delta t = 0.002$. Additional reduction of δt has been confirmed to leave the results unaffected. Apart from direct simulations of the ensemble dynamics for $N = 500$ and $N = 700$, the persistence of clustering phenomena has been verified by a method intended to probe the asymptotical behavior of the system in the thermodynamic limit $N \to \infty$, see subsection 5.3.1. The two sections to follow are aimed at characterizing the temporal structure of the two- and three-cluster states. The former are demonstrated to be stationary and the latter dynamical by nature [179], the distinction based on whether the neurons are allowed to cross back and forth between the clusters.

5.3 Properties of the two-cluster state dynamics

Enhancing the noise amplitude, the two-cluster states are first encountered at $D \approx 0.00025$ for $\tau = 2$. It is noteworthy that the given D values lie close to the crossover domain between the incoherent and the coherent collective dynamics. A useful approach is to consider first the phase portrait for the macroscopic variables $X = N^{-1} \sum_{i=1}^{N} x_i$ and $Y = N^{-1} \sum_{i=1}^{N} y_i$, deemed

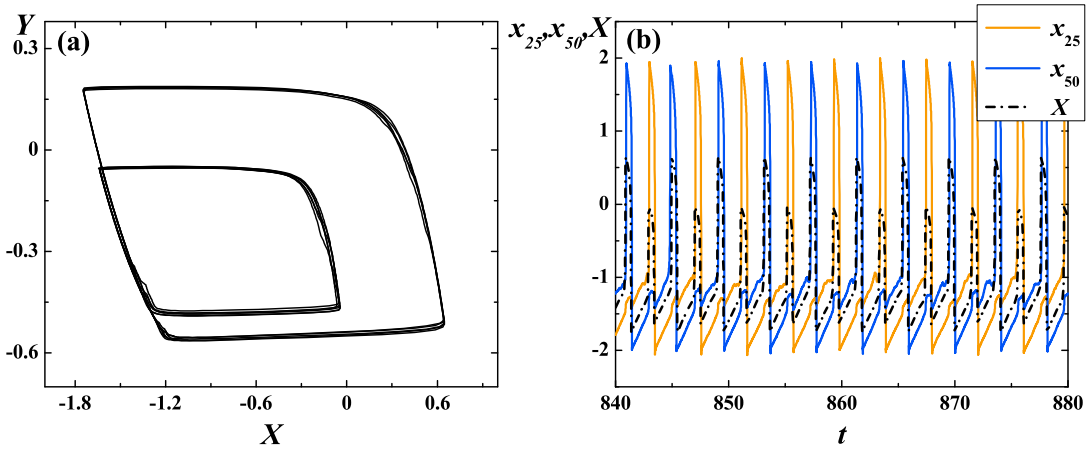

Figure 5.4: Two-cluster states at small D and τ. (a) As a signature of the population split, the phase portrait for the collective dynamics shows a twisted limit cycle orbit, where the two discernible segments reflect the action of the clusters. (b) A section from the $X(t)$ series (dashed line) is overlaid by the $x_i(t)$ series (solid lines) for two arbitrary neurons from the distinct clusters. A high-level coherence within the subsets is witnessed by the fact that the peaks of the global potential perfectly match the ones of the local potentials. The latter series imply that the firing of clusters is locked in antiphase. The data are provided for the case $c = 0.1, D = 0.00025, \tau = 2$.

as suitable descriptors since the higher amplitude of the peak global potential reflects a larger portion of neurons firing in synchrony. For such collective motion, Fig. 7.5(a) yields a twisted orbit made up of two clearly discernible segments that coincide with the macroscopic fractions of the population activated in turns, whereby the approximate synchronization within the subsets is maintained. In other words, the structureless population is in a dynamical fashion split into clusters, such that one's activation is accompanied by the neurons in the other cluster being refractory. This goes along with the observation in Fig. 7.5(b), demonstrating the overlap between the $X(t)$ spikes and the individual action potentials evoked in arbitrary neurons from the distinct clusters. One also learns how each of the two latter series displays high regularity, with the phase difference between their respective pulses apparently locked to π. The particular phase shift implies a splay state [162, 180], meant in general as an n-cluster partition where the phase difference between any two groups amounts to an integer multiple of $2\pi/n$.

To display the above behavior, the neurons have to be entrained to a single frequency, a point reflected in the distribution of local jitters r_i [55, 123] over the population. The jitters are defined as normalized variations of the interspike intervals T_k extracted from the individual time series x_i

$$r_i = \frac{\sqrt{< T_k^2 > - < T_k >^2}}{< T_k >}, \tag{5.3}$$

such that their smaller values indicate more regular firing patterns. Expectedly, for $(D, \tau) = (0.00025, 2)$, the r_i distribution in Fig. 7.6(a) is unimodal with a narrow peak and a maximum at a very low value $< r_m > \approx 0.01$, all the points indicative of the approximately uniform neuron frequencies across the population. Also, the mutual interaction acts within the clusters so to give rise to a form of a recovery mechanism, which rapidly suppresses any neuron from displaying large fluctuations in the firing period, the type of behavior that potentially leads to escaping the cluster. Though the stochastic background of the system dynamics may resurface causing occasionally the local interspike intervals (ISIs) to depart noticeably from the mean, one finds such perturbations resolved already in the next firing cycle. This is witnessed in Fig. 7.6(b), where the first return map of the ISIs for an arbitrary neuron shows a large majority of points tightly bunched. The latter holds irrespective of the cluster the given neuron belongs to, the point confirmed by the virtually indistinguishable ISI distributions for the members of the distinct subsets, viz. the inset in Fig. 7.6(b).

In terms of variations of the two-cluster partition $\{N_1, N_2\}$ under different stochastic realizations, it is interesting how for small D and τ the system appears less disposed to a splay state with equal sized fractions. Instead, one finds the fractions' ratio fluctuating around $2 : 1$, displaying the stronger convergence to an asymmetrical state if the population size N were increased, which rules out the possibility of this being the finite-size effect. In fact, it has more to do with the reduced ability of small amplitude

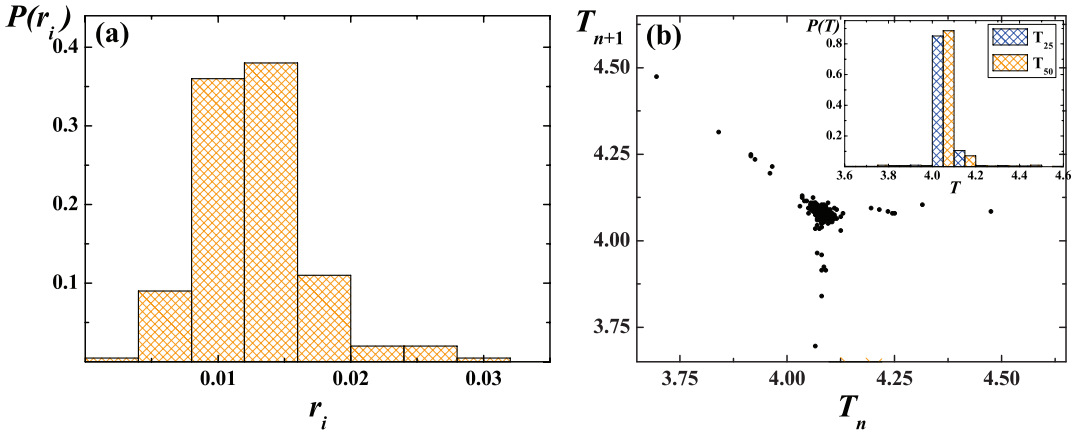

Figure 5.5: Properties of single neuron dynamics. (a) The distribution of local jitters $P(r_i)$ implies that highly regular spiking patterns are maintained across the ensemble. (b) The first return map of the firing periods T_n for an arbitrary neuron illustrates how any larger deviations from the mean value are rare, further subdued already within the following cycle. The latter is upheld independent on the particular cluster a neuron belongs to. This is witnessed in the inset, which shows the ISI distributions $P(T_n)$ for two arbitrary neurons from the distinct subsets. The parameter set is $(c, D, \tau) = (0.1, 0.00025, 2)$.

noise to draw more neurons away from the main bunch.

At certain τ longer than the average cycle of the isolated neuron, the two-cluster states are found to span the range $D \in (0.0004, 0.0008)$, a domain where the homogeneous coherent states are obtained in the case $\tau = 0$. Though at first sight of Fig. 7.7, illustrating the typical phase portrait for the ensemble averages under these parameters, it may seem plausible just to carry over the arguments from above, one should still outline a couple of differences. On a lesser note, the maximum of the r_i distribution is seen to shift to $< r_m > \approx 0.19$ due to an overall reduced regularity of the firing patterns. Qualitatively, however, the system dynamics in respect to different stochastic realizations switches into a bistable regime which involves coexistence between the two-cluster and the disordered states. Also, the conditions where D and τ are increased seem to favor the symmetrical cluster state with equal fractions in the population partition. The tendency to $N_1/N_2 \approx 1 : 1$ ratio becomes more salient with the increased system size, but is manifested as well for a somewhat larger $\tau = 6$, if the D values lie in the already considered range.

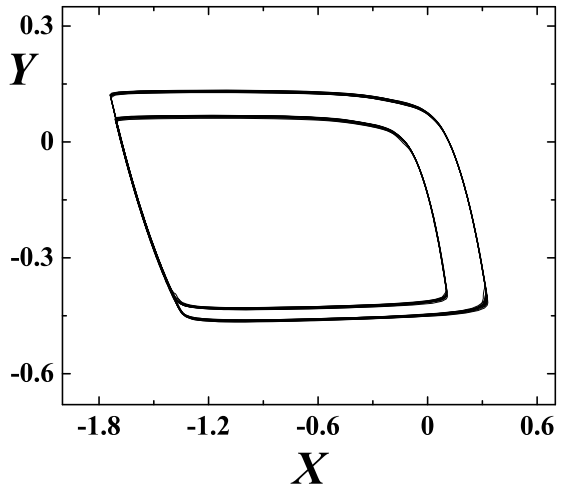

Figure 5.6: Two-cluster states at intermediate D and τ. Phase portrait for the global dynamics at $(c, D, \tau) = (0.1, 0.0005, 5)$ is projected in the $X - Y$ plane. The properties of the cluster partition N_1, N_2 are seen to depend on the parameter values, whereby the larger D and τ appear to favor the states closer to an equipartition $N_1/N_2 \approx 1 : 1$ over the asymmetric clustering.

Though it is not within the scope of the present chapter to extend the analysis in such a direction, one should still verify that the two-cluster states remain intact if one were to introduce heterogeneity into the intrinsic neuron parameters or the network coupling scheme. On the former, we have considered a population diversity scenario [148] where the excitability parameter is randomly drawn from a uniform distribution over a 2σ interval around $b = 1.05$. One should be careful to adjust σ so that the lowest possible b lies above the Hopf threshold $b = 1$. Nevertheless, the ensuing phase portraits for $(c, D, \tau) = (0.1, 0.00025, 2)$ and $(c, D, \tau) = (0.1, 0.0005, 5)$ are virtually unchanged compared to those in the homogeneous case, except for the minor variations in the cluster sizes occurring sporadically between the firing cycles. The other point concerns the persistence of the two-cluster states in case when the embedding network is randomly diluted. The dilution is carried out by randomly removing a certain fraction of links (synapses) from the fully (globally) connected network, as defined by the probability for removal p. Expectedly, at the above (c, D, τ) parameter sets we have found no modifications in the

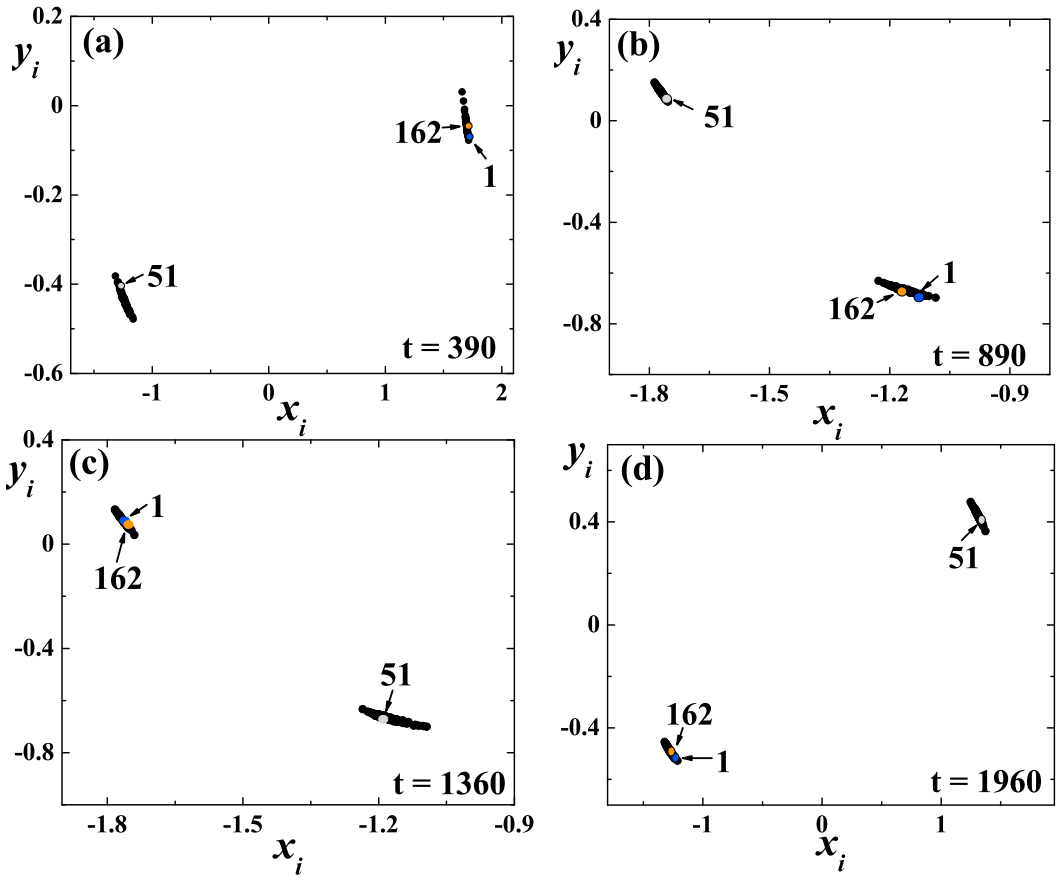

Figure 5.7: In case of the two-cluster state, evolution of the representative clouds for the distinct clusters is shown in the $x_i - y_i$ phase space. To indicate the stationary character of the cluster partition, we selected a triplet of neurons, including two arbitrary members (labeled by 1 and 162) from one cluster, and a single neuron (labeled by 51) from the other cluster. At any given moment, the neurons' respective positions, denoted by arrows, imply that there is no mixing between the clusters. The parameters are set to $(c, D, \tau) = (0.1, 0.0003, 2)$.

collective dynamics for the moderate p, say $p = 0.3$ or slightly above.

5.3.1 Asymptotic dynamics

This subsection covers the asymptotic dynamics related to the two-cluster state, both with respect to the long-term behavior and the increasing system size. On the former, one may inspect how are the representative points of neurons distributed in the $x_i - y_i$ phase space at different moments over the sufficiently long iteration period, viz. Fig. 7.8. This is helpful in demonstrating the persistence of clusters, especially their invariance to dissolution

and reconfiguration. The two representative clouds can be seen to maintain a clear separation and compactness throughout the simulation, as they should if the neurons are indeed forbidden to leave and exchange clusters. In practice, to assert the latter one may further select a triplet of neurons, where a couple belongs to the same cluster, and then show how these two are always clumped together, while the remaining neuron never has the spikes synchronized with them. This is further elaborated in Section 5.4.1, where the method of dynamical correlation coefficients is implemented.

So far, the arguments on the persistence of cluster states with increasing N have relied on the results of numerical simulations. Here we implement a method intended to probe the system dynamics in the thermodynamic limit $N \to \infty$. To this end, one introduces a type of a synchrony measure [12]

$$\chi^2(N) = \frac{\sigma_X^2}{\frac{1}{N}\sum_{i=1}^{N}\sigma_{x_i}^2}, \tag{5.4}$$

which presents the time-averaged variance of the global potential $X(t)$, $\sigma_X^2 = \langle X(t)^2\rangle_t - \langle X(t)\rangle_t^2$, normalized over the mean of the time-averaged variances of the local potentials $x_i(t)$, $\sigma_{x_i}^2 = \langle x_i(t)^2\rangle_t - \langle x_i(t)\rangle_t^2$. By the law of large numbers, for the systems of sufficient size $\chi(N)$ reads [12]

$$\chi(N) = \chi(\infty) + \frac{a}{\sqrt{N}} + O(1/N), \tag{5.5}$$

where $\chi(\infty)$ denotes the asymptotic component. Should there be genuine cluster states, the latter is expected to lie within a range between 0 and 1. The existence of the $\chi(\infty)$ term has been verified for the previously considered parameter sets, with the example for $(D, \tau) = (0.00025, 2)$ provided in Fig. 5.8. Notably, the $\chi(N)$ dependence makes it explicit that the near-asymptotic behavior sets in already about $N \approx 200$. This suggests that the implied stability of the two-cluster states in large populations cannot be affected by some mechanisms absent at small N.

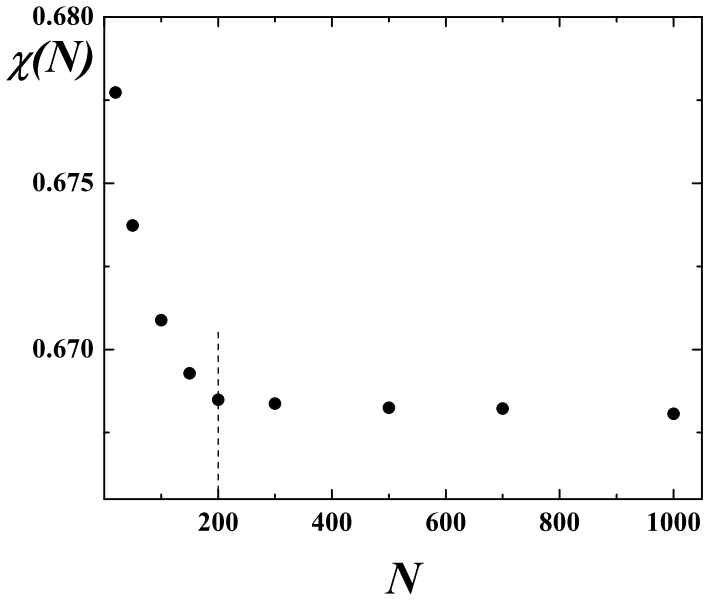

Figure 5.8: $\chi(N)$ dependence for the two-cluster state at $(c, D, \tau) = (0.1, 0.0005, 5)$. The existence of an asymptotic component $\chi(\infty) \in (0, 1)$ suggests the persistence of clustering in the thermodynamic limit, whereby the onset of the near-asymptotic behavior is found about $N \approx 200$. The latter makes it unlikely that the stability of the two-cluster states in larger populations may be altered by some mechanisms absent at smaller N.

5.4 Three-cluster state dynamics

The cluster states addressed so far can be considered stationary in terms of stability against reconfiguration, that is the changes in population partition due to neurons switching back and forth between the clusters. Adding up to a polymorphous character of the clustering phenomena, we also report on the existence of three-cluster states dynamical by nature [179], where the ability of neurons to exchange cluster survives even in the asymptotic regime. One stresses how such a scenario, encountered with further increase of D and τ about $D \approx 0.0013$ for $\tau = 10$, does not include a splay state with the clusters at any moment staggered by the $2\pi/3$ phase difference, so it should by no means be related with stochastic fluctuations around such a partition. Instead, there is a weaker cluster separation, which is best analyzed applying the methods laid out in Section 5.2, drawing a comparison to the results on the properties of binary and weighted

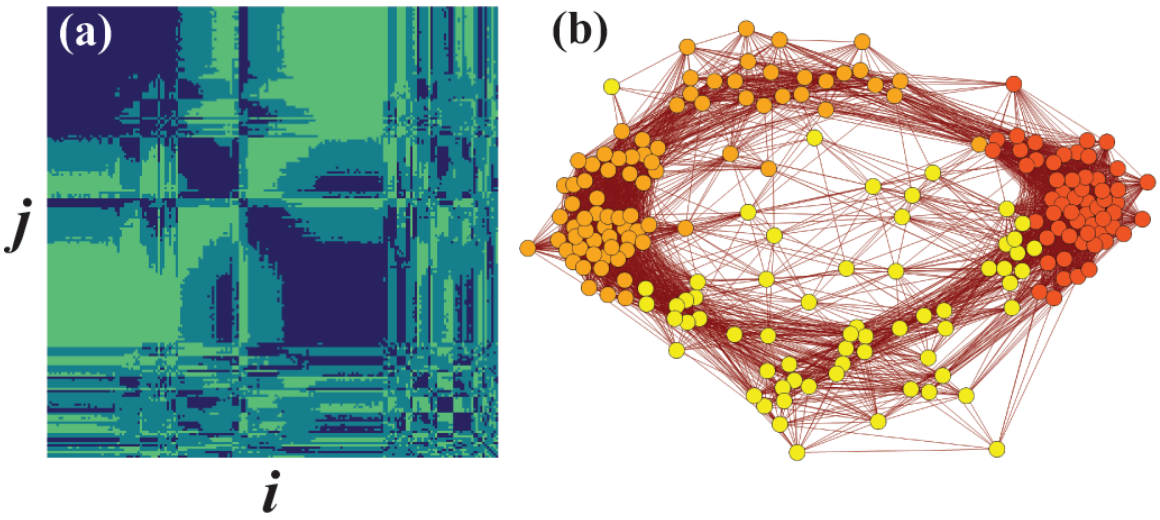

Figure 5.9: Global properties of the three-cluster state. (a) Compared to Fig. 7.2(c), the weight matrix for the weighted coherence network displays larger off-diagonal terms, indicating less clear cluster separation. (b) The binary coherence network reveals the three-cluster partition if the threshold level is raised to $\Theta \gtrsim 0.45$. The data refer to the parameter set $(c, D, \tau) = (0.1, 0.0013, 10)$.

coherence networks derived in Section 5.3.

In particular, the pairwise coherence matrix in Fig. 5.9(a) yields the inter-cluster elements much larger than those in the two-cluster state. A further indication on this is received from the corresponding binary network, whose structure now shows a strong dependence on the threshold parameter Θ, a point announced earlier on. If one chooses too low a threshold, there is insufficient resolution to distinguish between the three clusters, so one may end up with a seemingly two-cluster partition. However, any choice of Θ should be justified in a self-consistent fashion, such that no qualitative changes emerge after it is increased. In this context, it may readily be verified how a rise in Θ reveals the actual three cluster partition, viz. Fig. 5.9(b), corroborating with the findings from the coherence matrix approach.

Now let us focus on the origin and the long term behavior of the three-cluster states. In relation to the former, an important perspective lies with the local dynamics. Except for the brief episodes within the population cycle when all the units are refractory, at any given moment the three clus-

ters are roughly made up of neurons in refractory, spiking and resting (excitable) states, respectively, whereby the two latter subsets are proximal in the phase space. For this point alone, the three-cluster state may best be understood as derived from the two-cluster state instability, where the mutual entrainment fails to maintain the proper inter-cluster phase difference, giving way to noise. Moreover, the instability is self-sustained, as the stochastic effects are amplified by the very properties of the partition that has two subsets firing in close succession. Note how for any neuron participating the cluster states there are but two effective sources of noise, one explicit, embodied by the D term in the y_i subsystems, and the other implicit, due to interaction in the fast variable subsystems. On the latter, consider first the example involving the two-cluster partition. There, one finds a kind of subdivision imposed between the interaction terms, such that each neuron feels the action of its cluster co-members strongly, while the impact of the other subset amounts to noise, which is a consequence of tuning between the delay and the duration of neuron firing cycles. To some extent, this carries over to the three-cluster state. In particular, the intra-cluster interactions still provide ”periodical forcing” necessary to conserve the mutual entrainment, whereas the action of neurons from the other two clusters may be treated, apart for some zero-measure intervals due to imperfect adjustment of spiking periods relative to τ, as interaction-induced noise with zero mean values and small amplitudes. Nevertheless, the combined effects of the enhanced noise ”proper” and the ”interaction noise” can make an excitable neuron susceptible to exchanging clusters. This can take place under the scenarios of ”spike skipping” or ”premature firing”. In the former case, a neuron is denied a spike by getting caught in vicinity of the equilibrium, so that it misses out on its cluster beat. In the event of premature firing, a sufficiently large interaction term influences a neuron passed beyond the halfway of the mean interspike interval, making it escape the refractory branch of the slow manifold. Once the given unit

discharges ahead of the remaining subset co-members, there is a high likelihood for it to become assimilated into the cluster active around that time.

An intuitive perspective on the long-term behavior behind the three-cluster states may be gained by considering the features of the appropriate r_i distribution (not shown). Two points deserve special attention, both at odds with what is obtained for $(D, \tau) = (0.0005, 5)$. First, the distribution peak is around $< r_m > \approx 0.09$, the value substantially higher compared to 0.19 from the previous case, and second, the distribution has a longer tail to the right. The former is not easy to grasp, as it can hardly be attributed solely to a $D - \tau$ co-effect. In view of the very narrow D interval occupied by the three-cluster state, one may rather hypothesize a more subtle development, a putative interplay between the noise proper and the interaction-induced noise, which is not too far off the scenarios for the mixed-mode oscillations exhibited by isolated neurons subjected to additive noise in both the fast- and slow-variable subsystems. As for the longer tail of the r_i distribution, the three-cluster partition apparently exhibits a form of disorder related to the broken balance between the refractory and the spiking branches of the population at any given moment. This is likely to make the state non-generic, meant as sensitive to all kinds of parameter inhomogeneities, including the nonuniform connectivity patterns and the diversity introduced by letting b vary over the ensemble.

From the analysis of the available mechanisms by which the neurons exchange clusters, as well as the findings on the r_i distribution, it is justified to conclude that the gross-structure of the three-cluster states involves a nucleus made up of two clusters and a non-negligible fraction of ”itinerant” neurons, switching between the hard cores. This is not to say how the former are free from cluster exchange, it is only that on the average they execute considerably less jumps than the latter. An instance showing one of the itinerant neurons switching between the core clusters via the ”premature firing” scenario is provided in Fig. 5.10. Curiously enough, in spite

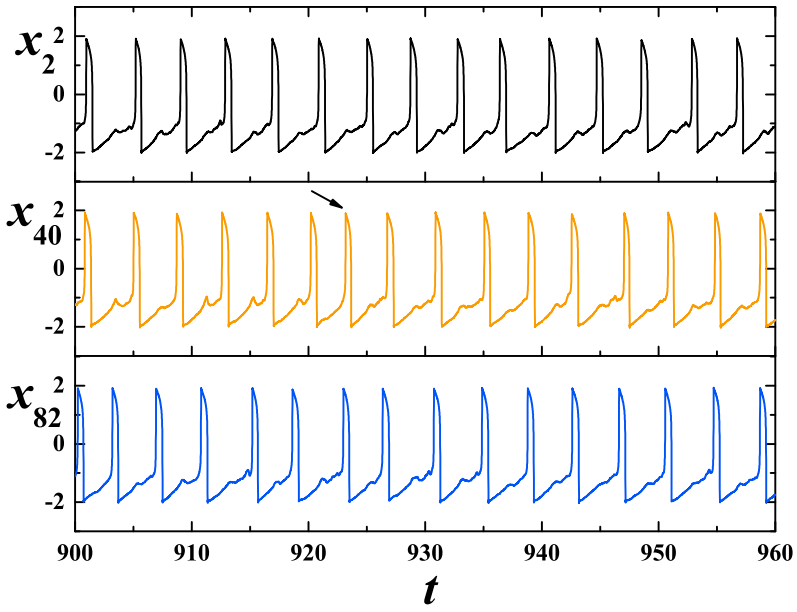

Figure 5.10: Illustration of the dynamical clustering typifying the three-cluster states. The top and bottom panels show sections from the $x_i(t)$ series for two arbitrary neurons, labeled 2 and 82, which belong to distinct core-clusters. The middle panel refers to a minority subset that exhibits switching between the cores, with its behavior characterized by the neuron 40. Within the interval $t \in [900, 922]$, spiking in the middle series is in step with the top series, whereas for $t \in [923, 960]$ it is synchronized with the firing series from the bottom panel. The moment when the neuron 40 jumps between the two core-clusters $t \approx 922$ is indicated by an arrow in the middle panel. The data are provided for $(c, D, \tau) = (0.1, 0.0013, 10)$.

of being involved in an apparently random activity, the itinerant neurons do not behave in an independent fashion, but rather maintain some degree of mutual coherence. In terms of the corresponding distribution of local jitters, the nucleus comprises the values centered around its peak, whereas the rest of the population reflects its tail. Altogether, both the intra- and the inter-cluster synchronization are intermittent by nature, but the neurons with more frequent coherent episodes are more likely to commit to synchronous firing again.

5.4.1 Dynamical correlation coefficients as means to quantify dynamical clustering

Appreciating the discussion above, we implement a method illustrative of the extent of co-activity which qualifies the neurons as members of the same cluster. Focusing on characterization of the coherent episodes, one considers the evolution of the dynamical correlation coefficients [181]

$$c_k^{ij} = \frac{< T_i T_j >_k - < T_i >< T_j >_k}{\sqrt{(< T_i^2 >_k - < T_i >_k^2)(< T_j^2 >_k - < T_j >_k^2)}}, \tag{5.6}$$

each reflecting the variation of the pairwise correlation between the respective ISIs sampled over the moving frame. The frame's length should scale with the characteristic duration of the episodes or be taken so to encompass a meaningful number of events, say in the range of tens of spikes. In Eq. 7.6, T_i and T_j denote interspike intervals for neurons i and j, whereas the angled brackets indicate averaging over the k-th frame. $c_k^{i,j}$ belong to the interval $(-1, 1)$ and highlight how well are the fluctuations in firing patterns of one neuron matched by those of the other on a low level of temporal coarse-graining. The values close to the upper (lower) boundary indicate correlated (anti-correlated) spiking, while near zero values point to the lack of correlation.

In Fig. 5.11, the objective is to clearly distinguish between the asymptotically stable two-fraction and unstable three-fraction partitions by plotting side-by-side the $c_k^{i,j}$ time dependencies which illustrate the typical inter-cluster (dotted lines) and intra-cluster (solid lines) correlations. The (i, j) couples for each partition are chosen so to keep one neuron fixed, while extracting from its own and the distinct cluster the other neuron. If large fluctuations in $c_k^{i,j}$ are encountered, one may resort to an appropriate smoothing algorithm. As expected, in Fig. 5.11(a) which refers to the two-cluster state, there is persistent correlated (anti-correlated) spiking within (between) the clusters, whereby the corresponding curves display no mix-

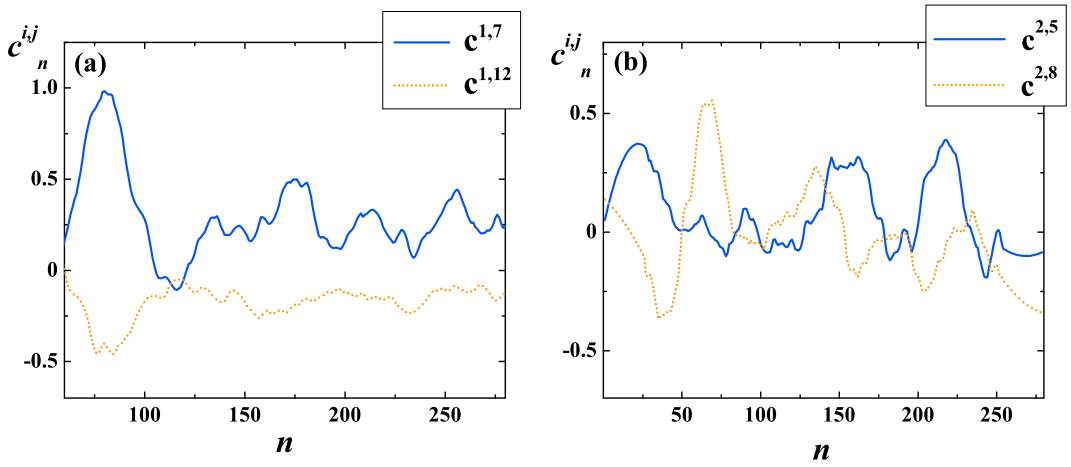

Figure 5.11: Asymptotic vs intermittent synchronization between the neurons. (a) and (b) refer to the two-cluster state at $(c, D, \tau) = (0.1, 0.0005, 5)$ and the three-cluster state for $(c, D, \tau) = (0.1, 0.0013, 10)$, respectively. In both panels are plotted the time variations of $c_k^{i,j}$ for an arbitrary pair of neurons in the same cluster (solid lines) and from the distinct clusters (dotted lines). (a) implies stable correlated (anti-correlated) spiking within (between) the subsets. The mixed picture in (b) indicates that correlated episodes occur for neurons occupying both the same cluster and the distinct ones, but are more abundant in the former case. The smoothed curves are obtained by applying the second-order Savitzky-Golay algorithm.

ing. Nevertheless, in case of the three-cluster state, see. Fig. 5.11(b), two points should be outlined. At variance with Fig. 5.11(a), not only has the difference between the dynamical correlation coefficients for the members of the same and the distinct subsets reduced, but also episodes can be found where the inter-cluster correlation exceeds the intra-cluster one. This also corroborates with the statement on how the intermittent synchronization facilitates the formation of the three-cluster state: compared to the neurons in different clusters, those within the same cluster enjoy prolonged intervals of mutually coherent spiking with rare and short interruptions.

In the following section, the aim is to lay out the unifying framework behind the clustering phenomena, drawing on the analysis of the common properties exhibited by the individual phase portraits. The interest lies with the macroscopic mechanisms that allow the cluster states to emerge and provide for the necessary robustness against perturbations.

5.5 Explanation of the clustering dynamics

Having discussed clustering from the macroscopic point of view, it is of interest to explain the way it is induced by and how it is manifested in the behavior on a microscopic level. An improved understanding on how the dynamics of neurons participating the distinct clusters is mutually adjusted can be gained by drawing an analogy between the motion of the fast variables and that of particles in a double-well potential [77]. Making a change of variables $t = \epsilon t'$, one can rewrite the equations for x_i from (7.1) in the form $dx_i = -\frac{\partial V(x_i,y_i,X)}{\partial x_i}dt'$. The V_i potentials reduced to each of the fast subsystems then read

$$V_i(x_i, y_i, X) = -\frac{1}{2}(1-c)x_i^2 + \frac{1}{12}x_i^4 + x_i y_i - c x_i X, \tag{5.7}$$

incorporating both the intrinsic and the interaction terms. It is natural to treat y_i and the delayed ensemble average $X(t-\tau)$ as parameters, with the former changing at a rate much slower than x_i. One notes how the local minima and the maximum of the given V_i coincide with the intersections that the curve $y_i - cX = const$, referring to the "dressed" slow variable makes with the fast variable nullcline. The latter's profile is, apart from the flattening effect due to interaction (the y-values at the knees are $\pm\frac{2}{3}(1-c)^{3/2}$), very much the same as that displayed in Fig. 7.1(a). In particular, of the three branches, the minima are tied to the refractory and the spiking ones, whereas the maximum is linked to the unstable branch. Within this framework, the spiking dynamics can be understood in terms of crossing the potential barrier between the two wells.

One may capture how the variations of the barrier's height and the wells' depth are reflected in the local dynamics by monitoring the simultaneous positions the arbitrary members of the distinct clusters occupy in relation to the corresponding V_i curves, see Fig. 5.12. The focus is on the changes in the form of the potential induced by the neurons visiting some

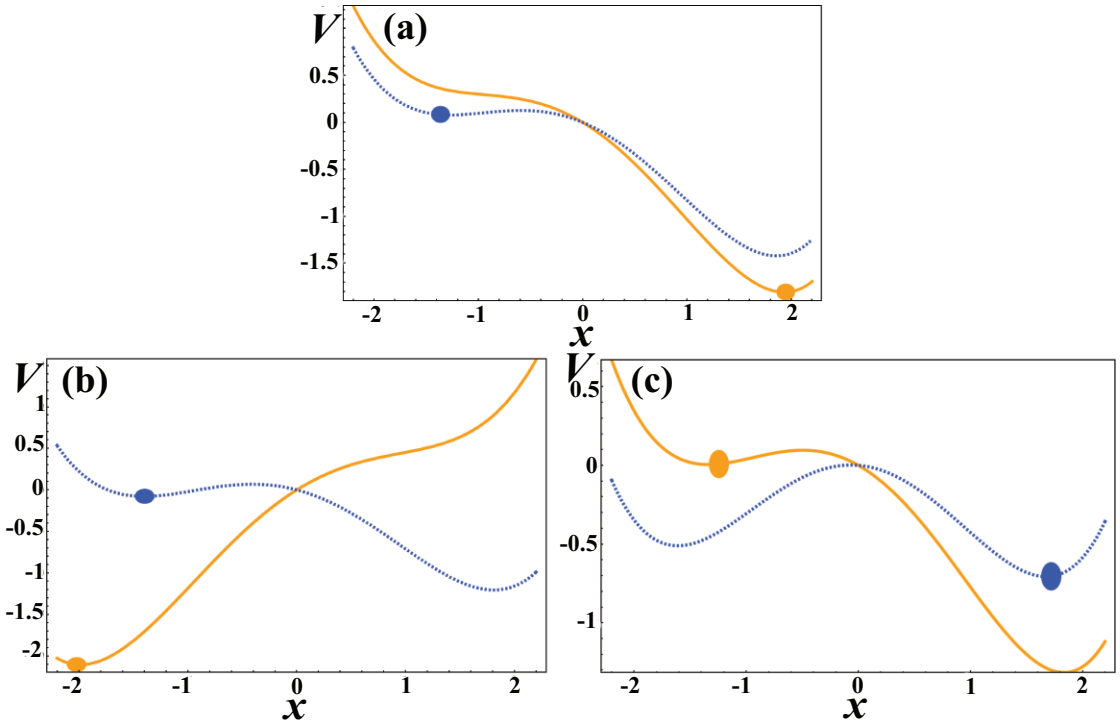

Figure 5.12: Analysis of the local dynamics in analogy to motion of particles in a double-well potential. The solid and dotted curves $V_i(x_i(t), y_i(t), X(t-\tau))$ indicate the respective potentials attributed to representative neurons from the distinct clusters. Transitions between the refractory ($x \lesssim -1$) and the spiking ($x \gtrsim 1$) branches are interpreted as hopping over the potential barrier, whose height depends on the interaction term. (a) reflects the setup where one neuron is active, and the other is refractory. The configuration in (b) shows both neurons on the refractory branch, with one having just completed a spike, whereas the other approaches the left knee. In (c) one of the neurons is trapped on the refractory branch, which constitutes a hallmark of clustering on the local level.

characteristic points along the orbit. For ease of presentation, one neuron (solid V_i curves) is selected as referential, such that the Figs. 5.12(a), 5.12(b) and 5.12(c) coincide, in the respective order, with the peak of the spike, the onset of the refractory period and the resting state approaching the left knee of the slow manifold. In the first two instances, the transition barriers are expectedly high, whilst the other neuron assumes notably less stable positions on the refractory branch. Nevertheless, the most important point concerns Fig. 5.12(c), aimed to convey the actual signature of the clustering phenomena impressed on the local dynamics. What is demonstrated amounts to a trapping effect, where the neuron nearby, but sufficiently above the left knee, faces a very low barrier. However, its po-

tential is almost, yet not quite enough to escape from the refractory to the spiking branch. In fact, it can be shown that the neuron is kept frustrated precisely due to the interaction term, which raises the barrier up on the value determined solely by y_i, enough to make the transition impossible. This type of behavior is maintained over the lower section of the refractory branch, with the net result of the spike generated later than the "barren" neuron dynamics would yield under the same conditions.

The discussion related to Fig. 5.12(c) can be appreciated by drawing a comparison between the individual phase portraits typical for neurons participating the homogeneous coherent states and the cluster states, see Figs. 5.13(a) and 5.13(b), respectively. It immediately strikes that the latter possesses a kink on the refractory branch of the slow manifold [115], which derives from the trapping effect described above. For the moment, we refer to the two-cluster state, a natural approach knowing the three-cluster state to be descended from it. Either way, the presence of the kink is the key manifestation of the self-regulation mechanism based on the D-τ co-effect which gives rise to the ensemble split into clusters and allows the established phase relationship among them to be maintained. The role of the kink consists in keeping the neurons frustrated on the refractory branch so to postpone the phase point's descent toward the left knee. This scenario conforms to a lock-and-release type of behavior, where the delayed interactions primarily give rise to the former, and the action of noise to the latter part. If a fraction of neurons were to move past the left knee while the rest lagged behind, for the convenient D and τ the kink emerges to stabilize the inter-cluster separation, simultaneously strengthening the inner cluster cohesion. The location of the kink, which depends on the parameter set, is a decisive factor for the trapping effect to succeed: it has to be placed nearby the knee of the refractory branch, where the neuron dynamics is most susceptible to perturbation, yet the sufficient distance to the equilibrium has to be maintained.

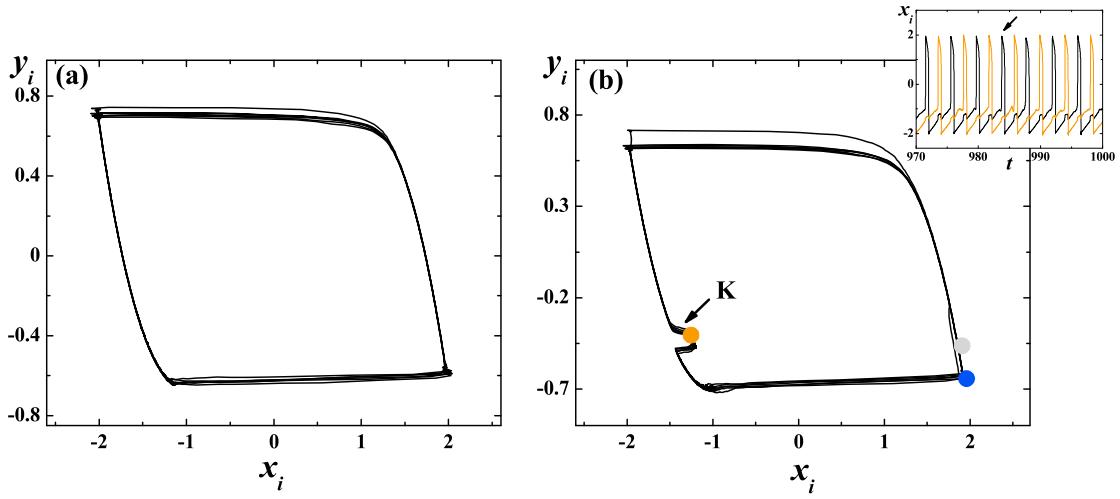

Figure 5.13: (a) and (b) display the phase portraits for the local dynamics of the homogeneous coherent states and the cluster states, respectively. The latter are distinguished by the kink K, which reflects the $D-\tau$ co-effect. The inset shows sections of $x_i(t)$ series for two arbitrary members of the distinct clusters, whereby an arrow indicates the neuron whose portrait is presented in the main frame. For an insight into the role of kink, we highlighted by bullets the respective positions of the involved neurons along the orbit at a given moment t. As a neuron lies at the kink, the other's potential is at the peak of the rising phase (farthest right bullet). In addition, at $t-\tau$, the former is located very close to the peak, which illustrates how the delay affects the adjustment between the clusters' dynamics. The parameter are set to $(c, D, \tau) = (0.1, 0.0005, 6)$ in (a) and $(c, D, \tau) = (0.1, 0.00025, 2)$ in (b).

The episode at the kink onset presents the sole section along the limit cycle where the interaction term prevails over the noise proper. Then, for a brief period, prompted by the rise in x_i the evolution of y_i gets accelerated to match the rate of change in the direction orthogonal to the slow manifold, the whole event driven by the spiking subset of the population. Note that the condition on the trapping interval duration is imposed as prerequisite to sustain the entrainment to a single frequency between the neurons. This frequency agrees with the one in a delay-free case, ensuring that the system dynamics takes on the form most resilient against small perturbations. Such a remark, combined with the established π phase difference for the two-cluster partition, implies that clustering may prefer some delay values over the others. One should recall here the earlier stated approximate formula for the clustering-resonant delays $\tau_r = T_0/2 + n * T_0$, where

T_0 stands for the period of coherent oscillations in case of $\tau = 0$. The given expression and the subdivision of interaction terms in which the ”periodical forcing” prevails over the ”implicit noise” are in fact two sides of the same coin, as forcing cannot fulfill its role unless the delay is not properly adjusted so that cluster compactness can be maintained. As for the noise, the increase of τ has to be countered by the larger D to facilitate relaxation from the kink to the slow manifold while retaining the entrainment to the proper frequency. In this context, the larger noise amplitudes may begin to manifest in a wider spread of the active subset. One can see conceptually how the enhanced delays are then required to cancel, or rather average out such an effect, instating a form of control through delayed feedback.

Building on the analysis so far, we provide an additional perspective on the dynamical instability found in the three-cluster states, viz. Sec. 5.4. Looking back at the proposed scenarios, one is seen as emerging in parallel to the kink's occurrence, and the other is tied to its collapse. In the former case, a neuron may exchange clusters by skipping to fire within its subpopulation beat, as it sticks too long in a close proximity of the equilibrium, performing a turn around the fixed point before resettling to the original limit cycle. Within the framework involving the double-well potential, the postponed firing instability unfolds via a scenario where a delayed rise in the interaction term combined with a small y_i value effectively cause an inhibitory effect. This reestablishes the barrier in lieu of the single solution on the spiking branch, setting the neuron temporarily back in the vicinity of the potential minimum on the refractory branch.

Under the alternative scenario, the neuron firing may precipitate the rest of its cluster by virtue of the interaction terms winning over the action of noise proper. This prevents the relaxation to the refractory branch of the slow manifold, so that the neuron traverses instead a smaller orbit inside the area of phase space encircled by the typical limit cycle. The effective disappearance of the kink is tied to the collapse of the V potential barrier,

the reason for it lying in that the interaction term acquires a positive value while the neuron's phase point has not yet reached the left knee. The collapse leaves the minimum at the spiking branch as the only solution, such that getting further descent terminated promotes a smaller limit cycle orbit. To put this matter into a broader perspective, one may recall the distinction between the CR and the SISR phenomena on non-interacting neurons, whose respective limit cycles exhibit a similar relationship [77]. In view of the detailed structure of the interaction terms, it may be tempting to interpret the local dynamics behind the two-cluster partition as the CR-like behavior, and the second scenario on dynamical instability as a sign of a mixed mode [79] where SISR-like phenomena step in.

Following the study on how the collective activity is reflected in that of individual neurons, the final section deals with the macroscopic dynamics from the perspective of the mean-field (MF) approximation we have derived. Two main points are introduced: first, one shows the MF model to undergo a global bifurcation for the parameter set where the exact system exhibits the onset of clustering, and second, there is further clarification on the role of noise within the D-τ interplay inducing the cluster states.

5.6 The MF model and clustering

Appreciating the all-to-all coupling scheme, one is led to develop a MF approximation to the exact model (7.1), an approach where the thermodynamic limit $N \to \infty$ on the population size enters in a natural way. In general, the MF treatment consists in reducing the original set of SDDE to a novel system of DDE in terms of cumulants or the moments of distribution describing deviations around the ensemble averages. In either case, the equation for the quantity of arbitrary order may involve a number of higher orders, leaving an issue of how to truncate the series that may appear unclosed [67]. In this sense, the cumulant method is more convenient

for it provides a plausible closure hypothesis within the Gaussian approximation, which states that the instantaneous distributions of local variables are Gaussian and that the ensemble averages at any given moment coincide with the expectation values of the appropriate distributions. If these two conditions are met, all the cumulants above second order are supposed to vanish. The detailed derivation based on these broad assumptions has been presented in Section 5.6, whereas the final result reads

$$\begin{aligned}\epsilon\frac{dX(t)}{dt} &= X(t) - X(t)^3/3 - \frac{X(t)}{2}\left\{1 - c - X(t)^2 + \sqrt{[c - 1 + X(t)^2]^2 + 4D}\right\} \\ &\quad - Y(t) + c[X(t-\tau) - X(t)], \\ \frac{dY(t)}{dt} &= X(t) + b, \end{aligned} \tag{5.8}$$

The particular form of the system (7.8) is a corollary of an observation exclusive to the problem at hand, which establishes the characteristic time scales of the second-order cumulants to be much longer than those of the first-order ones.

Though a simplification, the MF model should still reflect, at least qualitatively, the dynamical regimes of the exact system. The previously carried out analysis on local bifurcations displayed by the approximate system with respect to D and τ as control parameters [139, 143] has revealed a succession of supercritical and subcritical Hopf bifurcations under increasing delay if past the noise amplitude $D \approx 0.0025$. This is corroborated in Fig. 5.14 numerically by means of the DDE-biftool [182, 183], an adaptable package of Matlab routines suitable for handling the sets of DDE with constant delays. There is a clear interpretation on these results. The supercritical Hopf bifurcations account for the transitions between the stochastically stable fixed point and the stable limit cycle, the latter implying the existence of the parameter regions where the exact system becomes equivalent to the deterministic one. Likewise, the subcritical bifurcations suggest how introducing specific delays may put out the global coherent oscilla-

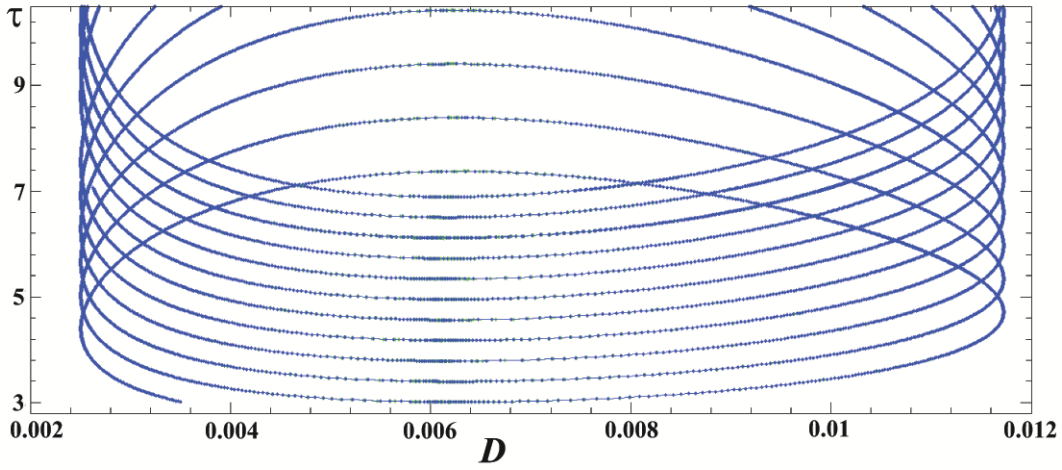

Figure 5.14: Sequence of Hopf bifurcation curves for the MF model under increasing D and τ. Though the curves can account for the transitions between the stochastically stable fixed point and the stable limit cycle, one cannot associate them with the cluster formation.

tions. Nonetheless, all the implicated noise amplitudes are $D \gtrsim 0.0025$, too far up on the values where the cluster states are seen to kick in, which makes it legitimate to rule out any of the local bifurcations of the approximate system as linked to the phenomenon.

However, an important point we pursue is that the MF model is capable of anticipating the onset of cluster states in a range of small D, c and τ. In particular, one finds the system (7.8) to undergo a global bifurcation at the parameter values around $\tau = 2, D = 0.00025, c = 0.08$. Under the given D and τ, for $c < 0.08$ there is only the equilibrium, whereas about $c \approx 0.08$ a large and a small limit cycle are born via the fold-cycle scenario. On the latter, note how the phase portrait for the MF system in Fig. 5.15(a) acquires the form reminiscent of the one for the exact system, viz. Fig. 7.5(a). The two discernable segments on the orbit are supposed to mirror the action of the subsets emerging within the actual population. This structure of the limit cycle goes unstable with increasing c and τ, in both cases suffering from the stronger impact of the interaction term. An interesting point on the MF model is that the complex-shaped limit cycle coexists with the fixed point, a behavior apparently absent in the exact sys-

tem. However, mapping the respective basins of attraction in Fig. 5.15(b) yields that the equilibrium is nested very close to their boundary, meaning it is stochastically unstable and therefore unobservable in the exact model for an arbitrarily small noise. On the particular choice of initial function for the mean-field variables X and Y, the evolution within the time interval $t \in [-\tau, 0]$ is obtained by numerically integrating the set (7.8) for $c = 0$ starting off from X_0 and Y_0. Making an analogy to the exact system, this is equivalent to assuming that all the neurons act as noninteracting elements for $t \in [-\tau, 0]$. Nonetheless, it is found that the main result on the equilibrium lying close to the boundary between its attraction basin and that of the limit cycle, also stands for other forms of the initial function.

Though the approximate system is less likely to provide accurate predictions once D and τ are enhanced, one can still gain some insight on the nature of their coaction and its influence on the dynamics of the real system. This especially refers to setups with larger τ which admit clustering. Under these conditions, the equilibrium appears as pseudo-stable in the MF dynamics, that is the limit cycle orbits remain too long nearby the fixed point, rendering the population periods longer than in the actual model, see Fig. 5.15(c). Extending the last analogy, such a behavior may be interpreted as exaggerating the likelihood for the "skip to fire" events, or in other words, overestimating the possibility to observe in the real system the minor oscillations around its fixed point. The distinct phenomena due to the lack of stochastic effects in the MF approximation can in fact pose "fortunate failures", since they might help us pinpoint the role played by the noise in the exact model. Here it is suggested how noise may be constructive in maintaining the cluster partition by keeping the neurons from mingling outside their subsets, i.e. it is assumed to suppress the excessive cluster exchange by cutting on its leading contribution from the "skip to fire" mechanism. The two discussed instances at small and moderate D and τ demonstrate that the MF approximation can be sensitive enough to

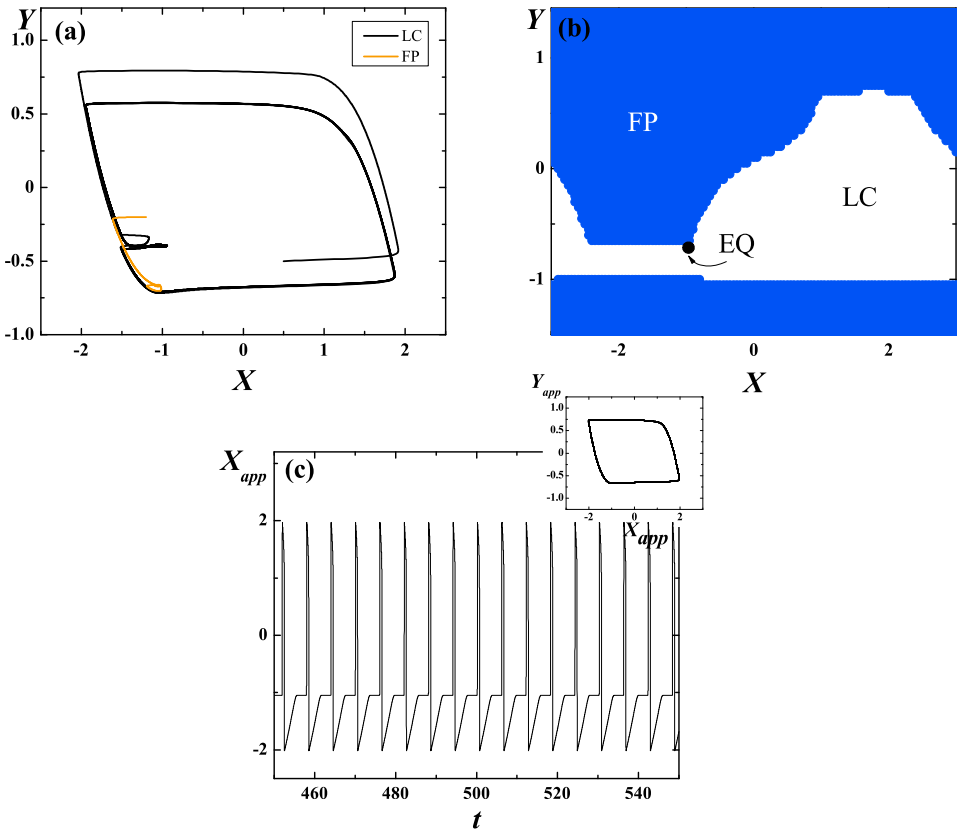

Figure 5.15: Behavior of the MF model in the parameter domains related to clustering. (a) and (b) illustrate bistability observed for $D = 0.00025, \tau = 2$ at $c = 0.1$. (a) shows the examples of trajectories converging either to the fixed point or the limit cycle, contingent on the initial conditions. In (b) are mapped the corresponding basins of attraction, with the equilibrium (EQ) found to lie very close to their boundary. (c) refers to the "fortunate failure" of the approximate model under the increased D and τ. The time series and the phase portrait are provided for $(D, \tau, c) = (0.0005, 6, 0.1)$.

account, both qualitatively and quantitatively, for the complex phenomena in the collective dynamics of the actual model. Nevertheless, in terms of reaching an explanation, its application is not a straightforward one, with the pitfalls related to establishing the proper analogies between the behaviors the given two systems display.

5.7 Chapter summary and discussion

We have studied the dynamics of a collection of stochastically perturbed Fitzhugh-Nagumo excitable units with time-delayed diffusive couplings.

In particular, our interest has lied in analyzing the spontaneous formation of clusters, whereby the neurons within each subset are synchronized, but different clusters become active at different phases of the population oscillation. Apart from discussing the means to characterize the cluster states and their dependence on the parameter set, we have gained an insight into the dynamical mechanism responsible for clustering. In conditional terms, i.e. having fixed the excitability property of neurons, the adjustment between noise intensity and time delay is found to provide the sufficient and necessary conditions that allow for the cluster states to emerge. The latter refers to the demonstrated resonant character of the clustering effect in general, rather than making a claim on the particular set of parameter values that admit clustering. No heterogeneity in the coupling scheme or the distribution of the intrinsic neuronal parameters is required for the clusters to emerge. Nevertheless, the two-cluster partition has been verified to be robust if a small disparity of these model parameters is introduced.

Several techniques have been employed to describe and understand the synchronization clustering, starting off with the methods to detect and visualize the clusters. To that end, the pairwise coherence κ_{ij} (7.2) was used. In fact, after applying a convenient transformation, the matrix κ_{ij} assumes a block-matrix form where the diagonal blocks mirror the clusters, and the off-diagonal blocks present the inter-cluster correlations. Two- and three-cluster distributions have been observed for different parameter values. Global coherence κ, obtained as the average of κ_{ij}, is used to study the dependence of the cluster formation on the parameters D, τ and c, viz. the noise intensity, time-lag and the coupling strength, respectively. In order to investigate the dynamical properties of clusters, we have considered the distribution of local jitters (7.3), turning out to be quite useful in highlighting the differences between the dynamical properties of the two- and three-cluster regimes. The long-term behavior and the asymptotic dynamics as the population size N is increased have also been discussed. On the

former, the two-cluster partition has been established as stable, whereas the internal structure of the three-cluster states has been found to involve a two-cluster nucleus and a non-negligible fraction of neurons jumping between the hard cores. The difference between the dynamical behaviors of two- and three-cluster states (stationary against the dynamical clustering) is also reflected in the dynamical correlation coefficient (7.6). Following on that, we turned to an explanation of the mechanism behind clustering, based on treating the evolution of the neuronal fast variables as if it referred to the motion of particles subjected to a double-well potential (7.7). A local manifestation of clustering is shown to be the kink formation nearby the knee of the refractory branch of the individual neuron orbit, a finding one can use to provide the qualitative explanation on the conditions necessary for the occurrence of clusters. Finally, we have demonstrated that a global fold-limit cycle bifurcation in the approximate MF model can indicate the onset of the cluster states, further elaborating on how the proper interpretation of the reasons for some of the apparently artificial behavior displayed by the MF may serve to clarify the roles played by the particular parameters in the exact system.

Numerous recent studies have revealed formation of synchronization clusters in networks of oscillators or excitable neurons [13, 21]. However, for the most part the phenomenon is seen to arise due to the locally variable parameters, viz. [184, 185] or as induced by the dynamically varying couplings, e.g. [186]. The collection of neurons studied here is completely structureless, so that the synchronization clusters are formed by the subtle interplay of noise, interaction time-delay and the excitable nature of the units. Nevertheless, at least some of the spontaneous clustering is shown to be stable under small perturbations of the local parameters and the pattern of neuron interconnections. Such resilience may be interpreted as further indicator of possible real world applications, in particular in the context of facilitating the neural encoding or improving its capacity. Most

prominently, this refers to cognitive processes of binding and segmentation. In the former instance, multiple representations of the same object may be bound into a cluster state, whereas in the latter, clustering is supposed to contribute in discriminating between the distinct perceptual entities [21, 187]. At variance with the beneficial roles, certain pathological brain rhythms linked to the epileptic seizures involve a high frequency firing of neural populations that might emerge through the interspersed action of several clusters [13]. On the formal side, it would be interesting to investigate whether the spontaneous synchronization clustering also occurs in networks of excitable systems with a different type of excitability.

Chapter 6

Mean field approximation of two coupled populations of excitable units

---

Chapter abstract The analysis on stability and bifurcations in the macroscopic dynamics exhibited by the system of two coupled large populations comprised of N stochastic excitable units each is performed by studying an approximate system, obtained by replacing each population with the corresponding mean-field model. In the exact system, one has the units within an ensemble communicating via the time-delayed linear couplings, whereas the inter-ensemble terms involve the nonlinear time-delayed interaction mediated by the appropriate global variables. The aim is to demonstrate that the bifurcations affecting the stability of the stationary state of the original system, governed by a set of $4N$ stochastic delay-differential equations for the microscopic dynamics, can accurately be reproduced by a flow containing just four deterministic delay-differential equations which describe the evolution of the mean-field based variables. In particular, the considered issues include determining the parameter domains where the stationary state is stable, the scenarios for the onset and the time-delay induced suppression of the collec-

tive mode, as well as the parameter domains admitting bistability between the equilibrium and the oscillatory state. We show how analytically tractable bifurcations occurring in the approximate model can be used to identify the characteristic mechanisms by which the stationary state is destabilized under different system configurations, like those with symmetrical or asymmetrical inter-population couplings.

The onset and mutual adjustment of collective rhythms are regarded as the dynamical paradigm for the macroscopic phenomena in a wide range of biological and inorganic systems. Such a framework has already proven indispensable for understanding the normal and pathological patterns of brain activity [12–14, 21], coordination of cellular clocks governing the circadian rhythms [11], the mechanisms regulating heartbeat [188] or lying behind certain forms of social behavior [15, 16], entrainment of electrochemical oscillators [9], as well as the dynamics of Josephson junction circuits [7] and the arrays of coupled lasers [8]. The emergence of macroscopic rhythms in ensembles of oscillating units is mediated by the synchronization based self-organization [17, 189]. The latter is often influenced or facilitated by noise on one hand [29, 57, 143, 190], while on the other hand, the interaction over the appropriate communication channels is typically susceptible to transmission delays or there may be a time lag due to the system components' latency in response to input variations [67, 136, 137, 144, 146, 147]. A pervasive idea in nonlinear dynamics is to treat an assembly exhibiting a collective mode as a macroscopic oscillator [3], which could in turn be subjected to an external drive or be exposed to a single or multiple collective rhythms from other populations. In this context, an important issue is to consider the relationship between

the ensemble's global variable and the external forcing or the relationship between the corresponding global variables.

In terms of the dynamical complexity of the observed behavior and the methods available for the analytical study, one has to make a distinction between the cases where the populations are built of self-sustained (autonomous) oscillators or the excitable units. In the former instance, it is possible to obtain a more compact description of the interacting ensembles' dynamics by applying the phase reduction techniques [25, 104, 191–193]. Given that the phase cannot be attributed to the system residing at the equilibrium, excitable populations are not amenable to such methods. Nonetheless, on the level of elementary behavior associated with the macroscopic variables, populations consisting of excitable or self-oscillating units undergo qualitatively similar forms of dynamics. In particular, the ensuing collective modes may synchronize [30, 31], become phase-locked or get suppressed by the action of the coupling delay (delay-induced amplitude death) [1]. Beyond such simple cases, there are more complex forms of collective behavior tied exclusively to populations of interacting oscillators. A few prominent examples include the self-organized quasiperiodicity [3] and the partially synchronous chimaera states [45, 128], which have been found to emerge in systems of identical phase oscillators under the action of the external forcing or by coupling to another population, respectively. The former regime is characterized by the frequency of the collective mode being distinct from that of the single elements, while the other involves a broken symmetry between the dynamics of two interacting populations.

In this study, the focus lies with the two delay-coupled populations of identical excitable units modeled by the Fitzhugh-Nagumo elements. The behavior of the latter is representative for the type II excitability [75], which in contrast to type I, lacks a sharp threshold in a sense that the amplitude of the response depends continuously on the size of the applied

stimulus. Though the considered framework is quite general, the basic motivation admittedly draws from the observations on neuronal assemblies, with the adopted model of local activity typically invoked in such a context. The analysis of the underlying system dynamics may be approached from two different angles. For one, a numerical study can be carried out to look for the states of the increasing dynamical complexity. Instead, we take on a strategy that consists in examining how well is the behavior of the exact system matched by that of the coupled mean-field (MF) systems, having derived the MF model as an approximation for the activity of a single ensemble. The concept aims to fully exploit the analogy between the assemblies and the macroscopic oscillators, such that the original set of equations for the microscopic dynamics is reduced to a flow which describes the evolution of the global variables, incorporating the cross-population interaction in a natural way. An important ingredient for the setup is that both the intra- and the cross-population coupling terms include the transmission delays. Note that the layout with two populations may constitute a paradigm, or rather serve as a nucleus for the "network of networks" [31, 128, 194], which can be realized as a hierarchy of multiple networks, or it could be thought of as an idealization for a single network with a strong modular structure and a large number of elements in each community (subnetwork). Both configurations are common in biological systems [31], ranging from the cellular level to the distributed anatomical areas of the brain, and also encompassing the populations of cells responsible for the rhythmic activity in heart, kidney, pancreas, to name but a few. As for the comparison with the MF model, the attempts at providing a reduced description instead of using the complete set of equations for each and every population constituent, have a particularly long history within the neuroscience [67, 103, 195–197]. Apart for the gains on the modeling side, they have initially been instigated by the finding that the EEG and MEG recordings may be linked to an average behavior, viz. the massively

summed action potentials emitted within the strongly coupled, but remote cortical areas [135, 197]. Though the given approach inevitably includes simplifying assumptions that eventually constrain the repertoire of possible system behaviors just to periodic motion, some of the realism may readily be sacrificed for a more parsimonious representation if the emergence of the collective mode and the related dynamics are reproduced with sufficient fidelity.

So far, the MF models have proven at least partially successful when handling the isolated population dynamics [5, 198, 199], but have rarely considered the scenarios with combined presence of noise and coupling delay [138, 139, 195]. Nonetheless, the rigorous results on interacting ensembles, especially those made up of excitable units, are still lacking. Hence, the key set of issues addressed in this study amounts to identifying the conditions for the stability of the stationary state, the onset of the collective mode, bistability between the equilibrium and the oscillation state, as well as the time-delay induced suppression of the collective mode. One notes that the applied term ”collective mode” here implies the existence of a limit cycle for the total system of interacting populations. Though the intention is not, or rather cannot be to account for any experimental observation of such phenomena, some elementary comparison can still be drawn. For instance, the notion that the emergence and the synchronization properties of collective rhythms arising in the macroscopic neural populations are critically influenced by the coupling strength and the interaction delay [135] has its clear analogue in the results we arrive at. Consistent with the stated objectives, the study of the approximate system is concerned with the local bifurcation analysis, carried out analytically and corroborated by the numerical means, to determine *i*) the parameter domains of stability of the steady states, *ii*) the scenarios for the emergence or the suppression of the collective mode, and *iii*) the parameter domains admitting the bistability between the equilibrium and the oscillatory state.

The chapter is organized as follows. In Section 6.1, the details of the exact model of interacting populations are laid out in parallel with the derivation of its MF counterpart. Section 6.2 is focused on the local bifurcation analysis of the approximate model, providing for the analytical results. In Section 6.3, we demonstrate that the approximation based on two coupled MF systems is able to accurately predict the behavior of the exact system in terms of the stability of the equilibrium, as well as the onset and the suppression of the collective mode. It is also pointed out how different system configurations affect the scenarios for the emergence of the oscillatory state and influence the parameter domains supporting its coexistence with the equilibrium. The results are briefly summarized and discussed in the concluding section.

6.1 Background on the exact model and derivation of its MF counterpart

6.1.1 Details of the exact model

Each population comprises a collection of N identical Fitzhugh-Nagumo elements [75, 125, 126], whose dynamics is given by

$$\begin{aligned}
\epsilon dx_{i,1} &= (x_{i,1} - x_{i,1}^3/3 - y_{i,1} + I_1)dt + \frac{g_{in,1}}{N}\sum_{j=1}^{N}[x_{j,1}(t-\tau_{in,1}) - x_{i,1}(t)]dt \\
&\quad + g_{c,1}\arctan[X_2(t-\tau_{c,1}) + b_2]dt, \\
dy_{i,1} &= (x_{i,1} + b_1)dt + \sqrt{2D_1}dW_{i,1} \\
\epsilon dx_{i,2} &= (x_{i,2} - x_{i,2}^3/3 - y_{i,2} + I_2)dt + \frac{g_{in,2}}{N}\sum_{j=1}^{N}[x_{j,2}(t-\tau_{in,2}) - x_{i,2}(t)]dt \\
&\quad + g_{c,2}\arctan[X_1(t-\tau_{c,2}) + b_1]dt, \\
dy_{i,2} &= (x_{i,2} + b_2)dt + \sqrt{2D_2}dW_{i,2},
\end{aligned} \tag{6.1}$$

where the subscripts $k = 1, 2$ specify the population, indices $i = 1, ..N$ denote a particular unit within the population, and $X_k = (1/N) \sum_{i=1}^{N} x_{i,k}$ stand for the macroscopic variables that typify the global population behavior. The small parameter $\epsilon = 0.01$ imposes a wide separation between the characteristic time scales for the evolution of $x_{i,k}$ and $y_{i,k}$. In the context of neuronal activity the set of fast variables embodies the membrane potentials, whereas the slow-variable set is supposed to account for the gross kinetics of the potassium ion-gating channels. In the absence of an external stimulation $I_1 = I_2 = 0$ applies. The impact of a noisy background activity is reflected by the $\sqrt{2D}dW_i$ terms, which represent the stochastic increments of the independent Wiener processes specified by the noise amplitude D, expectation values $\langle dW_i \rangle = 0$ and the correlations that satisfy $\langle dW_i dW_j \rangle = \delta_{ij} dt$ for each population.

Owing to the system configuration, the local dynamics involves two types of interactions, each characterized by the coupling strength and the delay. The respective parameters associated with the intra-ensemble terms are $g_{in,k}$ and $\tau_{in,k}$, and those related to the cross-population terms are $g_{c,k}$ and $\tau_{c,k}$. Within the populations, the elements communicate via the simple linear (diffusive) couplings, such that τ_{in} may account for the transmission delays due to finite rate of signal propagation or the latency in unit responses. Given the objectives stated in the Introduction, it is not unjustified to make use of some simplifying assumptions, like the all-to-all pattern of interconnections and the uniformity of coupling strengths inside the ensembles, which are the abstractions often invoked in the relevant literature [27, 127]. As for the cross-population interactions, at the current stage no particular model is considered to be preferred over the others. However, we make use of an analogy to neural systems by noting how a variety of models display a common feature. In particular, the evoked postsynaptic potentials can be expressed in a symbolical form $h = s \otimes m$, where m refers to an average density of presynaptic input arriving from the

transmitter population, and s presents the threshold-like response of the neurons of the receiving population [135]. Adhering to this concept, the output of the transmitter population is integrated by the macroscopic variables $X_k = (1/N)\sum_{i=1}^{N} x_{i,k}$, which reflect the global behavior in a sense that the better the synchronization among the constituent elements, the larger the amplitudes of X_k. In terms of the nonlinear threshold function, there is a degree of arbitrariness, so the arctan form applied here is as good a choice as any. Unlike the interactions within the populations, which are characterized by the specific strengths per link, the inter-population terms involve the cumulative strengths, consistent with the idea of viewing each population as a single macroscopic oscillator. The bidirectional couplings between the ensembles, being either symmetrical or asymmetrical, may be important from the aspect of neuroscience, given that the brain connectivity patterns are known to exhibit a large portion of reciprocal interactions [197]. Note that the parameters b_k, assumed to be uniform within each population, appear in (7.1) in two different contexts, one related to the single unit dynamics, and the other associated with the cross-population coupling. On the former, b_k plays the key role in modifying the unit's excitability. Given an isolated unit in the noiseless case, it is known that the condition $|b_k| = 1$ determines the Hopf bifurcation threshold, above which the system possesses a unique equilibrium, whereas below it one finds a limit cycle [77, 79]. Setting b_k slightly above 1, the population elements are poised close to the Hopf threshold. This gives rise to excitable behavior, meaning that an adequate stimulation, be it by the noise or the interaction terms, may evoke large transients in the phase space before the orbit converges back to the rest state. Here we keep the discussion general by allowing for $b_1 \neq b_2$, whereas the results in Section 6.3 are provided for $b_1 = b_2 = 1.05$. The role of b_k in the cross-population coupling terms is explained as follows. First note that the x-coordinate of equilibrium of each element within a population is given by $x_{i,k} = -b_k$, as implied by the

equations for $y_{i,k}$. Consequently, for the equilibrium of the system of global variables holds $X_{k,EQ} = -b_k$. Then, the argument of the inter-population coupling is defined in the form $X_k - X_{k,EQ} = X_k + b_k$, so that the impact of the global state X_k is felt stronger if it lies further away from the equilibrium.

6.1.2 Note on how the MF model is obtained

Here we only make a few brief remarks on how the appropriate MF model is obtained, given that the procedure leans almost entirely on what has already been laid out in 5.6. This is so because the cross-population coupling terms involve only the average dynamics of the respective transmitter populations. In terms of building the approximate system, the latter implies a two step derivation, such that the focus first lies with the internal dynamics of the ensembles, treating them temporarily as if they were independent, whereas the inter-population interaction is included in the second step. In particular, continuing from (2.17), which finalizes the first step, the MF approximation for the dynamics of the two interacting populations is completed by taking into account the cross-population terms, arriving at the

following set of four equations

$$\begin{aligned}
\epsilon\frac{dm_{x,1}(t)}{dt} &= m_{x,1}(t) - \frac{m_{x,1}(t)^3}{3} - \frac{m_{x,1}(t)}{2}(1 - g_{in,1} - \\
&\quad m_{x,1}(t)^2 + \sqrt{(g_{in,1} - 1 + m_{x,1}(t)^2)^2 + 4D_1}) - \\
&\quad m_{y,1}(t) + g_{in,1}(m_{x,1}(t - \tau_{in,1}) - m_{x,1}(t)) + \\
&\quad g_{c,1}\arctan(m_{x,2}(t - \tau_{c,1}) + b_2) \\
\frac{dm_{y,1}(t)}{dt} &= m_{x,1}(t) + b_1 \\
\epsilon\frac{dm_{x,2}(t)}{dt} &= m_{x,2}(t) - \frac{m_{x,2}(t)^3}{3} - \frac{m_{x,1}(t)}{2}(1 - g_{in,2} - \\
&\quad m_{x,2}(t)^2 + \sqrt{(g_{in,2} - 1 + m_{x,2}(t)^2)^2 + 4D_2}) - \\
&\quad m_{y,2}(t) + g_{in,2}(m_{x,2}(t - \tau_{in,2}) - m_{x,2}(t)) + \\
&\quad g_{c,2}\arctan(m_{x,1}(t - \tau_{c,2}) + b_1) \\
\frac{dm_{y,2}(t)}{dt} &= m_{x,2}(t) + b_2
\end{aligned} \tag{6.2}$$

Note that the adopted form of the MF system describing a single population activity incorporates the additional adiabatic-like approximation already explained in Chapter 2, since the intention is to construct a model that is fully tractable analytically. As to be expected, for $D_1 = D_2 = 0$, the obtained system strongly resembles the case of two interacting Fitzhugh-Nagumo elements subjected to delayed feedback.

Before proceeding to the main results, several brief remarks on the applied numerical integration schemes are in order. The time series for both the exact and the approximate models are obtained by implementing the Euler method with the fixed time step $\Delta t = 0.005$ in the former, and $\Delta t = 0.01$ in the latter case, having verified that no changes occur for the smaller Δt. Also, on either occasion, we have adopted the standard and physically plausible initial functions, based on the assumption of the units evolving independently within the time interval $t \in [-\tau_{min}, 0]$, where $\tau_{min} = min\{\tau_{in,1}, \tau_{in,2}, \tau_{c,1}, \tau_{c,2}\}$. This effectively amounts to integrating the

systems (7.1) and (7.8) by disregarding any interaction for $t \in [-\tau_{min}, 0]$, with the initial conditions in each instance taken in the vicinity of the fixed point. The results for the exact model refer to populations made up of $N = 200$ elements, but have been verified to persist if the larger assemblies are considered.

6.2 Analytical results of the local bifurcation analysis of the approximate system

In the two following sections, we first provide the details of the local bifurcation analysis performed on the approximate system and then examine whether and how well do these results match the behavior of the exact system, whereby the latter dynamics is represented by the typical sample paths obtained from numerical integration of (7.1) for the sufficiently large N with $D_1, D_2 \neq 0$. On the first part, the analysis covers the stability of the attractor states for the total system of coupled populations, such that both of them are either found lying in the equilibrium or exhibiting oscillations. The main focus is on the stability of the fixed point and its destabilization under variation of the cross-population coupling strengths and delays. Apart for the onset of the oscillatory state, it is also considered how the coherent rhythms may become suppressed, this primarily attributed to the action of the inter-ensemble time lags. As a final matter, we demonstrate the existence of the parameter domains admitting the bistable regime, where the stationary and the oscillatory state coexist. Altogether, an inference confirmed later on is that the MF approximation can capture the behavior of the exact system much better if the collective dynamics is such that the deterministic component, controlled by the coupling strength and time delay, prevails over the stochastic component. The points enumerated above exhaust the corpus of problems that may approximately be treated by the local bifurcation theory, in a sense of explaining the qualita-

tive changes arising in the system's asymptotic dynamics due to parameter variation. Outside the scope remain the more complex phenomena occurring for larger D-s and τ-s, which could cause the behavior of single units within the populations to become substantially stratified. Such issues would fall under the notion of stochastic bifurcations [134], meaning that one should consider how the parameter modification influences the changes of the respective stationary distributions of the local variables.

Since we discuss the scenarios with symmetrical and asymmetrical cross-population couplings, as well as the setups where the inherent ensemble dynamics is the same or distinct, the analytical results of the local bifurcation analysis on the system of interacting MF models are presented in most general terms with respect to the system parameters. First, it is established that the system (7.8) possesses a unique equilibrium given by

$$m_{x,k} = -b_k; m_{y,k} = \frac{b_k}{2}[1 + \frac{b_k^2}{3} + g_{in,k} - \sqrt{(g_{in,k} - 1 + b_k^2)^2 + 4D_k}] \quad (6.3)$$

with $k = 1, 2$. The local stability of (7.9) depends on the roots of the characteristic equation of the system (7.8). To obtain the latter, one linearizes (7.8) around the equilibrium, assuming that the deviations are of the form $\delta m_{x,k}(t) = A_k e^{\lambda t}, \delta m_{y,k}(t) = B_k e^{\lambda t}$ and $\delta m_{x,k}(t - \tau_{in,k}) = A_k e^{\lambda(t-\tau_{in,k})}$. This results in a set of algebraic equations for the coefficients A_k and B_k, which has a nontrivial solution only if

$$\Delta_1(\lambda)\Delta_2(\lambda) - \lambda^2 g_{c,1} g_{c,2} e^{-\lambda(\tau_{c,1}+\tau_{c,2})} = 0 \quad (6.4)$$

is fulfilled, where $\Delta_k(\lambda) = -\lambda F_k + \epsilon\lambda^2 - g_{in,k}\lambda e^{-\lambda\tau_{in,k}} + 1$ with $F_k = F_k(g_{in,k}, b_k, D_k)$. The condition (7.10) poses the desired characteristic equation, whose being transcendental reflects the presence of (multiple) time delays in (7.8). Though (7.10) has an infinite number of roots, it is well known how there may be only a finite number of exceptional roots equal to zero or with a zero real part [200, 200–202]. One recalls that tangent to the subspace

spanned by the associated eigenvectors lies the center manifold [203, 204], where the qualitative features of the system's dynamics, such as the local stability, are contingent on the nonlinear terms.

Bifurcations of the stationary state take place for the parameter values where the roots of (7.10) cross the imaginary axis. Given that Eq. (7.10) does not admit the possibility $\lambda = 0$, we look for the pure imaginary roots of the form $\lambda = \imath\omega$, adopting ω to be real and positive. Substituting for λ in (7.10), one obtains

$$\begin{aligned}
&[-\imath\omega(F_1 - \imath\epsilon\omega + g_{in,1}(\cos\omega\tau_{in,1} - \imath\sin\omega\tau_{in,1})) + 1]\times \\
&[-\imath\omega(F_2 - \imath\epsilon\omega + g_{in,2}(\cos\omega\tau_{in,2} - \imath\sin\omega\tau_{in,2})) + 1]+ \\
&\omega^2 g_{c,1}g_{c,2}(\cos(\omega(\tau_{c,1}+\tau_{c,2})) - \imath\sin(\omega(\tau_{c,1}+\tau_{c,2}))) = 0
\end{aligned} \tag{6.5}$$

which, after equating both the real and the imaginary parts with zero, provides for the implicit relations of ω and the system parameters

$$\begin{aligned}
-\omega^2 P_1P_2 + Q_1Q_2 &= -\omega^2 g_{c,1}g_{c,2}\cos(\omega(\tau_{c,1}+\tau_{c,2})) \\
\omega P_1Q_2 + \omega P_2Q_1 &= \omega^2 g_{c,1}g_{c,2}\sin(\omega(\tau_{c,1}+\tau_{c,2})),
\end{aligned} \tag{6.6}$$

where

$$\begin{aligned}
P_k &= F_k + g_{in,k}\cos(\omega\tau_{in,k}) \\
Q_k &= \epsilon\omega^2 + g_{in,k}\omega\sin(\omega\tau_{in,k}) - 1
\end{aligned} \tag{6.7}$$

applies for $k = 1, 2$. Squaring and adding the relations (6.6), one arrives at

$$(\omega^2 P_1P_2 - Q_1Q_2)^2 + \omega^2(P_1Q_2 + P_2Q_1)^2 = \omega^4 g_{c,1}^2 g_{c,2}^2, \tag{6.8}$$

which can be used to express the cross-population coupling strengths in terms of ω, while keeping the values for the subset of the intrinsic parameters $g_{in,k}, \tau_{in,k}, b_k$ and D_k fixed. Obtained in a similar fashion, the analogous result for the critical cross-population coupling delays may be written in

the compact form

$$\tau_{c,1} + \tau_{c,2} = \frac{1}{\omega} \arctan\left(\frac{\omega P_1 Q_2 + \omega P_2 Q_1}{\omega^2 P_1 P_2 - Q_1 Q_2}\right). \tag{6.9}$$

The last two equations combined define the curves in the appropriate delay-strength parameter plane. Bear in mind that Eq. (6.9) actually defines multiple branches of the Hopf bifurcation curves, these given by $\tau_{c,1} + \tau_{c,2} + j\pi$, where $j = 0, 1, 2....$ Naturally, the above relations further simplify once the inter-ensemble couplings are taken to be symmetrical and/or the populations' intrinsic parameters are assumed to be identical. Note that the expressions such as these could not be obtained if we were to retain the initial MF model (7.7) containing the full dynamics of the second order cumulants. As for the type of bifurcations whose location is indicated by (6.9), the very form of the solution adopted for the characteristic equation is consistent with the Hopf bifurcations, though a rigorous proof would require one to verify whether the conditions on non-hyperbolicity, transversality and genericity are satisfied [75, 201, 202, 204]. Without entering into unnecessary details, it suffices to say that the system (7.8) admits both the supercritical and subcritical Hopf bifurcations, whereby the former (latter) result in the creation of a stable (unstable) limit cycle. In addition, recall that either of these types can be direct or inverse [203], depending on whether an unstable two-dimensional manifold for the fixed point (7.8) appears or vanishes when crossing the bifurcation curve, respectively, having the fixed point unfold on the unstable or the stable side. The results derived analytically are corroborated numerically by means of the DDE-biftool [182, 183], an adaptable package of Matlab routines suitable for handling the sets of DDE with constant delays.

6.3 Qualitative comparison between the dynamics of the exact and the approximate system

For the systematic study, we first consider the layout with two populations made up of independent excitable elements ($g_{in,1} = g_{in,2} = 0$) subjected to a common, comparably small noise ($D_1 = D_2 = 0.0001$), whereby the cross-population coupling terms are taken to be symmetrical, so one may introduce $g_{c,1} = g_{c,2} = g_c$ and $\tau_{c,1} = \tau_{c,2} = \tau_c$. The parameters are such that for $g_c = 0$, the populations exhibit the asymptotically (stochastically) stable equilibrium in the MF (exact) model. Though it appears marginal at first sight, the described setup is still important, since the MF model is here strongly indicated to match the behavior of the real system. In a sense, this scenario is reminiscent of a null-hypothesis, given that the stated parameters are fully compliant with the nominal conditions for the validity of the MF approximation. One would further expect to gain some insight into the phenomena occurring for the more complex system configurations, or may at least obtain a reference point to isolate the effects of certain parameters, such as g_{in} or τ_{in}. In the remainder, the bifurcation diagrams are accompanied by the close-up views focused on the most relevant parameter domains, having those referred to in the text indicated by the representative symbols. Also, to distinguish between the different bifurcation curves, each is denoted by two types of indices. The $+/-$ sign specifies whether the curves coincide with the direct or inverse bifurcations, respectively, while the numerical index points to the order in which the given branches are encountered as the inter-population coupling delay is increased.

From the bifurcation diagram in Fig. 7.1(a), a major point concerns the prediction on the existence of the critical strength g_0 for the instantaneous couplings ($\tau_c = 0$), where the stationary state loses stability. Figure 7.1(b) presents a zoom in of Fig. 7.1(a), focussed on the parameter region where equilibrium changes stability. In particular, for $g_c < g_0$, viz. the open circle

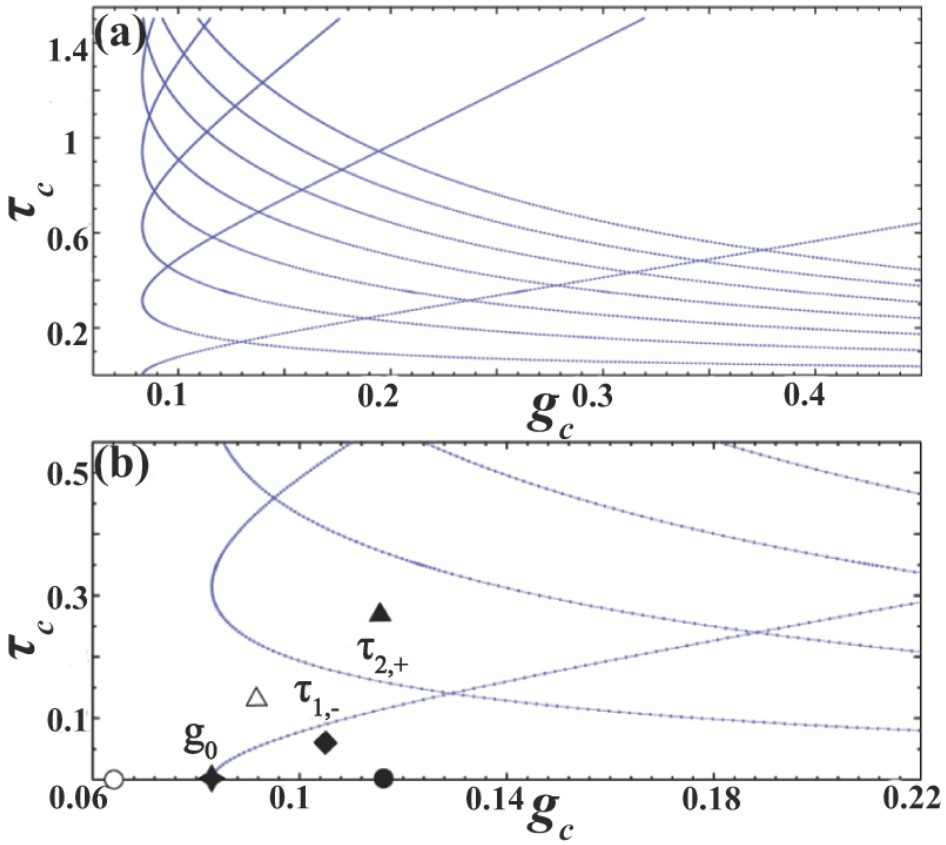

Figure 6.1: First few branches of the Hopf bifurcation curves $\tau_c(g_c)$ for the MF based approximation of the system of two symmetrically coupled ($g_{c,1} = g_{c,2} = g_c, \tau_{c,1} = \tau_{c,2} = \tau_c$) populations, each made up of noninteracting units ($g_{in,1} = g_{in,2} = 0$). In (b) is shown the enlarged section of (a), where the equilibrium changes stability. The equilibrium is destabilized via the supercritical Hopf bifurcation, but the form of the collective mode is found to be influenced by the interplay with the global fold-cycle bifurcation. All the units are subjected to noise of the amplitude $D = 0.0001$.

in Fig. 7.1(b), the equilibrium is stable, whereas for $g_c > g_0$ (solid circle) there is only the oscillatory state. The bifurcation scenario coincides with the direct supercritical Hopf bifurcation, and the numerical simulations imply that the unstable manifold for the equilibrium $m_{x,1} = m_{x,2} = m_x$ and $m_{y,1} = m_{y,2} = m_y$ around $g_c = g_0$ supports the oscillations in-phase, this being an example of synchronization between the units due to a common input. By the term "oscillations in-phase", it is meant that the MF approximation indicates a solution with the exact synchronization between the global variables, which is stochastically perturbed in the exact system. What is described applies not only for $\tau_c = 0$, but also holds in any instance

when the curve $\tau_{1,-}$ is crossed in the direction of increasing g_c with τ_c kept fixed. However, note that there is an additional subtlety to this transition derived from an interplay with the fold-cycle bifurcation, a global event which cannot be accounted for by the present type of analysis. Such an interplay is reflected in the form of the collective mode exhibited by the system. In this context, one may identify four distinct domains of g_c values, characterized by the stable solutions of the system's dynamics. The latter are illustrated in Fig. 7.2 by the corresponding $m_x(t)$ series, demonstrating the changes of the attractors with increasing g_c as follows. For the sufficiently small g_c, the equilibrium is the unique stable solution, see Fig. 7.2(a), such that any excitation eventually dies out. Then, for $g_c \approx 0.055$, the system undergoes a global fold-cycle bifurcation, which gives rise to an unstable and a large stable limit cycle. This points to an interval $g_c < g_0$ where the stationary and the oscillatory state coexist, viz. Fig. 7.2(b), with their attraction basins separated by the unstable limit cycle. Above g_0, the incipient limit cycle born via the Hopf bifurcation emerges around the former position of the equilibrium. The large limit cycle remains unaffected by the local bifurcation, so that there exists a narrow g_c interval around $\tau_{1,-}$ corresponding to a bistable regime with a small and a large amplitude limit cycle, viz. the solid diamond in Fig. 7.1(b). The two distinct limit cycles are illustrated by the time series in Fig. 7.2(c). Note that the described bistability may be difficult to observe in the exact system due to sensitivity of the incipient cycle to stochastic perturbation, as even the very small noise amplitudes can be sufficient to force the ensuing orbits away from its neighborhood. Nonetheless, it also turns out that the incipient cycle cannot fully grow with the supercriticality because it is enclosed by the unstable limit cycle created in the global bifurcation. This implies that with increasing g_c, there is a point where the stable cycle of small amplitude and the unstable limit cycle eventually collide and disappear in an inverse fold-cycle bifurcation. Therefore, for $g_c >> g_0$, all the trajectories are drawn to

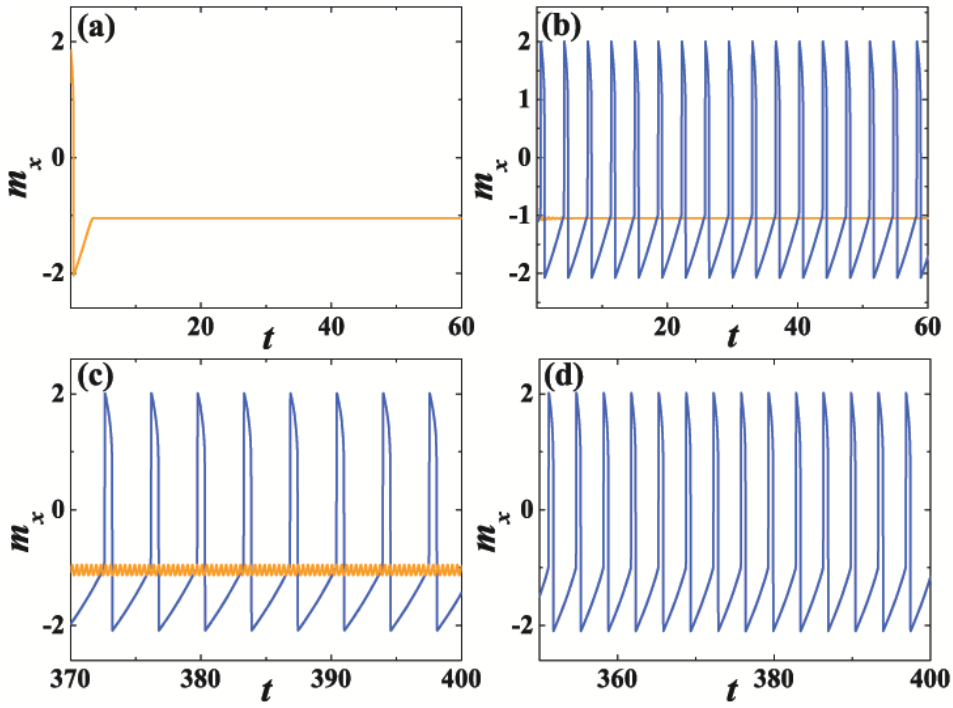

Figure 6.2: Time series $m_x(t)$ illustrating four characteristic types of stable solutions exhibited by the setup analyzed in Fig. 7.1 under increasing g_c at $\tau_c = 0$. Moving from (a) to (d), g_c assumes values $g_c = 0.05$, $g_c = 0.07$, $g_c = 0.083$ and $g_c = 0.1$, respectively. (a) For $g_c << g_0$, the unique attractor of the system is the fixed point. (b) In the intermediate region, the global fold-cycle bifurcation gives rise to a large stable limit cycle, which coexists with the stable equilibrium. The corresponding series are indicated by the blue (dark grey) and orange (light grey) lines, respectively. (c) In a relatively narrow interval around $g_c \gtrsim g_0$, the large limit cycle born via global bifurcation coexists with the incipient (small amplitude) cycle from the Hopf bifurcation. The $m_x(t)$ series corresponding to the former is shown by the blue (dark grey) line, and the latter by the orange (light grey) one. (d) Following an inverse fold-cycle bifurcation, where the incipient cycle annihilates with the unstable one, the sole attractor of the system is the large limit cycle, first seen in (b).

the large limit cycle, derived from the global bifurcation. The $m_x(t)$ series typical for this g_c domain is shown in Fig. 7.2(d).

To proceed with, we consider the effects of increasing τ_c under fixed coupling strength $g_c > g_0$. Crossing the first bifurcation curve from below $\tau_c > \tau_{1,-}$, viz. the domain indicated by an open triangle in Fig. 7.1(b), the equilibrium is seen to regain stability via the inverse supercritical Hopf bifurcation. Given the analogy of the underlying mechanisms, this could have been interpreted as a genuine example of the delay-induced amplitude death, if there were not for the large limit cycle which is unaffected

by the local bifurcation. Instead, this stability domain is characterized by the coexistence between the stationary and the oscillatory state. Nonetheless, enhancing the delay above $\tau_{2,+}$ gives rise to a region of instability, represented by the solid triangle in Fig. 7.1(b), where one encounters only the two populations oscillating in phase. Such an outcome is due to a supercritical Hopf bifurcation, which is reflected by the equilibrium gaining an unstable plane. Note that the analysis cannot extend to larger delays, since the underlying phenomena do not fall within the framework of the current study. It should be emphasized that the oscillation frequency of the MF model has been verified to match the one of the exact system almost perfectly. This point applies for two parameter domains highlighted by the solid circle and the solid triangle in Fig. 7.1(b). Under $\tau_{1,-}$, the respective oscillation period of the approximate model is $T_{\bullet,MF} = 3.664$ in arbitrary units, whereas the associated average period for the exact system is $T_{\bullet,EX} = 3.668$. Likewise, in the domain instantiated by the solid triangle, $T_{\blacktriangle,MF} = 3.874$ and $T_{\blacktriangle,EX} = 3.869$. The cited data indicate that the MF model is able to predict the average frequency of macroscopic oscillations of the exact system with remarkable accuracy. Regarding the comparison between the real and the approximate systems, one should also look back at the values of the critical strength g_0. The agreement here is weaker, whereby the MF model is found to overestimate the value. This is not unexpected, given that the local phenomena are mediated by the background global bifurcation. Still, the tendency and rate by which g_0 decreases with enhancing D is reflected reasonably well by the MF model.

The main results in this Section concern the canonical setup involving two identical populations of interacting excitable neurons ($g_{in,1} = g_{in,2} = 0.1$), whereby the cross-population couplings are taken to be symmetrical [30, 128]. The intrinsic ensemble parameters $D = 0.0001, \tau_{in} = 0.3$ warrant that the equilibrium is the only asymptotically (stochastically) stable state for the approximate (exact) model. Inspecting the appropriate bifur-

cation diagram in Fig. 7.3(a), one readily realizes how, at variance with the previously discussed case, there is not one, but two scenarios for the destabilization of equilibrium. Which of the scenarios actually applies is contingent on the inter-population coupling strength g_c: if $g_c < g_0'$, viz. Fig. 7.3(b), the equilibrium goes unstable via the direct supercritical Hopf bifurcation, while for $g_c > g_0'$, the onset of the collective mode rests with the direct subcritical Hopf bifurcation. In the latter instance, where g_c notably outweighs g_{in}, an unstable limit cycle collapses at the fixed point making it unstable. Away from criticality, in the domain marked by the solid circle in Fig.7.3(b), the system's trajectory eventually gets drawn to a distant limit cycle attractor. Again, both the stable and the unstable limit cycle derive from the fold-cycle bifurcation, whereas the numerical simulations confirm that the unstable manifold of the equilibrium at $(g_c, \tau_c) = (g_0', 0)$ supports the symmetrical oscillatory state. Below the curve $\tau_{1,-}$, which is barely distinguishable from the g_c-axis in Fig. 7.3(b), one finds a narrow interval of coupling strengths $g_c \gtrsim g_0$ where the emanating branch of the unstable solutions apparently folds back. As a corollary, the system of coupled MF models is seen to exhibit a bistable regime, such that the equilibrium and the collective mode coexist. However, such bistability is difficult to observe in the dynamics of the full system for the sensitivity of the equilibrium to stochastic perturbation. Interestingly, the approximation for the critical coupling strength g_0' is significantly improved when compared to the previous system configuration, this possibly owing to the influence of the inter-ensemble interactions that were excluded earlier on. Crossing into the domain $\tau_{1,-} < \tau_c < \tau_{2,+}$ represented by the open square in Fig. 7.3(b), the MF system undergoes an inverse subcritical Hopf bifurcation, such that the fixed point loses an unstable plane. Looking in a more general picture, this region of parameter space is supposed to be bistable between the equilibrium and the large limit cycle born via the global bifurcation. In parallel, the unstable limit cycle from the Hopf bifurcation should act like

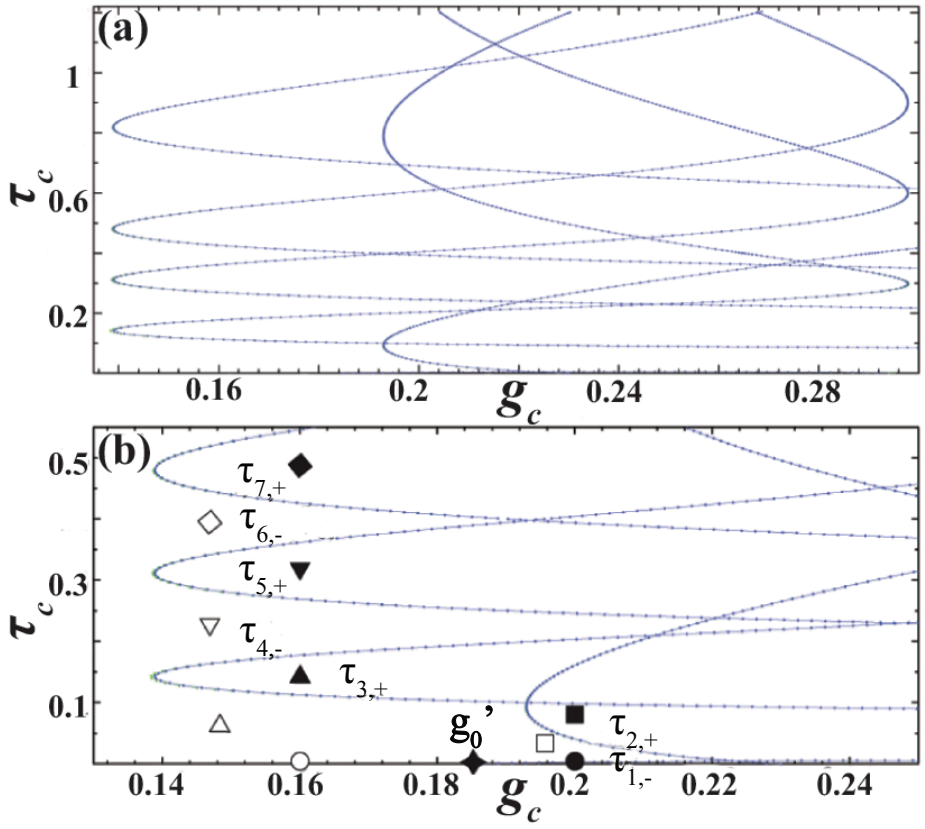

Figure 6.3: Hopf bifurcation curves $\tau_c(g_c)$ in case of two identical, symmetrically coupled populations, each comprised of globally connected elements whose interactions are characterized by $\tau_{in} = 0.3$ and $g_{in} = 0.1$. The two latter parameter values, together with $D = 0.0001$, warrant that the isolated populations (single MF systems) exhibit the stochastically (asymptotically) stable stationary state. (b) presents a close-up view of (a), focused on the parameter region where the stability of the equilibrium changes. Depending on g_c, the equilibrium is destabilized either by the supercritical or the subcritical Hopf bifurcation. As in Fig. 7.1, the exhibited collective mode is found to be a result of the interplay between the local bifurcations and the global fold-cycle bifurcations.

a threshold for switching between the two solutions. However, the stochastic component in the underlying dynamics prevents us from observing the bistable regime in the exact system. Above $\tau_{2,+}$, the equilibrium loses stability, giving way to the limit cycle as the sole attractor of the system's dynamics.

Next we turn to the sequence of bifurcations obtained for $g_c < g_0'$, which is a physically more plausible range since g_c lies closer to g_{in}. Below $\tau_{3,+}$, the stationary state is stable for both the real and the approximate system, with the appropriate parameter domain highlighted by the open up-triangle

in Fig. 7.3(b). Crossing $\tau_{3,+}$ from below, the system undergoes the supercritical Hopf bifurcation, such that the equilibrium becomes unstable, and the emerging oscillations are symmetrical. An interesting point for the transition between the domains marked by the open and solid up-triangles in Fig. 7.3(b) is that for the moderate coupling strength, under not too large a noise the time lag turns out to be a necessary ingredient should the equilibrium be destabilized. For the more comprehensive view, one again has to consider the effects of the interplay with the global fold-cycle bifurcation, whereby a general remark is that everything stated on the direct supercritical Hopf bifurcation regarding the diagram in Fig. 7.1(b) can carry over to this case. In brief, apart for the equilibrium, the system's phase space below $\tau_{3,+}$ also exhibits an unstable limit cycle enclosing the fixed point and a large stable limit cycle. Above the latter curve, the incipient limit cycle grows only until colliding with the unstable one, both being annihilated in an inverse fold-cycle bifurcation. Then, all the trajectories are eventually drawn to the large limit cycle, left as the sole attractor. As for the predictions of the approximate system, one stresses that there is an excellent agreement between the oscillating waveforms, in particular when comparing the anticipated frequency with the average one for the real system, viz. $T_{\blacktriangle,MF} = 3.836$ vs. $T_{\blacktriangle,EX} = 3.833$. This is illustrated in Fig. 7.4, showing side-by-side the sequences from the time series $m_{x,i}(t)$ and $X_i(t)$ for $i = 1, 2$ below (top row) and above (bottom row) the curve $\tau_{3,+}$.

Further enhancing τ_c to step into the domain highlighted by an open down-triangle in Fig. 7.3(b), one encounters the bistable dynamics, such that the system, depending on the initial conditions, may display either the stationary or the oscillatory state. The area is bounded by $\tau_{4,-}$ from below and $\tau_{5,+}$ from above. The found bistability regime is the consequence of the inverse subcritical Hopf bifurcation, where the emanating unstable cycle effectively acts to stabilize the fixed point, allowing for it to coexist with the collective mode, the latter present due to the global bifurcation.

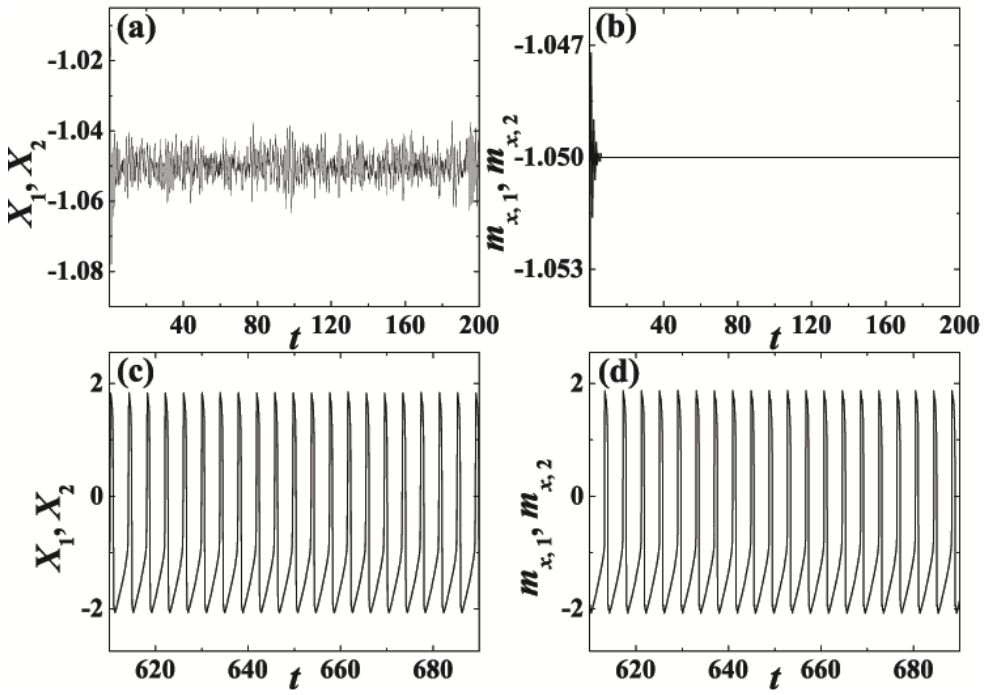

Figure 6.4: The exact (left column) and the approximate system (right column) are demonstrated to undergo the direct supercritical Hopf bifurcation when crossing the curve $\tau_{1,+}$ from Fig. 7.3(b). (a) and (b) show that below the curve ($g_c = 0.16, \tau_c = 0.06$), the fixed point is stochastically stable for the exact, and asymptotically stable for the approximate system, respectively. The onset of oscillations above the curve ($g_c = 0.16, \tau_c = 0.14$) is illustrated for the exact system in (c), and the approximate system in (d). The intrinsic population parameters are set to $D = 0.0001$, $g_{in} = 0.1$ and $\tau_{in} = 0.3$.

The possibility of observing bistability in the exact system is likely facilitated by the unstable limit cycle, whose amplitude is sufficient to separate more clearly between the attraction basins of the oscillatory solution and the equilibrium in spite of the stochastic perturbations induced by the relatively small, but non-negligible noise. The bistable regime is illustrated in Fig. 7.5, which demonstrates the coexistence of the stationary (top row) and oscillatory states (bottom row) for both the exact model and the MF approximation. Note that the change in oscillating frequency in the real system, associated with crossing $\tau_{4,-}$ from below, is well matched by the approximate system. Stepping into the domain $\tau_{5,+} < \tau_c < \tau_{6,-}$, marked by the solid down-triangle in Fig. 7.3(b), the key change consists in the switch from the bistable to a monostable regime, the latter characterized by the oscillatory state with the synchronization in-phase. The switch occurs as the

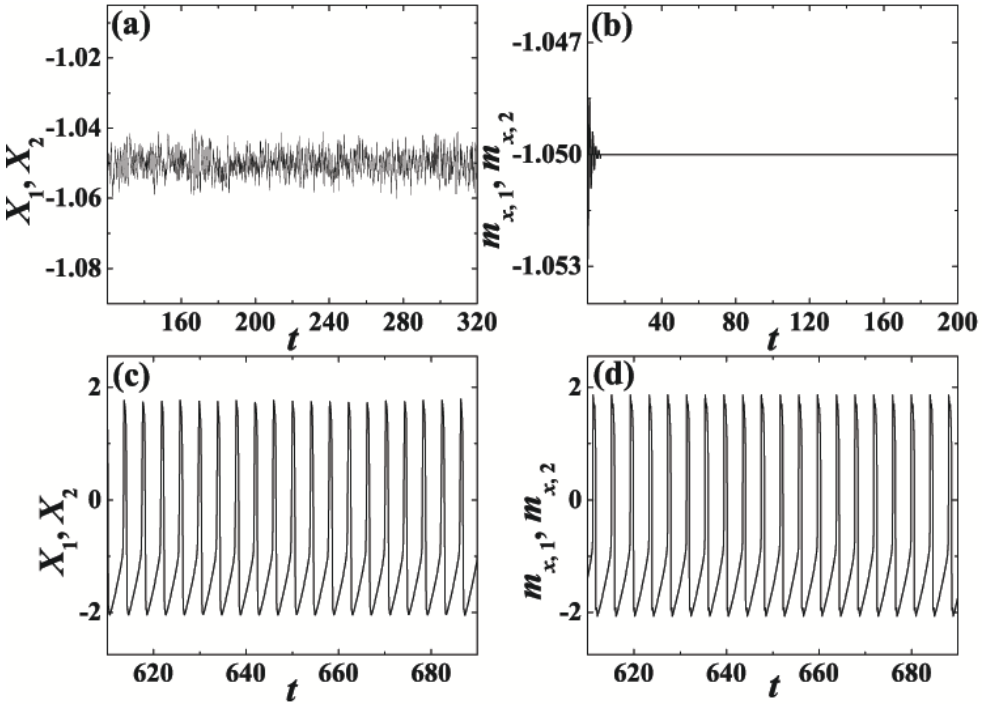

Figure 6.5: Illustration of how the same bistable regime, characterized by coexistence between the stationary and the oscillatory state, is exhibited both by the exact (left column) and the approximate system (right column). The top row indicates the corresponding stochastically and asymptotically stable fixed point, whereas the bottom row shows the two populations oscillating in-phase. The coupling strength and delay $(g_c, \tau_c) = (0.14, 0.22)$ lie within the domain highlighted by the open down-triangle in Fig. 7.3(b). The values for the intrinsic parameter subset are $D = 0.0001, g_{in} = 0.1$ and $\tau_{in} = 0.3$.

system undergoes the direct supercritical Hopf bifurcation, which adds unstable directions, altering the stability of the fixed point. The change from the bistable to the monostable regime occurs in the same fashion for the MF and the exact system. Setting τ_c above $\tau_{6,-}$, see the domain represented by the open diamond in Fig. 7.3(b), one finds the bistability regime reinstated. However, the transition is accompanied by the modulation of the oscillating frequency, the point well reflected by the approximate system, viz. $T_{\diamond,EX} = 4.097$ against $T_{\diamond,MF} = 4.119$. In general, the increase of coupling delay is biased toward reducing the oscillating frequency.

Note that the qualitatively similar sequence of bifurcations is verified to persist in a range of g_{in} values, if D and τ_{in} are set so to admit the stable stationary state as the sole attractor for the isolated populations. Nonethe-

less, in order for this framework to reflect accurately the behavior of the exact system, one should not consider too large noise amplitudes. The perturbation from larger D may be envisioned as if leading to an effective broadening of the bifurcation curves for the real system, which renders the entire sequence smeared, and the underlying qualitative changes difficult to discern. The question of assessing what noise amplitude is "too large" comes down to determining the D value which causes the failure of the Gaussian approximation, the ground assumption for the validity of the mean-field model. However, the actual value where this occurs depends on all the members of the parameter set $(g_c, \tau_c, g_{in}, \tau_{in})$. The discussion here is focused on the set $(g_c, \tau_c, g_{in}, \tau_{in}) = (0.16, 0.14, 0.1, 0.3)$ associated with Fig. 7.4(c), but the suggested means of analysis can be applied for an arbitrary set of values. In this context, one may first compare the stationary probability density for the global variables $P(X, Y)$ of the exact system with that for the mean-field variables $P(m_x, m_y)$ of the approximate model as D is increased. The two stationary distributions can be approximated numerically by observing the respective systems' evolution for the sufficiently long time period. In particular, the applied method consists in counting the number of representative points that fall within each cell of a 110×110 grid, obtained by partitioning the relevant ranges of X and Y, as well as m_x and m_y values into 110 bins each. It may be shown that there is an excellent match between the corresponding distributions for $D = 0.0001$, the value considered in Fig. 7.4(c), whereas $P(m_x, m_y)$ begins to appreciably depart from $P(X, Y)$ around $D \approx 0.0014$. The latter may serve as a rough estimate for the noise amplitude where the mean field approximation breaks down.

This conclusion is further supported by examining how close are the properties of the exact system to satisfying the Gaussian approximation when D is increased. Should the exact system conform to this requirement, the distribution $P(\vec{x})$ for the potentials of single neurons within each population $\vec{x} = (x_1, ..., x_N)^T$ at any moment of time is supposed to remain close

to Gaussian. This means that its third and fourth order semi-invariants should lie around zero, $I_3 = M_3 \approx 0$ and $I_4 = M_4 - 3M_2^2 \approx 0$. Here, M_k refers to the k-th moment of the centered distribution. Then, monitoring the values of I_3 for the numerically determined $P(\vec{x})$ distributions in the sufficiently long time period, one can obtain the appropriate histograms and calculate the mean values $< I_3 >$, characteristic for each given noise value D. It is found that the histograms $P(I_3)$ are expectedly centered around zero for small D, whereas their profiles exhibit tails as D is increased. The latter point reflects the discrepancy from the Gaussian approximation. Following the tendency of increasing positive fluctuations from the mean value, $P(I_3)$ eventually becomes a bimodal distribution for large D. The noise value where the tails become visible again turns out to be around $D \approx 0.0014$, corroborating the previously stated result on the breakdown of the mean-field approximation. As a measure of how distinct the $P(I_3)$ distributions at mentioned D values really are, one may compare the mean values for the third order semi-invariants $< I_3 > (D = 0.0001) = -0.0032$ vs $< I_3 > (D = 0.0014) = -0.0245$ or their fourth-order counterparts $< I_4 > (D = 0.0001) = -0.0305$ vs $< I_4 > (D = 0.0014) = 0.1471$. Finally, the conclusions so far can also be confirmed by determining the dependence of the time-averaged skewness and kurtosis for the $P(\vec{x})$ distributions in terms of noise. It can be demonstrated that such plots exhibit a sharp increase at values around $D \approx 0.0014$, again indicating where the significant deviation from the Gaussian approximation occurs for the given $(g_c, \tau_c, g_{in}, \tau_{in})$ parameter set.

A question that naturally arises is whether and how is the physical picture so far modified by taking the asymmetrical, rather than the symmetrical cross-population coupling terms. We have examined two different scenarios: by one, the couplings in either direction retain a common time lag, but attain different strengths, whereas in the other, strengths are the same, but the transmission delays are disparate. In the former case, the

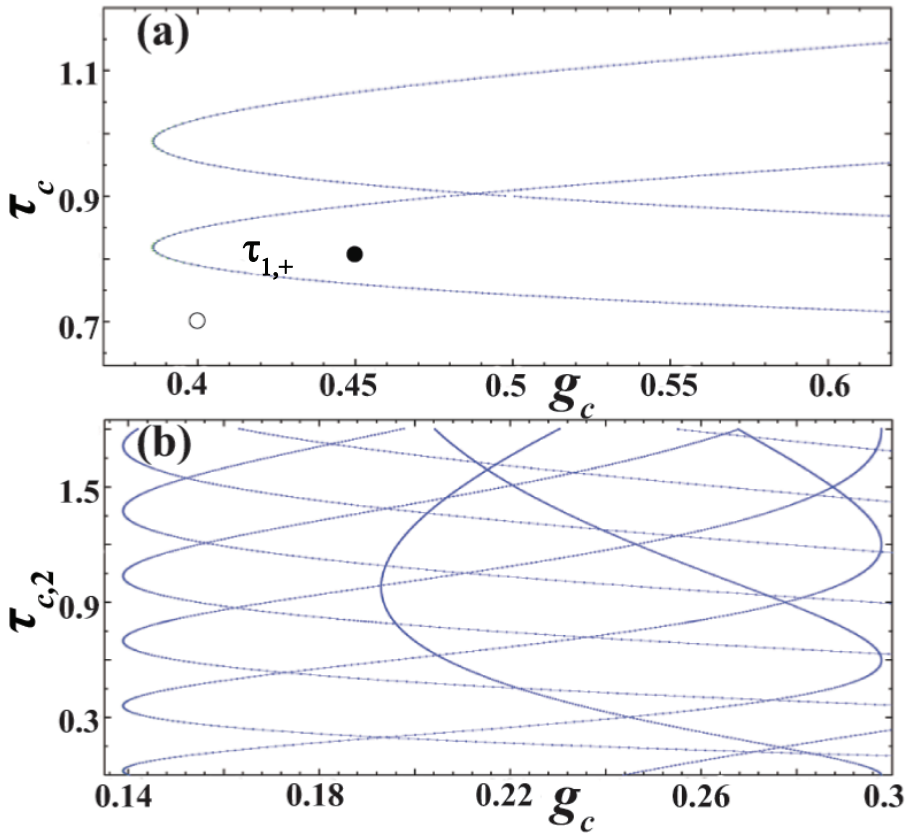

Figure 6.6: Results of the local bifurcation analysis of the approximate system for the two cases of the asymmetrical cross-population couplings, presented in the delay-strength parameter plane. (a) refers to the setup with the disparate coupling strengths, holding $g_{c,1} = 0.05$ and letting $g_{c,2}$ vary continuously. (b) is obtained for the uneven time lags, with $\tau_{c,1} = 0.6$ fixed and $\tau_{c,2}$ allowed to change. The intrinsic parameters $D = 0.0001, \tau_{in} = 0.3, g_{in} = 0.1$ are identical for both populations and warrant that the corresponding isolated system would exhibit the stationary state.

coupling strength in one direction, say $g_{c,1}$ is kept fixed, while $g_{c,2}$ varies continuously. The bifurcation diagram in the τ_c-$g_{c,2}$ plane is plotted in Fig. 7.6(a), whereby the intrinsic population parameters are identical to those stated in the caption of Fig. 7.3. One may immediately raise the issue of why is the bifurcation sequence profile much simpler compared to that in Fig. 7.3(a). The possible reason lies in that for the cross-population couplings asymmetrical by strength, the system's behavior is predominantly influenced by the global bifurcation phenomena dependent on $g_{c,1}$ and $g_{c,2}$. Nonetheless, one cannot neglect some qualitative resemblance between the dynamics of the MF and the exact system. For instance, below $\tau_{1,+}$ in Fig.

7.6(a), the equilibrium is stable for either system, but participates in the bistable regime. Along with the stationary state, one also finds an oscillatory state where the two populations are locked with a constant phase shift. This collective mode can only be attributed to the global bifurcation events. Crossing $\tau_{1,+}$ from below results in the creation of a limit cycle, leaving the equilibrium unstable. Both the real and the approximate model exhibit a single attractor supporting the phase-locked oscillations between the two populations, whereby the underlying frequencies are well matched, viz. $T_{\bullet,MF} = 4.281$ against $T_{\bullet,EX} = 4.302$. Notably, the oscillation waveforms above $\tau_{1,+}$ are more complex than those below, and bear the initial signatures of the quasiperiodic behavior. It has to be stressed that the qualitative resemblance between the dynamics of the exact and the approximate system heavily depends on how close is $g_{c,1}$ to g_{in}. In Fig. 7.6(a), $g_{c,1} = 0.05$ is comparably small to $g_{in} = 0.1$. Should $g_{c,1}$ approach g_{in} or exceed it, the effects of the global bifurcation phenomena become overwhelming, spoiling the predictions made by MF-based approximation.

We also briefly touch upon the setup where the cross-population couplings exhibit the disparate time lags, but attain the same coupling strength. Again, all the internal population parameters are equal to those linked to Fig. 7.3, whereas the notation on the asymmetrical coupling parameters is analogous to that used in the previous layout. The appropriate bifurcation diagram in the $\tau_{c,2}$-g_c plane is displayed in Fig. 7.6(b). Compared to Fig. 7.3(a), we learn how the main difference between this case of asymmetrical couplings and the case with symmetrical interaction lies in the domain of small delays. In particular, the destabilization of equilibrium occurs solely via the supercritical Hopf bifurcation, whereas the scenario involving the subcritical Hopf bifurcation is absent. This picture seems to be independent on the relation between the fixed time lag $\tau_{c,1}$ and τ_{in}.

Though it is not within the scope of the current study, one should still mention that the methods discussed can also be implemented for the sce-

narios where the two populations exhibit different types of kinetics, e.g. if one is made up of excitable, and the other of self-oscillating units. In this scenario, one effectively examines the interaction between the noise-induced and the noise-perturbed oscillations. The corresponding bifurcation diagram is not too distinct from the one in Fig. 7.6(b), except that the pattern of bifurcation curves is less dense. The critical coupling strength analogous to g_0 is naturally smaller than the one for the interacting excitable populations. Nevertheless, this setup is distinguished from those considered earlier in that the unstable manifold of the equilibrium supports the onset of the collective mode with the phase-locked rather than the in-phase oscillations, such that the firing of the ensemble with self-oscillating neurons precipitates the firing of the ensemble containing the excitable neurons.

6.4 Chapter summary and discussion

In the present chapter, we have pursued the analysis of the MF based approximation intended to accurately reflect the macroscopic behavior of two delay-coupled populations of stochastic excitable units in terms of the stability of the stationary state, the scenarios for the onset and the suppression of the collective mode, as well as the possibility of admitting bistable regimes, where the equilibrium and the oscillatory state are found to coexist. The described layout deserves attention, since it can be interpreted as the minimal model for the "network of networks", the configuration often brought into context of biological systems whose function relies on generation and adjustment between the multiple collective rhythms. The important ingredients of the exact system we consider include two types of delayed interactions, whereby those within the ensembles are assumed to be linear, and the inter-ensemble ones, mediated by the appropriate global variables, are taken to be nonlinear. The corresponding approximate sys-

tem is built by coupling the two MF models, derived to describe the activity of single populations. Such a framework follows the general idea that any ensemble of oscillating units exhibiting the collective mode can be treated as the macroscopic oscillator. The MF model integrates the cumulant approach with the Gaussian approximation, whereby the latter holds exactly for an arbitrary system if three conditions are satisfied. These include the thermodynamic limit $N \to \infty$ regarding the ensemble size, the negligible noise amplitude $D << 1$, as well as the negligible interaction between the units $g_{in} << 1$. Naturally, the term negligible does not allude to asymptotic limits $D \to 0$ or $g_{in} \to 0$, but refers to very small values of these parameters which correspond to an idealized, rather than the realistic setup. However, depending on the particular system, it often turns out that the validity of the MF based approximation extends beyond the initially prescribed parameter range, getting closer to the more realistic parameter values. This holds true in our case, where we have demonstrated that the approximate system is able to predict with sufficient accuracy the behavior of relatively large, but finite populations ($N \sim 100$) with the non-negligible internal interactions ($g_{in} \sim 0.1$), provided that the understandable requirement for not too large a noise amplitude is met. Regarding the latter, see the remarks on page 143 following the discussion on the setup with symmetrically coupled populations.

By stating the results in broad terms, the intention has been to stress their applicability to the class of systems made up of type II excitable units. Nonetheless, one recognizes that valuable motivation for the study comes from the field of neuroscience, which goes beyond the adopted model of local dynamics or the fashion in which the interactions are introduced. The methods for providing the reduced descriptions of the behavior of large neural assemblies are typically cast in the categories of the neural-mass and the MF models, whereby the former neglect, and the latter take into account the distribution of individual neuron states over the ensem-

ble. In these terms, the model considered here interpolates between the two classes. Recall that we have introduced an additional approximation on the second order moments to translate the five-variable MF system for a single population (2.16) into the two-variable form incorporated within (7.8), the latter being preferred as it allows for the appropriate bifurcation diagrams to be obtained analytically.

An inference from such an analysis is that the approximate system can undergo direct and inverse supercritical or subcritical Hopf bifurcations, such that the direct (inverse) ones lead to the destabilization (stabilization) of the stationary state. The complex bifurcation sequence under variation of cross-population coupling strengths and delays is found to depend on the details of the system configuration, like the symmetrical or asymmetrical character of the bidirectional interaction between the ensembles. The main set of results refers to the symmetrical case, where it is demonstrated that the equilibrium may lose stability according to two different scenarios. One involves a direct supercritical Hopf bifurcation and can be achieved for instantaneous couplings solely by increasing g_c, whereas the other scenario unfolds via the direct subcritical Hopf bifurcation. The latter involves an interesting point that for strengths $g_c \simeq g_{in}$ one finds a time-lag threshold necessary to destabilize the equilibrium. Increasing τ_c, there are parameter domains bounded from below (above) by the curves indicating subcritical (supercritical) bifurcations, where the stability of stationary state is regained. In many of such instances, the system is actually bistable, exhibiting coexistence between the equilibrium and the oscillatory state. This is a corollary of an interplay with the global fold-cycle bifurcation, as the large stable limit cycle born in this way remains unaffected by the local phenomena. Note that the global events may influence the system dynamics in several other instances. In particular, an unstable limit cycle created in a fold-cycle bifurcation may destabilize the fixed point in a direct subcritical Hopf bifurcation or may limit the growth of an incipient limit cycle

following the direct supercritical Hopf bifurcation. By numerical simulation, we have verified that the parameter domains of stability or instability of equilibrium for the exact system are reproduced by the approximate one with high accuracy. In addition, it has been shown that the average oscillation frequency for the global variable of the exact system is well matched by that of the corresponding MF variable. In the exact system, the ability to observe the bistable regimes, where the unstable limit cycle act as a threshold between the equilibrium and the large cycle, is contingent on the noise amplitude. In general, the predictions of the approximate system are better if the deterministic component, governed by the coupling strengths and delays, prevails over the stochastic component in the dynamics of the exact system. An interesting study complementary to the present one would be to examine whether the MF based model may reproduce the forms of synchronization between the generated collective rhythms the way they are exhibited by the exact system. These could include the in-phase and antiphase synchronization or the phase-locked states, as well as their coexistence. The preliminary results implementing the H-function approach suggest that the approximate system may account for the stability of the synchronization regimes and provide indications on the possible multistability.

Chapter 7

Stability, bifurcations and dynamics of global variables of a system of bursting neurons

---

Chapter abstract The analysis is focused on macroscopic behavior of an ensemble of delay-coupled Hidmarsh-Rose bursting neurons modulated by noise, having described the global coarse-grained dynamics in terms of collective averaged variables. Implementing the typical mean-field assumptions, we derive an approximate model constituting the set of nine deterministic delay-differential equations for the first and the second moments of the collective variables. Bifurcations observed in the global dynamics of the exact system under variation of different parameters, characterizing the time-lag, interaction strength and noise intensity, are compared to those displayed by the approximate model. Bifurcation analysis of the latter is carried out by numerical continuation. It is demonstrated that the domains of parameter space corresponding to stable quiescent behavior or to bursting collective mode of the exact system are correctly estimated by the much simpler approximate model.

Bursting is an important dynamical state of a real neuron and of collections of such neurons. It is believed that a burst of spikes is more reliable than a single spike in producing responses in postsynaptic neurons [75]. Small parts of the brain cortex may contain thousands of morphologically and functionally similar interconnected bursting neurons, and each of them is mathematically modeled by few nonlinear differential equations[75, 205, 206]. Dynamics of such neuronal network is crucially influenced by the interaction, i.e. synaptic delays [29, 57, 136, 137, 168, 169] (and [143] and the references therein), and by small perturbations of various origin which are commonly treated as noise [55, 67, 164, 166, 167, 207].

It is clear that relatively detailed mathematical model of a small part of realistic cortex should involve an extremely large system of nonlinear stochastic delay-differential equations (SDDE). Analysis of such complex models is impossible, even with the help of modern supercomputers, without more or less severe approximations. Our main goal in this chapter is to develop an approximation of large ensemble of coupled bursting neurons and to demonstrate that bifurcation analysis of the approximate model is possible and provides useful information about the exact large system.

Delay-differential equations with noise do not satisfy the Markov assumption [141, 208] which complicates their analysis. Stability of such SDDE's has been studied using extensions of the Lyapunov method long time ago [208], but with little influence in applications apart from models of mechanical devices. More recently, stability of synchronization in systems with noise involving DDE was studied analytically in the context of coupled realistic and formal neural networks. Liao and Mao [209](see also [141]) have initiated the study of stability in stochastic neural networks, and this was extended to stochastic neural networks with discrete time-delays in references [210, 211]. Some analytical techniques relevant

for delayed systems with noise have also been used in the study of coupled bistable systems with delays [212], and in noisy oscillators with delayed feedback [146, 213–217]. Small world and scale free networks of various neuronal models with noise and synaptic delays have been studied numerically for example in [147, 218–222]

Our approximation is based on ideas and assumptions of the mean field approach. The mean field approximation has been applied on systems of excitable neurons with noise but with no time-delay for example in [67, 111, 112, 129]. Otherwise a type of MFA was devised in [223] and [64] and applied on large clusters of noisy neurons with time-delayed interaction in [195]. Global dynamics of a system of delayed coupled noisy 1D elements was recently studied using the mean field approach in [224]. Recently an analytically tractable MFA for delayed-coupled noisy excitable FitzHugh-Nagumo neurons was developed [138] and used [139]. The mean field approximate model developed here, in section 7.1, is still too complicated for an analytic treatment, but the numerical bifurcation analysis, presented in section 7.2, is possible and the results of such analysis are the main topic of our chapter.

7.1 The exact large system and it's approximate model

Different types of bursting activity have been observed in real single neurons and collections of neurons [75]. Typical example of bursting dynamics is provided by the three dimensional model proposed by Hindmarsh and Rose (HR) [99]

$$\begin{aligned} dx/dt &= F_x = y + 3x^2 - x^3 - z + I, \\ dy/dt &= F_y = 1 - 5x^2 - y, \\ dz/dt &= F_z = -rz + rS(x - C_x). \end{aligned} \tag{7.1}$$

where x is the membrane potential, y represents the fast current, like N_a^+ or K^+, and z represents the slow current, for example Ca^{2+}. r, S and b are parameters which are in this chapter set to constant typical values $r = 0.0021, S = 4, C_x = -1.6$. The HR equations (7.1) describe the dynamics of a single neuron subjected to an external stimulus I. Depending on the values of the parameters r, S, C_x and the current I the model can have qualitatively different attractors corresponding to quiescent state, periodic firing and bursting with regular or chaotic sequences of bursts [225, 226]. The bursting dynamics is driven by the oscillations of the slow z variable, and occurs once they acquire sufficiently large amplitude, which is preferably induced by supplying an appropriate external stimulus I. The bursts of spikes endure during the period when z is increasing and the stable quiescent state is observed while $dz/dt < 0$.

In this chapter we shall analyze the bursting dynamics of collective variables in an ensemble of HR neurons. The model explicitly includes the interaction delays and stochastic perturbation represented by additive white noise, and is given by the following system of $3N$ stochastic delay-differential equations (SDDE)

$$\begin{aligned} dx_i &= [F_x(x_i, y_i, z_i) - \frac{1}{N}\sum_j^N c(x_i - x_j(t-\tau)]dt + \sqrt{2D}dW \\ dy_i &= F_y(x_i, y_i, z_i)dt, \\ dz_i &= F_z(x_i, y_i, z_i)dt, \quad i = 1, 2 \ldots N. \end{aligned} \tag{7.2}$$

where F_x, F_y, F_z are given by Eq. (7.1). There are two major types of inter-neuronal couplings: the chemical and the electrical synapses. Time-delay τ is important especially in the first type of synapses but plays also an important role in the electrical junctions and in the transmission of an impulse through the dendrite. In Eq. (7.2) we use the electrical coupling with the time-lag τ and the strength c that is equal for all pairs of neurons. The assumption that all internal neuronal parameters and all coupling con-

stants are equal is plausible if the neurons are found in a small patch of the brain cortex. The collective dynamics of such an ensemble of closely placed neurons would then be monitored by a single electrode in an EEG recording.

The terms $\sqrt{2D}dW_i$ represent stochastic increments of independent Wiener processes, i.e. dW_i satisfy

$$E(dW_i) = 0, \quad E(dW_i dW_j) = \delta_{i,j}dt, \tag{7.3}$$

where $E(\cdot)$ denotes the expectation over many realizations of the stochastic process. The intensity of the noise D and the stochastic properties of the noise are assumed to be the same for all neurons, but, of course, single realizations of the Wiener processes in the equations for x_i need not be the same functions of t for all i. Noise could be added also in the other equation of the fast subsystem. It is known that, in the case of excitable systems, the noise in the dx_i equation or in the dy_i equation produce different types of stochastic coherence effects [77]. The mean field approach, presented in this chapter, could be applied equally with almost no modification if the noise term was in the dy_i equation or in both dx_i and dy_i equations. Nevertheless, we arbitrarily decided to treat the case with the noise in the dx_i equation.

Before we start with the analysis of the system (7.2) with a large number of units it is instructive to recapitulate the synchronization properties of the system with only two neurons [57, 214, 227]. Transition from the quiescent or simple oscillatory state to bursting dynamics of two HR neurons can be induced either by increasing the external parameter I, the coupling strength $|c|$, the noise D or the time-lag τ. The bursting of the two neurons can be exactly synchronous, i.e. $x_1(t) = x_2(t)$, approximately synchronous $x_1(t) \approx x_2(t)$ or completely asynchronous. Sufficiently strong coupling with zero or small delay usually induces synchronization, which remains an approximate one as long as the noise is not too large. Non-zero time-

lag in a specific interval can induce synchronization of weakly coupled deterministic bursters but the synchronization completely disappears with the addition of a very small noise if the coupling remains weak. As for the synchronization in systems with a large number of noiseless and instantaneously coupled bursters, it is known that the synchronization can be achieved with weak coupling if each of the neurons is connected with (equal) sufficiently large number of other neurons [101]. As we shall see these facts are reflected in the properties of global bursting dynamics of the system with large N.

7.1.1 The mean field approximation

We are interested in the dynamics of the global averaged variables of the large system (7.2). These are defined as the space averages:

$$\begin{aligned} m_x(t) &= 1/N \sum_i^N x_i(t) \equiv < x_i(t) >, \\ m_x(t-\tau) &= 1/N \sum_i^N x_i(t-\tau) \equiv < x_i(t-\tau) >, \\ m_y &= 1/N \sum_i^N y_i \equiv < y_i >, \\ m_z &= 1/N \sum_i^N z_i \equiv < z_i > . \end{aligned} \tag{7.4}$$

In order to obtain a closed system of equations for the spatial averages and correlations we need several assumptions typical of the mean field approach. The assumptions are formulated using the centered first moments:

$$\begin{aligned} n_{x_i}(t) = m_x(t) - x_i(t), \;\; n_{y_i}(t) = m_y(t) - y_i(t), \\ n_{z_i}(t) = m_z(t) - z_i(t), \end{aligned} \tag{7.5}$$

and assume that they are statistically independent in different units. Next,

mean square deviations:

$$s_x(t) =< n_{x_i}^2(t) >,\ s_y(t) =< n_{y_i}^2(t) >, s_z(t) =< n_{z_i}^2(t) >, \tag{7.6}$$

and cross-cumulants:

$$u_{xy} =< n_{x_i} n_{y_i} >,\ u_{xz} =< n_{x_i} n_{z_i} > u_{yz} =< n_{y_i} n_{z_i} > \tag{7.7}$$

are introduced.

Next we shall assume that for sufficiently large N the global space averages (7.4) of local quantities, say $m_x(t)$, are equal to the expectations with respect to distribution of the corresponding variable $E(x_i(t))$. Because of the assumed Gauss distribution of each variable the first and the second order cumulants of the deviations (7.5) are equal to the first and second order centered moments of the variables x_i, etc.... Due to the same Gaussian assumption cumulants of order higher than second are equal to zero.

The well known formulas of the cumulant expansion up to the fourth order [124] are used to obtain, after some algebra, the expressions for higher order auto-correlations. In particular:

$$\begin{aligned}
< x_i^2(t) > &= s_x(t) + m_x^2(t) \\
< x_i(t)^3 > &= m_x^3(t) + 3m_x(t)s_x(t) \\
< x_i^4(t) > &= m_x^4(t) + 6m_x^2(t)s_x(t) + 3s_x^2(t) \\
< x_i(t)y_i(t) > &= u_{xy}(t) + m_x(t)m_y(t) \\
< x_i^2 y_i > &= m_y s_x + m_y m_x^2 + 2m_x u_{xy} \\
< x^3 y > &= 3s_x u_{xy} + 3s_x m_x m_y + 3m_x^2 u_{xy} + m_y m_x^3 \\
< xyz > &= U_{xy} m_z + u_{yz} m_x + u_{xz} m_y + m_x m_y m_z \\
< x^2 yz > &= s_x m_y m_z + m_x^2 u_{yz} + m_x^2 m_y m_z + 2u_{xz} u_{xy} \\
&\quad + 2u_{xz} m_x m_y + 2m_x m_z u_{xy} + s_x u_{yz}.
\end{aligned} \tag{7.8}$$

Using the first three equations (7.8) and the assumption that the spatial

average for large N is equal to the stochastic average, the spatial average of Eq. (7.2) becomes

$$\begin{aligned}
\dot{m}_x(t) &= -(m_x^3(t) + 3m_x(t)s_x(t)) + 3(s_x(t) + m_x^2(t)) \\
&\quad + m_y(t) - m_z(t) + I + c(m_x(t-\tau) - m_x(t)) \\
\dot{m}_y(t) &= 1 - 5(s_x(t) + m_x^2(t)) - m_y(t) \\
\dot{m}_z(t) &= r(S(m_x(t) - C_x) - m_z(t)).
\end{aligned} \tag{7.9}$$

In order to close the system (7.9) we need the evolution equations for $s_x(t)$. This involves other second moments, and the corresponding evolution equations are obtained using the Ito chain rule [124] and the equations (7.8). The second moments satisfy

$$\begin{aligned}
\dot{s}_x(t)/2 &= s_x(t)[6m_x(t) - 3m_x^2(t) - 3s_x(t) - c] \\
&\quad + u_{xy}(t) - u_{xz}(t) + D, \\
\dot{s}_y(t)/2 &= -10m_x(t)u_{xy}(t) - s_y(t), \\
\dot{s}_z(t)/2 &= S\,r u_{xz}(t) - r s_z(t), \\
\dot{u}_{xy}(t) &= u_{xy}(t)[6m_x(t) - 3s_x(t) - 3m_x^2(t) - 1 - c] \\
&\quad - 10m_x(t)s_x(t) + s_y(t) - u_{yz}(t), \\
\dot{u}_{xz}(t) &= u_{xz}(t)[6m_x(t) - 3s_x(t) - 3am_x^2(t) - r - c] \\
&\quad - s_z(t) + rS\,s_x(t), \\
\dot{u}_{yz}(t) &= rS\,u_{xy}(t) - u_{yz}(t)(1 + r) - 10m_x(t)u_{xz}(t).
\end{aligned} \tag{7.10}$$

Following the next step in the analogous analysis of the large system of excitable two dimensional FitzHugh-Nagumo neurons [138](see also the analysis of the FitzHugh-Nagumo neurons without the time-delay in [67, 129]) would consists in substitution of the stationary values for the second moments (7.10) into the equations (7.9) of the first moments. However, due to relatively complicated form of the right-hand sides of Eq. (7.10) the resulting three equations for the first moments would still be quite difficult

to analyze. Instead, we shall use the numerical continuation method to perform bifurcation analysis of the system of 9 DDEs (7.9) and (7.10). Predictions of this analysis will then be compared with numerical solutions of the exact large system.

7.2 Numerical stability and bifurcation analysis of the approximate system

Our goal in the next section will be to demonstrate that the qualitative agreement of the approximate and the exact system extends over a large range of parameters I, c, τ and for relatively small noise D, so that qualitatively different types of the exact dynamics are correctly reproduced by the approximate system. Let us stress that our claim will not be that the time series produced by the exact and the approximate equations are quantitatively similar but we shall claim that the approximate equations correctly predict the qualitative type of dynamics for parameters in the specified domains.

Given that the complexity of the approximate model seriously compromises, if not precludes an analytical treatment, one is compelled to consider some means of numerical bifurcation analysis. Before turning to details, let us point out that the destabilization of equilibrium generically occurs via the subcritical Hopf bifurcation. However, this does not rule out the existence of the more subtle secondary bifurcation phenomena in certain parameter domains, viz. the Bogdanov–Takens point is indicated for very small weights under the moderate stimuli and delays. Focussing on the subcritical Hopf bifurcation, the destabilization scenario consists in that an unstable limit cycle collapses on a stable fixed point making it unstable, whereas passed the bifurcation parameter value the trajectory moves over to a stable limit cycle, located further away in the phase space. Within this setup, the onset of bursting coincides with a pair of conjugate

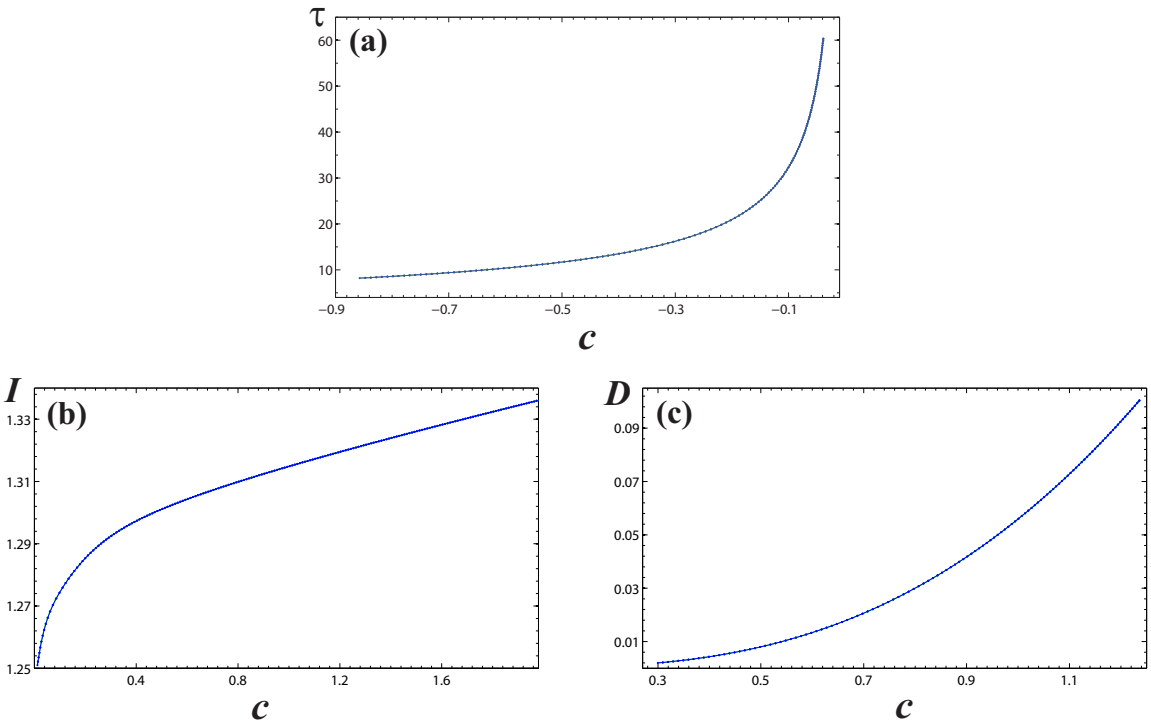

Figure 7.1: Bifurcation diagrams for the approximate model reflecting the destabilization of equilibrium via the Hopf bifurcation. Subfigures (a), (b) and (c) focus on the $\tau(c)$, $I(c)$ and $D(c)$ dependencies, respectively. The fixed point is stable (unstable) below (above) each of the curves. The remaining parameter values are $I = 1.25$, $D = 0$ in (a), $\tau = 8$ and $D = 0.001$ in (b), as well as $I = 1.29$, $\tau = 10$ in (c).

characteristic roots crossing the imaginary axes. The numerical analysis is carried out by implementing the DDE-biftool, which is a package of flexible Matlab routines appropriate for handling the systems of differential equations with constant delays [182, 183]. The calculation of the stability-determining characteristic roots itself involves two stages: the first, posing the approximation by the linear multi-step method, and the correction one, that rests on the Newton iteration method. Most notably, the software allows for numerical continuation over the Hopf bifurcation point, making it possible to switch to an emanating branch of periodic solutions.

The derived bifurcation curves, displayed in Fig. 7.1, are intended to demonstrate how the interplay of I, c, D and τ affects the destabilization of equilibrium for the approximate model, whereby the fixed point is stable (unstable) below (above) each of the curves. For instance, from Fig. 7.1(a)

one reads that under the action of small stimuli only excessive delays give rise to destabilization if $|c|$ is decreased. Nonetheless, at moderate τ, the bifurcation values of I show a sharp rise for smaller c, whereas they virtually reach saturation in the absence of noise (not shown), or exhibit a very slow growth once a small amount of noise is introduced, see Fig. 7.1(b). Finally, from Fig. 7.1(c) we learn that for intermediate I and τ the stronger the weights become, the larger D is required to destabilize the equilibrium. To reiterate, the formulation of the approximate model is justified if it yields the correct stability behavior of the equilibrium as compared to the exact system, a point witnessed later on by plotting the corresponding factual time series for the parameter values below and above the obtained bifurcation curves.

7.3 Numerical illustrations

For most part of our computations we have applied the Euler method of numerical integration, though at some instances the Runge-Kutta fourth and fifth order routines for the deterministic part of (7.2) have also been implemented. The results are compared with those obtained by the ready made programs for solving SDDE provided in the XPP package [228]. Many sample paths of (7.2) for the same parameter values have been computed, but in figures we represent the global variable $X(t)$ along parts of only one typical sample path, and compare these with numerical solutions of the approximate system of DDDEs (7.9),(7.10).

A system of delay differential equations with the time-lag τ is an infinite dynamical system, and the corresponding initial conditions are given by continuous functions on the interval $[-\tau, 0]$. In what follows we shall always use as the initial functions the solutions of (7.2) or (7.9),(7.10) with $c = 0$ and with specified values of the variables at $t = 0$. If the values of a given local variable at $t = 0$ are equal for all i we shall say that the initial

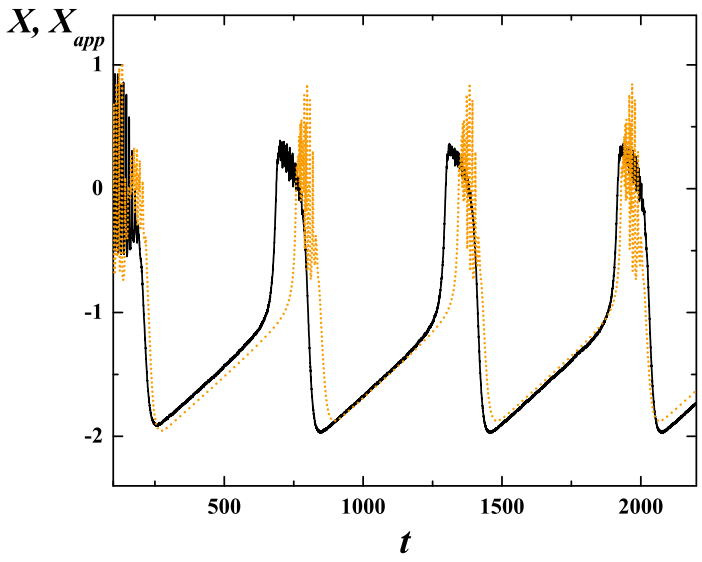

Figure 7.2: Examining whether there are parameter regions that favor precise matching between $X(t)$ and $X_{app}(t)$, provided the initial conditions are analogous. Throughout the chapter we adhere to a representation scheme where the exact series are shown by the black solid lines, while the approximate data are displayed by the dotted lines, coded orange (light gray). Contrary to the common logic, there are instances of close quantitative agreement of the data sets even under large D. Here, the parameter values are $N = 200$, $I = 1.3$, $c = 1$, $\tau = 10$ and $D = 0.04$.

data are equal, and if the local values at $t = 0$ are Gauss distributed we shall say that the initial data are Gauss distributed. In this case the initial data for Eq. (7.9),(7.10), i.e. the values of the first and the second moments at $t = 0$ are fixed by the Gaussian distribution of the local variables.

Of course, the dynamics of the global variables along the sample paths of the exact system (7.2), which is stochastic for $D \neq 0$, can not be exactly reproduced by the orbits of the deterministic approximate model (7.9),(7.10). However, the qualitative dependence on the parameters and their bifurcation values are still well predicted. Furthermore, the difference between the values of the global variables on different sample paths for the same values of the parameters is already at $D = 0.001$ of the same order as the difference between the values given by the approximate model and any of the sample paths.

Apart from the qualitative agreement between the exact system and the approximate model in terms of equilibrium destabilization, an additional

gain would be to determine whether there are parameter regions that warrant the close quantitative match between the corresponding time series of global potentials, designated X and X_{app} in the remainder of the chapter. By common logic, one expects this to be fulfilled in the absence of noise. However, the comparison of the data obtained for the exact system extended to $N = 200$ neurons and the approximate model (Fig. 7.2) under the analogous initial conditions sees the two series converging irrespective of the large D. Here it should be cleared out that the exhibited tendency persists beyond the displayed time interval. Such an outcome makes it explicit how the possible overlap between $X(t)$ and $X_{app}(t)$ is also influenced by the parameters other than noise, notably the stimulation current. What matters about the particular value $I = 1.3$ is that it would be sufficient to induce bursting in the noiseless case if the rest of parameters were to remain as in Fig. 7.2.

In view of the stated above, we proceed to the analysis of the sets of data provided by the exact system and the approximate model under the analogous initial conditions. The results are compared for the parameter values lying below and above the bifurcation curves from Fig. 7.1. The validity of the $\tau(c)$ dependence displayed in Fig. 7.1(a) is exemplified by the time series in Fig. 7.3, where the delay is gradually increased keeping the remaining parameters fixed. For τ below the bifurcation threshold, there are only relaxation oscillations of the global potentials X and X_{app}, whereas just above it one encounters the fixed point destabilized, as the regime of periodic spiking sets in. Further enhancement of τ leads to an onset of bursting. Aside from the fact that the approximate model reproduces all of the major regimes exhibited by the exact system, it strikes that the approximate series seem to best fit the exact one for very large $\tau = 50$.

Figure 7.4 illustrates the qualitative agreement between the data obtained and the $I(c)$ dependence from Fig. 7.1(b). Again, we find the damped oscillations below the bifurcation current and the bursting regime

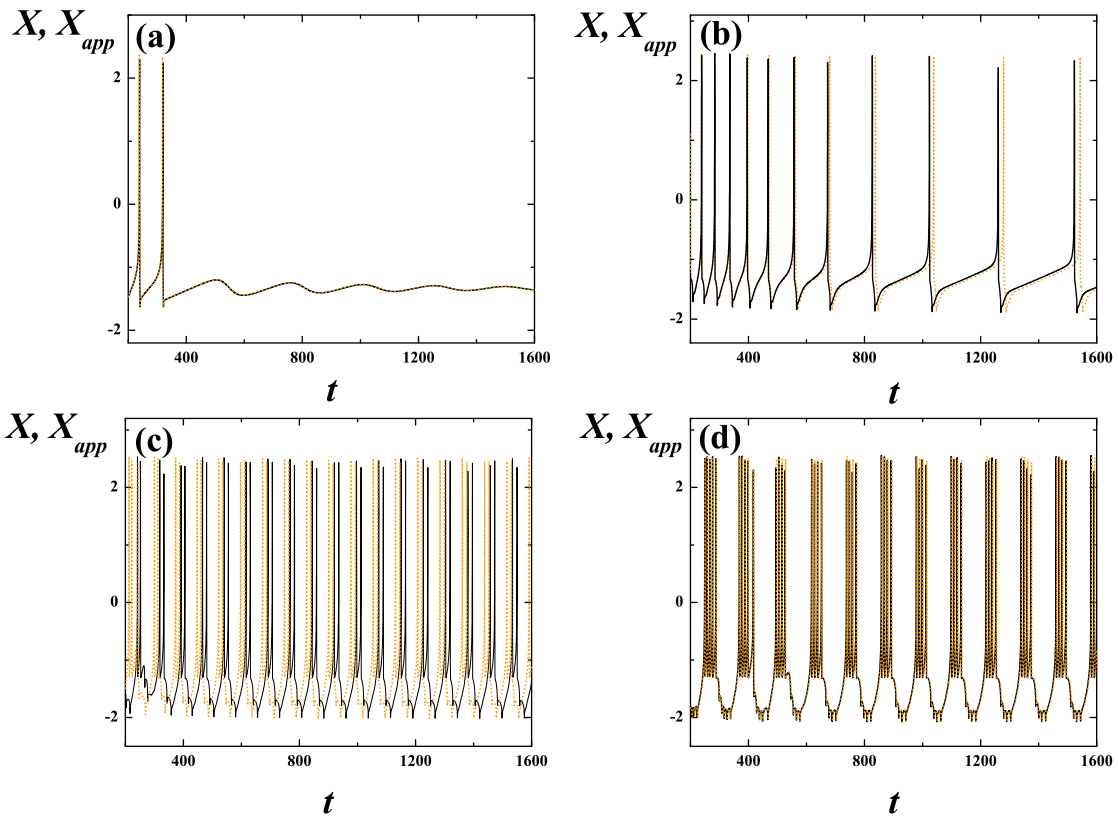

Figure 7.3: Destabilization of equilibrium under the increase of τ. We argue for the qualitative agreement between the approximate model and the exact system in a sense that their time series should reflect how the fixed point is stable (unstable) for the parameter values lying below (above) the bifurcation curve in Fig. 7.1(a). For sub-bifurcation delay $\tau = 2$ in (a) the quiescent behavior is asymptotically stable. Once above the bifurcation value, the neurons first engage in periodic bursting, as seen at $\tau = 9$ in (b), whereas further enhancing the delay gives rise to bursting shown for $\tau = 25$ in (c) and $\tau = 50$ in (d). The remaining parameters take values $I = 1.25$, $c = -0.8$, $D = 0$ and $N = 70$.

taking place above it. In the former case, $X(t)$ and $X_{app}(t)$ provide an excellent match under the analogous initial conditions, whereas they are slightly shifted in the latter. On the qualitative side, the above argument also holds up for the displayed in Fig. 7.5 that relates to the $D(c)$ bifurcation diagram in Fig. 7.1(c). However, the greatest departing so far between the approximate model and the exact system deserves some additional attention. The reason behind this lies in the stimulus value $I = 1.29$, which, connoted with the remaining set of parameters, makes the induced bursting exclusively noise-driven. With this in mind, one cannot expect the deterministic approximate system to replicate the exact dynamics of the stochastic one

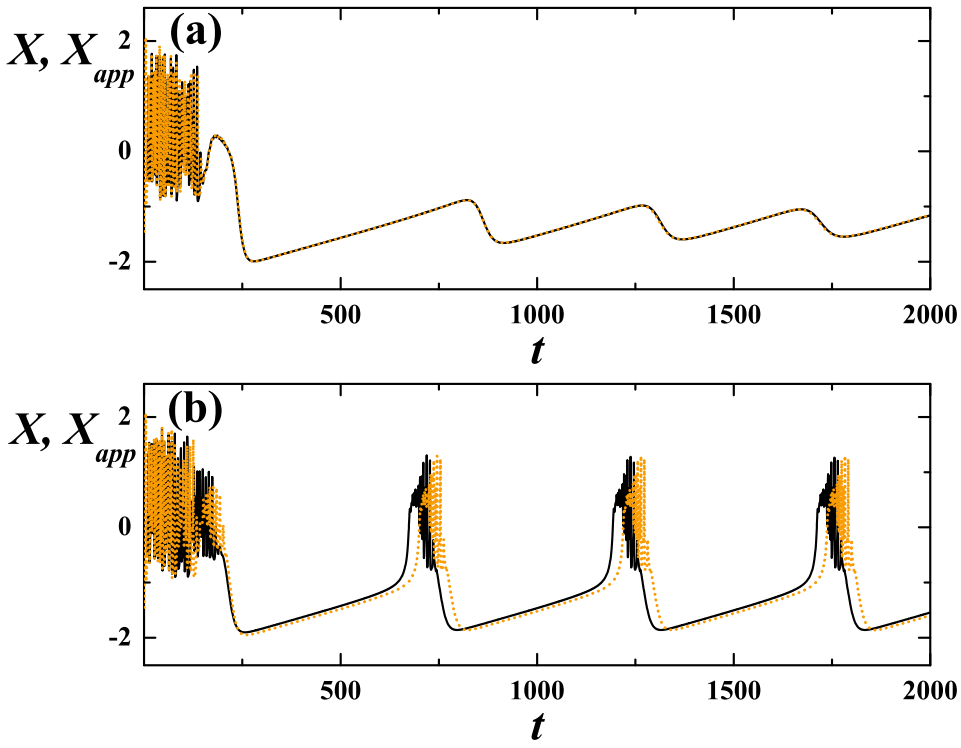

Figure 7.4: System dynamics undergoes transition from asymptotically stable quiescence to bursting under the increase of I in correspondence to the bifurcation diagram displayed in Fig. 7.1(b). $X(t)$ and $X_{app}(t)$ under the analogous initial conditions are obtained for $I = 1.29$ in (a) and $I = 1.32$ in (b), with the rest of parameters being $\tau = 8$, $c = 1$, $D = 0.001$ and $N = 70$.

with any significant fidelity. On a final note, the proposed approximate model is put to the test by considering the noiseless and the delay-free case, where the perfect match with the exact series should occur. To this end, we compared the data obtained for the damped oscillations and the bursting regime, recovering a complete agreement in either event, see Fig. 7.6.

All the examples of the different dynamical phenomena illustrated so far have been obtained for relatively strong coupling $c = 1$ or $c = -0.8$ between the neurons. Figure 7.7 is intended to illustrate the changes introduced by decreasing the coupling. Strong coupling prompts synchronization between the neurons which is only slightly perturbed by small noise. Thus, the local bursters discharge in an almost synchronous fashion and the global averages also display clear burst with large amplitude.

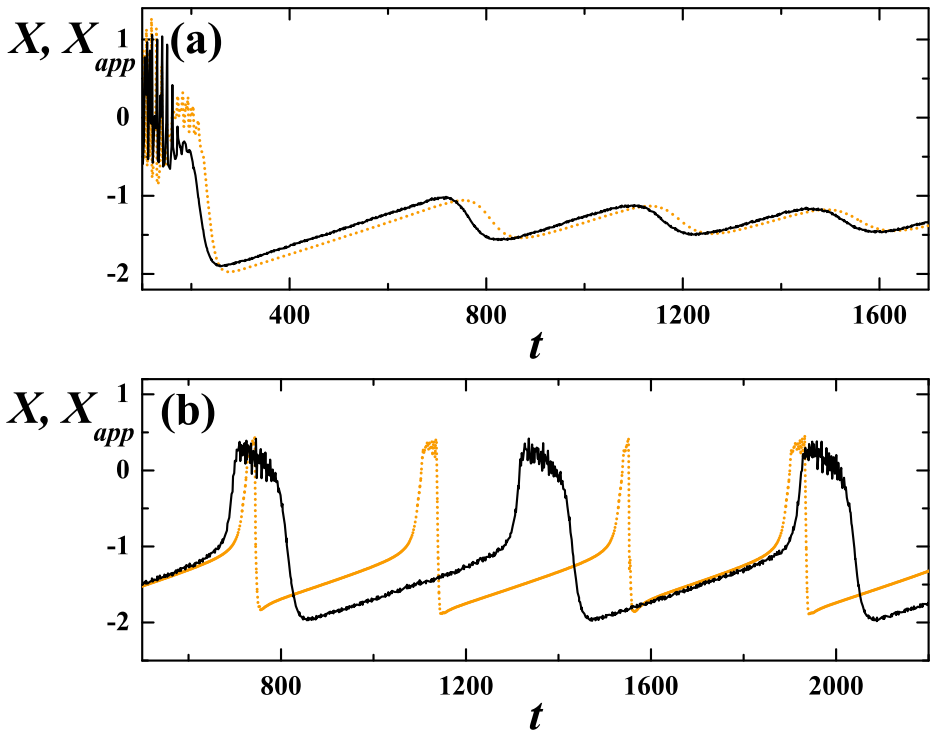

Figure 7.5: Prompted by the increasing noise, the system dynamics undergoes transition from stable quiescent behavior to bursting, as anticipated by the bifurcation diagram in Fig. 7.1(c). The noise values are $D = 0.01$ in (a) and $D = 0.057$ in (b), with the remaining parameters set at $I = 1.29$, $\tau = 10$ and $N = 70$. $X(t)$ and $X_{app}(t)$ depart from each other, in particular for the ascending and the descending sections of bursts being much sharper in the latter, as the observed transition is exclusively driven by noise.

This is illustrated in Figs. 7.7(a), (b) and (c) by showing only one burst in the exact dynamics of $X(t)$, the dynamics of its approximation $X_{app}(t)$ and $x_1(t)$ versus $x_8(t)$. $X_{app}(t)$ is qualitatively similar to $X(t)$, and all pairs of local bursters $x_i(t), x_j(t)$ are almost synchronous. On the other hand, weak coupling also implies synchronous dynamics of local bursters with zero noise, but this synchrony is completely destroyed by arbitrarily small noise. Because of this noise induced de-synchronization the global variables only display dumped bursting as is illustrated in Fig. 7.7(d). The stationary state is unstable, but the individual bursting is de-synchronized so that spatial averaging only produces dumped bursting in global variables. The approximate model correctly predicts that the stationary state is unstable, but it undergoes clear bursting dynamics which is quantitatively

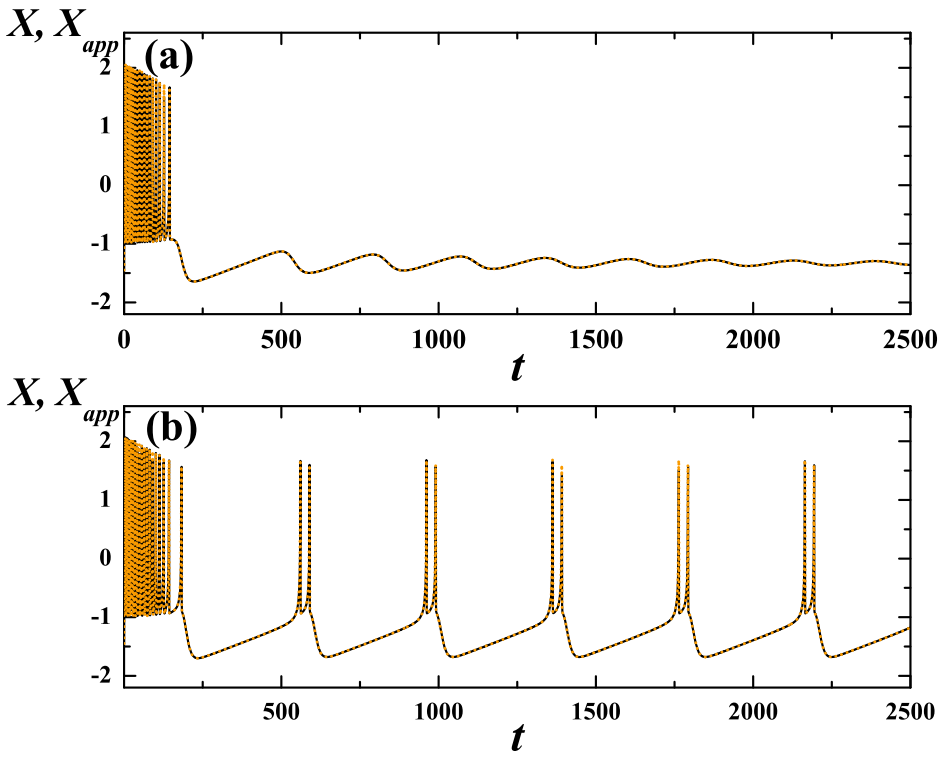

Figure 7.6: Comparison between $X(t)$ and $X_{app}(t)$ under the analogous initial conditions in the noiseless and the delay-free case. Increasing I, there is an excellent agreement both for the damped oscillations and the bursting regime. The results are presented for $I = 1.265$ in (a) and $I = 1.272$ in (b), with the remaining parameters being $c = 1$ and $N = 70$.

different from the exact system global variables. Figure 7.7(f) shows that the weakly coupled local bursters are completely de-synchronized by the small noise.

It is expected that the estimates of the critical parameter values corresponding to different bifurcations that are provided by the approximate model (7.9),(7.10) become more accurate as the number of units of the exact system is increased. For example, consider the transition from the bursting dynamics (with the unstable stationary state) that occurs in the approximate system for the fixed parameter values $\tau = 8$, $c = 1$, $D = 0.001$ somewhere between $I = 1.275$ (stable, no bursting) and $I = 1.295$ (unstable, bursting). This transition occurs in exact system with $N = 70$ for the same parameter values and in the indicated interval of I. This is illustrated in Fig. 7.8. On the other hand, the exact system with $N = 65$ for

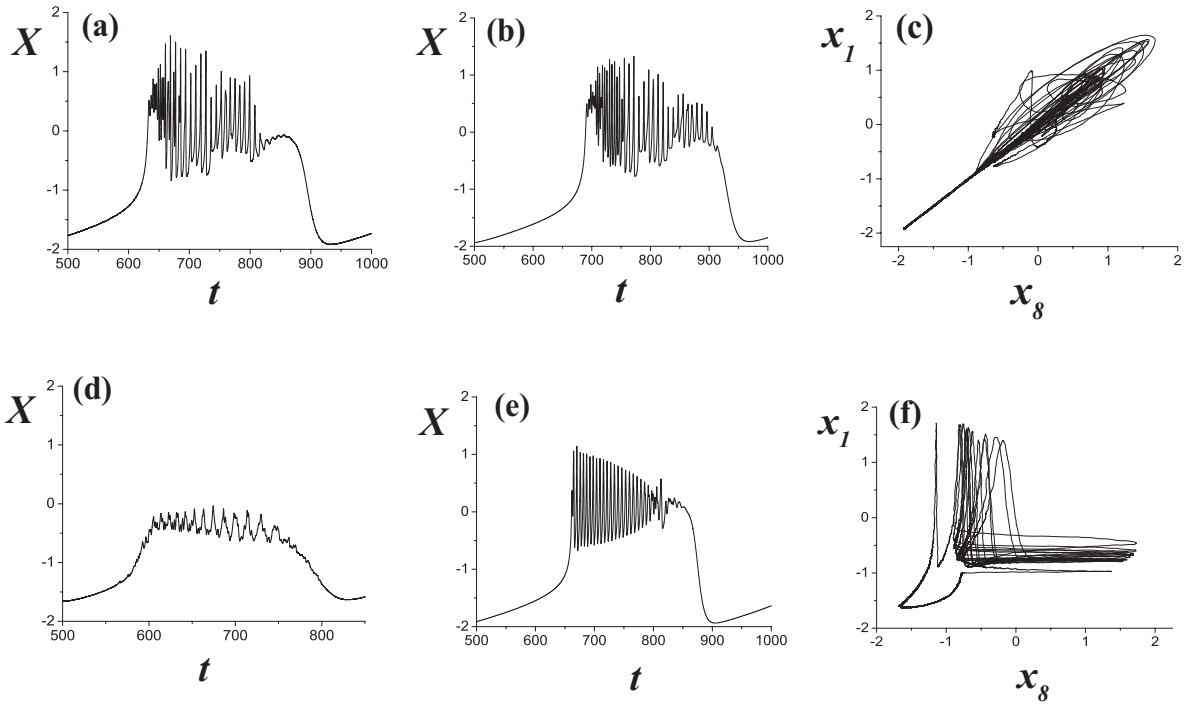

Figure 7.7: Illustration of the influence of coupling strength c on the bursting global dynamics in the case when the parameters $I = 3, \tau = 0, D = 0.001$ are such that each individual neuron is bursting. In a) (exact) and b) (approximate) $c = 1$, and in d) (exact) e) (approximate) $c = 0.1$. In c) $c = 1$ and f) $c = 0.1$ $x_1(t)$ vs. $x_8(t)$ are shown.

the same fixed parameters and for $I = 1.275$ has an unstable stationary state and the global dynamics displays bursting. For $N = 65$ the cessation of bursting and stabilization of the stationary state occurs somewhere between $I = 1.22$ (stable, no bursting) and $I = 1.23$ (unstable, bursting). The critical value of I for $N = 50$ is between $I = 1.2$ (stable, no bursting) and $I = 1.22$ (unstable, bursting), which is even further away from the value estimated with the approximate system than in the $N = 65$ case. For $N = 10$ the transition occurs between $I = 1.15$ (stable, no bursting) and $I = 1.17$ (unstable bursting). We see that, as expected, the estimated critical value becomes more accurate as the number of units in the exact system is increased.

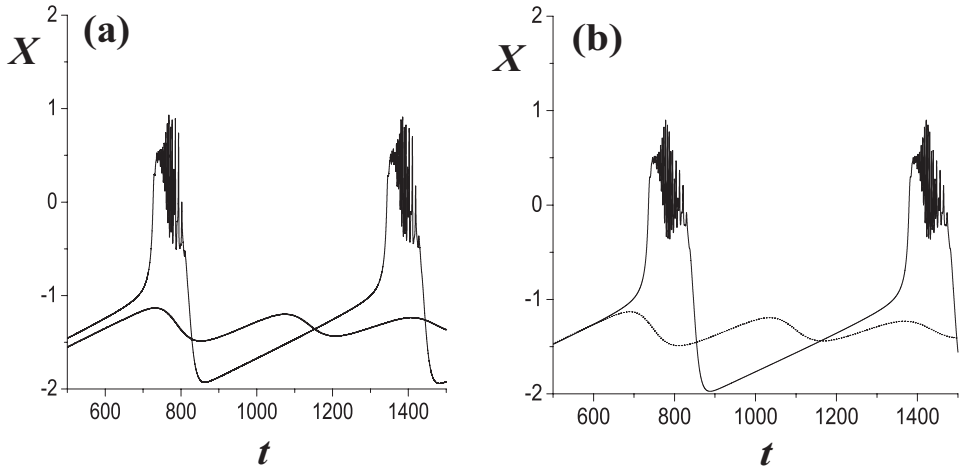

Figure 7.8: Illustrating the point that for $N = 70$ the bifurcation value of the parameter I, which implies destabilization of the stationary state and the transition to the bursting dynamics of the global variables in the exact system (a), is predicted by the approximated model (b) with the accuracy better than two percent. Accuracy for smaller N is commented in the main text. The parameters are $I = 1.275$ (dotted), $I = 1.295$ (full) and $c = 1, D = 0.001, \tau = 8$.

7.4 Chapter summary and discussion

We have studied stability and bifurcations that induce the bursting dynamics of the global variables of a large ensemble of coupled bursting neurons. Each of the neurons is represented by Hidmarsh-Rose model which is known to be able to display the bursting dynamics for sufficiently strong external perturbation. Influence of noise is modeled by additive white noise in each neuron. It is supposed that each neuron is coupled to all other neurons by electrical junctions and the synaptic delays are explicitly included. It is also assumed that all neurons are equal and interact via synapses of equal efficiency. This is justified if the neurons are assumed to occupy nearby positions in the brain cortex. For example, such a collection of similar neurons would be found in a patch of the brain cortex monitored by a single electrode of an EEG measurement. Another possibility, which could also be analyzed by the methods of this chapter, would be to assume random uniform distributions with small fluctuations of the internal parameters, the interaction constants and the time-lags.

Thus, the model is given by a large set of stochastic delay-differential equations. We have focused on the dynamics of the collective variables represented as the spatial averages of the local ones.

Typical assumptions of the mean field approach are used to derive the set of nine deterministic delay-differential equations for the first and the second moments of the collective variables. The main assumption in the derivation is that the system represents an ensemble of Gaussian distributed independent random variables. One expects this to be a plausible assumption if the intensity of the noise and the coupling are not very large.

Various bifurcations due to variations of different parameters I, c, τ, D are observed in the dynamics of global variables of the exact system with large number of units, and the bifurcation values are compared with those predicted by the approximate model with only nine deterministic equations. It is observed that variations of any of the parameters I, c, τ, D can destabilize the quiescent global behavior and introduce bursting. Domains in the parameter space corresponding to stable quiescent behavior or to the bursting of the collective variables of the large exact system are correctly predicted by the approximate model. The predictions of the approximate model become more accurate as the number of units is increased. In this sense the approximate model represents a very useful tool for an efficient numerical treatment of the global dynamics of the large system of delayed coupled noisy bursters.

It would be interesting to extend this type of analysis on the system of bursters coupled by some model of the chemical synapse.

Chapter 8

Conclusion

The main topic of the present thesis has been the analysis of the self-organization phenomena emerging due to synchronization in large populations of stochastic excitable or bursting units subjected to interaction delays. Apart from considering the scenarios for the onset of the spiking and bursting collective modes, we have also reported on the novel paradigm for cluster synchrony, reflected in the spontaneous splitting of structureless assemblies of excitable units into subsets whose members are approximately synchronized in phase, whereas the subsets themselves may display constant or variable phase differences. Throughout the thesis, the local excitable dynamics has been represented by the Fitzhugh-Nagumo model, canonical for type II excitability, while the activity of bursting units has been described by the Hindmarsh-Rose model, typically generating square-wave bursts. Though both models derive from the field of neuroscience, their potential range of applications spans a variety of systems, from assemblies of cardiac cells to kinetics of electrochemical reactions. In terms of interaction patterns, for the most part we have considered the fully connected networks, this being a preferred approach if one is interested into building minimal models that may capture some forms of collective behavior. What makes this approximation appealing is that one may treat each unit as if it is driven by the mean-field, produced by all the members of the assembly. Regarding macroscopic phenomenology, another important

point is that the effects of noise and delay are not perceived as detrimental or destabilizing, but rather as potentially biased toward creating dynamical structures in networks homogeneous both with respect to connection topology and the local parameters.

Our study incorporates two complementary lines of research: one aimed at determining if and how can the complex forms of collective behavior displayed by the populations of autonomous oscillators be generalized to systems of coupled excitable units, whereas the main contribution from the other line of research lies in developing mean-field based approximations to collective dynamics of systems microscopically described by large sets of SDDEs. Regarding the first line, we have discussed in detail the phenomenon of cluster formation in assemblies of excitable units, showing that its mechanism rests solely on the interplay of excitability feature, noise and interaction delay. In this context, one recalls that clustering presents a fairly common occurrence in populations of self-sustained oscillators. Nevertheless, cluster states we have found emerge via the distinct mechanism, and are further distinguished by the fact that they always coexist with the homogenous states. On a conceptual side, the given phenomenon is important for several reasons. The setup itself is different from most other models exhibiting cluster synchrony because it does not involve heterogeneity in the local parameters or connectivity patterns. On the other hand, it underlies the point that the inclusion of interaction delays significantly alters the physical picture on the excitable media established so far. The latter, reflecting solely the effects of noise, has been built on the idea that under increasing noise intensity excitable media switch between three generic regimes, namely the non-oscillatory state, the coherent oscillatory state and the incoherent (chaotic) oscillatory state. It is also noteworthy that given the spontaneous character of the considered phenomenon, one may expect it to occur under real-world conditions, especially in certain biophysiological systems.

With respect to long-term behavior, the cluster states we have found may be cast either as asymptotically stable ones, where the units are firmly bound to their subsets, or dynamical, where the units may exchange subsets. It turns out that the two-cluster states generically fall into the former class, while the three-cluster states belong to the latter. The stability of cluster partition is reflected in the relative phase differences between the subsets' activities. In the two-cluster case, an approximately constant π phase-shift is maintained, such that if one cluster is active, the other one is resting. On the other hand, in case of three-cluster partitions, the approximately constant phase difference cannot be maintained. Intuitively, the existence of only two- and three-cluster states may be understood as a consequence of the excitability feature and the strong time-scale separation between the fast and slow variables. Put briefly, the two-cluster states may be seen as reflecting the existence of two stable branches of the slow manifold, where the refractory and spiking states lie. Regarding the stability of the two-cluster partition, one invokes the point that in the limit $\epsilon \to 0$ for $D \simeq 0$, the two branches virtually act as attractors. As for the three-cluster partition, the excitable state comes into play as well, with the possibility for some fraction of units to become frustrated in the vicinity of the equilibrium. The ensuing inability to maintain approximately constant phase differences between the subsets may be linked to variable longevity of the excitable states.

In order to characterize the structure of the cluster states and determine the parameter domains admitting clustering, several tools have been applied. The basic description rests on the notion of pairwise coherence, employed to construct the appropriate coherence matrices, as well as the binary or weighted functional ("coherence") networks. Within the latter, a link between the two units is defined in such a way that its presence or strength indicates the degree of long-term coordination of the units' activity patterns. While the properly arranged coherence matrices can be used

to assess and conveniently visualize the structure of the cluster states, the properties of functional networks, like the distribution of connectivity degrees, may allow one to distinguish more easily between the dynamical cluster states and some complex incoherent states. The phenomenon of dynamical clustering has further been analyzed by introducing the method of dynamical correlation coefficients. From their evolution and the long-tail feature of the distribution of local jitters, one may infer that the three-cluster partition involves two core subsets and a cluster of itinerant units, jumping between the cores. Note that in statistical terms, the jumping events of different itinerant units are highly correlated.

Given the stable character of two-cluster partitions for relatively large network sizes, we have been interested into verifying two additional points: (*i*) whether one can demonstrate the persistence of clustering in the thermodynamic limit $N \to \infty$, and (*ii*) whether the two-cluster states are robust against heterogeneity in local parameters or the connectivity pattern. Regarding (*i*), the quantity relevant for examining the asymptotic behavior of the two-cluster states in the limit $N \to \infty$ turned out to be the synchrony measure $\chi^2(N)$, defined as the ratio of the time-averaged fluctuations of $X(t)$ vs the sum of the averaged fluctuations of $x_i(t)$. Apart from explicitly demonstrating the existence of the asymptotic component $\chi^2(\infty)$, which is known to warrant the persistence of two-cluster states in the thermodynamic limit, we have verified that the convergence toward the asymptotic behavior with increasing N is a fast one, with $\chi^2(N)$ approaching $\chi^2(\infty)$ already for $N \sim 10^2$. With respect to (*ii*), the two-cluster states have been shown to persist under heterogeneity of the local excitability parameters b_i, if their values are drawn from a uniform distribution keeping notice that all of the units remain excitable ($b_i > 1$). Nonetheless, two-cluster states have also been found in systems of network-coupled, rather than globally coupled excitable units. In particular, we have verified that clustering may occur in scale-free and random diluted networks, provided that the connec-

tivity degrees of individual units do not become too small. The scale-free networks have been generated via the modified Barabasi-Albert algorithm, whereby the scaling exponent $\gamma \approx 2$ lies close to values seen in certain biophysiological systems. Though the intention has been to outline only the key ingredients behind clustering, rather than examine the less salient effects, such as the dependence on network topology, the obtained results seem to corroborate the claim that the clustering phenomenon persists in networks with more realistic connectivity patterns.

To gain insight into the parameter domains admitting clustering, we have monitored the dependence of the global coherence κ on τ and D. This is based on the notion that for the cluster states κ-values lie around $\kappa \simeq 0.5$, which is substantially smaller from what is obtained for the homogenous coherent states ($\kappa \gtrsim 0.8$) and significantly above the values typical for the homogeneous incoherent states ($\kappa \lesssim 0.35$). The non-trivial character of the parameter domains supporting the cluster states is manifested by the fact that clustering takes place for the parameter values around the local minima of the $\kappa(\tau)$ and $\kappa(D)$ families of curves. Overall, the system's behavior may be understood in terms of collective dynamics occurring on two characteristic time-scales, the noise-driven and the delay-driven one, which results in the competition between two types of collective modes. The oscillation period $T_0(D)$ of the noise-driven mode corresponds to the delay-free case $\tau = 0$, whereas the period of the delay-driven mode scales with τ. We have explicitly demonstrated that clustering bears the features of a resonance phenomenon with respect to τ, such that the delay-resonant intervals are centered around $\tau_r \approx T_0/2 + n * T_0$ with $n = 0, 1, 2$. On the level of competition between the two modes, one may explain this as follows. For the most part, the delay-driven mode wins over, giving rise to the homogeneous (coherent) states. On the other hand, the onset of the cluster states coincides with the parameter domains where the delay-driven mode gives way to the noise-driven one. This is corroborated by the fashion

in which the scaled average ISI intervals $\langle T_X \rangle / \langle T_0 \rangle$ and $\langle T_X \rangle / \langle \tau \rangle$ for the global variable X depend on τ. Proximity to the "center" of the resonant delay interval is found to influence the properties of the cluster partition: close to the center, the symmetrical split involving almost even fractions is preferred, whereas approaching the interval's boundaries, the partition becomes increasingly asymmetrical.

Note that the approximate relation for τ_r is reminiscent of the expression already seen in systems of coupled phase oscillators, but is distinct in that it holds an implicit dependence on D. The intervals of noise values which support clustering for $\tau \approx \tau_r$ are relatively narrow. This indicates that clustering in excitable systems is a result of the noise-delay coeffect, viz. that it requires fine tuning between the two parameters. Though the impact of coupling strength c on cluster states appears marginal, one should still mention that its values should not be overly large, since that would suppress the influence of noise-driven mode altogether.

From the microscopic perspective, the mechanism behind the onset of cluster states and the fashion in which they are maintained can be explained by drawing analogy between the motion of a representative unit and a particle subjected to a double-well potential. Within such a framework, noise provides for the thermal fluctuations eliciting jumps between the two branches of the slow manifold, whereas the delay influences the height of the potential barrier which the particle has to overcome when executing the jump. One may state that for most parameter values, the escape rates become adjusted with τ, whereas for the cluster-resonant delay intervals the rates are in fact noise-dependent, as if $\tau = 0$.

Having summarized the results on the first line of research covered within the thesis, we turn to the main points regarding the second line. The latter has been concerned with building the mean-field based approximate models describing the evolution of global variables for systems whose microscopic dynamics is given in terms of large sets of SDDEs. Given that

such systems are not susceptible to analysis within the Fokker-Planck formalism, the models we have derived rest on the cumulant approach complemented with the Gaussian approximation. The principal gain consists in that the collective dynamics of the exact system, comprised of kN coupled equations where k refers to the number of local variables per each unit, may be represented by only $\frac{k(k+3)}{2}$ deterministic DDEs for the mean-fields and the related variances and covariances. By doing so, the yet unresolved problem of treating the stochastic bifurcations of the original system is translated into the framework of bifurcation analysis on the approximate system, where D may act as a control parameter. It is reasonable to infer that the correspondence between the dynamics of the exact and approximate models is enhanced if the deterministic, delay-driven component in the collective behavior prevails over the stochastic one. Nevertheless, the mean-field model provides accurate predictions on the following set of issues:

i) the conditions for the stability of the stationary state,

ii) the scenarios affecting the onset of the collective mode or its suppression via time-delay,

iii) the regions of bistability, characterized by coexistence between the equilibrium and the collective mode, or between two collective modes.

These points are qualitatively satisfied independent of the form of local dynamics, be it excitable or bursting. Note that the scenarios for the onset and the suppression of collective modes involve the approximate system undergoing direct and inverse Hopf bifurcations, respectively. The appropriate diagrams, indicating sequences of such bifurcations under increasing τ, have been obtained both in $(D - \tau)$ and $(c - \tau)$ parameter planes. On the quantitative side, the average ISI interval of the global variable for the assembly of excitable units is matched well by the oscillation period of the corresponding mean-field variable. The similar point holds in case

of the bursting collective mode regarding the duration of the average cycle exhibited by the exact system and the cycle displayed by the approximate model.

Apart from single populations, we have also considered the setup where two populations of excitable units interact in a nonlinear fashion, such that the corresponding threshold-like coupling function depends explicitly on the respective global variable. The exact system involves noise acting locally within each assembly, as well as two types of interaction delays, namely the intra- and inter-population ones. Consistent with the notion that population exhibiting a collective mode may be treated as a macroscopic oscillator, the approximate system has been built by coupling the two appropriate mean-field models. Our main result concerns the typical case of two symmetrically coupled populations, where the approximate system has been demonstrated to accurately predict the two scenarios giving rise to the collective mode of the total system. In particular, the oscillatory solution can emerge via

i) direct supercritical Hopf bifurcation, which may occur for zero inter-population coupling delay τ_c solely due to increasing the coupling strength g_c between the populations;

ii) direct subcritical Hopf bifurcation, which occurs only above a certain threshold value of τ_c.

Apart from the results on the local bifurcation analysis, an interesting point is that the mean-field model also anticipates the parameter domains where the exact system undergoes a global fold-cycle bifurcation. The latter has been shown to influence the collective behavior in two ways, both tied to the appearance of the saddle cycle. In particular, the saddle cycle emerging from fold-cycle bifurcation may induce subcritical Hopf bifurcation of the equilibrium, or may limit the growth of the incipient limit cycle born via supercritical Hopf bifurcation. Note that the effects of global bifurcation

are also considered in the context of single populations, where the former is found to immediately precede the onset of two-cluster states under variation of the appropriate system parameters. Regarding the setup with two populations, the oscillation period of the mean-field model shows remarkable agreement with the mean ISI interval of the exact system for all the considered configurations. Nevertheless, the results on properties of the collective mode and the bifurcation diagrams obtained for the configuration with symmetrical couplings between populations are significantly modified by introducing asymmetry in coupling functions or if the setup is changed such that one population consists of excitable, and the other of self-oscillating units.

From the theoretical standpoint, an important part of the study concerns determining the parameter domains where the mean-field models accurately reflect the behavior of the respective exact systems, which translates into the issue of examining the conditions under which the mean-field assumptions hold. In these terms, the behavior of populations made up of bursting or excitable units is somewhat distinct. In a sense, the mean-field models built in the former case are more conventional, given that the conditions for their validity may be stated as simple requirements for weak interactions and small noise intensity. This does not apply for the assemblies of excitable units, where the mean-field assumptions, namely the quasi-independence and Gaussian one, need to be adapted to the strong time-scale separation ratio and the significant impact of noise. Having refined the formulation of these two assumptions, we have been able to identify the generic scenarios for their validity, which reflect the properties of local and global dynamics. In particular, the assumptions hold if both the local and global dynamics converge to a unique attractor of the same type, either the fixed point or the limit cycle, provided that D is not excessive. Conversely, if the local and global motion follow different attractors or display multistability, at least one, if not both mean-field assumptions fail. Note

that these qualitative requirements may be satisfied for parameter domains spanning intermediate c and D ranges. This implies that for assemblies of excitable units, the commonly stated requirements on small c and D would effectively understate the range of mean-field model's applicability. Such an outcome is partly due to the impact of interaction delays.

What makes our approach interesting is the ability to estimate the rate in which the fulfilment of the mean-field assumptions deteriorates with increasing noise. This is especially useful given the relationship between the mean-field model and the results of the bifurcation analysis: even if the mean-field assumptions are not satisfied in the absolute terms, the prediction regarding the stability of equilibrium and the onset of the collective mode may still be qualitatively correct. With respect to the fulfilment of the Gaussian approximation in populations of excitable units, the increase of noise intensity is most strongly felt in stochastic phase fluctuations between the different realizations of the stochastic process. Nonetheless, the validity of the quasi-independence assumption has been tested by two methods: (i) an indirect one, verifying whether the distribution of the collective variables for different realizations of the stochastic process is Gaussian; (ii) a direct one, examining the synchronization properties between the units' activities. The rationale for (i) derives from the central limit theorem, by which the sum of independent equally distributed random variables is a Gaussian variable. As for (ii), it has been shown that the coupling term involving the interaction delay may cause the dynamics of two units to appear virtually independent if their activities are synchronized, even in spite of the potentially large c. The method described under (ii) has enabled us to draw additional conclusions on the intervals of τ where the mean-field assumptions are satisfied. A set of minor results concern the statistical properties of local and global oscillations. For the delay-driven dynamics, both in case of local variables and the collective mode, it has been shown that the effective phase description may be applicable. The

same inference can be made for the noise-driven dynamics, provided that D is not too large. Last but not the least, we make a remark on the validity of mean-field assumptions for assemblies of excitable units by looking into the relation with the behavior of the mean-field model itself. In particular, one can demonstrate that if the latter exhibits bistability, involving coexistence of the fixed point and the limit cycle or the two cycles, one born via Hopf and the other via fold-cycle bifurcation, the mean-filed assumptions break down. This is explained by the fact that in the exact system, the corresponding orbits effectively engage in stochastic switching between the attractors given by the mean-field model, hence explicitly violating the above requirements for the assumptions' validity. Therefore, behavior of the mean-field model may be used to predict the domains where the mean-field assumptions fail in the self-consistent fashion.

Having provided the summary of the results obtained, putting them in the appropriate context and commenting on their relevance from the theoretical point of view, we briefly outline the scenarios for potential practical application, further touching upon suggestions for future research. As already iterated, the forms of local dynamics studied within the thesis are typical for the biophysiological systems, though excitability is seen in a wider range of fields. On the other hand, areas where systems on a variety of spatial and temporal scales generate coherent rhythms and communicate by adjusting them are ubiquitous in nature. Nonetheless, the setup involving two interacting populations is important since it may serve as paradigm for the "network of networks" [127, 128] or may represent the basic element of a highly modular network [194]. With respect to self-organization phenomena in complex networks, cluster states are also a common occurrence. For instance, in the field of neuroscience, clustering is found to accompany the cognitive processes of feature binding and segmentation [21, 187]. On the former, multiple representations of the same object may be bound together into a cluster state, whereas in the latter case, cluster-

ing is likely to contribute to discriminating between the different items perceived. Apart from the beneficial side, cluster states may also play a role in the onset of certain pathological brain rhythms linked to epileptic seizures [13].

The results obtained on clustering phenomena in assemblies of excitable units justify pursuing further the research on analogies between the complex forms of self-organization in populations of excitable units and those made up of autonomous oscillators. In particular, it would be interesting to determine the conditions for the onset of chimera states, especially focussing on the issue of whether they may exist in presence of coupling delays [47, 229]. From the neuroscience perspective, chimeras pose the dynamical paradigm behind the so called "bump states" [230–233], occurring in macroscopic systems that allow for some regions to exhibit coherent oscillations, while other remain in the asynchronous regime. As a more distant goal, it would be interesting to examine whether an effective phase description can be developed for the assemblies of excitable units. Note that certain promising results in this direction, though only for a single unit, have already been reported [4, 81]. In terms of the mean-field based approximations, one may address the issue of improving the models derived here in several ways. For instance, an attempt can be made to refine the models by abandoning the quasi-independence approximation altogether [103]. At a first glance, such an approach is certain to provide better accuracy by accounting for the correlations between the local variables, but would also reopen the problem of treating the impact of interaction delay [195]. A more easily obtainable goal concerns adapting the present mean-field models to apply when more realistic network topologies, such as the small-world or scale-free, are considered. Apart from including heterogeneity in the connectivity patterns, it would also be interesting to examine how the collective behavior is modified by introducing heterogeneity in the excitability parameter, thus arriving at mixed populations of excitable and

self-oscillating units.

References

[1] Rosenblum, M. and Pikovsky, A. *Phys. Rev. Lett.* **92**, 114102 (2004). 1, 2, 4, 14, 32, 82, 121

[2] Rosenblum, M. and Pikovsky, A. *Phys. Rev. Lett.* **98**, 064101 (2007). 2, 3

[3] Baibulatov, Y., Rosenblum, M., Zhanabaev, Z., Kyzgarina, M., and Pikovsky, A. *Phys. Rev. E* **80**, 046211 (2009). 1, 2, 14, 120, 121

[4] Schwabedal, J. and Pikovsky, A. *Phys. Rev. E* **81**, 046218 (2010). 6, 8, 9, 14, 182

[5] Zaks, M., Neiman, A., Feistel, S., and Schimansky-Geier, L. *Phys. Rev. E* **68**, 066206 (2003). 1, 16, 37, 47, 81, 123

[6] Komarov, M. and Pikovsky, A. *Phys. Rev. E* **84**, 016210 (2011). 1, 2

[7] Wiesenfeld, K., Colet, P., and Strogatz, S. *Phys. Rev. Lett.* **76**, 404 (1996). 1, 120

[8] Kim, M., Roy, R., Aron, J., Carr, T., and Schwartz, I. *Phys. Rev. Lett.* **94**, 088101 (2005). 1, 120

[9] Kiss, I., Zhai, Y., and Hudson, J. *Science* **296**, 1676 (2002). 1, 120

[10] Chiang, W.-Y., Lai, P.-Y., and Chan, C. *Phys. Rev. Lett.* **106**, 254102 (2011). 1, 9, 22

[11] Yamaguchi, S., Isejima, H., Matsuo, T., Okura, R., Yagita, K., Kobayashi, M., and Okamura, H. *Science* **302**, 1408 (2003). 1, 120

[12] Golomb, D., Hansel, D., and Mato, G. volume 4 of *Handbook of Biological Physics*. Elsevier, Amsterdam (2001). 1, 98, 120

[13] Velazquez, J. and Wennberg, R., editors. *Coordinated Activity in the Brain: Measurements and Relevance to Brain Function and Behavior*. Springer, New York, (2009). 76, 77, 117, 118, 182

[14] Buzsaki, G. *Rhythms of the Brain*. Oxford University Press, Oxford, (2006). 1, 77, 120

[15] Strogatz, S., Abrams, D.M, M. A., Eckhardt, B., and Ott, E. *Nature (London)* **438**, 43 (2005). 1, 120

[16] Néda, Z., Ravasz, E., Brechet, Y., Vicsek, T., and Barabasi, A.-L. *Nature (London)* **403**, 849 (2000). 1, 120

[17] Pikovsky, A., Rosenblum, M., and Kurths, J. *Synchronization, A Universal Concept in Nonlinear Sciences*. Cambridge University Press, Cambridge, (2001). 1, 2, 120

[18] Strogatz, S. *Sync: The Emerging Science of Spontaneous Order*. Hyperion, New York, (2003).

[19] Balanov, A., Janson, N., Postnov, D., and Sosnovtseva, O. *Synchronization: from simple to complex*. Springer, Berlin, (2009). 1

[20] Kuramoto, Y. *Chemical Oscillations, Waves and Turbulence*. Springer, Berlin, (1984). 2

[21] Tass, P. *Phase Resetting in Medicine and Biology: Stochastic Modelling and Data Analysis*. Springer, Berlin Heidelberg, (2007). 2, 3, 14, 32, 63, 77, 82, 83, 117, 118, 120, 181

[22] Levnajić, Z. and A., P. *Phys. Rev. E* **82**, 056202 (2010). 2, 8, 14

[23] Schwabedal, J., Pikovsky, A., Kralemann, B., and Rosenblum, M. *Phys. Rev. E* **85**, 026216 (2012). 2

[24] Acebron, J., Bonilla, L., Pérez Vicente, C., Ritort, F., and Spigler, R. *Rev. Mod. Phys.* **77**, 137 (2005). 2

[25] Ott, E. and Antonsen, T. M. *CHAOS* **18**, 037113 (2008). 2, 3, 14, 121

[26] Pazo, D. *Phys. Rev. E* **72**, 046211 (2005). 2

[27] Rosenblum, M. and Pikovsky, A. *Phys. Rev. E* **70**, 041904 (2004). 2, 14, 32, 82, 125

[28] Childs, L. and Strogatz, S. *CHAOS* **18**, 043128 (2008). 2

[29] Popovych, O., Hauptmann, C., and Tass, P. *Phys. Rev. Lett.* **94**, 164102 (2005). 2, 4, 64, 77, 120, 152

[30] Montbrio, E., Kurths, J., and Blasius, B. *Phys. Rev. E* **70**, 056125 (2004). 3, 121, 137

[31] Barreto, E., Hunt, B., Ott, E., and So, P. *Phys. Rev. E* **77**, 036107 (2008). 121, 122

[32] Sheeba, J., Chandrasekar, V., Stefanovska, A., and McClintock, P. *Phys. Rev. E* **79**, 046210 (2009). 3, 14

[33] Kuznetsov, S., Pikovsky, A., and Rosenblum, M. *CHAOS* **20**, 043134 (2010). 3

[34] Kuptsov, P., Kuznetsov, S., and Pikovsky, A. *Phys. Rev. E* **87**, 032912 (2013). 3

[35] Dahms, T., Lehnert, J., and Schoell, E. *Phys. Rev. E* **86**, 016202 (2012). 3

[36] Kori, H. and Kuramoto, Y. *Phys. Rev. E* **63**, 046214 (2001).

[37] Maistrenko, Y., Popovych, O., Burylko, O., and Tass, P. *Phys. Rev. Lett.* **93**, 084102 (2004). 3

[38] Strogatz, S. and Mirollo, R. *Phys. Rev. E* **47**, 220 (1993). 3

[39] Zillmer, R., Livi, R., Politi, A., and Torcini, A. *Phys. Rev. E* **76**, 046102 (2007). 3

[40] Baibolatov, Y., Rosenblum, M., Zhanabaev, Z. Z., and Pikovsky, A. *Phys. Rev. E* **82**, 016212 (2010). 3

[41] Pikovsky, A. and Rosenblum, M. *Physica D* **238**, 27 (2009). 3

[42] van Vreeswijk, C. *Phys. Rev. E* **54**, 5522 (1996). 3

[43] Abrams, D. M. and Strogatz, S. *Phys. Rev. Lett.* **93**, 174102 (2004). 3

[44] Omel'chenko, O. E., Maistrenko, Y. L., and Tass, P. A. *Phys. Rev. Lett.* **100**, 044105 (2008).

[45] Abrams, D., Mirollo, R., Strogatz, S., and Wiley, D. *Phys. Rev. Lett.* **101**, 084103 (2008). 121

[46] Laing, C. *CHAOS* **19**, 013113 (2009).

[47] Wolfrum, M., Omel'chenko, O., Yanchuk, S., and Maistrenko, Y. *CHAOS* **21**, 013112 (2011). 3, 182

[48] Hagerstrom, A., Murphy, T., Roy, R., Hövel, P., Omelchenko, I., and Schöll, E. *Nature Physics* **8**, 658 (2012). 3

[49] Watanabe, S. and Strogatz, S. H. *Phys. Rev. Lett.* **70**, 2391 (1993). 3

[50] Ott, E. and Antonsen, T. M. *CHAOS* **19**, 023117 (2009). 3

[51] Tsimring, L. and Pikovsky, A. *Phys. Rev. Lett.* **87**, 250602 (2001). 4, 10

[52] Pototsky, A.and Janson, N. *Phys. Rev. E* **77**, 031113 (2008). 4

[53] Chen, Y., Ding, M., and Kelso, J. *Phys. Rev. Lett.* **79**, 4501 (1997). 4

[54] Masoller, C. *Phys. Rev. Lett.* **86**, 2782 (2001). 4

[55] Pikovsky, A. and Kurths, J. *Phys. Rev. Lett.* **78**, 775 (1997). 4, 5, 10, 11, 28, 29, 30, 66, 76, 80, 94, 152

[56] Nesse, W., Del Negro, C., and Bressloff, P. *Phys. Rev. Lett.* **101**, 088101 (2008). 4, 5

[57] Dhamala, M., Jirsa, V., and Ding, M. *Phys. Rev. Lett.* **92**, 074104 (2004). 4, 64, 77, 120, 152, 155

[58] Herrero, R., Figueras, M., Rius, J., Pi, F., and Orriols, G. *Phys. Rev. Lett.* **84**, 5312 (2000).

[59] Doiron, B., Lindner, B., Longtin, A., Maler, L., and Bastian, J. *Phys. Rev. Lett.* **93**, 048101 (2004). 4

[60] Denker, M., Timme, M., Diesmann, M., Wolf, F., and Geisel, T. *Phys. Rev. Lett.* **92**, 074103 (2004). 4

[61] Ernst, U., Pawelzik, K., and Geisel, T. *Phys. Rev. Lett.* **74**, 1570 (1995).

[62] Yeung, M. and Strogatz, S. *Phys. Rev. Lett.* **82**, 648 (1999). 4, 88

[63] Janson, N., Balanov, A., and Schoell, E. *Phys. Rev. Lett.* **93**, 010601 (2004). 4, 11

[64] Hasegawa, H. *Phys. Rev. E* **70**, 021911 (2004). 4, 15, 16, 81, 153

[65] Masoller, C. and Marti, A. *Phys. Rev. E* **94**, 134102 (2005). 5

[66] Kestler, J., Kopelowitz, E., Kanter, I., and Kinzel, W. *Phys. Rev. E* **77**, 046209 (2008). 5

[67] Lindner, B., Garcia-Ojalvo, J., Neiman, A., and Schimansky-Geier, L. *Phys. Rep.* **392**, 321 (2004). 5, 6, 7, 8, 9, 10, 11, 12, 16, 27, 28, 29, 30, 37, 42, 47, 76, 81, 111, 120, 122, 152, 153, 158

[68] Goldobin, D. and Pikovsky, A. *Phys. Rev. E* **71**, 045201 (2005). 5

[69] Sagués, F., Sancho, J., and García-Ojalvo, J. *Rev. Mod. Phys.* **79**, 829 (2007). 5

[70] Gammaitoni, L., Hänggi, P., Jung, P., and Marchesoni, F. *Rev. Mod. Phys.* **70**, 223 (1998). 5

[71] Chialvo, D., Longtin, A., and Mueller-Gerking, J. *Phys. Rev. E* **55**, 1798 (1997).

[72] Jung, P. *Phys. Rep.* **234**, 175 (1993). 5

[73] Yoshimura, K. and Arai, K. *Phys. Rev. Lett.* **101**, 154101 (2008). 6, 8

[74] Teramae, J., Nakao, H., and Ermentrout, G. *Phys. Rev. Lett.* **102**, 194102 (2009). 6

[75] Izhikevich, E. *Dynamical Systems in Neuroscience: The Geometry of Excitability and Bursting*. MIT Press, Cambridge, Massachusetts, (2007). 6, 7, 8, 9, 12, 13, 23, 31, 79, 121, 124, 132, 152, 153

[76] Khovanov, I. A., Polovinkin, A. V., Luchinsky, D. G., and McClintock, P. V. E. *Phys. Rev. E* **87**, 032116 (2013). 7, 10, 23, 25, 26, 27

[77] Lee DeVille, R. E., Vanden-Eijnden, E., and Muratov, C. *Phys. Rev. E* **72**, 031105 (2005). 7, 8, 10, 11, 25, 26, 27, 29, 80, 81, 106, 111, 126, 155

[78] Muratov, C., Vanden-Eijnden, E., and Weinan, E. *Physica D* **210**, 227 (2005). 8, 10, 26, 29, 81

[79] Muratov, C. and Vanden-Eijnden, E. *CHAOS* **18**, 015111 (2008). 10, 23, 26, 28, 80, 81, 111, 126

[80] Brandstetter, S., Dahlem, M., and Schoell, E. *Phil. Trans. R. Soc. A* **368**, 391 (2010). 7, 8, 25, 26, 27, 28

[81] Schwabedal, J. and Pikovsky, A. *Phys. Rev. Lett.* **110**, 204102 (2013). 8, 182

[82] Morris, C. and Lecar, H. *Biophys. J.* **35**, 193 (1981). 9

[83] Fitzhugh, R. *Biophys. J.* **1**, 445 (1961). 9, 22

[84] Nagumo, J., Arimoto, S., and Yoshizawa, S. *Proc. IRE* **50**, 2061 (1962). 9, 22

[85] Gerstner, W. and Kistler, W. *Spiking Neuron Models: Single Neurons, Populations, Plasticity*. Cambridge University Press, Cambridge, (2002). 9, 22

[86] Yacomotti, A., Monnier, P., Raineri, F., Ben Bakir, B., Seassal, C., Raj, R., and Levenson, J. *Phys. Rev. Lett.* **97**, 143904 (2006). 9

[87] Dubbeldam, J., Krauskopf, B., and Lenstra, D. *Phys. Rev. E* **60**, 6580 (1999). 9

[88] Larotonda, M. A., Hnilo, A., Mendez, J., and Yacomotti, A. *Phys. Rev. A* **65**, 033812 (2002). 9

[89] Sridhar, S., Le, D.-M., Mi, Y.-C., Sinha, S., Lai, P.-Y., and Chan, C. *Phys. Rev. E* **87**, 042712 (2013). 9

[90] Ciszak, M., Euzzor, S., Arecchi, F., and Meucci, R. *Phys. Rev. E* **87**, 022919 (2013). 9, 22

[91] White, J., Rubinstein, J., and Kay, A. *Trends in Neurosci.* **23**, 131 (2000). 9

[92] Li, Q. and Lang, X. *Phys. Rev. E* **74**, 031905 (2006). 11

[93] Hauschildt, B., Janson, N., Balanov, A., and Schoell, E. *Phys. Rev. E* **74**, 051906 (2006). 11

[94] Muratov, C., Vanden-Eijnden, E., and Weinan, E. *PNAS* **104**, 702 (2007). 12

[95] Kaluza, P., Strege, C., and Meyer-Ortmanns, H. *Phys. Rev. E* **82**, 036104 (2010). 12, 37, 64, 81

[96] Ibarz, B., Cao, H., and Sanjuan, M. *Phys. Rev. E* **77**, 051918 (2008). 12

[97] Ivanchenko, M., Osipov, G., Shalfeev, V. D., and Kurths, J. *Phys. Rev. Lett.* **93**, 134101 (2004). 12

[98] Elson, R., Selverston, A. I., Huerta, R., Rulkov, N., Rabinovich, M. I., and Abarbanel, H. *Phys. Rev. Lett.* **81**, 5692 (1998). 12

[99] Hindmarsh, J. and R.M., R. *Proc. R. Soc. London, Ser. B* **221**, 87 (1984). 13, 153

[100] Schimansky-Geier, L., Anishchenko, V. S., and Neiman, A. volume 4 of *Handbook of Biological Physics*. Elsevier, Amsterdam (2001). 13

[101] Belykh, I., de Lange, E., and Hasler, M. *Phys. Rev. Lett.* **94**, 188101 (2005). 156

[102] Franović, I. and Miljković, V. *EPL* **92**, 68007 (2010). 13

[103] Hasegawa, H. *Physica D* **237**, 137 (2008). 14, 15, 51, 81, 122, 182

[104] Kawamura, Y., Kawamura, Y., Nakao, H., Arai, K., Kori, H., and Kuramoto, Y. *Phys. Rev. Lett.* **101**, 024101 (2008). 14, 121

[105] Atay, F. *Phys. Rev. Lett.* **91**, 094101 (2003). 14

[106] Mackey, M. C. and Nechaeva, I. G. *Phys. Rev. E* **52**, 3366 (1995). 15

[107] Guillouzic, S., L'Heureux, I., and Longtin, A. *Phys. Rev. E* **59**, 3970 (1999). 15

[108] Ohira, T. and Yamane, T. *Phys. Rev. E* **61**, 1247 (2000). 15

[109] Gaudreault, M., Lépine, F., and Viñals, J. *Phys. Rev. E* **80**, 061920 (2009). 15

[110] Gaudreault, M., Berbert, J., and Viñals, J. *Phys. Rev. E* **83**, 011903 (2011). 15

[111] Tanabe, S. and Pakdaman, K. *Phys. Rev. E* **63**, 031911 (2001). 16, 38, 47, 153

[112] Rodriguez, R. and Tuckwell, H. *Phys. Rev. E* **54**, 5585 (1996). 16, 47, 153

[113] Acebron, J. A., Bulsara, A., and Rappel, W.-J. *Phys. Rev. E* **69**, 026202 (2004). 16, 81

[114] Franović, I., Todorović, K., Vasović, N., and Burić, N. *submitted to Phys. Rev. E* . 19

[115] Franović, I., Todorović, K., Vasović, N., and Burić, N. *Phys. Rev. Lett.* **108**, 094101 (2012). 19, 33, 43, 49, 77, 87, 108

[116] Franović, I., Todorović, K., Vasović, N., and Burić, N. *CHAOS* **22**, 033147 (2012). 19

[117] Franović, I., Todorović, K., Vasović, N., and Burić, N. *Phys. Rev. E* **87**, 012922 (2013). 19, 47

[118] Franović, I., Todorović, K., Vasović, N., and Burić, N. *CHAOS* **21**, 033109 (2011). 20

[119] Bonhoeffer, K. *J. Gen. Physiol.* **32**, 69 (1948). 22

[120] Kadar, S., Wang, J., and Showalter, K. *Nature* **391**, 770 (1998). 22

[121] Baer, M. and Erneux, T. *SIAM J. Appl. Math.* **46**, 721 (1986). 26

[122] Peng, B., Gaspar, V., and Showalter, K. *Phil. Trans. R. Soc. Lond. A* **337**, 275 (1991). 26

[123] Gao, Y. and Wang, J. *Phys. Rev. E* **83**, 031909 (2011). 28, 37, 66, 81, 94

[124] Gardiner, C. *Handbook of Stochastic Methods*. Springer, Berlin, (2004). 29, 40, 47, 157, 158

[125] Atay, F., editor. *Complex Time-Delay Systems*, volume 16 of *Understanding Complex Systems*. Springer, Berlin, (2010). 31, 47, 79, 124

[126] Schoell, E., Hiller, G., Hovel, P., and Dahlem, M. *Phil. Trans. R. Soc. A* **367**, 1079 (2009). 31, 79, 124

[127] Luccioli, S. and Politi, A. *Phys. Rev. Lett.* **105**, 158104 (2010). 32, 82, 125, 181

[128] Olmi, S., Politi, A., and Torcini, A. *EPL* **92**, 60007 (2010). 32, 82, 121, 122, 137, 181

[129] Zaks, M. A., Sailer, X., Schimansky-Geier, L., and Neiman, A. B. *CHAOS* **15**, 026117 (2005). 38, 42, 153, 158

[130] Neiman, A., Anishchenko, V., and Kurths, J. *Phys. Rev. E* **49**, 3801 (1994). 38

[131] Anishchenko, V. and Neiman, A. *Int. J. Bifurcation Chaos* **2**, 979 (1992). 38

[132] Desai, R. and Zwanzig, R. *J. Stat. Phys.* **19**, 1 (1978). 38

[133] Pikovsky, A. and Ruffo, S. *Phys. Rev. E* **59**, 1633 (1999). 38

[134] Arnold, L. *Random Dynamical Systems*. Springer-Verlag, Berlin, (1998). 38, 130

[135] David, O. and Friston, K. *Neuroimage* **20**, 1743 (2003). 42, 123, 126

[136] Ramana Reddy, D. V., Sen, A., and Johnson, G. *Phys. Rev. Lett* **80**, 5109 (1998). 42, 64, 77, 120, 152

[137] Strogatz, S. H. *Nature* **394**, 316 (1998). 42, 64, 77, 120, 152

[138] Burić, N., Ranković, D., Todorović, K., and Vasović, N. *Physica A* **389**, 3956 (2010). 43, 47, 48, 55, 77, 78, 123, 153, 158

[139] Burić, N., Todorović, K., and Vasović, N. *Phys. Rev. E* **82**, 037201 (2010). 43, 66, 71, 78, 112, 123, 153

[140] Laing, C. and Lord, G., editors. *Stochastic Methods in Neuroscience*. Oxford University Press, New York, (2010). 47

[141] Mao, X. *Exponential Stability of Stochastic Differential Equations*. Marcel Dekker, New York, (1994). 47, 152

[142] Kloeden, P. E. and Platen, E. *Numerical Solution of Stochastic Differential Equations*. Springer, Berlin, (1999). 47

[143] Burić, N. and Todorović, D. *Phys. Rev. E* **67**, 066222 (2003). 64, 77, 78, 112, 120, 152

[144] Pikovsky, A., Zaikin, A., and de la Casa, M. A. *Phys. Rev. Lett* **88**, 050601 (2002). 64, 120

[145] Pikovsky, A., Zaikin, A., and de la Casa, M. A. *Phys. Rep.* **392**, 321 (2004).

[146] Burić, N., Todorović, K., and Vasović, N. *Phys. Rev E* **75**, 026209 (2007). 120, 153

[147] Wang, Q., Chen, G., and Perc, M. *PLoS ONE* **6**, e15851 (2011). 64, 120, 153

[148] Sailer, X., Hennig, D., Beato, V., Engel, H., and Schimansky-Geier, L. *Phys. Rev. E* **73**, 056209 (2006). 64, 96

[149] Yi, M. and Yang, L. *Phys. Rev. E* **81**, 061924 (2010). 65, 83

[150] Sun, X., Perc, M., Lu, Q., and Kurths, J. *CHAOS* **20**, 033116 (2010). 65, 83, 87

[151] Moss, F. and Gielen, S., editors. *Neuro-Informatics and Neural Modelling*. Elsevier, Amsterdam, (2000). 66, 68

[152] Ward, L. *Trends Cogn. Sci.* **17**, 553 (2003). 76

[153] Jensen, O., Kaiser, J., and Lachaux, J.-P. *Trends Neurosci.* **30**, 317 (2007).

[154] Engel, A. K., Fries, P., and Singer, W. *Nat. Rev. Neurosci.* **2**, 704 (2001).

[155] Varela, F., Lachaux, J., Rodriguez, E., and Martinerie, J. *Nat. Rev. Neurosci.* **2**, 229 (2001).

[156] Buzsaki, G. and Draguhn, A. *Science* **304**, 1926 (2004). 76

[157] Baker, S., Kilner, J. M., Pinches, E. M., and Lemon, R. N. *Exp. Brain. Res.* **128**, 109 (1999). 76

[158] Cassidy, M., Mazzone, P., Oliviero, A., Insola, A., Tonali, P., and Di Lazzaro, V. *Brain* **125**, 1235 (2002).

[159] Sanes, J. N. and Donoghue, J. *Proc. Natl. Acad. Sci. USA* **90**, 4470 (1993).

[160] Murthy, V. N. and Fetz, E. E. *J. Neurophysiol.* **76**, 3949 (1996). 76

[161] McDonnell, M. and Ward, L. *Nat. Rev. Neurosci.* **12**, 415 (2011). 76

[162] Josić, K., Rubin, J., Matías, M. A., and Romo, R., editors. *Coherent Behavior in Neuronal Networks*. Springer, New York, (2009). 93

[163] Smith, C. Academic Press, San Diego, CA (1992).

[164] Longtin, A. *Phys. Rev. E* **55**, 867 (1997). 152

[165] Manjarrez, E., Rojas-Piloni, J., Mendez, I., Martinez, L., Velez, D., Vazquez, D., and Flores, A. *Neurosci. Lett.* **326**, 93 (2002).

[166] Pankratova, E. V., Polovinkin, A., and Spagnolo, B. *Phys. Lett. A* **344**, 43 (2005). 152

[167] Valenti, D., Augello, G., and Spagnolo, B. *Eur. Phys. J. B* **65**, 443 (2008). 76, 152

[168] Abarbanel, H., Huerta, R., and Rabinovich, M. I. *Neural Comput.* **8**, 1567 (1996). 77, 152

[169] Rossoni, E., Chen, Y., Ding, M., and Feng, J. *Phys. Rev. E* **71**, 061904 (2005). 77, 152

[170] Golomb, D. and Rinzel, J. *Physica D* **72**, 259 (1994). 77

[171] Okuda, K. *Physica D* **63**, 424 (1993).

[172] Ernst, U., Pawelzik, K., and Geisel, T. *Phys. Rev. E* **57**, 2150 (1998). 77

[173] Sporns, O. *Networks of the brain*. MIT Press, Cambridge, (2011). 83

[174] Bullmore, E. and Sporns, O. *Nat. Rev. Neurosci.* **10**, 186 (2009).

[175] Sporns, O., Chialvo, D., Kaiser, M., and Hilgetag, C. *Trends Cogn. Sci.* **8**, 418 (2004). 83

[176] Eguíluz, V. M., Chialvo, D., Cecchi, G., Baliki, M., and Apkarian, A. *Phys. Rev. Lett.* **94**, 018102 (2005). 83, 84

[177] Fries, P. *Trends Cogn. Sci.* **9**, 474 (2005). 83

[178] Schmid, G., Goychuk, I., and Hänggi, P. *Physica A* **325**, 165 (2003). 89

[179] Ermentrout, G. and Terman, D. *Mathematical Foundations of Neuroscience*. Springer, New York, (2010). 92, 99

[180] Chik, D., Coombes, S., and Wang, Z. *Phys. Rev. E* **70**, 011908 (2004). 93

[181] Franović, I. and Miljković, V. *Chaos Soliton. Fract.* **44**, 122 (2011). 104

[182] Engelborghs, K., Luzyanina, T., and Samaey, G. Technical report, Department of Computer Science, K. U. Leuven, Leuven, Belgium, (2001). 112, 132, 160

[183] Engelborghs, K., Luzyanina, T., and Roose, D. *ACM Trans. Math. Softw.* **28**, 1 (2002). 112, 132, 160

[184] Jirsa, V. K. *Cogn. Neurodyn.* **2**, 29 (2008). 117

[185] Li, M., Guan, S., and Lai, C.-H. *New J. Phys.* **12**, 103032 (2010). 117

[186] Niyogi, R. and English, L. *Phys. Rev. E* **80**, 066213 (2009). 117

[187] Singer, W. and Gray, C. *Annu. Rev. Neurosci.* **18**, 555 (1995). 118, 181

[188] Glass, L. and Mackey, M. C. *From Clocks to Chaos: The Rhythms of Life*. Princeton University Press, Princeton, NJ, (1988). 120

[189] Boccaletti, S., Kurths, J., Osipov, G., Valladares, D., and Zhou, C. *Phys. Rep.* **366**, 1 (2002). 120

[190] McDonnell, M. D. and Ward, L. *Nat. Rev. Neurosci.* **12**, 415 (2011). 120

[191] Kawamura, Y., Nakao, H., and Kuramoto, Y. *Phys. Rev. E* **75**, 036209 (2007). 121

[192] Kori, H., Kawamura, Y., Nakao, H., Arai, K., and Kuramoto, Y. *Phys. Rev. E* **80**, 036207 (2009).

[193] Kawamura, Y., Nakao, H., Arai, K., Kori, H., and Kuramoto, Y. *CHAOS* **20**, 043109 (2010). 121

[194] Skardal, P. and Restrepo, J. G. *Phys. Rev. E* **85**, 016208 (2012). 122, 181

[195] Hasegawa, H. *Phys. Rev. E* **72**, 021912 (2004). 122, 123, 153, 182

[196] Hasegawa, H. *Phys. Rev. E* **72**, 056139 (2005).

[197] Stefanescu, R. A. and Jirsa, V. K. *PLoS Comput Biol.* **4**, e1000219 (2008). 122, 123, 126

[198] Hasegawa, H. *Phys. Rev. E* **67**, 041903 (2003). 123

[199] Hasegawa, H. *Phys. Rev. E* **70**, 066107 (2004). 123

[200] Hale, J. and Lunel, S. V. *Introduction to Functional Differential Equations*. Springer-Verlag, New York, (1993). 130

[201] Campbell, S. A. Springer-Verlag, Berlin Heidelberg (2007). 132

[202] Campbell, S. A. Springer-Verlag, New York (2009). 130, 132

[203] Wiggins, S. *Introduction to Applied Nonlinear Dynamical Systems and Chaos*. Springer, New York, Cambridge, 2nd ed. edition, (2000). 131, 132

[204] Kuznetsov, Y. A. *Elements of the Applied Bifurcation Theory*. Springer-Verlag, New York, 3rd ed. edition, (2004). 131, 132

[205] Kandel, E., Schwartz, J., and Jessel, T. *Principles of Neural Science*. Elsevier, New York, 3rd ed. edition, (1991). 152

[206] Haken, H. *Brain Dynamics: Synchronization and Activity Patterns in Pulse-Coupled Neural Nets with Delays and Noise*. Springer-Verlag, Berlin, (2006). 152

[207] Smith, C. E. MIT Pess, Cambridge MA (1989). 152

[208] Elgolc, L. and Norkin, S. Nauka, Moskva (1971). 152

[209] Liao, X. and Mao, X. *Stoch. Anal. Appl.* **14**, 165 (1996). 152

[210] Blythe, S., Mao, X., and Shah, A. *Stoch. Anal. Appl.* **19**, 85 (2001). 152

[211] Sun, J. and Wan, L. *Phys. Lett. A* **343**, 331 (2005). 152

[212] Goldobin, D., Rosenblum, M., and Pikovsky, A. *Physica A* **327**, 134 (2003). 153

[213] Goldobin, D. and Pikovsky, A. *Physica A* **351**, 126 (2005). 153

[214] Burić, N., Todorović, K., and Vasović, N. *Chaos Soliton. Fract.* **40**, 1127 (2009). 155

[215] Shinohara, Y., Kanamaru, T., Suzuki, H., Horita, T., and Aihara, K. *Phys. Rev. E* **65**, 051906 (2002).

[216] Sainz-Trapaga, M., Masoller, C., Braun, H. A., and Huber, M. *Phys. Rev. E* **70**, 031904 (2004).

[217] Sethia, G., Kurths, J., and Sen, A. *Phys. Lett. A* **364**, 227 (2007). 153

[218] Chun-Biao, G., Perc, M., and Qing-Yun, W. *Chin. Phys. B* **19**, 040508 (2010). 153

[219] Wang, Q., Perc, M., Duan, Z., and Chen, G. *Phys. Rev. E* **80**, 026206 (2009).

[220] Wang, Q., Perc, M., Duan, Z., and Chen, G. *CHAOS* **19**, 023112 (2009).

[221] Wang, Q., Perc, M., Duan, Z., and Chen, G. *Europhys. Lett.* **83**, 50008 (2008).

[222] Wang, Q., Perc, M., Duan, Z., and Chen, G. *Physica A* **389**, 3299 (2010). 153

[223] Hasegawa, H. *Phys. Rev. E* **68**, 041909 (2003). 153

[224] Pototsky, A. and Janson, N. *Int. J. Bifur. Chaos* **20**, 1825 (2010). 153

[225] Wang, X.-J. *Physica D* **62**, 263 (1993). 154

[226] Perz, M. and Marhl, M. *Phys. Rev. E* **71**, 026229 (2005). 154

[227] Burić, N. and Ranković, D. *Phys. Lett. A* **363**, 282 (2007). 155

[228] Ermentrout, B. http://www.math.pitt.edu/~bard/xpp/xpp.html. 161

[229] Sethia, G. and Sen, A. *Phys. Rev. Lett.* **100**, 144102 (2008). 182

[230] Compte, A., Brunel, N., Goldman-Rakic, P., and Wang, X.-J. *Cereb. Cortex* **10**, 910 (2000). 182

[231] Renart, A., Song, P., and Wang, X.-J. *Neuron* **38**, 473 (2003).

[232] Sakaguchi, H. *Phys. Rev. E* **73**, 031907 (2006).

[233] Omel'chenko, O. E., Wolfrum, M., and Maistrenko, Y. L. *Phys. Rev. E* **81**, 065201 (2010). 182

CURRICULUM VITAE
Igor Franović

Personal data
Current position: researcher
Present address:
Faculty of physics, University of Belgrade
PO Box 44, 11001 Belgrade, Serbia
e-mail: igor.franovic@gmail.com

He was born in Belgrade in 1979. He applied to the Faculty of Physics at the University of Belgrade in 1997. He graduated with excellent marks in 2002. presenting the diploma thesis "Analysis of the Jahn–Teller effect on the example of the transition metal complex $[Cr(NH_3)_6]^{3+}$". After graduation, he attended advanced courses in the theory of phase transitions, nonlinear dynamics, percolation structures and processes, diagrammatic methods in quantum statistical physics, as well as magnetism. He received Master's degree in 2011. completing the thesis entitled "Percolation phase transitions at spatiotemporal fractal structures in *ex-vivo* and *in-vitro* neuronal cultures", where the proposition of functional cell assemblies of transiently synchronized neurons was introduced to explain for the formation and the properties of patterns of activity propagation in mesoscopic cultured networks.

Since 2007, he has participated as a researcher within the project "Phase transitions and nonlinear phenomena in biological and inorganic materials", while at the moment he is engaged on the project "Phase transitions and characterization of inorganic and organic systems", supported by the Serbian Ministry of Education and Science. So far, his contribution amounts to several research papers published in high-level international journals, such as the Physical Review Letters, Physical Review E, Europhysics Letters and Chaos, with the complete list of references appended below. His numerical skills involve the application of numerical methods and programming in C++, Mathematica and Matlab. The fields he is presently interested in cover the topics of combining the methods of nonlinear dynamics in modeling the activity of individual neurons and neuronal populations

subjected to noise and time-delay, different forms of synchronization and emergent phenomena in assemblies of excitable and self-oscillating units, critical behavior exhibited in neural networks and the implementation of the theory of complex networks in the context of the relation between the structural and functional neural networks.

In 2012, he has been a DAAD fellow at the University of Potsdam, Germany.

REFERENCES

1. I. Franović, K. Todorović, N. Vasović, N. Burić, "Mean-field approximation of two coupled populations of excitable units", Physical Review E **87**, 012922 (2013).

2. S. Kostić, I. Franović, K. Todorović, N. Vasović, "Friction memory effect in complex dynamics of earthquake model", accepted in Nonlinear Dynamics (2013).

3. I. Franović, K. Todorović, N. Vasović, N. Burić, "Spontaneous formation of synchronization clusters in homogenous neuronal ensembles induced by noise and interaction delays", Physical Review Letters **108**, 094101 (2012).

4. I. Franović, K. Todorović, N. Vasović, N. Burić, "Cluster synchronization of spiking induced by noise and interaction delays in homogenous neuronal ensembles", CHAOS **22**, 033147 (2012).

5. I. Franović, V. Miljković, "Possibilities of introducing different functional circuits on top of a structural neuron triplet: where do the gains lie?", Chaos, solitons and fractals **45**, 527 (2012).

6. I. Franović, K. Todorović, N. Vasović, N. Burić, "Stability, bifurcations, and dynamics of global variables of a system of bursting neurons", CHAOS **21**, 033109 (2011).

7. I. Franović, V. Miljković, "Functional motifs: a novel perspective on burst synchronization and regularization of neurons coupled via delayed inhibitory synapses", Chaos, solitons and fractals **44**, 122 (2011).

8. I. Franović, V. Miljković, "The effects of synaptic time delay on motifs of chemically coupled Rulkov model neurons", Communications in nonlinear science and numerical simmulation **16**, 623 (2011).

9. I. Franović, V. Miljković, "Phase plane approach to cooperative rhythms in neuron motifs with delayed inhibitory synapses", Europhysics Letters **92**, 68007 (2010), selected for publication in Virtual Journal of Biological Physics Research 21(3).

10. I. Franović, V. Miljković, "Power law behavior related to mutual synchronization of chemically coupled map neurons", European Physical Journal B **76**, 613 (2010).

11. I. Franović, V. Miljković, "Percolation transition at growing spatiotemporal fractal patterns in models of mesoscopic neural networks", Physical Review E **79**, 061923 (2009), selected for publication in Virtual Journal of Biological Physics Research 18(1) and Virtual Journal of Nanoscale Science and Technology 20(1).

12. I. Franović, V. Miljković, "Fractal properties of percolation clusters in Euclidian neural networks", Chaos, solitons and fractals **39**, 1418 (2009).

13. I. Franović, V. Miljković, "Percolation approach to formation of synfire chains in two dimensional neural networks", NEUREL 2006: Eight Seminar on Neural Network Applications in Electrical Engineering, Proceedings, p. 69-72 (2006).

Izjava o autorstvu

Potpisani mr Igor Franović
broj indeksa D-39/2011

Izjavljujem

da je doktorska disertacija pod naslovom

Collective Dynamics and Self-organization of Stochastic Neuronal Systems Influenced by Synaptic Time Delay

- rezultat sopstvenog istraživačkog rada,
- da predložena disertacija u celini ni u delovima nije bila predložena za dobijanje bilo koje diplome prema studijskim programima drugih visokoškolskih ustanova,
- da nisam kršio autorska prava i koristio intelektualnu svojinu drugih lica.

Potpis doktoranda

U Beogradu,

26.11.2013.

Izjava o istovetnosti štampane i elektronske verzije doktorskog rada

Ime i prezime autora mr Igor Franović

Broj indeksa D-39/2011

Studijski program fizika kondenzovane materije i statistička fizika

Naslov rada Collective Dynamics and Self-organization of Stochastic Neuronal Systems Influenced by Synaptic Time Delay

Mentor Prof. dr Nikola Burić

Potpisani mr Igor Franović

izjavljujem da je štampana verzija mog doktorskog rada istovetna elektronskoj verziji koju sam predao za objavljivanje na portalu **Digitalnog repozitorijuma Univerziteta u Beogradu**.

Dozvoljavam da se objave moji lični podaci vezani za dobijanje akademskog zvanja doktora nauka, kao što su ime i prezime, godina i mesto rođenja i datum odbrane rada.

Ovi lični podaci mogu se objaviti na mrežnim stanicama digitalne biblioteke, u elektronskom katalogu i u publikacijama Univerziteta u Beogradu.

Potpis doktoranda

U Beogradu,

26.11.2013.

Izjava o korišćenju

Ovlašćujem Univerzitetsku biblioteku "Svetozar Marković" da u Digitalni repozitorijum Univerziteta u Beogradu unese moju doktorsku disertaciju pod naslovom

Collective Dynamics and Self-organization of Stochastic Neuronal Systems Influenced by Synaptic Time Delay,

koja je moje autorsko delo.

Disertaciju sa svim prilozima predao sam u elektronskom formatu pogodnom za trajno arhiviranje.

Moju doktorsku disertaciju pohranjenu u Digitalni repozitorijum Univerziteta u Beogradu mogu da koriste svi koji poštuju odredbe sadržane u odabranom tipu licence Kreativne zajednice (Creative Commons) za koju sam se odlučio.

1. Autorstvo
2. Autorstvo-nekomercijalno
3. Autorstvo-nekomercijalno-bez prerade
4. Autorstvo-nekomercijalno-deliti pod istim uslovima
5. Autorstvo-bez prerade
6. Autorstvo-deliti pod istim uslovima

Potpis doktoranda

U Beogradu,

26.11.2013.